A study into the origins and significance of white etching cracks in bearing steels

by

Francesco Manieri

A thesis submitted to the University of London in fulfilment of the requirements for the degree of Doctor of Philosophy and Diploma of Imperial College

May 2018

Tribology section

Department of Mechanical Engineering

Imperial College London

Acknowledgements

I thankfully acknowledge SKF for financing this research project.

I would like to express my gratitude to my supervisor, Amir Kadiric, for offering me the great opportunity to carry out this research at very high standards. Many thanks for the guidance during initial stages of the PhD and the trust upon me throughout these years of study.

I am thankful to all the people in SKF for their availability and support. Special thanks go to Guillermo Morales for being a source of inspiration and to Kenred Stadler for the help and sharing of his great knowledge of the subject.

Many thanks to all the colleagues in the Tribology Group for their support and friendship.

To Nico, Ale, Anto, Thanos, Sorin, Johanna, Damon, Pawel, Artemis, Debashis, Alexis for all the trips, parties, pints and many other uncountable things we had together in these four years which I do not want to forget.

To my ethernal friends, Beppe, Tiziano, Marco, Alessio, Davide, Marina, Chiara, which maybe do not have a clue of what I have done in my PhD and, regardless, they were always by my side.

Thanks to my family, mom, dad, Martha, Magda, Mariarita. Thanks for believing in me unconditionally.
Special thanks to my little happiness, Carletto, who still cannot say a word but able to make me smile every time, keeping me away from my lowest times.

Finally, thanks to Antonella for her unique love.

Abstract

Modern machine elements, such as bearings and gears, are often subjected to harsh operating conditions, arising from increased power densities and reduced lubricant film thickness and, often, unpredictable load histories. Such conditions can lead to excessive rates of premature failures i.e. failure rates that were not predicted by basic life theories. A prominent example of this are the relatively high failure rates of rolling bearings employed in wind turbine gearboxes. Such failed bearings exhibit large crack networks decorated by microstructural alterations that appear white when etched and examined under an optical microscope. Hence, these cracks are known as white etching cracks or simply WECs and their appearance in parallel with premature failures, sometimes as early as 1-20% of expected L_{10} life, has led many to directly associate the failures with WECs themselves. Given the ever increasing importance of wind in the overall energy generation throughout the world, WECs have received significant attention in the last decade form both industry and academia. However, despite a significant body of recent relevant research, there is yet no agreement on the root causes of WECs, with numerous theories having been proposed in this regard. Furthermore, literature is focused on WECs themselves while their significance to actual failures is not widely discussed or established at all. This study attempts to address some of these deficiencies.

The primary objective of this study is to establish the root causes of WEC formation, through reproduction of WECs under controlled lab conditions and consequently, discuss their significance in relation to premature bearing failures. A triple-contact disc machine is used in this research to reproduce and examine WECs in AISI 52100 bearing steel under controlled laboratory conditions. This part of the study focuses on exploring the influence of the potential root-causes of WECs, namely lubricant composition, slide-roll ratio, lambda ratio and nominal contact pressure. , TEM analysis showed that these WECs were representative of those from the field. Hence, pure oils were also used to investigate the influence of additives on WEC formation. WECs were produced with all oils employed here, fully-formulated commercial transmission oil, widely referred to as 'WEC critical oil', a commercial mono-grade diesel engine oil as well as group I mineral base oil and group IV PAO base oil. These results led to the conclusion that, despite contrary suggestions in WEC related literature, oil formulation is not a primary cause of WEC generation in bearing steels.

From direct observation of results arisen from this study under rolling contact fatigue conditions, the hypothesis that microstructural changes along the crack path were produced by crack-face rubbing was made, as no WEAs were detected without an associated crack. Hence, a new experiment was set up, consisting of a reciprocating ball on a flat disc, to ascertain whether it was possible to produce WEAs under pure rubbing conditions. Using this set-up, white etching areas were reproduced under pure reciprocating rubbing conditions over a range of strokes, loads and frequencies and under lubricated and non-lubricated conditions.

WECs were reproduced over a wide range of slide-roll-ratio and under positive and negative sliding, varying film thickness and contact pressures in line contact configuration where a strong edge effect is present at the beginning of the test, due to the specific

geometry of specimens. WECs were not reproduced under elliptical contact configuration, unless a source of stress was conveniently introduced.

The above evidence points that applied stress is the main driver of WEC formation and that it is the following specific mechanism that is responsible for WECs formation in present rolling contact fatigue tests: a high stress excursion early in life initiate fatigue cracks; subsequently the contact operates at a lower nominal stress; the early cracks therefore propagate slowly and their faces beat and rub with each other for a prolonged period of time; this rubbing generates microstructural alterations in the vicinity of the crack that exhibit themselves as white etching areas; finally, pitting occurs which can be formed by a crack that is non-white etching as well as a crack that is white etching depending on the location of the crack and its propagation rate.

This mechanism also helps to explain the occurrence, or lack of it, of WECs to ‘premature’ bearing failures: WECs are simply a symptom of a specific stress history, not a cause of eventual component failure. Failure of a component at a time earlier than predicted by current life theories cannot automatically be attributed to presence of WECs. Instead both the ‘premature failure and presence of WECs are caused by a third factor: a short lived, high stress event occurring at an early stage of operation followed by operation at a moderate nominal stress.

Declaration of originality

I, Francesco Manieri, declare that this thesis is my own original work. The use of information coming from other sources has been properly referenced.

Copyright declaration

Lists of conferences and journal papers resulting from this PhD thesis:

- World Tribology Congress (Beijing, China), September 2017 "Premature failures in 52100 bearing steel and their relationship to WECs"

- Society of Tribology and Lubrication Engineers' 72nd Annual Conference (Atlanta, USA), May 2017 "Root causes for WEC initiation and propagation in bearing steel"

- Manieri, F.; Stadler, K.; Morales-Espejel, G. E. and Kadiric, A.; 2018, "Origins of White Etching Cracks in Bearing Steels and Their Significance to Early Bearing Failures"; International Journal of Fatigue, paper submitted for review

Table of Contents

1 Introduction

In this chapter, a brief background to this study is provided to outline the motivation for the research and its primary objectives. In addition, the layout of the thesis is described.

1.1 Background

As a preliminary foreword to the present study, it is worth underlining its significance in the context of wider research on tribological aspects of rolling bearings and its importance in terms of practical aspects of bearing performance.

Higher than expected occurrence of premature rolling bearing failures in wind turbine gearbox applications is one of the main problems that the wind energy industry is currently facing. The failures necessitate costly repairs, exacerbated by remote locations of wind turbine installations which are often in harsh offshore environments, and more importantly, lead to significant downtime of the affected turbine and hence reduced energy generation. The failures are proving to be a significant hindrance in achieving the ambitious growth targets for wind energy generation [1].

Rolling bearings experience a multitude of failure modes, including smearing, pitting, micropitting and false brinelling. Many of those, such as smearing and fretting, can be prevented through adequate lubrication and design, but rolling contact fatigue failure leading to pitting or spalling, is difficult, or impossible, to design against, and therefore is generally considered the life-limiting mode of rolling bearings. In wind turbine applications, bearing failure rates appear to be higher than those predicted with basic bearing life models which are based on rolling contact fatigue as the dominant filaure mode. Consequently, these failures are termed ‘premature’. Premature failures occur in many applications, but over the last decade or so the wind turbine installations have become a prominent example of the phenomena, with in-service L_{10} bearing life of between 1 and 20% of the expected value widely reported [2].
Failed bearings from wind turbines have been shown to exhibit large crack networks decorated with microstructural alterations of bearing steel which appear white under optical microscope after etching. Such cracks have become to be known as white etching cracks (WECs). Unsurprisingly, the parallel occurrence of WECs and premature bearing failures, has led to a common assumption that it is the WECs that are directly causing the early bearing failures.

Given the ever increasing importance of wind energy to overall power generation in many areas of the world, this problem has received significant attention from researchers in both industry and academia. The next chapter of this thesis presents an extensive survey of the relevant literature but for the purposes of this introduction, it can be said that WECs from the field have been extensively analysed by many authors, using destructive and non-destructive methods, thanks to which it has been possible to accurately describe the crack morphology and the associated microstructural alterations while other works have focused on reproducing WECs under controlled conditions using either real bearings or specific tribometers. However, a glance on relevant literature clearly indicates that there is as yet no agreement on the root causes of WECs. More importantly, there appears to be very little work on attempting to establish the significance of WECs to premature bearing failures, which is surely the issue that carries more practical significance. Literature is beset by multiple theories on WEC formation that are often at odds with each other. These include:

- Hydrogen embrittlement [4], [5], [6], [7]
- Steel cleanliness (role of non-metallic inclusions) [5], [6]
- Environmental effects (corrosion [8], contaminants, electric currents)
- Composition [9] and self-charging of lubricant [10]
- Impact loading (also known as hammering wear impact fatigue, through adiabatic shear bands) [3]
- Brittle fracture [8]
- Frictional energy dissipation criteria [3–5].

Some of the proposed theories listed here are difficult to reconcile with tribological conditions prevailing in rolling element bearing contacts; for example, in the hypothesis of the impact loading, it is not clear how the very small clearance between the rolling elements and the rings can cause such a relevant hammering to obtain an initial cracking or a microstructural alteration in the steel. The brittle fracture hypothesis implies a very high value of friction within the contact, exceeding that which can be achieved even under boundary lubrication. It was also proposed that the lubricant could self-charge and cause the damage of the steel by transmitting an electric current, but there is no precise indication about the value of current that one needs to have in order to produce the failure. At least one of the initial theories on WEC generation, that of thermal stresses due to discharge current impulses flowing through bearing steel [6], has subsequently been shown to be infeasible by some of its original authors [7].

Other factors discussed in relation of WECs, such as the influence of tribo-chemistry, hydrogen embrittlement and presence of inclusions, are known to be important in the performance of tribological contacts and fatigue failures. However, it is not clear why these factors would become more important in wind turbines or other applications exhibiting WEC failures, or in case of inclusions, why the current bearing life theories are unable to predict resulting lifetimes given that they are based on subsurface crack initiation. These factors are almost certainly significant in terms of fatigue failures, but whether or not they are the primary or even a necessary, factor in WEC generation remains unclear.

Given the importance of WEC associated failures, and the apparent discrepancy in literature on root causes of WEC formation, the motivation of the present study is to provide a better understanding of mechanisms responsible for WEC generation, and subsequently, to discuss the significance of WECs in terms of premature bearing failures. The primary objectives of this study are listed next.

1.2 Objectives

In general, the present research will systematically assess potential mechanisms of WEC formation using lab experiments under closely controlled conditions and based on the generated understanding, attempt to establish the relevance of WECs to premature rolling contact fatigue failures. The primary objectives and research tasks may be described as follows:

- Generate white etching cracks in lubricated rolling contacts of bearing steels under controlled laboratory conditions that are representative of those found in real failed bearings;
- Once a procedure to successfully generate WECs is established, conduct appropriate experiments to investigate the influence of selected tribological contact conditions on formation of WEAs and WECs, namely: lubricant composition, direction and magnitude of sliding, contact pressure, lambda ratio and contact geometry and load history.
- Propose the fundamental mechanism(s) that lead to WEC formation;
- Based on the established mechanism, explore the significance of WECs to real bearing failures;
- Propose potential solutions for prevention of premature bearing failures associated with WECs, including potential improvements to rolling contact fatigue life predictions to address the apparent inability of basic fatigue life models to predict what is consequently termed 'premature' failures.

1.3 Layout of the thesis

This thesis consists of 8 chapters. After this brief introduction, Chapter 2 presents a detailed review of existing literature on WECs and premature bearing failures. The studies concerned with characterising WECs and associated microstructural changes are described, various approaches used by authors for WEC generation and studies are explored and finally the multiple theories proposed by researchers as mechanisms of WECs generation are described.

Chapter 3 illustrates the experimental design and techniques employed in the present study, based on the use of a triple-disc contact machine to reproduce WECs under controlled laboratory conditions. The way in which experimental conditions are controlled so that the influence of any one variable can be isolated and studied at a time is described including a thermal network of the triple disc rig employed to ensure consistent lubrication conditions. Characteristics of all experimental specimens, including lubricants used in the experiments, are also presented in this chapter.

Chapter 4 introduces the equipment used for the present study, including details about specimens and lubricants. Moreover, the experimental procedure of inspection of specimens prior and post-testing is presented.

Chapter 5 contains all the results of the rolling contact fatigue experiments, analyzing the effect of various tribological parameters of potential relevance to WEC formation including lubricant composition, direction and magnitude of sliding, specific film thickness, contact geometry and load history, spanning from the standard configuration of the MPR rig to the different contact geometries that have been adopted to study the phenomenon of WECs in its entirety.

Chapter 6 contains details of an additional study performed to directly observe formation of white etching areas under rubbing condition, designed to confirm whether a hypotheses proposed in Chapter 5 of crack face rubbing being responsible for WEA formation is valid. The relevant reciprocating ball-on-disc set-up is first explained, followed by results obtained under various frequencies and amplitudes of oscillation as well as different lubricants and non-lubricated contacts.

Chapter 7 discusses the findings of this study in relation to potential mechanisms of WEC formation and in view of related theories in literature. Based on the substantial evidence presented in this thesis, a new theory on mechanism of WEC formation is proposed focused on contact stress history. In addition, based on the newly proposed theory, this chapter also provides a further discussion on the significance of WECs in relation to premature bearing failures in an attempt to address the lack of similar treatments in existing literature.

Finally, Chapter 8 summarises the main findings of this study including the proposed theory of WEC formation and significance of WECs to bearing fatigue life. In addition, this chapter also proposes some potential future research that would be useful to further advance our knowledge of the subject and ability to better predict bearing failures.

2 Literature review

In this chapter a review of relevant literature on white etching cracks and premature bearing failures is presented. First of all, the description of the problem is given, describing the context in which premature failures and WECs should be treated. Subsequently, a general description of WEC/WEA characteristics and morphology is given, considering observations and findings from the field. In the second part of the review the proposed drivers for WEC formation and failures are examined. Finally, the gaps in the current understanding of WEC mechanisms and their significance to bearing failures are summarised and the motivation and aims of the present thesis are discussed in relation to this.

2.1 Introduction: definition of the problem

(Note: Parts of this Chapter are based on a related journal paper by this author [8]*)*

It is common for a rolling element bearing, being subjected to rolling contact fatigue (RCF), to fail eventually by spalling or pitting. Such a failure means that a part of the material is permanently detached from the surface of the bearing ring or rolling element. The bearing failure lifetimes due to contact fatigue are statistically distributed and in the absence of additional external factors follow Weibull statistical distribution. For this reason bearing lifetimes are not expressed as absolute values but in terms of probability for a bearing to reach a specified number of revolutions (or hours of operation at a specific speed). Commonly, the L_{10} life (DIN ISO 281) is quoted which represents the RCF life of a given bearing population, at a given operating condition, at which 10% of the bearings are expected to fail, or the lifetime within which bearing failure probability is 10%.

However, in the last two decades, a high number of early or premature failures have been reported in wind turbine applications, particularly at bearing locations within the wind turbine gearbox [2]. It is important to realise that the term *premature failures* here is simply used to describe a failure rate higher than the one predicted by conventional standard bearing life formulas i.e. the word 'premature' is in context should not be interpreted as meaning that there necessarily anything wrong with the bearing itself causing it to fail earlier than it should, but simply that the failure was not expected based on current fatigue models. In wind turbine gearbox bearing applications such premature failures have been reported to occur at 5-20% of L_{10} life.

Figure 1 below shows a set of failure lifetimes of a particular wind turbine gearbox bearing in real world operation [2,9]. Each blue dot represents a real "in-service" recorded failure. One can clearly see the large number of documented failures that happen well before the expected L_{10} life time of 24 years. As indicated in the picture the actual L_{10} is 6 month only, i.e. less than 3% of the predicted L_{10} lifetime.

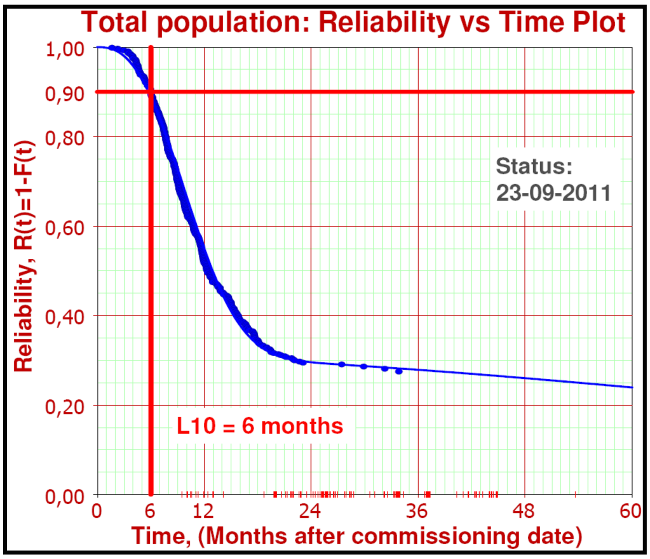

Figure 1 In-service recorded wind turbine failures [2]

It is known [10] that bearings suffering such premature failures commonly exhibit white etching cracks (WECs), a network of cracks decorated with microstructural alterations, known as white etching areas (WEAs). An example of white etching crack network in a premature failure from the field is shown in Figure 2. As a result of this simultaneous occurrence of WECs and early failures, there appears to be a tendency in the literature to interchangeably refer to premature failures or WECs, although no cause-effect relationship has been established.

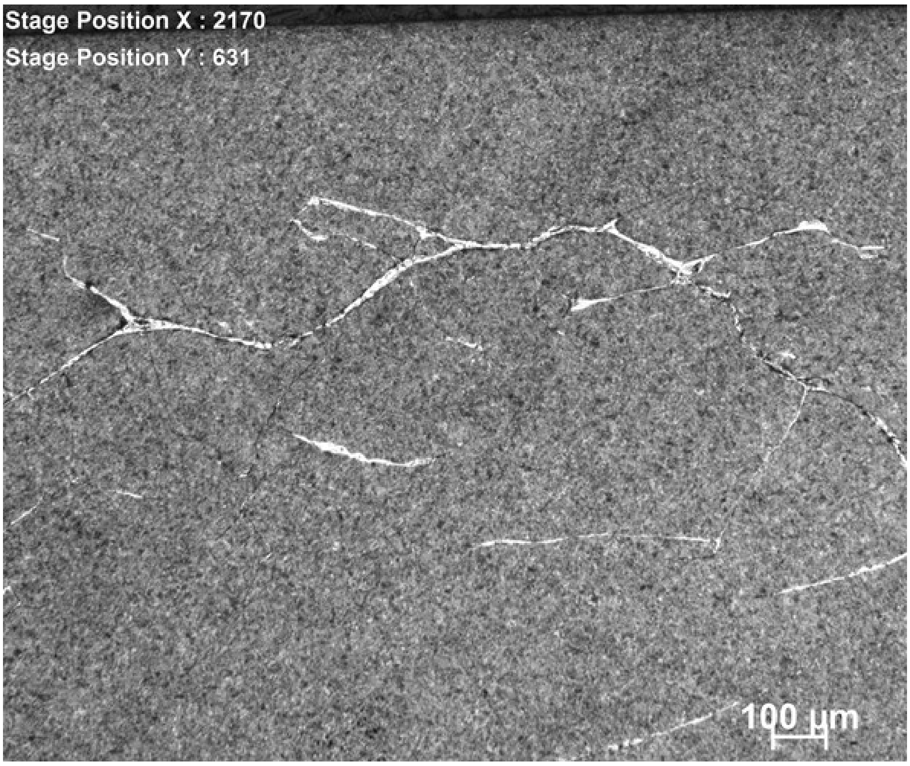

Figure 2 A typical example of a white etching crack in a cross section of an inner ring from a spherical roller bearing in AISI 52100 steel. Courtesy of SKF.

Moreover, it should be noted that WECs are not peculiar of wind turbine industry alone; in fact, they have been shown to occur in automotive gearboxes and similar applications

[11]. Furthermore, they are not exclusive to a particular type of bearing steel, with WEAs found in case-carburised steel as well as through-hardened steel [12,13]. However, it is in wind turbine applications that the problem assumes more importance, given the size of the bearings and consequently the exorbitant costs of the repair and system downtime.

2.2 The basics of rolling contact fatigue

Before going specifically to talk about premature failures and white etching cracks, it is good to know how a crack can generally form within the bearing steel matrix under a lubricated rolling contact.

Figure 3 illustrates a typical rolling bearing, composed of an outer ring and an inner ring, the rolling elements (spherical rolling elements in the illustration) and a cage or separator that holds the rolling elements at right separation. A failure could initiate on each one of those components, but rolling contact fatigue failures, pitting or spalling, are most commonly found on the bearing rings given their relatively lower hardness and the number of stress cycles they are subjected to.

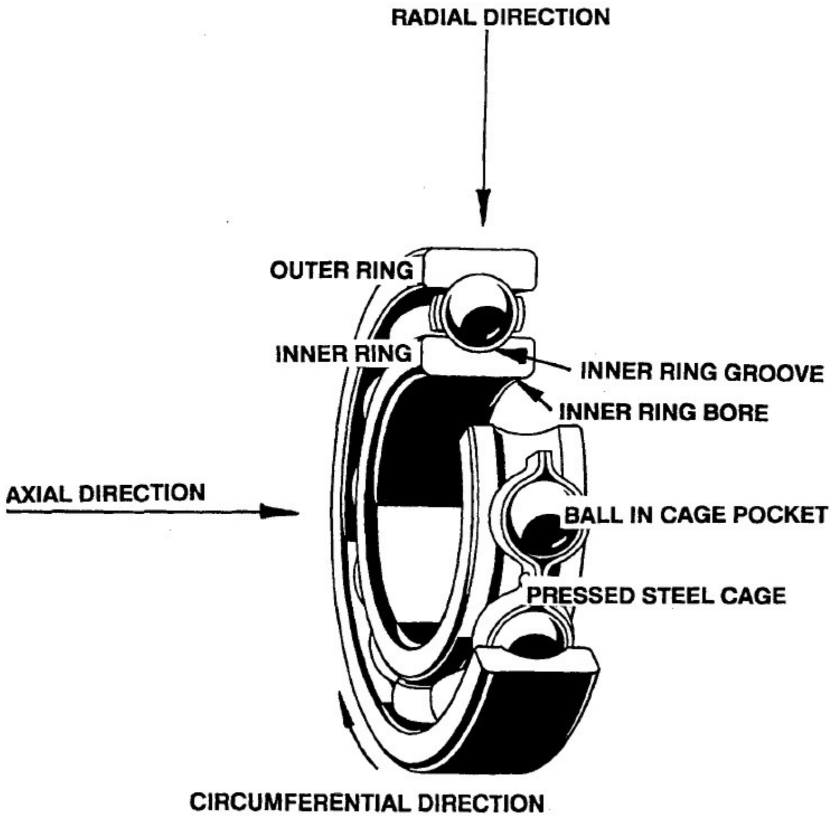

Figure 3 Sketch of a spherical roller bearing [14]

During its function, a bearing operates under rolling contact fatigue (RCF). RCF is a specific type of fatigue occurring in rolling contacts subjected to cyclic contact stresses, such as those due to passage of rolling elements over rings in rolling bearings or meshing of gear teeth. Relative to classical fatigue, RCF possesses several peculiarities, such as multi-axial, mainly compressive stress system, governed by the Hertzian theory

[15], as well as presence of lubricant and surface roughness (and hence random asperity stress history). Given a plane of the principal axes, the stress history at a point below the surface is non-proportional, since the stress components do not follow a trend proportional to each other: while the normal stresses are always compressive and follow the same trend, the orthogonal shear stress reverses direction and its maxima do not coincide with those of direct stresses as illustrated in Figure 4 below.

Another peculiarity of RCF lies in the fact that in non-conformal frictional contacts, the planes of maximum orthogonal shear stress amplitude constantly change during a stress cycle. For this reason identifying the plane of maximum fatigue damage is very complicated.
Moreover, there is a high hydrostatic stress component which is absent in classical fatigue phenomena (tension, compression or bending fatigue) [16,17]. These factors make RCF rather difficult to study, but the fundamental mechanisms of crack initiation and propagation are likely to be the same, as argued in Rycerz et al. [18].

Bearings steels need to have high elastic limit to deal with the cyclic load during the operation and avoid plastic deformation. The elastic response during cyclic loading can be affected by microstructural alterations of the steel that could arise during operation. Therefore, a localized micro-plastic deformation can take place, bringing the material to be exposed to damage and crack initiation.

The state of stress illustrated in Figure 4, represents the situation in an ideal, ‘smooth’ case. In real applications, the stress field is much more complex due to the presence of imperfections within the material, either on the surface (in the form of scratches or dents) or subsurface (in the form of non-metallic inclusions or voids). Those defects modify the Hertzian stress in their vicinity and usually expose the material to a higher intensity of stress.

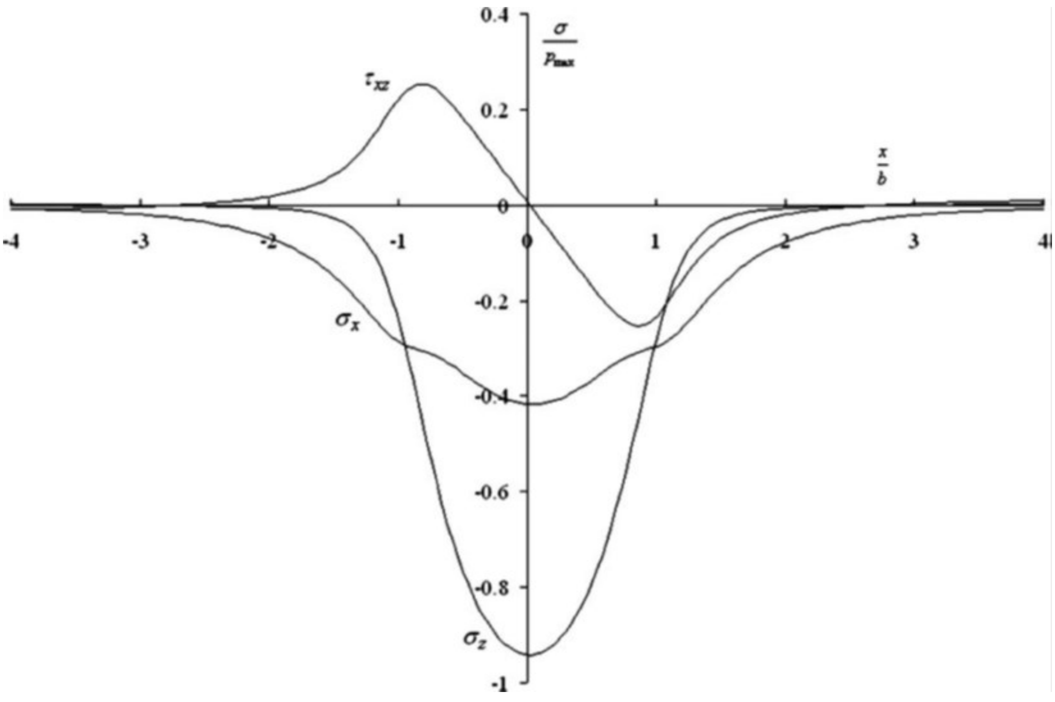

Figure 4 Stress history at a subsurface point in a Hertzian line contact [17]

Rolling contact fatigue failure is generally characterized by final flaking from the surface of one of the raceways or rolling elements. One differentiates between surface originated and subsurface originated failures, also known as 'pitting' or 'spalling'. The occurrence of one of these instead of the other depends on surface condition, steel cleanliness and lubrication conditions. The opening and propagation of the crack will then depend on surface traction, hydraulic pressure from the penetrating lubricant and sliding direction [19–26].

Surface initiated failure is more likely to occur when the initial fresh surface presents defects like dents or scratches due to the machining process employed. In this case, those imperfections act as stress raisers and hence a crack is more prone to start at the surface. The appearance on the surface is a v-shaped growth. In cross section, the cracks is seen to generally propagate at a very shallow angle (about 30 deg) into the inner material; Secondary cracks can branch back towards the surface, which acts to detach a bit of material and eventually form a pit [27]. Figure 5 illustrate the entire sequence of a surface crack started at a dent [27].
Other forms of damage initiate at the surface and are very common to occur in bearing and gear application, such as micro-pitting, considered to be a particular subset of pitting [27,28].

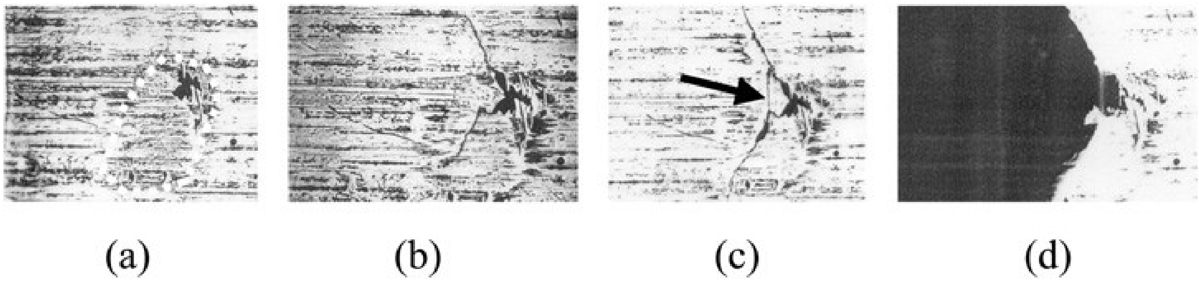

Figure 5 Sequence of propagation of a surface crack due to presence of a dent. (a) The dotted line highlights the debris dent; (b) v-shaped growth; (c) secondary crack (d) final pit [27]

Subsurface originated failure, on the other hand, takes place when a micro-crack forms beneath the surface at some inhomogeneity within the material, such as non-metallic inclusions or voids [29]. In this case, if such discontinuity is positioned within the stress field, it will cause a subsurface stress concentration. After crack initiation, it will propagate towards the raceway causing a final spall. This form of failure is more likely to happen in case of very smooth surfaces and under good lubrication conditions i.e. full film EHL regime. Figure 6 shows an example of subsurface failure due to edge loading on a tapered roller bearing. Generally, the depth of the final spall on the surface tends to be larger than pits in surface initiated failure [30].

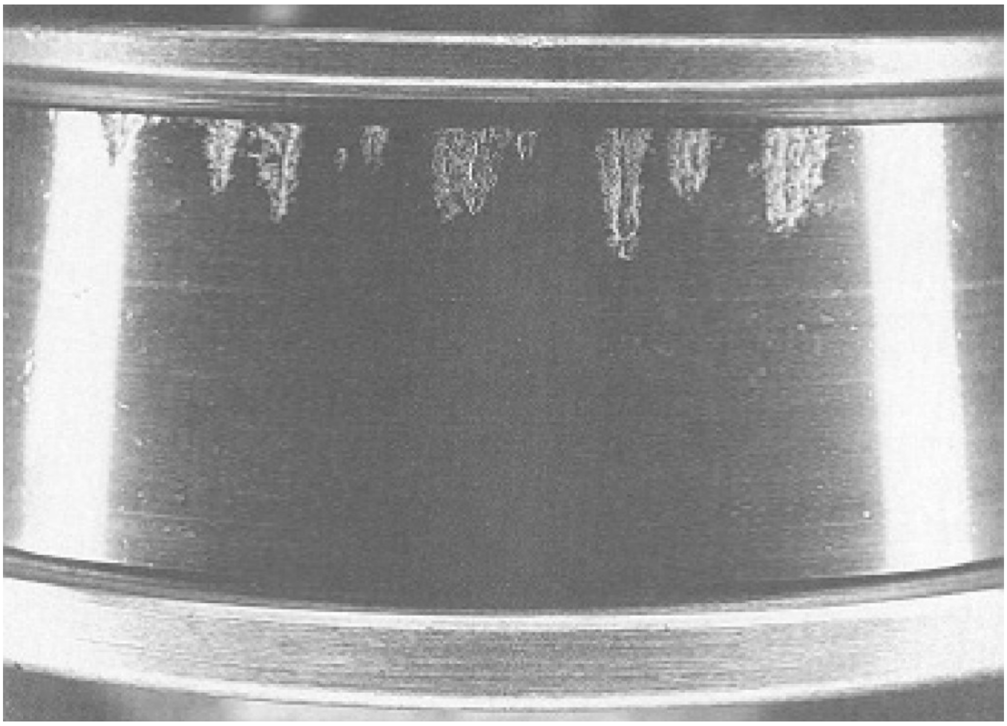

Figure 6 Subsurface initiated spalling due to edge loading in a tapered roller bearing raceway [30].

After initiated, either on the surface or subsurface, a crack tends to propagate within the bulk material with increasing number of cycles. As soon as crack initiation occurs, however, the Hertzian state of stress is drastically altered, now varying at the crack tip, where stresses have a different form and depend on the geometry of the crack but are proportional to the applied overall stress. The constant of proportionality is the so called *stress intensity factor* as commonly used in fracture mechanics [31,32] to estimate the intensity of stress at the crack tip and predict the propagation of the crack. Three different modes of crack propagation are then possible: mode I, opening of the crack; mode II, in-plane shear; mode III, out-of-plane shear [17,33,34]. It is generally believed that a RCF crack is initiated under mode I or II, due to tensile or shear stress, and then it propagates due to shear.

When a population of identical bearings is subjected to the same operating conditions, those bearings fail at different number of cycles. The problem of determining the life of a component subjected to RCF has a probabilistic nature [30]. The first mathematical model for bearing life was developed by Lundberg and Palmgren in 1947 [35] and later in 1952, who utilized earlier works of Weibull [36]. They essentially applied his earlier probability theory of fatigue to the rolling contact fatigue life. Their bearing life formula indicates the survival probability, S (%) of a bearing in terms of the Hertzian contact parameters according to the following equation:

$$ln\frac{1}{S} \approx N^e \frac{\tau_0^c}{z_0^h} a z_0 l$$

N is the number of load cycles, l is the length of the contact, τ_0 is the maximum shear stress at the depth z_0, a is the contact semi-width in the transverse direction of rolling, e is the Weibull exponent and c and h are other experimental exponents. By expressing the Hertzian contact parameters τ_0, z_0 and a in terms of applied load and contact geometry, the compact formula derived from their study for the L_{10} life or rolling bearings can be expressed as follows:

$$L_{10} = \left(\frac{C}{P}\right)^{p},$$

where C is the bearing basic dynamic load rating, which is provided by the manufacturer and represents the load of constant direction and magnitude at which a sufficiently large population of bearings can endure the basic rating L_{10} life of 1 million cycles; P is the equivalent load during operation. The exponent p is 3 for ball bearings and 10/3 for roller bearings. In the following years, this formula was adopted by ISO with the addition of multiplicative constants to account for material properties, contamination and lubrication conditions. In 1985 the concept of fatigue limit was introduced by Ioannides and Harris [37] who extended the Lundberg-Palmgren approach with the idea that the probability of fatigue initiation depends on the magnitude of the alternating shear stress above a threshold value; therefore, if the bearing is not loaded beyond this limit, its theoretical fatigue lifetime is infinite and its general performances would be limited only by external factors, such as contamination or lubrication issues. Ioannides-Harris model also adopts a numerical approach for the determination of the stressed volume and the stress cycle magnitude; this allows taking into account the influence of residual stress and asperity contact stress. These bearing life models are based on sub-surface crack initiation as the dominant mode of failure, although they are widely and successfully applied to surface initiated failures, and assume that crack propagation period is negligible. These assumptions may not necessarily hold in all cases but since models are empirical in their basic forms and utilize constants obtained from a vast number of real bearing failures, they produce valid results for most cases.

Standard ISO bearing life formulas do not seem to be able to predict the failures rates experienced in some applications, such as those in wind turbines, which are subject of this study. Due to this, many works in literature [4,5,38–40] have tended to conclude that these ‘premature’ failures are not caused by RCF. However, one needs to consider that in cases of variable stress history, the standard formulas are based on the well-known Miner linear damage accumulation rule [41], previously and independently proposed also by Palmgren in 1924. This method estimates the fatigue damage potential of random sequence of cyclic loading applied for different amount of cycles to be the same as the equivalent load worked out using the linear damage accumulation rule. Hence, it does not in any way account for the actual order in which load levels are applied and hence the non-linear effect of transient events which are very likely to occur during operation of many mechanical systems, not least wind turbines.

2.3 Wind turbine gearbox bearings and their operating conditions

Figure 7 shows a typical layout of a wind turbine. Every intervention of maintenance, repair or replacement in case of wind turbine applications is very complex, mainly due to the size of its single components; an onshore failure takes around 250 hours to repair, this time being even more in case of an off-shore turbine [42,43].

A review on WECs by Evans [44] reports that more than two-thirds of wind turbine gearbox failures initiate in the bearings with most of them associated with WEC appearance [45].

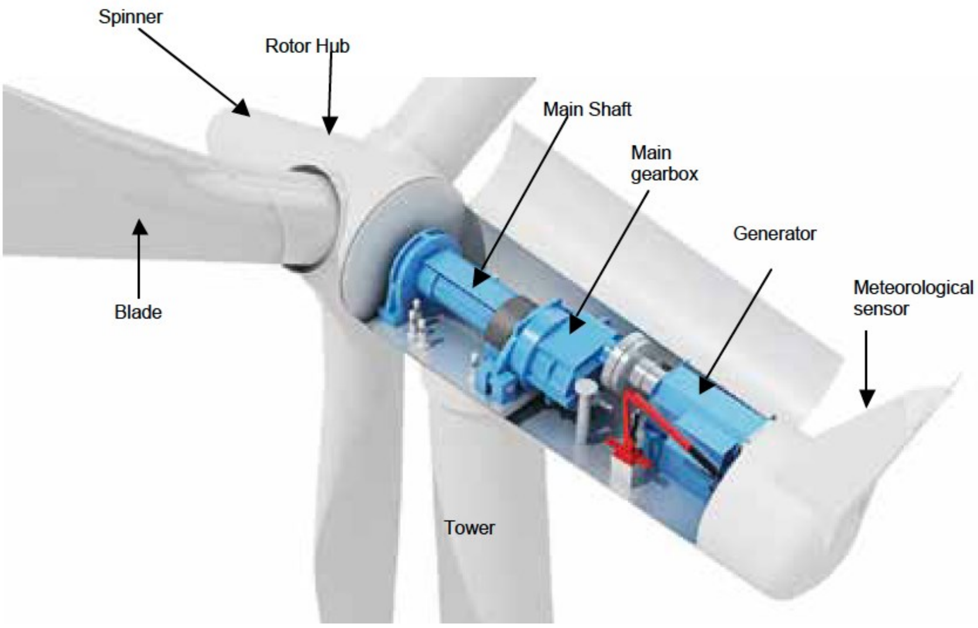

Figure 7 Layout of a wind turbine [46]

Wind turbine gearboxes (see Figure 8) generally have about 15 bearings distributed between the low-speed stage, in which the gearbox is connected to the rotor input rotating at approximately 25 rpm, intermediate stage, and the high-speed stage where the output for AC generation is located, rotating at much higher speeds in the range 1500 to 3000 rpm depending on the grid frequency and electronics [44].

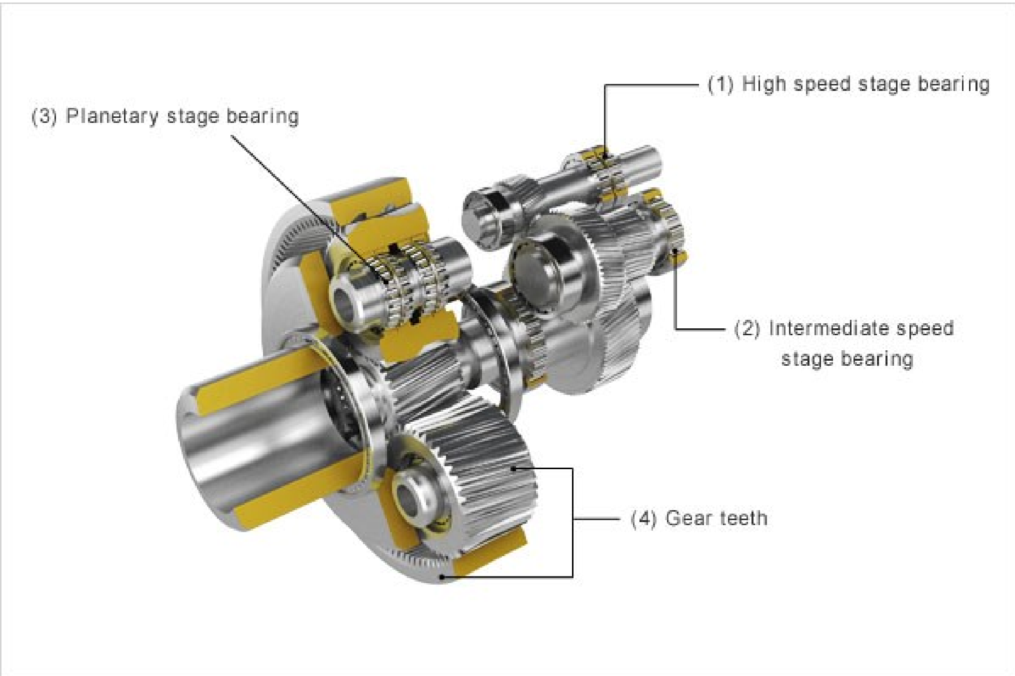

Figure 8 Scheme of a typical wind turbine gearbox; courtesy of [47]

Other than the RCF related issues mentioned in the related section, there are several other reasons that could co-operate to drastically reduce the performance of a bearing and damage on raceway (see Figure 9); these being related mainly to poor lubrication, environmental action, cleanliness and residual stresses of the steel.

Figure 9 Surface damage on an inner ring of a wind turbine tapered roller bearing [48]

The bearing steels commonly used for wind turbine gearbox bearings are the standard through-hardened AISI 52100 bearing steel, and less frequently case-hardened steel. Through-hardened steel can present a martensitic or bainitic microstructure. Microstructure of this kind of steel is very complex and includes the presence of retained austenite, primary cementite, tempered carbides, and martensite or bainite needle structure [49,50]. Carbides and non-metallic inclusions are commonly the locations for crack initiation; in this sense, it is important to improve cleanliness of the steel.

Martensitic and bainitic through-hardened steels and case-hardened steels have different residual stresses after manufacturing. Although the presence of a residual stress is important to determine the overall state of stress of the component, it is reported [14,49,51,52] that WECs are observed both in martensitic and bainitic steels, independent on the nature of the initial residual stress.

Lubrication of wind turbine gearboxes is very important to allow the components to work in adequate film regimes despite the harsh environments and varying conditions in different parts of the gearbox. The same lubricating oil lubricates both gears and bearing from the low-speed to the high speed stages. Due to severe conditions in which bearings and gears operate, it is frequent to meet poor lubrication conditions, this causing damage on the surface such as wear, fretting corrosion, scuffing.

In addition, during the operation, these bearings can be subjected to transient and unexpected events, including wind gusts, abrupt disconnections from the grid, misalignment and vibrations [42,43]. Of course, all those factors can contribute to reduction in life and, since they are mostly unexpected events, it is not easy to account for them.

2.4 **WEC/WEA observations from the field**

Despite the proliferation of WEC related research papers in the past decade or so, WECs are not a recent phenomenon. There are publications as far back as 1960s that testify observations of cracks associated with steel microstructure alterations that manifest themselves as white etching areas. Wren and Moyer [25], in 1964, reported presence of white alterations related to oxide inclusions in a tapered roller bearing; Figure 10 shows what nowadays one would call a "butterfly" (see next section). Scott et al. [53] in 1966 noticed a fine carbide precipitate and dissolution that caused the hardness of these alterations to be higher than the initial microstructure. He attributed the microstructure refinement to yielding or plastic flow. It is important to notice that, although the WEC problem is evidently mentioned as a peculiarity of the wind turbine bearings, Scott's paper and observations were not related to wind applications but just to 52100 bearing steel.

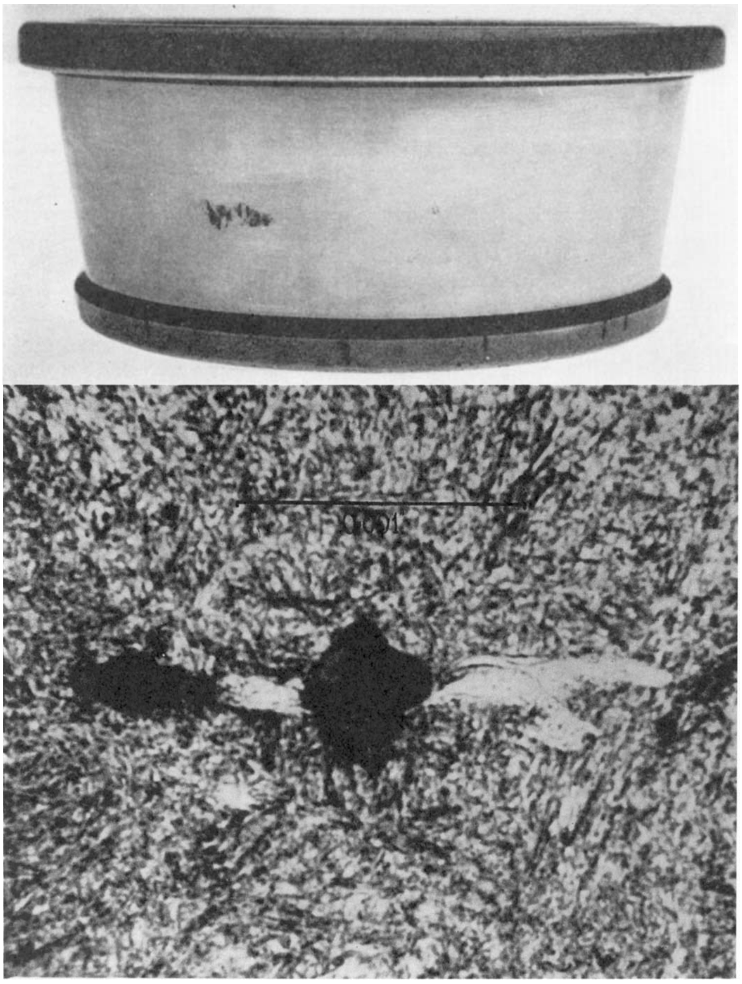

Figure 10 Oxide inclusion associated with initial cracking and alterations in the microstructure [25]

After Scott's paper, the use of more sophisticated techniques such as transmission electron microscope with focused ion beam analysis, EBSD, X-ray diffraction gave a great contribution in the comprehension of the morphology of WECs but the finding of a root cause for their formation and the solution of the problem still seem to be far as WECs develop in several different cases and under different conditions.

One of the reasons why the formation mechanisms of WECs are not still understood lies on the fact that their morphology is variable and gives space to different interpretations. With the term white structure flaking one tends to indicate the final spall resulting from WEA/WEC formation (see Figure 11). Whether WECs are surface initiated or subsurface initiated is one of the points that need to be still clarified. In fact, WECs networks related to the surface (Figure 12) are observed, as well as the entirely subsurface WECs in Figure 13 which are in contrast with the previous ones.

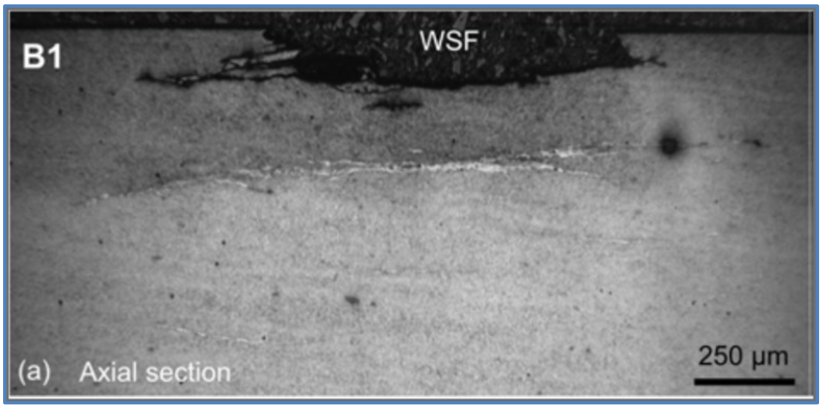

Figure 11 WSF of a bearing from the field [54]

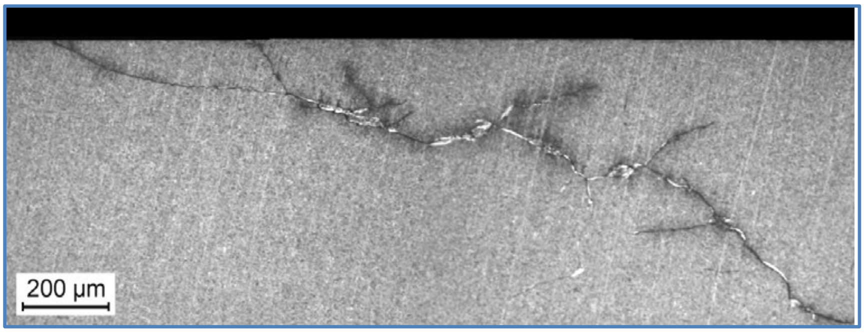

Figure 12 WEC related to the surface [55]

Figure 13 Subsurface WECs in a failed bearing from a high-speed shaft of a wind turbine gearbox [55]

In the literature there are several investigations of failed bearings that researchers have provided [10,13,56]). This direct analysis from the field is particularly recent; there are in fact no publications on WEC of failed bearings from wind turbine gearboxes before 2010. Thanks to those observations, it is possible to define few peculiar characteristics about the morphology of these cracks and characteristics of their associated white areas.

In their analysis, Greco et al. [10] sectioned and observed four different types of bearing from the field that differed from each other with regards to the steel (through hardened steel and case carburized steel) and to the type of rollers (cylindrical and tapered roller bearings). They found axial cracks in all the bearings, like the ones showed in Figure 14, apart from the only one that was case-carburized; this particular bearing, located on the main shaft and hence outside the gearbox, did not show surface cracking or spalling but only subsurface WECs. Every bearing showed microstructural alterations of different lengths within 1 mm below the surface. All four bearings showed WECs and fractographic analysis revealed the connection between axial cracks and white etching areas that were located at the crack edges (indicated by the arrows in Figure 15). In the conclusions they mentioned unsteady operational conditions as a possible cause for the high plastic deformations which lead to microstructural changes and WECs formation.

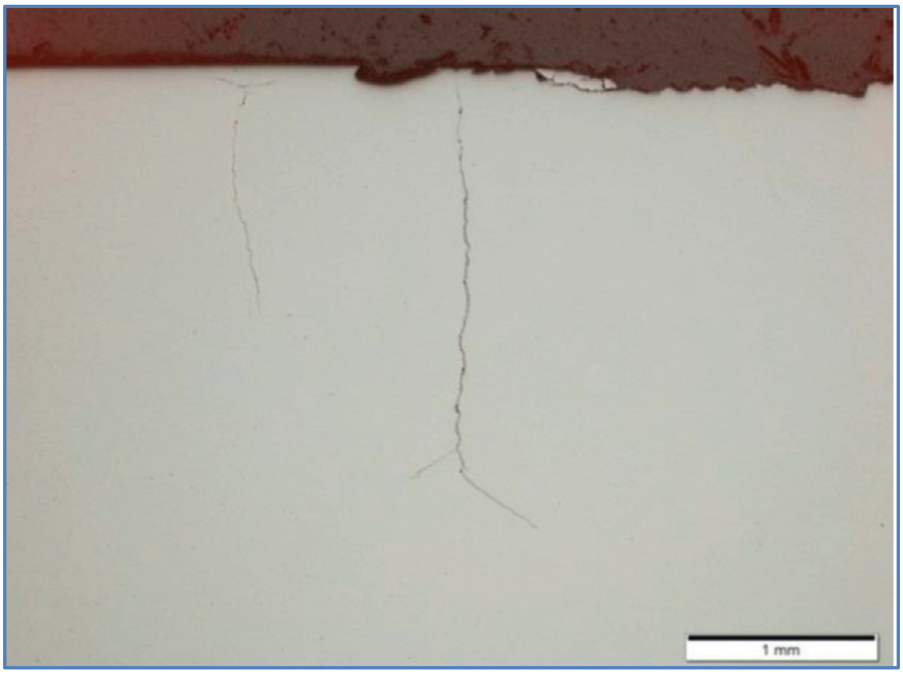

Figure 14 Axial cracks in a high-speed through hardened TRB [10]

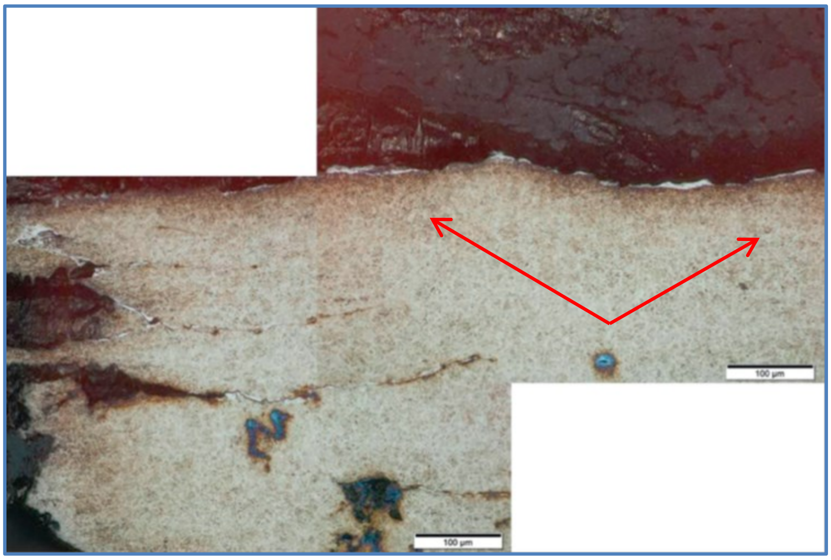

Figure 15 Optical fractograph of a high-speed through hardened CRB that shows WEAs at crack edges. [10]

Errichello et al.[13] analysed both through hardened steel bearing and case-carburised steel bearings from the field, recognising substantial difference in their failures. They stated that through hardened bearings failed by axial cracks which were showing irregular WEAs, whereas carburised bearings failed due to macro-pitting. They suggested that the presence of WEAs along the crack network in carburised steel was dependent on the content of retained austenite: if this content is at least 20%, carburised bearing might be immune to WEAs occurrence, they concluded.

Gould et al. [56] recently published another analysis of a failed bearing from the field using a non-destructive technique based on X-ray tomography. The study highlights the fact that the four different cracks observed were completely subsurface with no connection to the raceway. The propagation seems to follow the axial direction, as in other examples of observed failures. According to the authors, the existence of a source of tensile stress in the circumferential direction could be the reason of this axial propagation, rather than adiabatic shear bands via impact loading as claimed in [6,57,58]. Regarding the interactions with inclusions, from their observations the authors concluded that WECs could be generated either in connection or independently on subsurface inclusions, although further evidence is needed to ascertain whether the inclusion could represent the initiation of the whole WEC network (Figure 16). Regarding the properties of microstructural changes associated with WECs, Gould et al. sustain they could be the evolution of a dark etching alteration that happens prior to WEA, as they noticed the microstructure in the vicinity of the cracks was showing some dark appearance after etching (Figure 17 shows regions of DEAs in the vicinity of the cracks. In the paper it is also commented that three point branching morphology cracks, as the crack indicated in the figure, are typical of cracks that follow retained austenite grain boundaries).

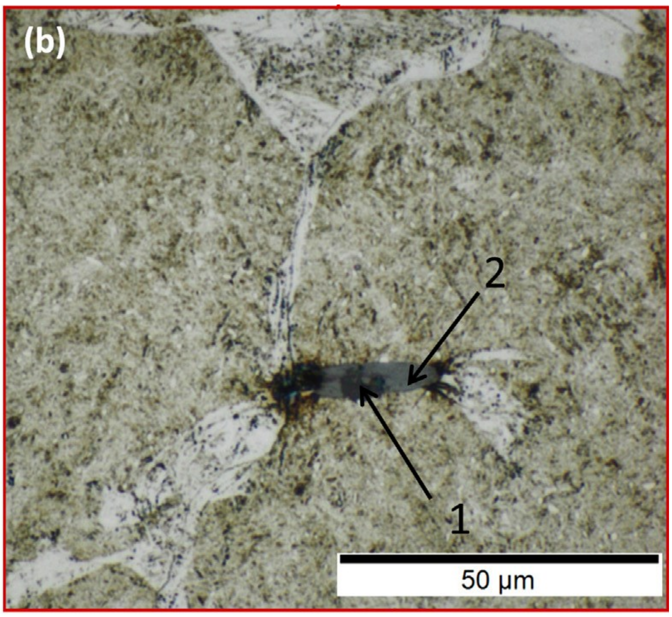

Figure 16 Non-metallic inclusion associated with WEC in a failed WT bearing [56]

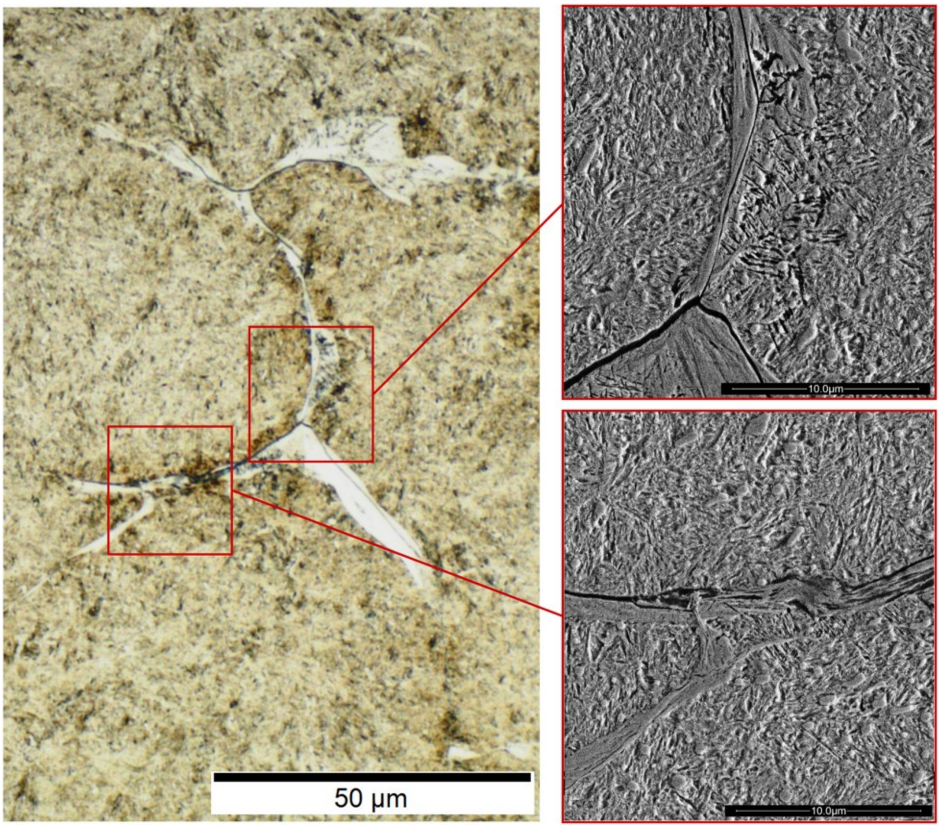

Figure 17 WEC and DEA in a failed WT bearing from the field [56]

After analysis of those WEAs decorating WECs, it has been noticed that the white etching areas are composed of a refined nano-ferritic structure [40,59–61], carbon supersaturated, characterized by the dissolution of the initial primary or tempered carbides. Nano-hardness measurements have also been carried out from which it has been found that WEAs are generally 30-50% harder than the surrounding matrix [38,61–63]. Other types of white etching alterations exist in bearing steels which differ from the ones observed in white etching cracks and these are presented in section 2.5.

2.4.1 Surface and subsurface WEC initiated failures

WEC appearance and morphology depend on several conditions and factors, such as the type of steel, bearing location and kinematics, and tribological parameters. Through-hardened steels, for example, have been reported to tend to exhibit preferentially axial cracks directly connected to the surface, whereas case-carburized steels seem more likely to be affected by subsurface cracks [10]. The morphology of a given WEC also depends on sectioning direction: in the circumferential section WECs tending to be branched and radially propagating towards the bulk; in the axial direction, on the other hand, WECs appear more parallel to the surface with less branching [10,13,44].

Fractography of WECs has also been carried out as an attempt to identify the location of their origin and propagation characteristics [38,64,65]. However, it is still debated whether WECs originate surface or subsurface. Using a non-destructive method [56] it was confirmed there is no relation between the crack and the contact surface, attributing the origin of the crack mainly to defects and inclusions dispersed in the bulk matrix and within the Hertzian stress zone. Butterflies may be considered as an example of subsurface originated WEC, in which cracks originate at inclusions, often MnS or Al_2O_3 non-metallic inclusions. Their characteristic wing-shaped pattern gives rise to the name “butterfly” (Figure 18). Evidence of interaction between butterflies and WEC networks has been reported [66], which led some researchers to postulate that butterflies are precursors for WECs [54], although this contradicts other cases in which no such connection was found [13].

In contrast, it has also been observed that WECs could be directly connected to the surface [55]. Some authors have suggested that WECs are similar to cleavage-like axial cracks and used this as a proof for surface initiation of WECs due to high frictional tensile stresses [38]. They argue that WECs present a semi-circular shape, similar to fish-eyes produced in bending fatigue, with presence of adiabatic shear bands. In the circumferential direction, they exhibit a stair-like pattern which extends in radial direction. It is proposed that cleavage-like axial cracks are driven by frictional tensile stress; shear stress on the other hand would drive those surface cracks which form a shallow angle with the contact surface [2,38].

However, it is author’s opinion that the observation of WECs connected to the surface does not necessarily mean that the initiation of the crack started at the surface; in fact, connection to the surface could just be posterior to a subsurface initiation. Furthermore, a brittle cleavage like failure is extremely unlikely in a rolling contact where stresses are mainly compressive. This is analysed later in the thesis, but in general for stress intensity to exceed fracture toughness of typical bearing steels, would require friction coefficients of 0.3 and higher which is practically impossible to achieve in a lubricated contact even under boundary lubrication.

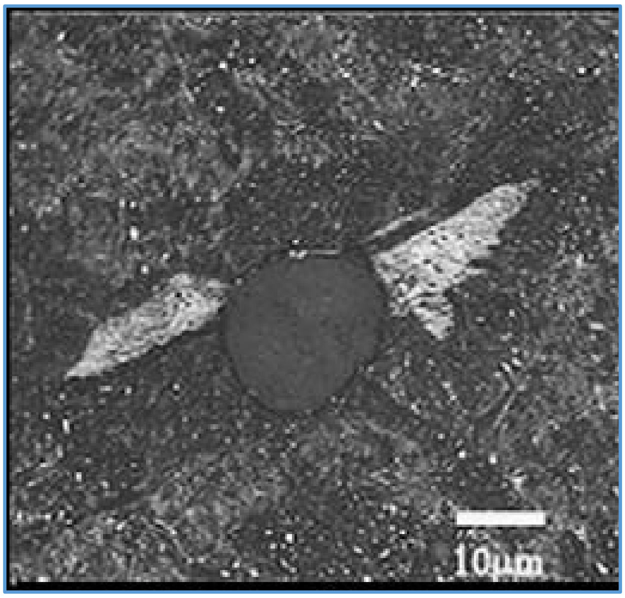

Figure 18 Butterfly formed around a Al_2O_3 inclusion [61]

2.5 White etching areas

The term white etching area refers to the altered steel microstructure decorating white etching cracks which appear white under an optical microscope after etching with Nital (a solution of 2% volume of nitric acid in methyl alcohol). Examples of WEAs are illustrated in Figure 19.

Figure 19 White etching areas around cracks in a rotor bearing from the field [13]

According to the initial microstructure, operating conditions can change the matrix of the steel due to different reasons. There are few other well-known examples in literature of alterations of the steel, with characteristics and conditions under which they occur that are different from WEAs in wind applications. These include white etching bands and dark etching regions in high cycle fatigue [63,67], white etching layers in railway applications [68]. In the following, a brief description of those alterations is given, in order to distinguish them from WEAs in premature failures.

It is possible to have formation of white etching bands in bearing steels under rolling contact conditions due to high cycle fatigue. The fatigue experienced by the bearing consists of a local cyclic plasticity. This is the cause for the formation of the dark etching regions and white etching bands (DERs and WEBs) widely studied by Lund in 1969 [69] and Swahn et al. [67]. Lund described the formation of these white bands as being mainly due to plastic deformation and he was the first one to show the presence of their characteristic orientations at 30 and 80 degrees (see Figure 20). He noticed that the 80° bands contained no carbon, whereas a very low content of carbon was found in the 30° bands. Swan et al. [67], using a standard SKF R2 endurance testing machine, were able to reproduce those bands. They proposed that DERs are formed prior to WEBs and represent the martensite decay at maximum shear stress direction. They also described the white bands as composed by lenticular carbides scattered in a ferrite matrix in thermal equilibrium. For this reason, as these bands are either characterised by a smaller content of carbon or could even be carbon-depleted, they show a lower value of hardness with respect to the bulk material. They also noticed no significant increase in temperature during the tests, meaning that the thermal effect could not be responsible for the alteration in the microstructure. The lower hardness of such WEB in high cycle fatigue is in contrast to the WEA observed around cracks in premature failures, which are generally harder than the surrounding matrix, suggesting that the two are indicative of different phenomena.

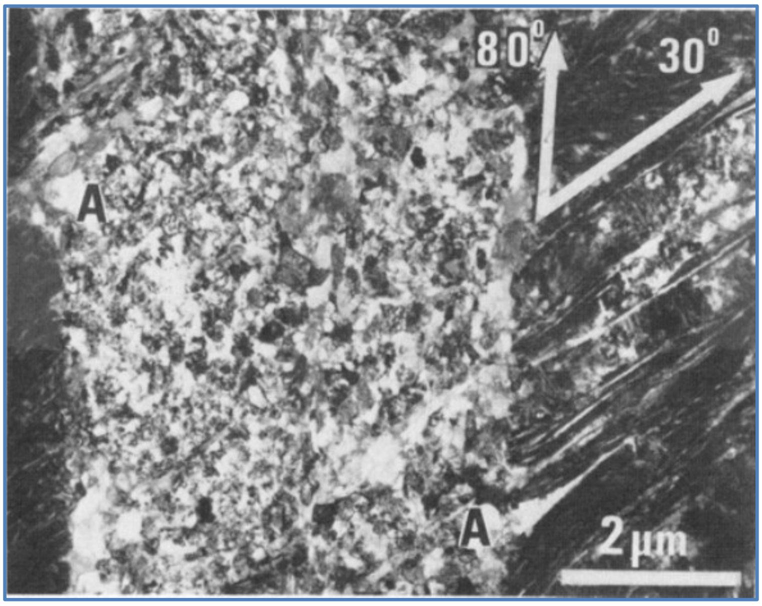

Figure 20 Formation of 80° and 30° WEBs in bearing steel [67]

In railway applications, similar alterations which are called white etching layers (WELs) are commonly observed. Zhang et al. [70] noticed that the microstructure of WELs consisted of carbon dissolved in ferrite within the deformed pearlite and the hardness of the new layers was found to be higher than the one of the original matrix. Carroll and Beynon [68] showed few examples of white layers (see Figure 21) due to the contact between two discs slide-rolling against each other. They proposed a hypothesis for crack initiation and propagation mechanism within the WEL that was created by sliding. In their particular application of a disc sliding and rolling against another, the WEL formed first due to sliding and eventually a crack is caused at the surface due to the combination of tensile and shear stresses. The crack then propagates rapidly within the layer and is deflected at the interface with the pearlite phase.

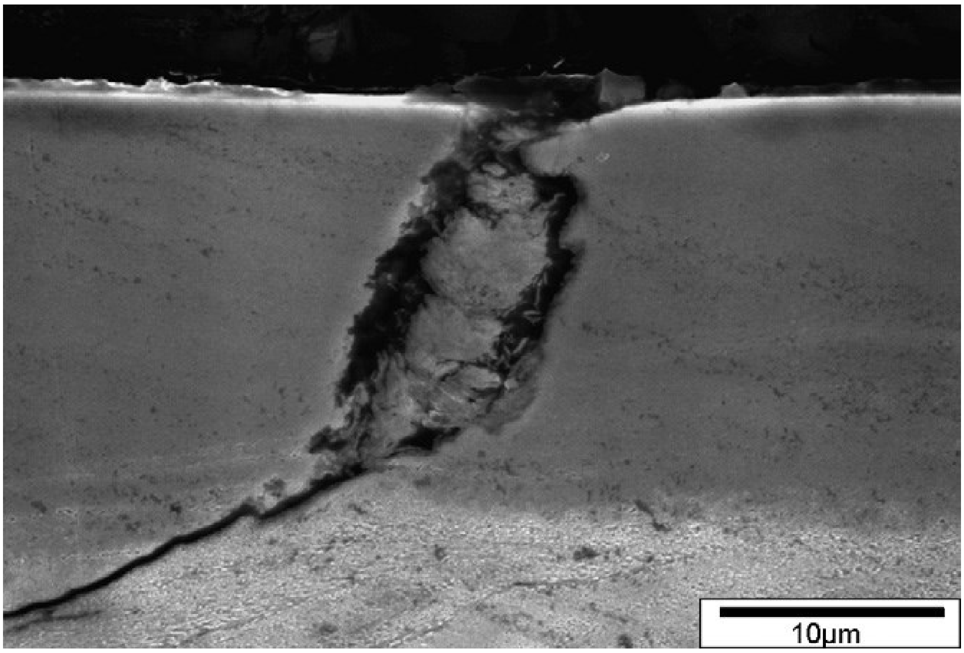

Figure 21 White etching layer in a railway application [68]

2.5.1 WEAs associated with WECs

WEAs in premature failures have been widely analysed. TEM analysis and X-ray diffraction patterns show that WEAs are a BCC nano-crystalline ferrite structure with grain size varying from 10 to 300 nm [60,71]. Due to carbide dissolution and martensite degradation, WEAs are claimed to be supersaturated with carbon in solid solution, with a high dislocation density [61,72]. Whether the microstructural change is progressive or instantaneous and whether WEA or WEC occur first is debated.

Sometimes the separation between WEAs and the surrounding matrix is very sharp; in other cases, it is possible to recognize elongated carbides at the boundary between WEAs and unchanged microstructure, suggesting that carbide dissolution is a result of a progressive action of plastic deformation and dislocation movement [61,71].

If the initiation of a crack occurs prior to WEA formation, it could be possible that shear stresses imposed on these pre-existing cracks may be responsible to form WEAs [73–77] via large plastic strains. Others have argued that dynamic recrystallization is difficult to take place in bearing steels under RCF, the time in the stress cycle being insufficient to initiate dynamic recrystallization; low temperature recrystallization process may instead occur [61]. On the other hand, if WEAs are prior to WECs, being harder than the surrounding matrix, they could cause subsequently brittle cracking during rolling contact fatigue generated stresses as a result of relaxing the stress, as the material cannot plastically yield like the original matrix [78].

In a relatively early paper, and prior to the more recent research efforts on WEC formation, Harada et al. [26] in 2005 published their observations on the formation of WEAs under rolling contact fatigue. They used a fatigue test rig with a disk-on-roller configuration. The tests were performed using traction oil and stopped at different number of cycles (4.2 GPa, 14% SRR, 100°C). Specimens flaked after 10^7 contact cycles and showed different microstructural transformations during the progress of the test. Figure 22 shows cross-sections of three different specimens that underwent different amount of cycles. Harada observed that WEAs were formed starting from an initial dark etching region; this is visible in Figure 22 (B), within the dotted semi-circle. Moreover, WEAs showed a preferred orientation of 30° and 160° to the rolling direction. This typology of formation seems to be more similar to white etching bands that one can find in high-cycle fatigue, rather than WEAs in premature bearing failures. TEM analysis showed that, although the microstructure was comprised of a very fine ferritic structure, which is what happens in WEAs in wind applications too, carbides were deformed but not dissolved after the formation of those white etching alterations.
Gould et al. [66] also suggest that dark etching areas can be observed prior to WEA formation.

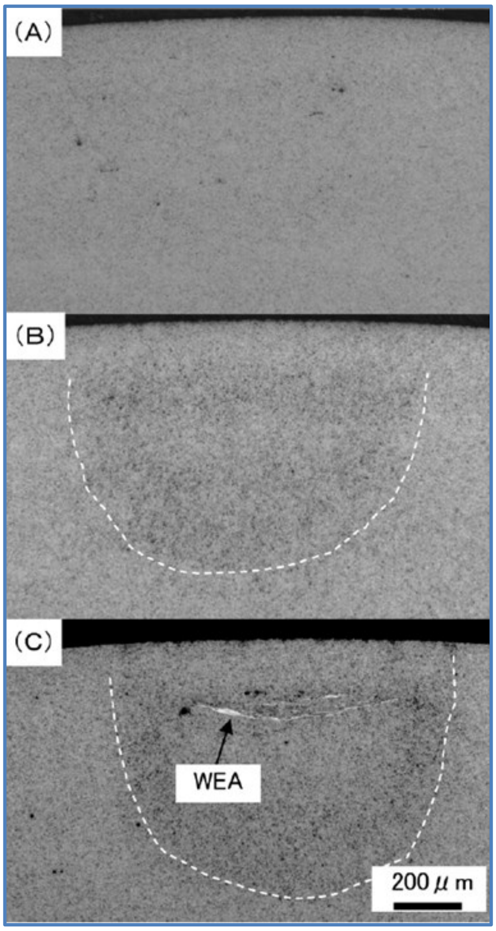

Figure 22 Alterations in microstructure at different number of cycles [59]

2.6 Crack-face rubbing

(Note: Parts of this Chapter are based on a related journal paper by this author [8]*)*

An important issue that is still subject of a considerable debate in WEC related literature is whether the white etching areas form first through microstructural changes in bearing steel, which then leads to cracking, as proposed, for example, by Diederich et al.[79], Holweger et al. [6], or whether the cracks form first followed by the white etching areas around the crack as suggested by various authors [56,65,75,80]. This distinction is important in terms of distinguishing the cause and effect relationships leading to early bearing failures: the first theory suggests that WEA themselves are the direct cause of bearing premature failures whereas the latter essentially proposes that the appearance of white etching areas is not of primary significance to premature failures.

An interesting hypothesis, known as crack-face rubbing, seems to be satisfactory in explaining the cause-effect relation between WECs and WEAs and it is presented here as follows. When a crack is formed within the steel microstructure, a discontinuity is created within the matrix. As it propagates, this crack can be seen as a 3d feature with crack faces coming into contact with each-other. It has been suggested that due to this crack face rubbing during repetitive contact cycles, WEAs form around the cracks.

At this regard, an interesting study from Solano-Alvarez and Bhadeshia [75], has showed formation of WEAs around pre-existing cracks that were introduced into the steel matrix through special heat treatment. After the RCF test, results showed formation of WEAs in the proximity of the cracks (see Figure 23), demonstrating that cracks formed first and WEA second i.e. white etching areas are a consequence of the crack not the cause of it. The hardness of those WEAs turned to be only 9% higher than the surroundings; authors suggest that this result should be interpreted as an underestimate due to their particular small dimensions compared to the large indents as visible from the figure. EBSD study showed that orientation of grains on both sides of cracks was different, suggesting that crack propagated along grain boundaries. Since WEAs originated around pre-existing cracks, their main conclusion was that WEAs were formed because of rubbing of crack faces against each other. Moreover, they pointed out that the narrower the crack, the wider is the area where the relevant microstructural changes take place due to more intense rubbing.

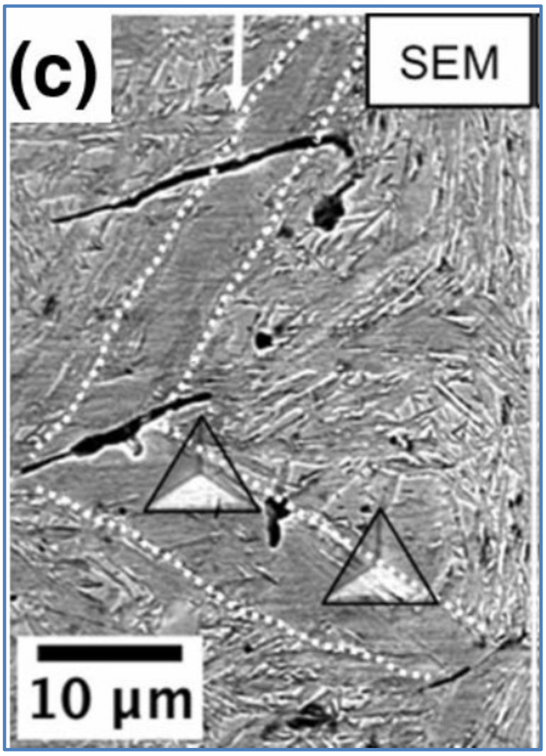

Figure 23 WEAs formation starting from initial cracks [75]

Indeed, completely unrelated to the relatively recent efforts on understanding WEA and WEC formation, previous fretting related research showed evidence for generation of WEA under reciprocating rubbing conditions of steel [81,82]. Hence, this mechanism of WEA formation due to crack face rubbing seems very plausible although direct evidence with bearing steels and representative lubricants is needed for confirmation. This is one of the aspects that will be explored in this present study.

It should also be added that the mechanism of crack-face rubbing is sometimes additionally linked to the theory of increased level of hydrogen in the steel as it is claimed that crack-face rubbing can promote formation of nascent steel surface and, hence, hydrogen absorption [44].

2.7 Reproduction of WECs under lab conditions

(Note: Parts of this Chapter are based on a related journal paper by this author [8]*)*

Several researchers recently attempted to reproduce WECs under controlled laboratory conditions using a full-bearing test rig [3,6,54,83,84]. Except for Ruellan et al. [3], they all used an FE8 FAG standard rig, which employs cylindrical roller thrust bearings, with a contact pressure between 1.2 GPa (in Evans et al. [54]) and 1.8-1.9 GPa (in Holweger et al. [6], Franke et al. [83] and Bader et al. [84]). Owing to the use of cylindrical rollers on flat washers, this bearing configuration produces very high slide roll ratios in the range of +12.5% to -12.5% on either side of bearing pitch diameter (i.e. the roller is slower that the contacting washer on one side and faster on the other). In all cases, the oil used was what is often referred to as ‘low reference oil’ as it has been suggested that it promotes formation of WECs. This oil is a fully formulated 75W80 transmission oil. The lubrication condition was very severe in Evans et al. with a lambda ratio of 0.1 and less severe, even though always mixed, in the other three cases with a lambda ratio of 1.1. Ruellan et al. used a NTN-SNR Machine standard rig for testing angular contact ball bearings with a thrust load of 6.5 kN and a radial load of 9.5 kN corresponding to a contact pressure of 3.4 GPa in an elliptical contact condition; the nominal lambda ratio was 4.2 although the authors state in the paper that at the edges of the contact this value could be markedly lower. In every case the steel tested was 100Cr6 (AISI 52100) through hardened steel. The elements affected by WECs were the washers in Holweger, Bader and Franke, the rolling elements in Evans et al. and the inner rings in Ruellan et al. In all of the five examples the edges of the contact showed the presence of WECs, but the conclusions that the authors deduced were different from each other.

In Evans et al. only five specimens out of thirteen showed surface initiated cracks, therefore they concluded that WECs should be a subsurface initiated phenomenon (see Figure 24) and inclusions would play a big role in their formation. They also noticed that cracking occurred in the region of maximum stress area, hence they supposed contact stresses to be relevant as well.

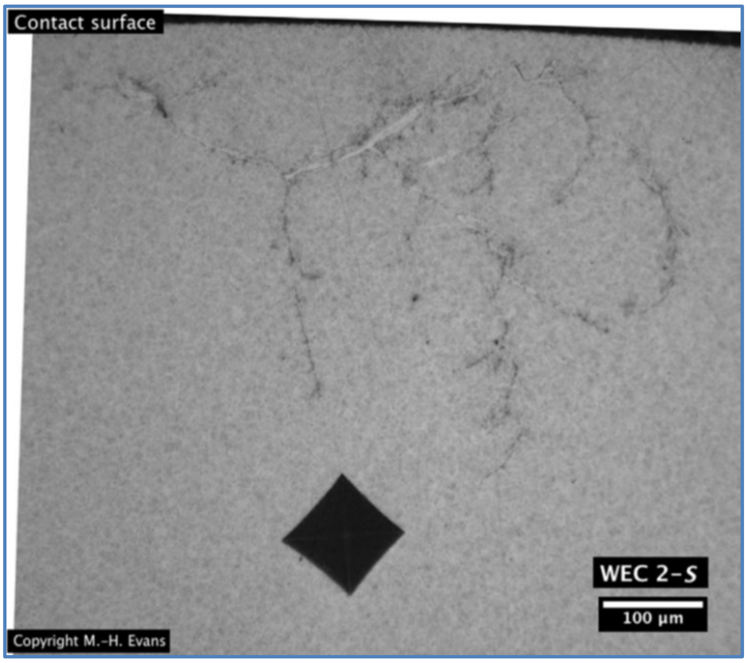

Figure 24 Sub-surface initiated WECs in lab conditions [54]

Franke et al. [83] focused on the role of lubricant and additives. They noticed WECs only with particular types of oil, the low reference fully formulated transmission oil and an oil they called “fail oil”. They noticed that by removing the Ca-Sulfonate additive from the oil, WECs did not occur, which led them to suggest that additives are the most important cause of WEC related failures.

Specimens from Ruellan et al. [3] showed cracks connected to the surface and in correspondence of the contact edges where the slippage is maximum. The relation between cracks and surface was evident also from fractograph analysis results shown in Figure 25. Therefore they claimed, unlike Evans et al. [54], that the contact stresses do not play a role in formation of WECs since in their elliptical contacts stress should have been lower near the contact edges. Another conclusion of the authors was that wear and high friction, promoting the generation of fresh surface, could enhance the permeation of hydrogen within the material and embrittle the steel, causing premature cracks.

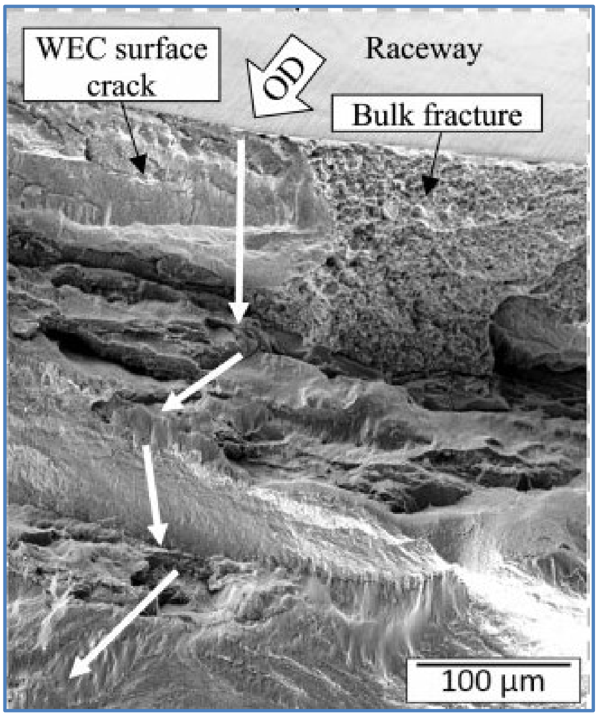

Figure 25 Fractograph analysis of a surface initiate crack [3]

Gutierrez et al. [85] more recently proposed that WEC formation can be influenced by lubrication conditions, specifically regarding the film thickness. By using a two-disc contact rig, they obtained WECs in mixed lubrication, whereas no damage of the specimens was recorded in full film conditions. The axial cracks they produced, present at the centre of the track did not show white etching alterations, but instead WECs were recorded in correspondence to the edges of the contact. It should be noted here that Gutierrez et al.'s set up consisted of two bearing rings pressed against each other, with one ring being narrower than the other. Given that bearing rings are flat in transverse direction, it is very likely, although not pointed out by the authors, that significant edge stresses existed in their tests; if so, this would strongly affect crack initiation and propagation behaviour in the reported tests.

Gould et al. [66] reproduced WECs using a triple-contact rig and line contact configuration specimens. They suggest the magnitude and direction of sliding to be significant in WEC formation and according to their results they proposed a threshold value of frictional energy that can be used as a criterion to predict occurrence of WECs. Their findings are described in more detail later in this thesis within the "slip and energy accumulation theories" section, 2.8.3.

It should be noted that Franke et al. [7], using the same triple-disc rig but with specimens in elliptical contact configuration, tried to reproduce results from a previous study [5] where WECs were obtained using the FE8 full-bearing rig. They were not able to get white etching cracks using the triple-contact rig with specimens in elliptical contact configuration; they explained this by stating that the amount of hydrogen absorption in the test chamber of the triple-disc rig was not enough to create WECs although they do not provide any direct evidence to support this statement or the importance of hydrogen in this respect in general. Furthermore, even when triple-disc rig specimens were pre-charged with hydrogen, failure occurred after 5 million cycles (much faster with respect to the uncharged specimen which endured more than 260 million cycles), but WECs were not observed after sectioning unlike in the case of FE8 rig results.

2.8 Proposed drivers for WEC formation

Recently, the focus of WEC research has moved to attempting to explain the driving factors and potential mechanisms of WEC formation. Unfortunately, the literature on this latter aspect seems to be littered with discrepancies and disagreements, with an ever increasing number of theories being proposed for the formation of white etching cracks. Given that numerous factors are at play in any rolling contact fatigue failure, research results seem to have led to different interpretations by different authors. Some of the factors that have been proposed as root causes of WEC formation include:

- Hydrogen absorption (mono-atomic hydrogen, either coming from the surrounding environment or from degradation of lubricant, can penetrate the steel causing its embrittlement and then cracking [39,40,86–88];
- Environmental effects (presence of contaminants in the lubricant, static electric currents generated from the relative motion between rotating and sliding components) [89];
- Degradation and detrimental action of additives in lubricants which are referred to as “low reference oils” or ‘WEC critical oils’ [83] and lubricant self-charging [6];
- Impact loading, also known as hammering wear impact fatigue, through adiabatic shear bands [2];
- Brittle fracture and corrosion fatigue [38];
- Friction energy accumulation or frictional power intensity, giving rise to related threshold parameters for WEC formation [3,5,64,66].

In the next section, some of these theories proposed for WEC generation will be analysed in more depth.

2.8.1 Lubricant and additives degradation

There are several studies on the apparently detrimental effects of lubricants on the occurrence of WECs. Studies report that oils containing ZDDP and CaS additive are prone to cause WEC failure, with WECs observed after few hours of testing [6,54] while with those those additives absent tests were stopped after more than 1000 hours without showing presence of WECs. This implies that WEC formation can be attributed directly to the chemical composition of the oil. In this regard, the use of a specific oil, known as ‘low-reference’ or ‘WEC critical’ oil, has become wide-spread in the literature. The oil is described as commercially available, fully formulated SAE 75W80 transmission oil. In their analysis, Paladugu et al. [80], amongst others, showed that it contains significant amounts of metallic elements, phosphorus and sulphur, all of which are pretty common constituents of many fully formulated lubricating oils.

Self-charging of the lubricant has been proposed [6] due to transportation of chemical components present in the lubricant itself. Although there is a lack of evidence, the authors suggest that a subsequent discharging would then cause an electro-magnetic induction that is transferred into the steel at the microstructure level, producing alterations in the steel. However, this theory has recently been disowned by some of its original authors [83].

Other studies reported that sulphur is able to promote hydrogen ions to enter the steel via recombination of molecular hydrogen; hence, anti-corrosive sulphonate additives are claimed to cause WEC failure [90]. Similarly, several commercial greases for WTG applications, containing poly-urea thickeners, have been considered to promote hydrogen absorption [11,64,89].

2.8.2 Hydrogen absorption and embrittlement

Hydrogen absorption is one of the most cited root causes for the formation of WECs. These theories generally claim that during operation, an increased level of hydrogen is introduced within bearing steel via chemical absorption. It is not clear how hydrogen can penetrate the steel. Cwiek [91] demonstrated that diatomic hydrogen is too large to enter the surface, therefore only the single atoms or their ions can be absorbed within the matrix. Few researchers suggest that lubricant degradation could promote the dissociation of hydrogen and showed presence of lubricant at the crack tip, but others claim that hydrogen absorption does not depend on chemical composition of the lubricant but instead is proportional to the amount of wear on the surface of the steel [92].

Indeed, a number of recent studies of white etching cracks related to wind turbine applications have employed hydrogen pre-charged samples in order to enable reproduction of WECs in their tests [39,87,88]. A WEC originated in a hydrogen pre-charged specimen is shown in Figure 26. However, there are divergent opinions amongst different studies. Richardson et al. [93] suggest a direct link between hydrogen diffusion into rollers during fatigue tests of cylindrical roller thrust bearings and WEC formation in the rollers; no WECs or hydrogen diffusion was observed in the raceways. In stark contrast, Paladugu et al. [80] categorically exclude the possibility that hydrogen was responsible for the short lives and WECs observed in their tests using the same bearing type and the same test rig (FAG-FE8 test rig)

Historically, prior to the more recent WEC related research and largely owing to significant research programmes in Japan since 1980s, it has been well established that hydrogen causes the steel to become more brittle; many researchers have proved it by charging their samples before testing [90,91,94–96] and others demonstrated that it can stay trapped at defects in the bulk material like, for example, non-metallic inclusions

[95,97]. There are also several theories that explain the harmful effect of hydrogen embrittlement on steel: hydrogen-enhanced localised plasticity (HELP) is one of those theories, sustaining that hydrogen promotes dislocation movement resulting in localised plasticity [98].

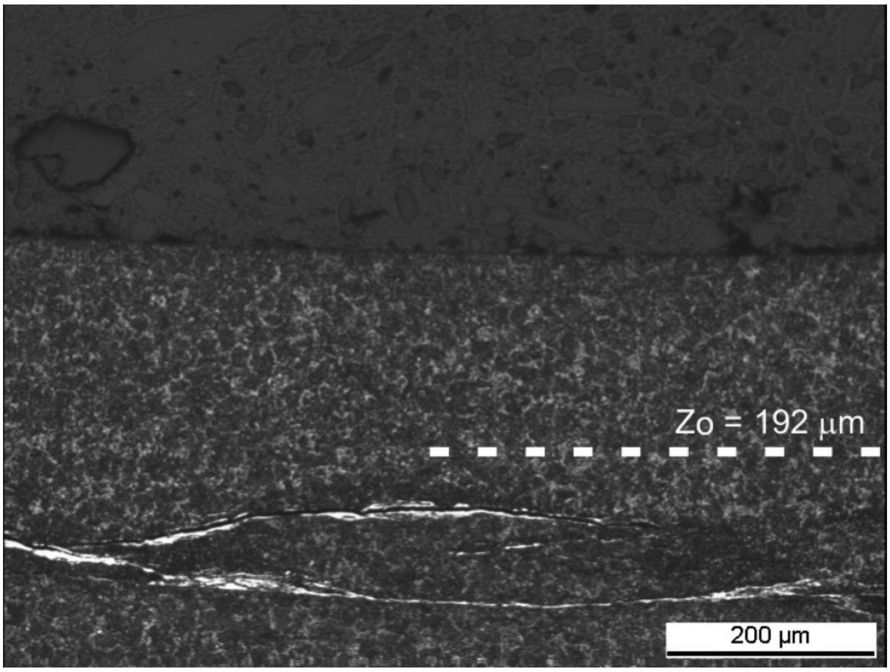

Figure 26 WECs in an hydrogen-charged sample [88]

Hence, hydrogen diffusion is detrimental for steel but there is no evidence that a high concentration of hydrogen occurs in real applications known to be suffering from WEC related failures. In fact, it is very difficult to measure hydrogen content after bearing operation, since it is very mobile and will escape the steel very quickly after the bearing operation. In laboratory conditions, samples can be frozen in liquid nitrogen or dry ice right after the experiments, to prevent the hydrogen to effuse from the steel. Thermal desorption analysis is used to measure the concentration of diffusible hydrogen. Hydrogen trapped in the steel could be non-mobile (trapped) or diffusible (mobile). Only mobile, diffusible hydrogen is taken into account as a driver for WECs. This hydrogen is released below the temperature of 400°C and it can be trapped at defects like inclusions, carbides, dislocations which may introduce a tensile stress field. It has been reported that decreasing the number of MnS inclusions is beneficial in term of WEC resistance: manganese sulphide inclusions are added into the steel to improve machinability; however, they are believed to be weak traps of mobile hydrogen that then easily release it into the steel when subjected to a high shear stress field [99].

Another proposed mechanism of hydrogen-driven WEC formation is that during mixed lubricated conditions, where damage in the form of wear is supposed to happen, hydrogen is diffused via consequent fresh nascent steel formation: hydrogen ions would diffuse through the steel by combining with electrons at the nascent contact surface, becoming monoatomic diffusible hydrogen attracted to inclusions or crack tips [92,100].

There are other proposed driver mechanisms described in the following sections, which are directly or indirectly linked to hydrogen absorption. For example, presence of inclusions (as already stated in this section), lubricant degradation, impact loading, and brittle fracture.

2.8.3 Slip and energy accumulation theories

Although the magnitude of sliding between rolling elements and rings in a bearing is generally low (<5-10%) under normal operation, more significant slip can occur in bearings during operation when the dynamic load rating is below a minimum value in the unloaded zone and during transient events. Tests with varying amount of slip have been conducted in different bench top rigs. Slip has been proposed to cause WECs by increasing the level of shear stresses near the surface [6,66,87,93,101], this in turn causing drop in tribo-film and subsequent formation of nascent surface for hydrogen migration [59,102]. Magnitude and direction of sliding is often cited as having an important influence on formation of WECs. FAG-FE8 test set-up which utilizes cylindrical roller thrust bearings (CRTB) is often used for reproduction of WECs. This type of bearing has relatively large magnitudes of sliding speed on either side of the bearing pitch. Based on the results from this set-up, Kruhöffer and Loos [5] report that WECs form preferentially within the inside radius region of the bearing washer i.e. where the washer is slower than the roller (commonly defined as negative sliding from the washer perspective). Paladugu [80] reported that, although cracks are formed across the contacting surface on the washer, only those within the regions of negative sliding exhibited white etching. Gutierrez et al [85] also report that white etching cracks are observed preferentially within the negative sliding region on a two-disc machine. Using a triple-contact machine, Gould et al. [66] proposed that the direction of sliding is important for WEC generation. Authors report that WECs were only observed in a test roller when the roller was faster than the ring (+ve slip according to the commonly accepted convention, although authors refer to this as positive slip) in a triple disc contact fatigue rig. Authors further reported that only relatively high magnitudes of sliding (slide-roll ratio of 0.3), resulted in WECs, while slide-roll ratio of 0.05 did not produce WECs. Based on these findings Gould et al. [4] proposed a criterion for WEC formation based on threshold frictional energy accumulation (a product of sliding speed, operational time, applied load and contact friction coefficient). Such frictional energy based criteria are commonly used for assessing the risk of scuffing [103] and their validity for assessing the risk of fatigue cracking is uncertain; indeed the authors themselves state that ‘correlation does not imply causation’.

The link between WEC formation and frictional energy was first made by Ruellan et al. [3] to explain WEC occurrences in their tests with angular contact ball bearings. They used the product of local pressure and sliding velocity (PV value) as the criterion. Others have claimed a link between the local PV value and the local hydrogen concentration as being of significance [55,102,104], hence once again a link with hydrogen theory is made.

A more recent criterion for WEC formation by Kruhöffer and Loos [5] is also based on critical frictional energy (as stated by the authors, although it has units of power intensity, [W/m^2]). This criterion considers the pressures at the asperity contacts (in this way the effect of lambda is included with the assumption that the pressure at the asperity level decreases with increasing lambda) and also incorporates the time between repetitive over-rollings through a ratio $t_{contact}/t_{reg}$, where $t_{contact}$ is the time elapsed during a single contact and $t_{reg,}$ the so called "regeneration time" which is the time span between two consecutive contact cycles. Using cylindrical roller bearings on a standard FE8 test rig, authors found that WEC failure was dependent on the number of rollers used during the test. They suggest that fewer rollers means higher value of regeneration time and that this may contribute to thicker tribo-film formation, which prevents hydrogen absorption.

2.8.4 Impact loading and brittle fracture

An important deficiency of most currently proposed theories of WEC formation, is the fact that they do not explain why the commonly used bearing life theories appear unable to predict the relatively high failure rates experienced in the field. Bearing life theories are of course based on rolling contact fatigue as the failure mode, so one WEC formation theory, due to Gegner [38], that could seemingly explain this mismatch is that of cleavage fracture being responsible for the premature bearing failures associated with WECs.

This theory, in fact, is not linked to rolling contact fatigue, proposing instead that the final failure is due to brittle fracture. It seems to, at least in part, arise from authors interpretation of the appearance of the fracture surfaces from prematurely failed bearings, which often show existence of elliptical region of smooth fracture with a small inclusion at its centre (often referred to as 'fisheye') surrounded by a region of rough fracture. Gegner et al. attribute the smooth central area to brittle cleavage fracture, followed by crack propagation due to corrosion fatigue, assisted by the lubricant additives. In fact, the literature reveals that such fracture morphology is entirely consistent with fatigue crack growth, rather than cleavage, the change from smooth to rough fracture surfaces being accounted for by a discontinuous change in crack propagation, with the associated mechanisms well established [105]. Given the predominantly compressive stress field in a rolling contact, it is not obvious how the tensile stresses of the magnitude needed to cause brittle fracture can be generated under such conditions. In this respect, Gegner and co-authors argue that high tensile stresses can be produced by high surface friction loading. However, considering a surface breaking crack of 10 μm in depth, an extreme value of friction coefficient of 0.4, and contact pressures of 2.5 GPa, which are the actual values cited by the authors, the stress intensity would be of the order of 10 MPa m$^{0.5}$. This is therefore not sufficient to cause brittle fracture of AISI 52100 bearing steel, where the K_{IC} has been quoted to be in the range 16-28 MPa m$^{0.5}$ [105]. In reality, friction coefficients in lubricated contacts rarely exceed 0.15, and if higher values were to occur on local asperity level, this would be offset by the smaller depth of tensile stresses, so that stress intensity factors are extremely unlikely to exceed fracture toughness in any case. Moreover, a recent study reported that cleavage-like cracks caused by mixed friction condition are very unlikely to occur, given that the value of fracture risk index (ratio between stress intensity factor and fracture toughness) was below 1 [87].

The apparent presence of cleavage-like axial cracks is also the motivation behind some other WEC theories such as impact loading causing WEC formation. This proposes that impact load, due to vibrations, misalignment, pressure peaks, generates a cleavage-like axial crack which propagates fast under tensile stress. Subsequently, a v-shaped crack forms and propagates in a stair-like direction (Figure 27, right), the radial segments caused by tensile stress, the parallel segments by shear. Hence, according to this theory, WEAs observed at the parallel cracks are caused by adiabatic shear bands [9].

Figure 27 Axial cracks on an inner ring raceway (left) and in circumferential section (right) [13]

2.8.5 Hoop stress

Rolling bearings are generally subject to a compressive stress field during operation. However, there are occasions where tensile hoop stresses can be introduced in bearing rings due to interference fits with the shaft. Presence of such hoop stresses has been linked to reduced bearing lives in the past, particularly in the case of large bearings [106]. More recently, some authors have also reported a link between tensile hoop stresses and WEC appearance [107,108], with enhanced risk of axial cleavage-like cracks too.

Propagation of WECs includes both axial and circumferential direction, as observed in several examples from the field. Hence, the presence of hoop stresses does not strictly appear to be a requirement for WEC formation. This is also supported by evidence in other tests, in which specimens loaded with hoop tensile stresses did not produce white etching cracks [64].

2.9 Critical discussion on existing literature and motivation for the current study

(Note: Parts of this sub-section are based on a related journal paper by this author [8]*)*

Some of the apparent discrepancies and omissions in literature are critically discussed in this sub-section and subsequently, the motivation and aims of the present study are put into context.

As was seen, lubricant composition is often mentioned to account for WEC formation. The use of a “bad reference oil” gained popularity in the literature at this regard. A number of studies [4–6,66,80,83,109], in fact, employ this oil to generate the white etching cracks in their tests and at least in part associate the formation of cracks to the composition of this oil. However, although this oil is often quoted as contributing to WEC formation, there appear to be very few published studies that specifically compare the performance of this low reference oil to other oils of known composition. A notable exception is the study of Paladugu, Wear 2018, which compared the performance of this oil to that of a mineral oil commonly used in bearing life tests and concluded that the low reference oil indeed does promote WEC formation and premature failure through formation of boundary films which result in high surface shear stresses; therefore, in this case the effect of oil formulation on damage is attributed to mechanical rather than chemical effects. Indeed, when performing comparative rolling contact fatigue studies with different oils, it is very difficult to ensure a valid comparison that is able to distinguish between chemical and mechanical effects of a particular oil formulation. A particular additive package will form a boundary film that may well have a different chemical composition to that formed with another oil, but at the same time the roughness and frictional properties of the two boundary films are also likely to be different so that contact stress fields and wear are different between the two different tests. From a practical point of view, where a choice needs to be made between different lubricants for particular application, this is perhaps less important, but it is absolutely crucial in the quest to understand the damage mechanisms and hence prevent similar failures in the future. A good example of a study that successfully distinguishes between the mechanical and chemical effects of an oil, is the work of Olver and co-authors [28,110] who showed that ZDDP anti-wear additives can increase the amount of micro-pitting damage on the surface while MoDTC friction modifier minimizes micro-pitting [111]. In both cases, the differences in damage were entirely accounted for by the changes in surface stresses caused by the additive action, and not to any chemical effects of different oil formulations; namely ZDDP increased the number of asperity micro-stress cycles due to its ability to suppress wear of the counterface, while MoDTC reduced friction and hence tensile stresses which are detrimental to contact fatigue lives. Concerning always the connection between chemical and mechanical effects of additives, also another study from Gatzen and co-workers [112] showed that the use of polymer additive-enhanced greases results in a reduction of friction by formation of boundary layer of lower surface hardness.

A plethora of rolling contact fatigue research over the past 70 or so years has established that the variable that has by far the greatest influence on rolling contact fatigue lives is the applied stress, with life for a given reliability being inversely proportional to stress to power of about 9 [35,113]. This fact does not always seem to be reflected in the recent research on WEC related failures resulting in multiple non-stress related mechanisms being proposed to explain what is essentially a contact fatigue failure. If nothing else, it is clear that a slight difference in friction or asperity contact pressure distribution between two different lubricants can have a large effect on observed RCF lives. Hence, if one is to decouple any chemical influences from this large mechanical effect, fatigue tests need to be carefully designed to minimize any differences in stresses between tests run with different oils, which occur primarily due to differences in friction and wearing-in of the test components; this is far from easy to achieve in practice given the complexity of rough surface contact interactions.

Lubricant composition is also used as a link to hydrogen embrittlement. In this case, degradation of lubricant during operation is claimed to release monoatomic hydrogen which is then absorbed by the steel. As seen, hydrogen is probably the most cited root cause for WEC formation. Hydrogen cracking is a well-known process that especially interests welded components, where it starts at stress concentrations such as the root of the weld and then propagates within the metal through the heat-affected zone. It is also known as hydrogen-induced cracking, hydrogen-assisted cracking or hydrogen delayed cracking [91,114–116]. After noticing the increased level of hydrogen after failure, hydrogen embrittlement was increasingly proposed as a mechanism of WEC formation in bearing steels. Studies show that hydrogen absorption and embrittlement in martensitic steel depends on tempering temperature with negative effects on the steel with temperatures above 300C [117], which is not the case of bearing steel, where tempering temperature is around 150C. It is far from simple to set up an effective experimental method to study hydrogen absorption. Isolating the several sources from which hydrogen could escape and be trapped in the steel is a real challenge, given also that the accuracy of instruments and sensors strongly affect the reliability of results. It has to be remarked also that hydrogen measurements are very subject to the method used and results can vary considerably from one measurement to another. Moreover, when looking for a single root cause for WEC formation, one needs to consider that the environment in which bearings operate is complex and involves a lot of phenomena taking place simultaneously. Popularity of hydrogen absorption as WEC formation theory may be because it can be linked easily to other theories. For example, if one proposes sliding effects on the surface as responsible for driving the formation of WECs, hydrogen absorption is called into play as well. In this case, in fact, two different implications could be recognized: from one side shear stress is present on the surface which is a direct consequence of sliding; on the other hand, sliding promotes creation of fresh nascent surface and this on turn implies absorption of hydrogen from the surrounding to the steel. Hence, it is not simple to isolate the two different aspects and understand which phenomenon is relevant for the initiation and which one is just an accelerator of the failure.

Regarding the implementation of a criterion to discern what conditions can bring to premature failure occurrence, one should not to overlook the fact that tests to produce WECs take always place in rolling contact conditions, which substantially means that the statistical nature of the phenomenon plays a big role in the interpretation of results. Hence, in order to account for this, a criterion should be based on a large dispersion of test results. Proposed criteria in literature seem not to be satisfactory in this regard.

Whether the initiation of the damage starts at the surface or subsurface is not clear and needs more investigation. This could help in understanding on what parameters to focus attention. If the problem is surface initiated, then the significance of roughness, slide-to-roll ratio and film thickness should be analysed in more detail. On the other hand, if the problem is subsurface initiated, the effect of tribological parameters or the effect of lubricant on the contact surface is likely to be of a secondary concern.

Another point which still needs to be clarified is whether the typical white etching alterations are prior or posterior to crack initiation. Understanding the order of appearance of the two phenomena is important to focus the attention on the aspect that takes on the most important role in premature failures. Crack-face rubbing is a hypothesis for WEA and cracks relationship. This assumption implies that the microstructure alteration takes second place of importance, since it does not represent the initiation of the damage. This would suggest that formation of initial cracks is at the heart of premature failure occurrence. Provided that the material is of sufficient quality without inherent cracking, formation of such cracks requires application of stress cycles, whether or not other factors, such as 'WEC critical oil' or hydrogen, may be present. At the same time, crack-face rubbing does not explain why the crack forms and hence, a more complete theory is needed to explain premature failures.

2.9.1 Primary aims of the present study in relation to literature findings

The previous section about the proposed drivers for WEC/WEA initiation serves to illustrate that there is clearly no agreement on the mechanisms of formation of the white etching cracks. Current studies of WECs seem pre-occupied with considering WECs as a phenomenon in their own right and there is a notable lack of literature linking WECs and early bearing failures, so much so that the significance of WECs as a potential cause of premature bearing failures has not been directly confirmed yet. This is clearly a significant omission, given that it is the reasons for premature bearing failures that are of greatest economic interest to wind turbine industry. In view of the discrepancies identified in literature, the present study sets out to answer the following primary questions:

- What are the primary mechanisms of WEC formation?
- What is the significance of WECs to premature bearing failures, in particular those observed in wind turbine applications?

In addition, given the existing disagreements in the literature on the primary causes of WEC formation, this work also attempts to establish the significance of some of the most commonly proposed WEC drivers in existing literature, namely:

- lubricant composition
- sliding magnitude and direction
- frictional energy input.

The experimental procedures and equipment employed in the present study are described next.

3 Experimental design

In this chapter, considerations in relation to the choice of experimental set-up and test conditions are discussed. In order to provide valid comparisons between different lubricants and test conditions the experiments need to be closely controlled so that the effects of a single variable of interest can be isolated one at a time. The justification for the chosen experimental methods is presented here with this in mind. The features and advantages of the chosen test rig are explained. Finally, the thermal network model of the rig used to ensure consistency of specific film thickness at different test conditions is described.

(Note: Parts of this Chapter are based on a related journal paper by this author [8]*)*

3.1 Background

As mentioned in the literature review, attempts to study white etching cracks under laboratory conditions can be divided mainly in two categories. Some researchers adopted the use of a full bearing test rig, such as FE8 FAG standard test machine, while others chose an experimental rig such as a two disc rig or a four-ball machine.

The first configuration is used when one wants to simulate the behaviour of a rolling bearing in its entirety, thus this represents a global approach in the study of the phenomenon of bearing failures, generally used because it is claimed to be more representative of the field conditions. The second set-up, on the other hand, focuses more on the phenomenon of the contact between two rolling elements, which represent for example the inner ring and the roller of a bearing. This approach is, then, a more fundamental study of the phenomenon of rolling contact fatigue.

Both of these approaches present some issues in the compromise between replicating realistic conditions and the need to control the effect of a specific tribological parameter. For example:

- It is claimed that the magnitude of slide-roll ratio plays a big role in the occurrence of WECs. The effect of this parameter cannot be isolated if using a full-bearing test rig;
- when running a rolling contact fatigue test aiming to reproduce a specific failure, such as pitting, there are many other competitive modes of failure which can occur, preventing the desired mode of failure to happen. In particular, it is important to control wear damage, which by changing the contact geometry can also cause a variation of the initially imposed Hertz pressure, and micropitting which can occur in mixed regime and also cause substantial changes to the surfaces of test specimens;
- The bearings that manifests WECs are believed to operate in relatively severe lubrication conditions of mixed regime. When trying to replicate these conditions, low entrainment speeds need to be employed leading to relatively

slow rate of cycle generation and hence a long and time consuming tests. This means that the number of fatigue tests that can be conducted within a specified time-frame of any one project can be relatively low;

- A practical advantage of using a single-contact test rig is that it is possible to cause the failure to happen on a specific disc or specimen, whereas in a full-bearing rig, the final failure can independently occur at any one of the rolling element or at one of the two raceways which are generally more difficult to prepare for inspection.

A major reason why one would opt for a lab based experimental rig rather than a full bearing is that, as anticipated above, in the latter configuration it is not possible to isolate the role of a single parameter which is essential if fundamental mechanisms for WEC development are to be revealed.

3.2 **Choice of test rig**

After considering difficulties in choosing the right parameters for a test and all the pros and cons of any given test configuration, it was decided that the present study should utilize the triple-disc contact fatigue machine. The initial incarnation of this triple-disc set-up was designed at Imperial College for studies of fatigue damage in helicopter transmissions. At the time, the rig utilized hydrostatic loading system and the same oil was used for both the test and to provide the load [118,119]. The number of slide-roll ratios was also limited and changing from one to another required modification to pulleys and belts in the drive system of the rig. The current version of the rig, designed and developed by PCS Instruments Ltd, overcomes most of these shortcomings by implementing a mechanical loading system and utilizing multiple electric motors so that infinite number of slide-roll-ratios can be achieved. PCS initially designed and marketed the rig for study of micro-pitting and therefore is often known as PCS Micro-Pitting Rig (MPR). This rig has been widely and successfully used for studies of rolling contact fatigue in the past at Imperial College and elsewhere, by, amongst others Benyajati [120], Laine [28] and Rycerz [18]. The rig is described in detail in the later section but for the purposes of this chapter, it should be noted that the main advantages of the rig are the fast generation of contact cycles in the test roller specimens, owing to the triple contact set-up, choice of contact configurations (line or elliptical with different contact dimensions) with specimens of repeatable quality and surface finish, and close control of test conditions including SRR, temperature, and load.

3.3 **Control of test parameters**

An explanation on how the most relevant parameters are controlled in tests is presented as follows.

3.3.1 Control of friction coefficient

After choosing a test machine for the present study, next step is to design how experiments will be carried out. In order to make comparison between different tests, it is important to change one parameter at a time. However, isolating the influence of the particular variable of interest while keeping all other contact conditions constant, is not easily achieved under lubricated RCF conditions. This is primarily due to the competing failure modes of pitting, micropitting and wear, with the outcome of that competition being very sensitive to any changes in conditions during the test [28,111,121] and the fact that RCF tests inevitably take a long time over which contact conditions can change unpredictably, due to unwanted wear for example. This means that when interpreting RCF results it is relatively easy to attribute any observed trends to a wrong mechanism.

Studying the effects of different lubricant formulations is particularly problematic in this respect as it is very difficult to separate chemical and mechanical effects that an oil may exert. For example, two oils with different chemical formulations are likely to result in different friction, different wear rates and different roughness evolution, all of which will affect contact stresses and hence have a profound influence on rolling contact fatigue lives. If not monitored, these purely mechanical influences could inadvertently be attributed to chemical effects of different formulations. Hence, the only way to conduct scientific studies that provide insight into physical mechanisms is to control the variables that are known to affect RCF as closely as possible so that the chemical influence of an oil formulation can be assessed. This was achieved here by ensuring that friction coefficient is the same for all oils tested and by monitoring the surface roughness and wear of the test roller and the counterface throughout the tests. To control friction, friction coefficient curves for different entrainment speeds were obtained for each of the tested oils and loading conditions, and then the entrainment speeds and temperatures for the RCF tests were adjusted as needed for each oil in order to ensure that tests were conducted at the same friction value each time. For example, as illustrated in Figure 28, if using two different oils, in order to run both tests at the same friction coefficient of, say, 0.09, the entrainment speed for Oil1 should be set at 1 m/s and entrainment speed for the other test, using Oil2, should be set at 2.4 m/s.

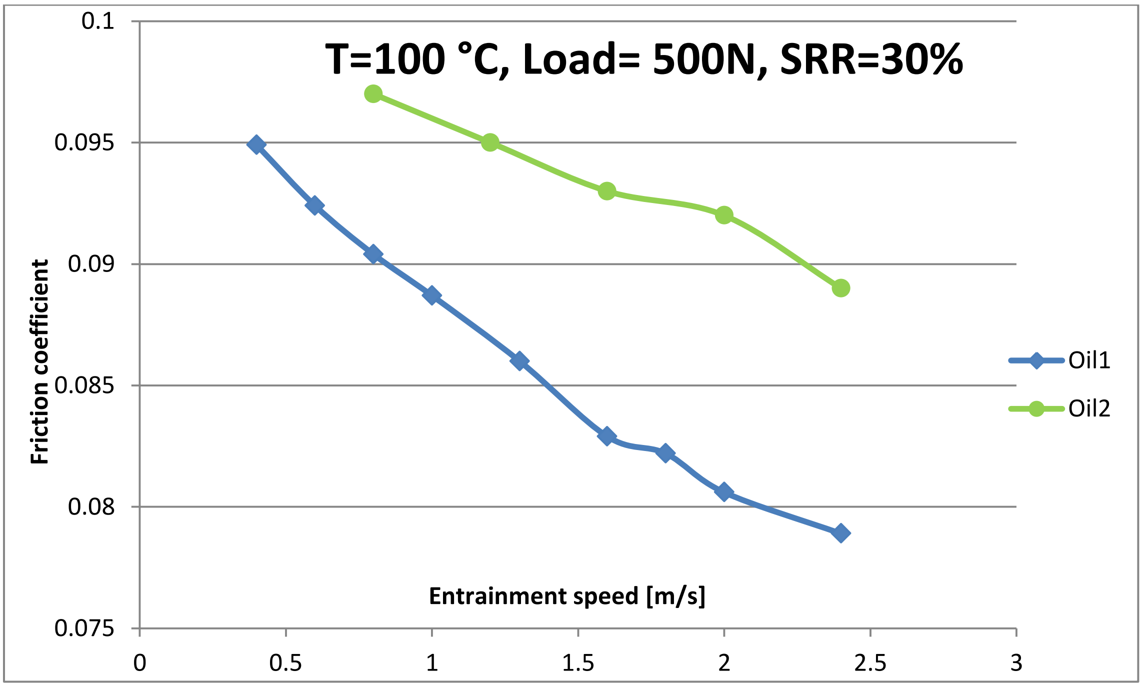

Figure 28 Friction coefficient vs entrain. speed for two different oils at the same temperature, load and SRR

This of course means that the specific film thickness values may change slightly for different lubricants, but given the gradient of the Stribeck curves in the mixed regime employed here, these changes are minimal so that all tests are conducted under the same mixed lubrication regime. In any case, since macro-pitting is considered here, small changes in lambda are far less important than changes in friction which affect tensile stresses and hence have a profound influence on crack propagation rates and RCF lives. In contrast, if micro-pitting was of interest small changes in lambda would be much more important [28,121,122].

3.3.2 Control of film thickness and thermal network calculations

Slide-roll-ratio (SRR) is another variable that can have multiple effects in the contact and hence lead to possible misinterpretation of mechanism at play. Higher slide-roll ratios increase the number of asperity stress cycles and hence affect the competition between micro-pitting, wear and pitting failure modes [121]. In addition, increasing SRR leads to an increase in bulk temperature of the test specimens in the triple disc machine and the subsequent drop in film thickness, which can be significant if relatively high values of SRR are used. Both of these effects can push the dominant contact damage mode into wear or microptting, rather than pitting, and hence totally invalidate any inferences in terms of SRR influence on WEC mechanisms.

To prevent this, current procedure employs two measures; firstly, the evolution of roller and counterface surfaces are monitored by measuring them with a stylus profilometer to ensure no significant surface wear is taking place so that valid comparisons can be made across different SRR and oils. Secondly, a previously devised approach [122] of predicting the bulk temperatures of the counterface discs and the test roller and hence the viscosity of the oil at the inlet to the roller-disc contact is employed for all test conditions when calculating film thicknesses, rather than using simple isothermal predictions. This ensures that any effect of SRR on film thickness can be compensated for, again ensuring that the comparison across different SRRs in terms of its effect on WECs is valid. Employing isotheral film thickness predictions which ignore these effects may lead to potential misinterpretation of results for extreme values of SRR and hence significant bulk temperature increases.

The thermal model employed here follows the general approach proposed by Olver et al in 1998 [123] for predicting contact temperature rise, and applied to the triple-disc rig by Rycerz and Kadiric [18,121,122]. It is based on Jaeger's theory of moving hot spots and a thermal network of the triple disc test set-up. When two surfaces come into contact, a frictional heat is generated by the relative sliding between the bodies and consequently, this heat is conducted into the material, so that the temperature of the two surfaces increases. Hence, the temperature, T_b, of the contacting surfaces is now higher than the temperature, T_a, of the surrounding, (which in the case of the test, is represented by the oil sump temperature), but in turn, is lower than the temperature, Tc, reached in the contact.

The rise of the bulk temperature depends on the dissipation of heat into each surface. In this case, it is assumed that for each contact part of the heat, portion α, enters the roller, body 1, and the remaining (1-α) portion of the heat is dissipated into the counterface disc, body 2. Consequently, the heat flow of the contact can be represented by the thermal network shown in Figure 29.

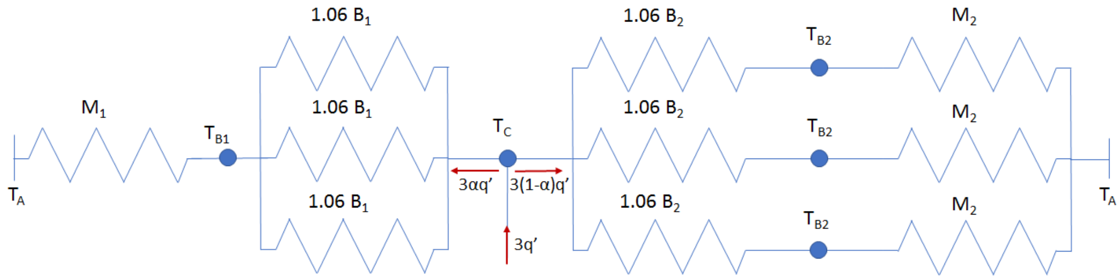

Figure 29 Thermal network model for the triple contact configuration

Making Jaeger's assumption that the mean contact temperature rise above ambient is the same for body 1 and body 2 the heat partition coefficient can be worked out as:

$$\alpha = \frac{1.06B_2 + M_2}{1.06(B_1 + B_2) + (3M_1 + M_2)}$$

So, the heat partition can be determined if both transient (B) and steady state (M) thermal resistances are known. The transient thermal resistance is derived from Jaeger's equations for the rise of flash temperature, by taking into account the material and contact parameters in the equations such that they are defined as

$$B_i = \frac{1}{Ak_i}\left(\frac{\chi_i b}{\upsilon}\right)^{1/2}$$

where i is an index which indicates the i-th body or surface, k is the thermal conductivity (W/mK), b is the contact half-width (m), υ is the speed of the surface (m/s), and A is the contact area (m^2). The thermal diffusivity, χ (m^2/s), is defined as

$$\chi = \frac{k}{\rho C_P}$$

where ρ is the density of the material (kg/m^3) and C_P is the specific heat capacity (J/kg°K).

For the calculation of the steady state thermal resistances, M, one considers that these depend upon the conductivity of the material, the geometry of the contact and the convective surface heat transfer coefficients of the surfaces. This calculation normally represents the most difficult part in the determination of the final temperature of the bodies. In this work, the approximation by Olver and Spikes [123] was adopted. The thin-disc approximation is here considered, hence for the counter discs (M_2), there are two heat exchanges (losses) to be taken into account: heat loss from the disc side and a simultaneous convection from the running track. Therefore, the total steady state thermal resistance for the counter discs is

$$\frac{1}{M_2} = \frac{1}{M_\infty} + \frac{1}{M_R}$$

M_∞ represents the heat loss from the track. The solution for this case, in line contact, with contact width l, is given by Cameron [1976]

$$M_\infty = \frac{1}{2\pi Rlh}$$

whereas, M_R is the heat loss from the disc side, which can be obtained considering the case of the annular fin of uniform thickness subjected to steady conduction in the radial dimension [Chapman, 1984]

$$M_R = \frac{1}{8.88(hkl)^{1/2} R \frac{I_1(nR)}{I_0(nR)}}$$

Here R is the radius of the disc (m), h is the surface heat transfer coefficient (W/Km^2), I_0 and I_1 are Bessel functions of the first kind (which one finds implemented in Matlab and Excel). And

$$n = \left(\frac{2h}{kl}\right)^{1/2}$$

Furthermore, the small disc approximation [Olver, 1991] was adopted for the small roller specimen. With analogy to the counterface disc, the steady state thermal resistance for the roller, M_1, can be calculated as follows

$$\frac{1}{M_1} = \frac{1}{M_\infty} + \frac{1}{M_A}$$

Calculation of M_∞ is analogous as the case of the disc and can be obtained with the same formula using the geometry of the roller and the solution for M_A can be derived considering the case of a straight fin of uniform thickness under steady conduction in the axial dimension

$$M_A = \frac{1}{4.44(hk)^{1/2} R^{1/2} [tanh(mL_l) + tanh(mL_S)]}$$

L_s and L_l (m) are respectively the distance from the top and the bottom of the roller to the middle of the running track, and

$$m = \left(\frac{2h}{kR}\right)^{1/2}$$

Now that the heat partition is calculated, the required surface temperatures can be obtained from the following equations

$$T_{B1} = T_A + 3\alpha q' M_1$$

$$T_{B2} = T_A + (1-\alpha) q' M_2$$

for the surface temperature of the roller and the counter discs respectively, where q' is the total amount of heat generated by the sliding in the contact area and it is obtained from

$$q' = \mu W \Delta v$$

where W is the normal load (N), μ is the friction coefficient, and Δv is the sliding speed (m/s).

The inlet surface temperatures T_{B1} and T_{B2} for each body are different; hence the inlet viscosity needed for the calculation of the desired film thickness is dependent on both. The formula for calculation of the effective inlet temperature according to Olver and Spikes [1998] is

$$T_B = \frac{v_1 T_{B1} + v_2 T_{B2}}{v_1 + v_2}$$

It is here anticipated that the temperature of a running test in the test rig chosen for the study is measured by a temperature probe which is at a certain distance from the contact; hence, the probe cannot obviously measure the exact temperature of the lubricant which is entrained into the contact. Therefore, the actual temperature of the entrained oil, T_B, is higher than the temperature of the oil measured by the probe (i.e. sump temperature, or supply oil temperature, T_A). The calculation of the film thickness takes into account this rise in temperature in order to obtain a more reliable value of the actual lambda ratio during the test. A detailed description of the rig set-up and its parts will be given in the next chapter but here, for the sake of clarity, in Figure 30 the location of temperatures T_A and T_B in the test chamber is illustrated.

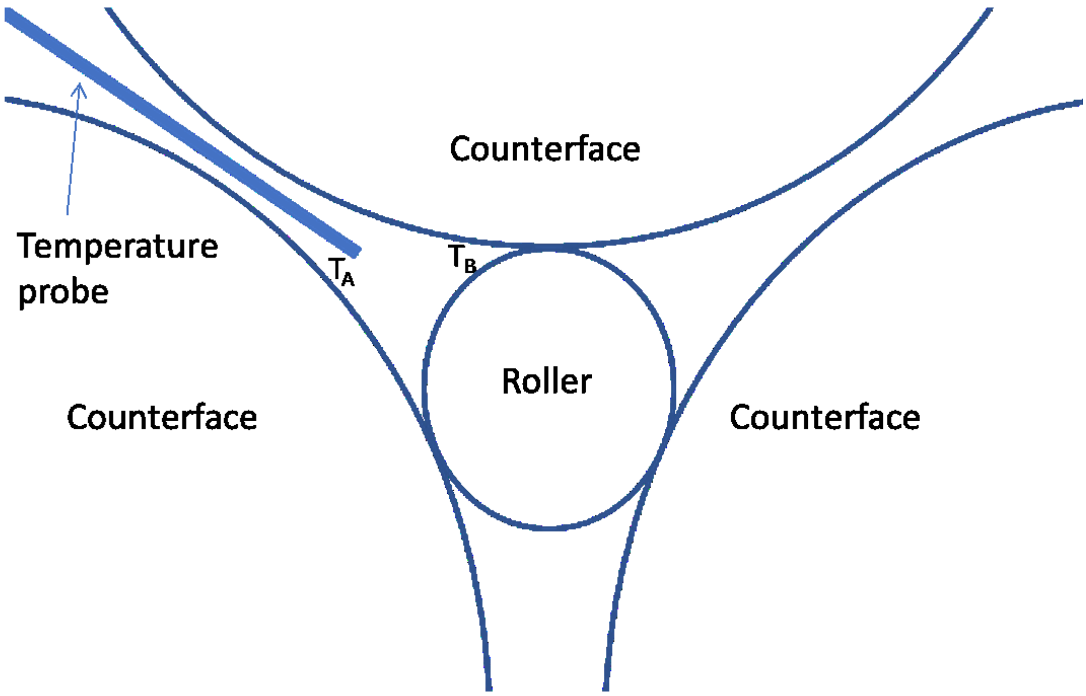

Figure 30 Position of temperature T_A, measured by the temperature probe of the rig, and T_B, temperature due to rise in the contact

After the inlet temperature T_B is obtained, the next step is to determine the inlet viscosity of the test lubricant at the effective inlet temperature. The AGMA method was employed in this study. The inlet viscosity can be calculated from:

$$loglog(\eta + 0.9) = c + dlog(T + 273.16)$$

where η is the dynamic viscosity (cP) at temperature T (°C) while c and d are constant, determined when the viscosities at 40 °C and 100 °C are known.

In addition, the pressure viscosity coefficient of the lubricant, α_p (Mpa^{-1}), at the effective inlet temperature can be obtained from the following equation:

$$\alpha_p = k\eta^s$$

Here, both k and s are constant values which are obtainable by knowing the pressure viscosity coefficient at two different temperatures, or by using the table provided in AGMA 925-A03 (for mineral oils and PAO synthetic oils at several viscosity grades).

Finally, after determining the inlet viscosity of the oil, the corresponding film thickness can be now calculated. The Dowson and Higginson's equation [124] and Chittenden's equation [125] were here employed in this work respectively for line and elliptical contacts and they are shown below:

$$\frac{h_0}{R'_x} = 2.65\bar{U}^{0.7}\bar{G}^{0.54}\overline{W_L}^{-0.13}, Dow.-Higg.eq, line\ contact$$

$$\frac{h_0}{R'_x} = 3.63\bar{U}^{0.68}\bar{G}^{0.49}\bar{W}^{-0.073}\left(1 - e^{-0.67\left(R'_y/R'_x\right)^{2/3}}\right), Chitt.eq., elliptical\ contact$$

h_0 is the minimum film thickness (m), and R'_x and R'_y are the reduced radii in the x and y direction, with x in the rolling direction. Considering indices $_1$ and $_2$ for indicating the two bodies in contact, the reduced radius in the x direction is:

$$\frac{1}{R'_x} = \frac{1}{R_{x1}} + \frac{1}{R_{x2}}$$

And same relation holds for the reduced radius in the y direction.

The equations of film thickness are both expressed in terms of three main non-dimensional groups defined respectively as speed parameter, materials parameter and load parameter:

$$\bar{U} = \frac{U\eta}{E'R'_x}$$

$$\bar{G} = \alpha_p E'$$

$$\overline{W}_L = \frac{W}{E'R'_x l}\ (for\ line\ contact, in\ Dow.-Higg.equation)$$

$$\bar{W} = \frac{W}{E' {R'_x}^2} \ (for\ elliptical\ contact, in\ Chitt.\ eq.)$$

where U is the entrainment speed, E' is the reduced Young modulus, l is the line width of the contact area.

Using this method, the corresponding film thickness could be determined given the range of entrainment speeds and the particular combination of other parameters used in the tests, such as load, SRR, bulk oil temperature and lubricant properties. The film thickness calculated in this way with thermal correction was adopted as a means to select lubrication conditions to be within the same range across all tests, considering also the range of friction coefficient as described above.

Finally, knowing the initial value of the roughness of the specimens, it is also possible to determine the so-called lambda ratio, λ, defined as the ratio between the film thickness and the composite roughness of the specimens.

3.4 Conclusions

This chapter presented the factors considered when setting up the current experiments in order to ensure the applicability of results to the problem studied and validity of comparison across different contact conditions. This description included the reason for the choice of the specific test rig used in the present work, together with the methods and criteria with which the tests should be conducted.

As a fundamental study of premature failures associated with WECs, a triple-contact rig was chosen mainly for two reasons: firstly, this rig allows accumulating rolling contact cycles three times faster with respect to an equivalent twin-disc rig and, furthermore, the control of important parameters such as SRR or load can be treated independently so that one can isolate their effects on WEC appearance.

Given that rolling contact fatigue is strongly affected by friction coefficient, particular attention should be addressed in keeping it constant across the tests in order to deduct the right interpretations. Stribeck curves for each oil were obtained in this sense and test conditions adjusted for each oil in order to ensure that mechanical and chemical influences of the oil can be separated.

Moreover, it is also necessary to maintain the lubrication regime within the same range in all the tests (of course, if this is not the parameter to be analysed). In this regard, a thermal model for calculation of film thickness was adopted, taking into account the effect of SRR in the rise of the surface temperatures of the bodies into contact.

The detailed description of the MPR rig, the type of specimens used and the test procedure in this analysis are presented in the next chapter.

4 Experimental Equipment and Procedures

In this chapter, the description of the test rig is presented, together with characteristics and geometry of specimens adopted in the tests. The lubricants used in this work are listed and their relevant properties given. Finally, the procedure for post-test inspection of the specimens is described in detail.

4.1 Description of the triple-disc RCF test rig

As stated in the previous chapter, the test machine adopted for this study is the so-called Micro-Pitting Rig (MPR). Figure 31 illustrates the main mechanical components of the MPR. Two electrical motors provide the rotation of the drive shafts through the gearbox; three of the four shafts drive the rings, while the central shaft is connected to the roller; the rings and roller are driven independently by each motor so that a desired value of sliding between the specimen and the counterfaces can be imposed; both rings and roller are enclosed in the test chamber. Load is applied by means of a loading system which incorporates a stepper motor and a loading arm.

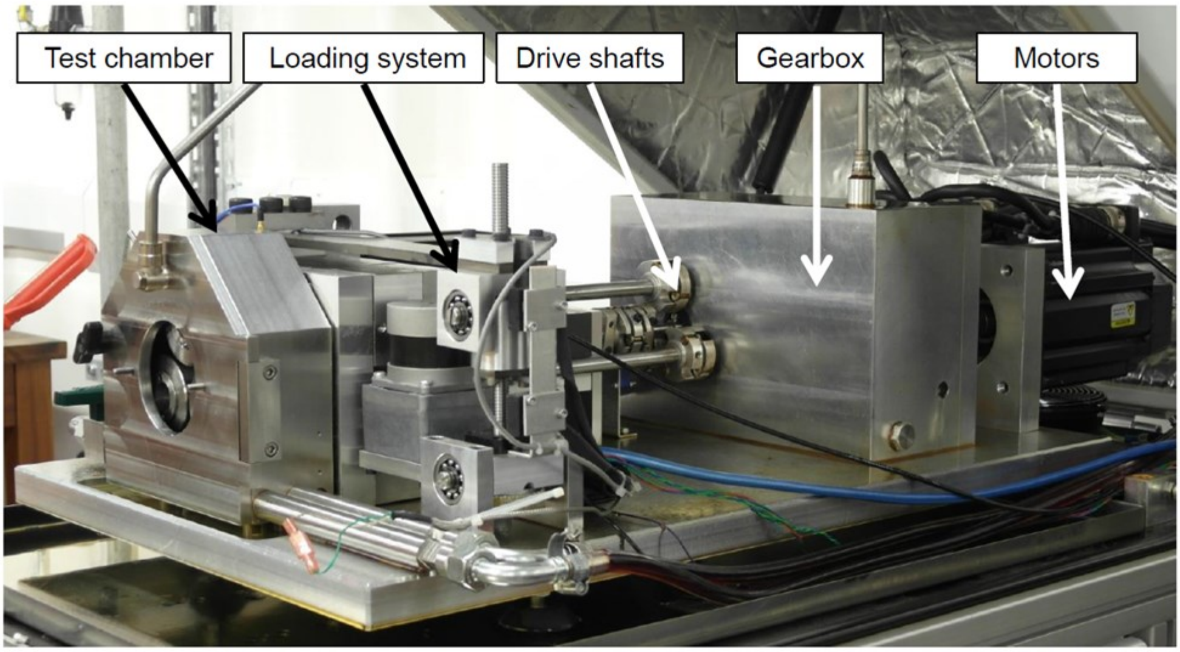

Figure 31 Main components of the Micro-Pitting Rig

The configuration of the MPR is a triple-contact set-up represented by three ‘counterface’ discs (or rings) of equal diameter, located at 120° from each other. A roller of smaller diameter is present in the middle of the counterface rings and is in contact with them. The roller is the actual specimen of the test. This particular arrangement allows the test roller to be subjected to a large amount of rolling contact cycles in a short time, significantly reducing the time of the test: this is important especially when dealing with rolling contact fatigue tests, where final failure could take large amount of cycles before occurring. Figure 32 shows the inner part of the test chamber and the configuration of the rings and the roller specimen.

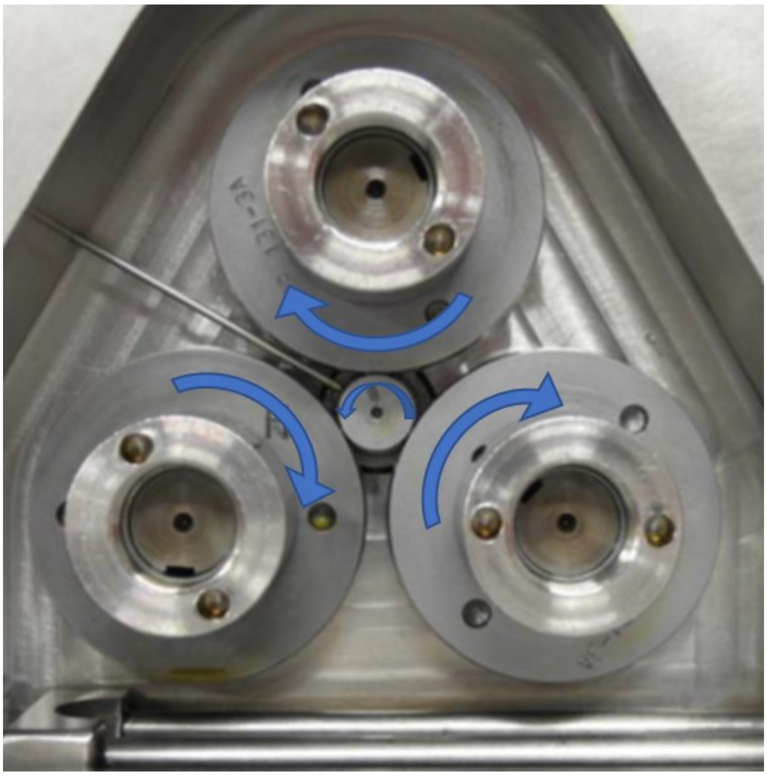

Figure 32 Test chamber of the MPR showing the triple contact configuration

Disc and roller speed, load, and sump temperature are automatically controlled by an on-board processor and software with which the rig is equipped. The rings and the roller are driven independently from each other and linked, by means of their respective shafts, to two servo-controlled motors. This arrangement allows the control of any combination of entrainment speed and sliding between the counterfaces and the roller. The slide-roll ratio in the software of the rig is defined as

$$SRR\ (\%) = \left[\frac{2 \cdot \left(U_{Ring} - U_{Roller}\right)}{U_{Ring} + U_{Roller}}\right] \cdot 100$$

It should be noted that from the perspective of the roller test specimen, this formula of SRR is the opposite of the usual convention adopted in rolling contact fatigue: a positive value of SRR for a test on the MPR, implies that the roller is slower and the negative value of SRR means that the roller is faster, in contrast to more common convention where the negative slide roll ratio would imply a slower roller. Nevertheless, this definition of SRR as implemented on the rig is adopted throughout this thesis.

The direction of sliding is important to establish the direction of friction coefficient on the running surface with respect to the direction of contact motion. As illustrated in Figure 32, the counterface rings always rotate clockwise, whereas the rotating direction of the test specimen (the roller) is anti-clockwise. The contact moves in the opposite way across the roller surface with respect to the rotating direction, so that the contact motion on the roller surface is then clockwise. The orientation of the friction coefficient is determined by the direction of sliding: if the roller is slower than the ring (SRR > 0), the direction of the friction force on the surface is anti-clockwise; on the other hand, when the roller rotates faster than the rings (SRR < 0), the friction force on the roller acts clockwise, i.e. concordant to the contact motion. This is shown in Figure 33.

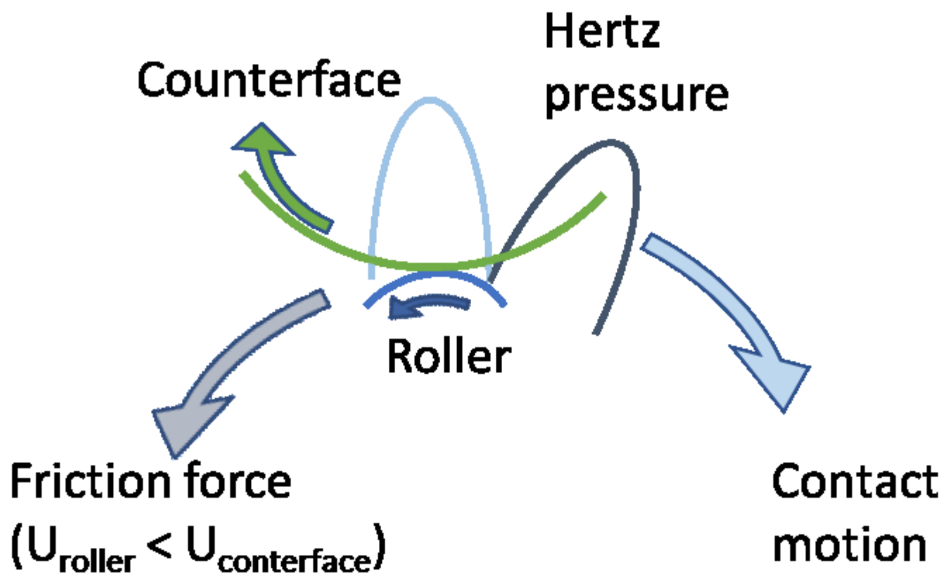

Figure 33 Directions of the friction force on the surface of the roller specimen according to the direction of sliding velocity. The qualitative Hertz pressure and its motion is shown, i.e. the contact motion

The provided software allows performing complicated test steps if one needs to change, for any reasons of analysis, the value of a particular input parameter. In this way, it is possible to obtain from the MPR rig a Stribeck curve of a lubricant, given a set of prescribed input conditions. This is achieved by uploading a desired number of step profiles with increasing entrainment speed. The friction coefficient is monitored over the test, so that at the end it can be plotted against the varying entrainment speed and a Stribeck curve is derived. This is what has been done in the present work for each test oil to design the initial conditions of the tests.

The rings and the roller are enclosed in a test chamber housing which is dip lubricated. The chamber requires only a little volume of oil (130-150 ml) and it is poured directly in the chamber through the front door of the housing. At the beginning of the test, the level of the oil is such that the two rings at the bottom are partially drowned in it. As the test starts with heating up the oil, the unloaded set-up of specimens rotates, allowing the oil to lubricate the whole chamber and the contact between roller and rings.

Electric cartridge heaters located in the steel housing are used to adjust the temperature of the oil in the sump. Two RTD temperature probes are present in the chamber, one in the oil sump and the other situated in proximity of the contact inlet (it cannot of course provide the exact temperature of oil at contact inlet but it gives an indication of any temperature differentials in the chamber). The measured temperature of the RTD in proximity of the contact inlet is then sent to the PC through a feedback control system, switching off the heater when the desired temperature is reached. This is illustrated in the Figure 34 below.

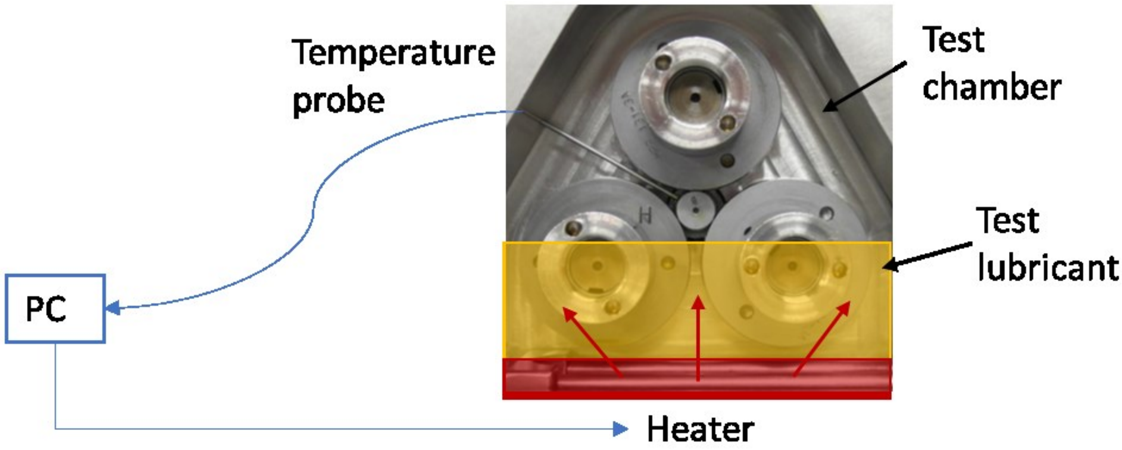

Figure 34 Schematic illustration of temperature control and measurement

A load is applied by means of a step motor, driving a ball-screw which then acts on the loading arm. The scheme of the load application is illustrated in Figure 35. The movement of the motorized ball-screw of the step motor causes the application of a load on the top ring. Given the fixed position of the bottom ring and the 120° separation between the contacts, the load applied to the top ring is transmitted to the bottom rings so that each contact sees the same load. The load is gradually increased during the initial step to finally reach the designated load for the running test. A strain gauge is attached on the loading arm for measuring the load continuously. Friction is measures by mean of a torque meter, located on the roller shaft.

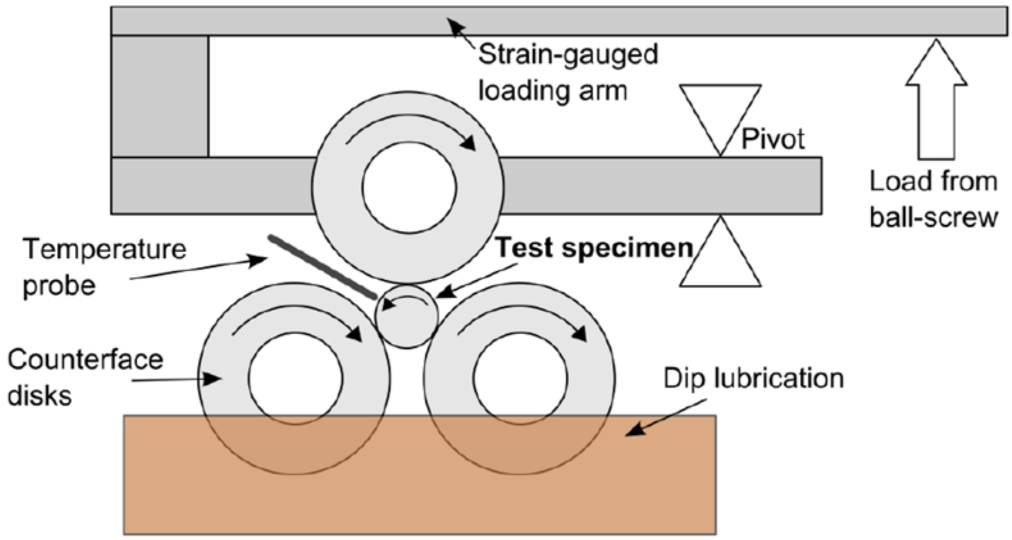

Figure 35 Schematic of the loading system of the rig

The rig contains an accelerometer screwed into the test housing and it is possible to automatically stop the test when a threshold value of vibration signal is reached. This usually indicates the presence of a macro-pit if the vibration signal varies abruptly, or it can also be representative of an excessive amount of debris in the chamber; in this latter case, level of vibrations will increase gradually. Of course, the test can also be stopped manually via the control software.

4.2 Description of test specimens

A set of specimens for each test consists of one roller and three rings. Different geometries of rings and roller are used in the present work to change the contact geometry accordingly with the purpose of studying the effect of different pressure distributions, varying from line to elliptical contact configuration. In this regard, three different set-up configurations of specimens are adopted in this work:

- Flat rings on a 1 mm chamfered roller, which give line contact
- 80 mm crowned rings on a flat roller, which give elliptical contact
- Flat 3 mm chamfered rings on a flat roller, which give line contact

In all three cases, the overall dimensions of rings and roller in the plane of rolling are the same, the diameter of the rings being 54.15 mm and the roller diameter being 12 mm. A schematic representation of the geometry of the three configurations is illustrated below in Figure 36, Figure 37 and Figure 38.

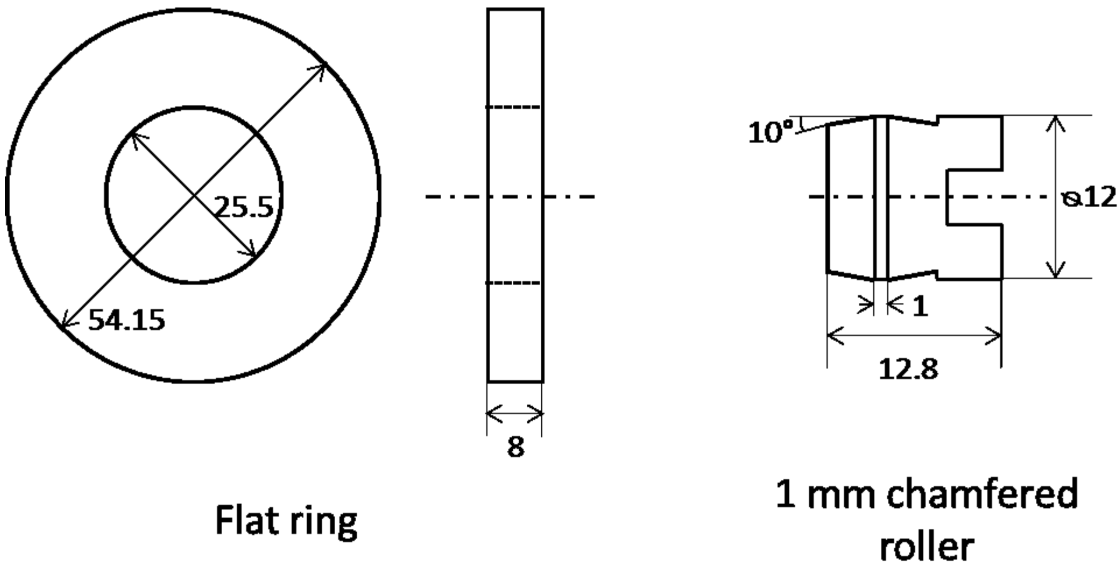

Figure 36 Line contact configuration: flat ring on 1 mm flat roller

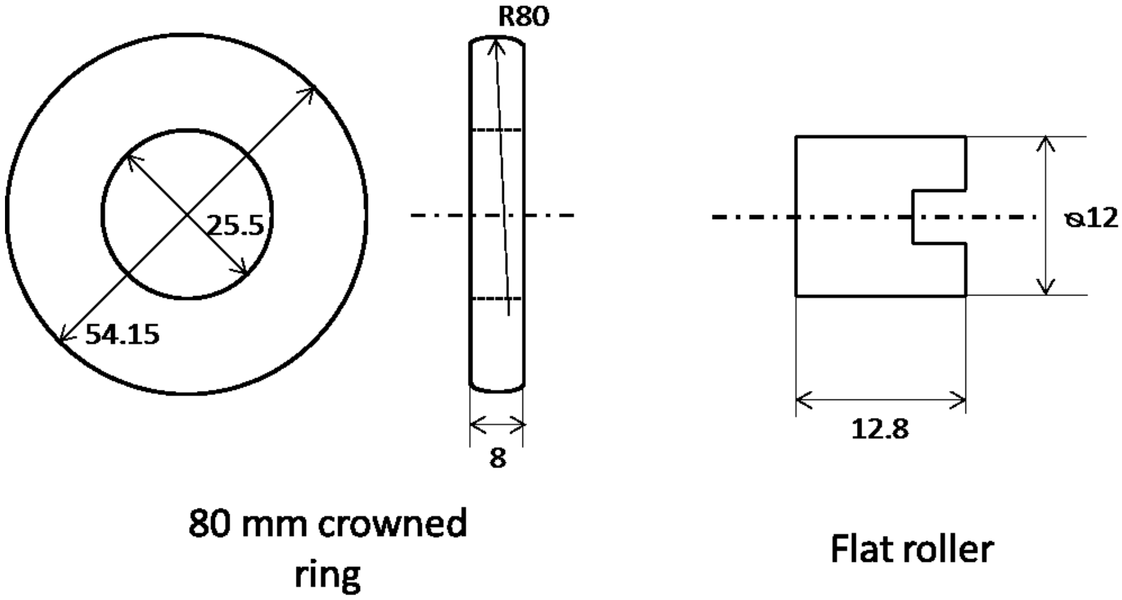

Figure 37 Elliptical contact configuration: Crowned ring on a flat roller

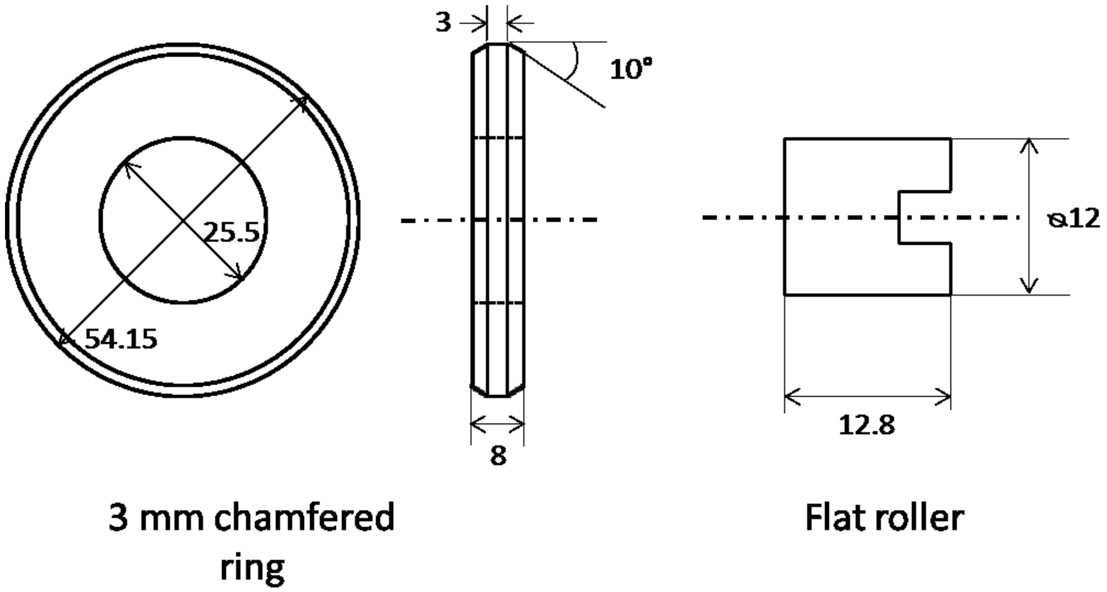

Figure 38 Line contact configuration: 3 mm chamfered ring on a flat roller

As seen, the third set-up of specimens, i.e. chamfered rings on a flat roller, corresponds to the same type of line contact configuration as the one with flat rings on a chamfered roller. Nevertheless, the chamfered rings on a flat roller were employed here in a few tests for a specific purpose of confirming some interesting observations; the details of this are explained in Chapter 5, when results of the tests will be presented.

Here, it is important to notice the different aspect of pressure distribution in the case of line and elliptical contacts. These are illustrated in Figure 39 below.

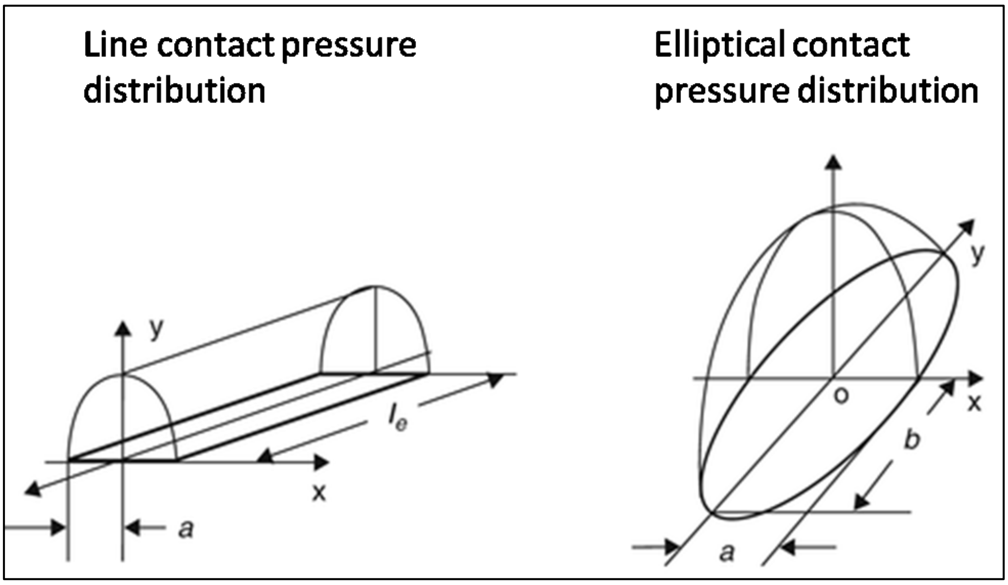

Figure 39 Pressure distribution in line and elliptical contacts

The main difference between the two configurations is the way the pressure is distributed along the direction transverse to rolling: in the line contact, Hertz pressure profile is uniform in this direction, whereas in the elliptical contact pressure has a semi-elliptical distribution in this direction as well as the rolling direction, with its maximum at the centre of the contact area and being zero at the boundaries.

All the specimens are manufactured from AISI 52100 steel, through hardened, vacuum arc remelted at a temperature of 820 °C, subsequently quenched and then tempered for 3 hours at a temperature of 150 °C. Chemical composition and mechanical properties of this material are listed in Table 1 and Table 2.

Table 1 Chemical composition of specimen material, AISI 52100 steel

Chemical compound	C	Cr	Si	Mn	S	P
Weight %	1.05	1.5	0.3	0.35	0.015	0.015

Table 2 Mechanical properties of AISI 52100 steel

Mechanical property	Value (units)
Density	7850 (kg/m3)
Young modulus	210 (GPa)
Poisson ratio	0.3
Thermal conductivity	41 (W/mK)
Specific heat capacity	0.46 (J/gK)
Hardness of rings	750 (HV)
Hardness of roller	700 (HV)

As indicated in the table above, the hardness of the counterface rings and the hardness of the roller differ from each other. The specimens were hardened and heat treated in such a way that rings resulted in deliberately higher hardness value than the roller. This causes the final failure always to occur in the roller, which represent the actual test specimen of the test. This also means that the ring surface is worn very little during the tests helping to ensure consistent conditions throughout (this would be even more important in micropitting tests).

Surface roughness of all samples is measured prior to each test using a stylus profilometer. Average nominal root mean square roughness for rollers and rings are obtained as described in 4.5 and are equal to $R_{q,roller}$=0.172 ±0.015 µm and $R_{q,rings}$=0.162 ±0.014 µm respectively. The chosen finishing process produces roughness with lay orientated in the rolling direction on all specimens, not unlike the roughness structure in real rolling bearings.

Some consideration can be made regarding the cleanliness of the steel adopted in this research as provided by PCS. Non-metallic inclusions are clearly observed when roller specimens are sectioned. Figure 40 below shows as an example of the presence of these inclusions. These inclusions mostly look circular in the circumferential section of the roller and appear, as evident from the figure, elongated along the axial direction of the specimen; this is due to manufacturing process, as roller specimens are produced from rolled bar stock.

Figure 40 Microstructure of the steel adopted in the present work is shown in a section parallel to the main axis of the roller. Presence of numerous carbides and non-metallic inclusions is reported

4.3 Test oils

In this research four kinds of oils have been used in the tests and they are listed below in Table 3.

Table 3 Lubricants in current tests and their properties

Lubricant	Measured viscosity (cSt)	Measured density (kg/m^3)

	@40°C - @100°C	@40°C - @100°C
75W80 Transmission commercial oil	66.6 – 9.7	864.4 - 826.9
SAE 40 Mono-grade diesel engine commercial oil	120.5 – 13.1	880.1 - 843.1
PAO [+ ZDDP (0.1% P, in weight)]	66.1 – 11.6	817.9 - 781.1
Group I mineral oil [+ ZDDP (0.1% P, in weight)]	15.1 – 3.4	842.4 - 803.7

The viscosity and the density of the various lubricants adopted for this research are indicated in the table. Those properties were measured by means of an SVM Stabinger Viscometer.

The first two oils in the list are fully formulated commercial oils. Hence their additive formulation is largely unknown. They are used in this study as they have been suggested to promote the formation of WECs. The transmission oil in particular, is the one that is referred to as 'WEC critical' or 'low reference' oil in literature.

However, since this research aims to establish the physical mechanisms of WEC formation, the use of fully formulated oils with largely unknown additive package is not acceptable. Instead, the use of model oils with fully known formulations is required. With this in mind, the last two oils listed in the table are pure base poly-alpha-olefin (PAO) and base Group I mineral oil. These have been used with addition of a little amount of ZDDP anti-wear, which gives 0.1% phosphorus in mass; this was done in order to avoid excessive wear during the test, preventing this competitive mode of damage to take place over pitting failure (the importance of which was described in detail in the previous chapter on experimental design). Furthermore, a few additional tests with pure (i.e. no ZDDP) PAO oil and pure Group I mineral oil have also been conducted and presented.

4.4 Experimental Procedure

4.4.1 Cleaning of specimens and rig prior to testing

Prior to starting a test, all the assembly components of the chamber and the specimens are ultrasonically cleaned for 10 minutes separately in toluene and isopropanol, then dried. While this process takes place, the chamber is subjected to an hour of "flushing" with the oil to be used in the test. This is done in order to remove traces of lubricants used in the previous test. Particular attention was made in this regard when carrying tests concerning the effect of additives on WEC formation, in order to always be sure that the residual lubricant was completely washed out from the chamber before running another test. This was assured by repeating the flushing steps for two consecutive times and carefully wiping the inner walls of the test chamber with standard industrial paper. If a particular test has produced considerable amount of damage, like wear or micro-pitting, it is, in this case as well, a good practice to repeat the flushing process twice. It should be noted that isopropanol solvent is also used after flushing, wiping walls of the test chamber, preventing contamination of the new test lubricant.

4.4.2 Test procedure

The three rings and the test roller are assembled in the test chamber. The test chamber is then filled with the desired oil. The test load, ring and roller speeds and test temperature are set at desired value. The choice of these values takes into account the considerations of friction coefficient and lambda ratio with different oils and SRRs as described in the previous chapter.

The test starts with heating up the oil via the control loop in the rig software. During this time the rings and the roller rotate at the same speed under zero load, to uniformly lubricate the chamber and accelerate the heating process. The heating step always takes place at the desired constant entrainment speed. Afterwards, the load is applied at a uniform rate over one minute. Then the sliding speed is applied by the electric motors to roller and rings.

In general, the MPR tests can be run until failure, i.e. until a final pit is formed on the surface of the specimen, without further input from the user. This event induces in the rig a peak in the vibration level, which can be easily detected by the accelerometer. An example of pit detection due to increased level of vibration/acceleration in the test chamber is shown in Figure 41 below. However, in the present study, in order to more closely study the progression of damage and attempt to ascertain what is going on in the contact, the roller is normally inspected after the first 2 million of rolling contact cycles using optical microscopy in order to note if undesired conditions are happening on the surface, such as excessive wear, oxidation, scuffing or micro-pitting. In addition, in a number of cases tests were interrupted at a series of further intervals before failure and roller and disc specimen surface inspected visually or using a profilometer. The details of this and the relevant observations will be discussed in the following chapter.

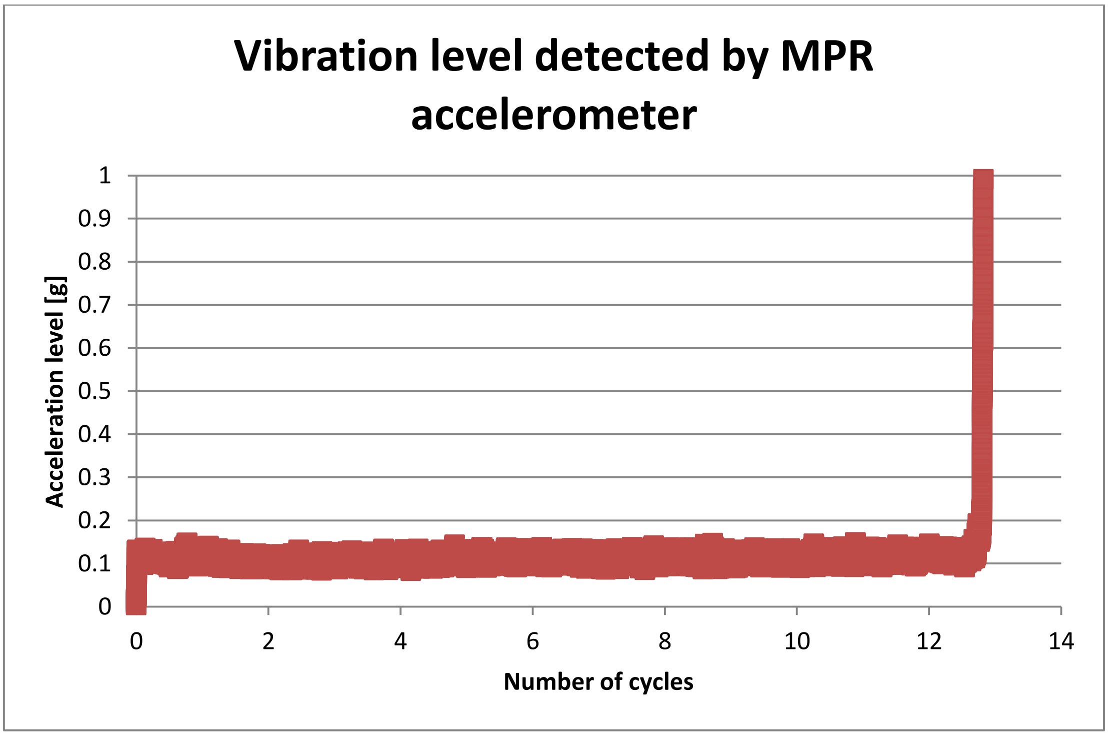

Figure 41 Example of pit detection due to increased level of acceleration in the MPR chamber. Data extrapolated from the MPR software

4.5 Post-test inspection of specimens

After the test is finished, the roller surface is inspected using various analytical techniques, and subsequently sectioned, polished and etched for further analysis.

At the end of the test, the roller is analysed under an optical microscope to take photos of the final pitted surface. The whole circumferential running track of the roller is observed using a custom built dial mounted on the microscope stand. The next inspection of specimens consists of measurement of the roughness of all the rings and roller. This is done by means of a stylus profilometer (Form Talysurf Series 2). A diamond stylus, having a tip of 2.5 µm radius, traverses the surface of the specimen and its vertical movement is converted in an electrical signal which is then amplified by the gauge. This signal is then fed into a PC for analysis, providing a rough profile of the surface which is subsequently filtered to obtain information about its roughness, waviness, and primary characteristics. For the rings and roller, the value of R_q is considered for estimating the lambda ratio of the tests. Three measurements are taken per each ring and four are taken for the roller. Final value of roughness is obtained for both rings and roller by averaging those measurements.

Next, a series of sections of the roller specimen are prepared. In most cases, circumferential sections (plane parallel to rolling direction) were prepared but in some instances roller was also sectioned axially. The roller is first embedded in bakelite. This process lasts for 7 minutes at 150°C. Afterwards, the specimen is cooled down for 4 minutes. Those are the minimum values of time and temperature allowed by the mounting press for the resin to cure properly. Once the specimen is mounted in the resin, a rough grinding disc is used to reach the desired section of the roller for analysis.

This is done as an alternative to the use of cutting blades, which could cause overheat of the steel and hence, alteration of the final microstructure after the test. The process of grinding is constantly cooled with flushing cold water, so that the steel is never subjected to overheat. After grinding, the polishing procedure takes place. This process is made in three different steps using diamond particles suspensions respectively of 9 μm, 3 μm and 0.05 μm in size. After polishing, the specimen is then etched with Nital, a solution of methyl alcohol and 2% volume of nitric acid. The etching process reveals the characteristics of the microstructure. Figure 42 shows an example microscope image of a roller section after etching. The etchant highlights the particular microstructure of the steel. In this case, the lath path of the martensite grains is visible, together with presence of carbides and non-metallic inclusions.

Figure 42 Example optical image of an etched specimen cross-section. The etchant brings in evidence the microstructure of the steel, made of lath martensite, primary and tempered carbides and possible non-metallic inclusions

Finally, after etching the specimen is again observed under optical microscopy, detecting the cross-section damage and possible microstructural alterations. A series of circumferential sections of the roller are prepared at different axial positions, starting from one edge of the contact track and moving towards the other edge of the contact track. The grinding and polishing processes serve to reach a desired section of analysis; in the case of the standard chamfered specimen, the sections which are of an interest for the analysis span over the range of the 1 mm track, which can be seen in a schematic representation of the roller in Figure 43. When starting to look for white etching cracks after the test, one always starts from the section corresponding to the first edge of the track, then proceeding towards the centre of the track, eventually until the second edge is reached. Distance from one section to another generally varies between 50 to 150 μm.

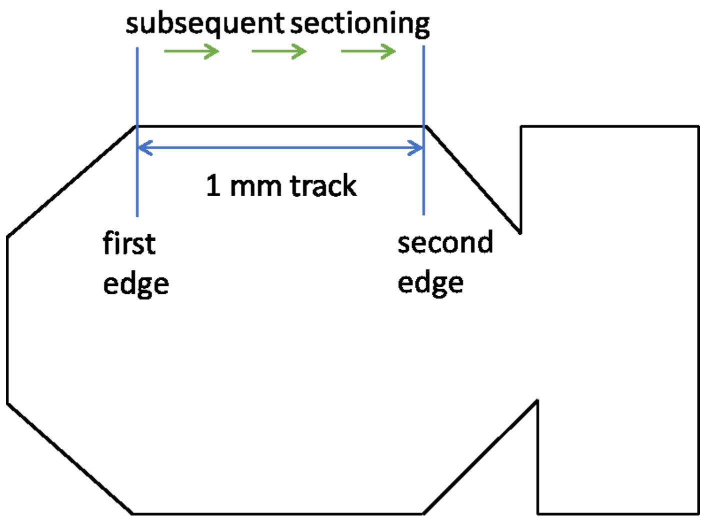

Figure 43 Schematic representation of the chamfered roller. The specimen is always sectioned starting from the first edge of the track, then proceeding towards the centre, until the second edge.

Optical images of circumferential sections of the roller generally are illustrated in the present work showing the surface of the roller and the etched subsurface, which may or may not contain damage or cracks. Direction of friction and contact motion is indicated as appropriate. When the surface of the roller is contained in the optical photograph, a black part is also generally visible on the bottom of the picture: this is the black resin in which the specimen has been embedded (see Figure 44).

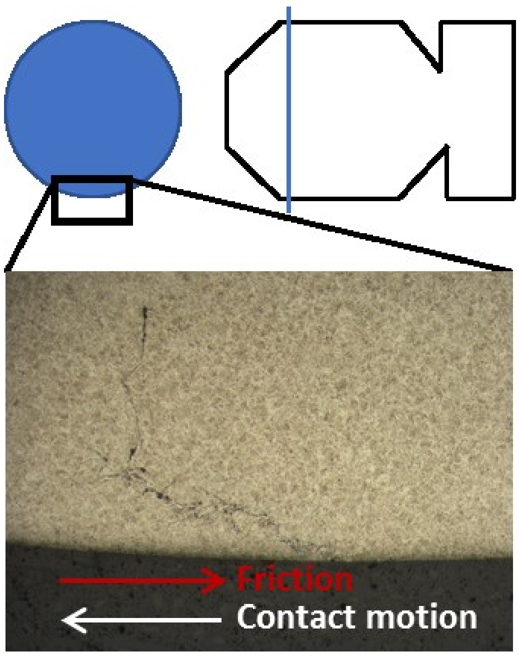

Figure 44 Typical circumferential section of the roller specimen

In order to analyse the particular microstructure alterations in more depth, TEM microscopy has also been utilised in the present study, using a FIB technique for sample preparation and subsequent X-ray diffraction. Given the costs and time needed for TEM analysis, only selected roller samples were subjected to this additional inspection. Details of this analysis will be provided in the following chapter.

4.6 **Conclusions**

The description of the triple-disc rolling contact fatigue test rig (MPR) and the specimens adopted for this study has been presented in this chapter. The controlled operating conditions and the way they are applied by the rig have been explained. The test oils and the sample preparation is also given, together with the description of practical procedures prior and posterior to testing, including, preparing, cleaning and testing sequence. Finally, the method of inspection of specimens is presented.

Experimental results of this work obtained on the MPR rig are systematically shown in the next chapter.

5 Results: triple-disc contact fatigue tests

In this chapter the main MPR fatigue test results of the present study are presented. The list of results starts with presenting the effect of the most important tribological parameters claimed to play a role in WEC formation. The different lubricants were first employed to evaluate their influence on the phenomenon of white etching cracks. Afterwards, SRR, nominal pressure and lambda ratio were also considered. Finally, contact configuration is analysed. In this regard, line and elliptical contacts are compared. The set of results involves the analysis of one parameter at a time, and it generally consists of presenting optical images of tested specimen surfaces, followed by analysis of etched and polished cross-sections to show whether or not the test produced white etching cracks under the given conditions. An example specimen is also analysed by means of a FIB-TEM technique, which provides more insight about the characteristics of microstructural changes produced after testing on MPR. Following this chapter, an additional set of results from reciprocating rubbing tests is presented in Chapter 6 to provide further insight into some of the observations made here.

5.1 Preliminary experiment to confirm feasibility of producing WECs on the MPR rig

A total amount of 65 tests in different rolling contact conditions were carried out in the present study, a selected number of which is presented in this chapter.

In order to confirm whether white etching cracks can be reproduced on the triple-disc MPR rig, preliminary tests were first run. Based on the findings in the literature, white etching cracks are thought to form when bearing is operating under relatively harsh conditions of low lambda ratio (mixed regime) and relatively high slide-roll ratio. The maximum nominal contact pressure in wind turbine gearbox bearings on the other hand is relatively moderate in the region 1.5 to 2 GPa. Therefore, the conditions for the preliminary tests were chosen accordingly and are listed in the list below. The contact configuration adopted is the standard specimen geometry of the MPR, i.e. line contact obtained with flat rings on 1 mm flat chamfered roller. This contact configuration is known to produce high edge stresses due to truncated line contact and is not usually used at Imperial College for pitting tests (crowned rings and elliptical coanct being preferred for such studies [18]). However, in this case, the effect of such stress concentrations was considered to be potentially significant in relation to WEC formation so the standard specimens with line contact were chosen. Parameters for the preliminary test are listed as follows:

- Load: 500 N
- SRR: 30% (roller slower)
- Test temperature: 100 °C
- Entrainment speed: 1 m/s

The reader is reminded that positive sliding in the present definition (in line with definition used in the MPR software) means that the roller test specimen is slower than the counterface rings. Given the load and the geometry of the specimens, the contact semi-width in rolling direction is 165 μm. The track width in transverse direction is of course 1mm owing to the specimen geometry. The resulting maximum Hertz pressure in the contact is equal to 1.93 GPa. Depth of maximum shear stress is 130 μm from the contact surface. The fully formulated transmission oil described earlier was used in these preliminary studies as they have been suggested to promote WEC formation.

The friction coefficient measured over the initial part of the test, corresponding to 0.5 million cycles is equal to 0.087. The average value of friction coefficient over the test duration was 0.083, less than 5% lower than the initial value. Given the initial value of friction coefficient and the other parameters of the test, using the MPR thermal model described previously, the calculated inlet temperature is equal to 118 C° (T_B), which gives a minimum film thickness of 34 nm and the resulting lambda ratio of 0.13. In the following tests presented in this study, given the small difference between initial and average friction (within 5-10%), initial value of friction is reported and used for film thickness evaluation (considering the average friction coefficient would give very similar values of lambda ratio with a change only in the second decimal place).

The roller specimen pitted after 23.3 million cycles. Figure 45 is an optical photograph that shows the final surface of the roller at the location of the produced pit.

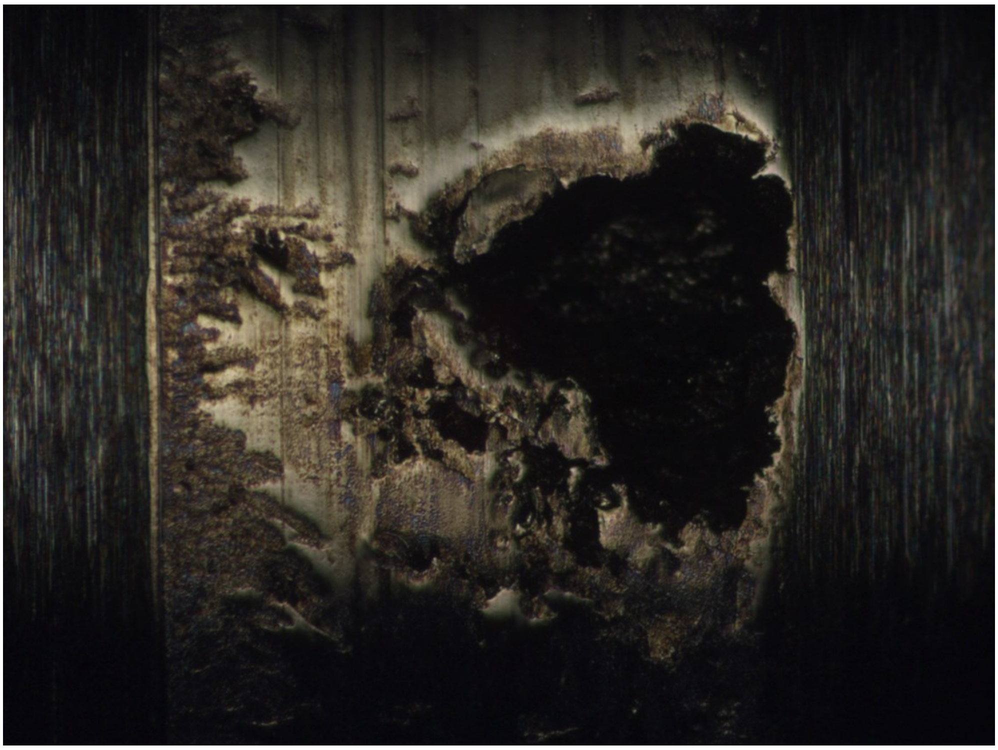

Figure 45 The pitted surface of the roller after 23.3 million cycles in the preliminary test with commercial transmission oil.

At the end of the test, the specimen was ground, polished and etched as described before.

Selected roller sections are shown below in Figure 46; they are all at a location between 100:200 µm from the first edge (see Figure 43) of the roller running track.

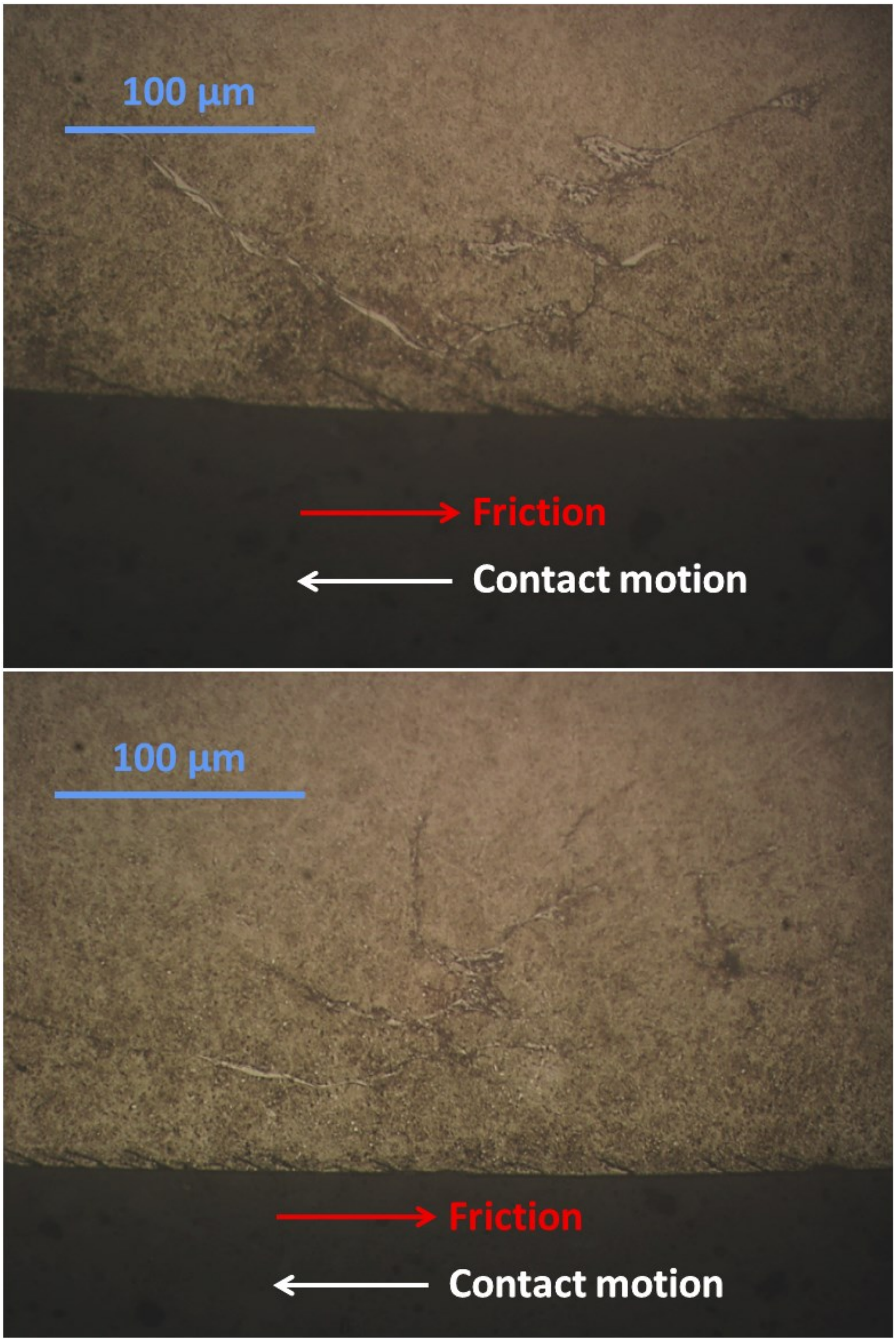

Figure 46 Selected sections from preliminary test with commercial transmission oil. Sections correspond to the initial 100:200 µm of the running track. WECs are observed

As visible in Figure 46, many cracks are present at the end of the test. Some of them are short and surface-breaking cracks while other cracks seem not to be directly connected to the surface. Definitely, the most important characteristic evidenced in these images is that many cracks do indeed show white decorations similar to those from failed bearings from the field, i.e. the MPR can successfully reproduce white etching cracks.

The results of this preliminary testing were promising and, although at this early stage it was not possible to make any significant conclusions about characteristics of produced WECs only, the conditions adopted here are obviously suitable for re-production of white etching cracks and for this reason they were adopted for further tests, results of which are shown in the following section.

5.2 Influence of lubricant composition on WEC formation

The first parameter to be analysed in terms of its potential influence on WEC formation was the lubricant composition. As was shown in the literature review section, lubricant composition is commonly claimed to be a significant, or even the primary, factor in WEC formation. This hypothesis will be examined here. Table 4 lists the tests performed for analysis of lubricant composition and their conditions.

Table 4 Test conditions for analysis of lubricant composition

	TEST 1	**TEST 2**	**TEST 3**	**TEST 4**
Lubricant	**Formulated Transmission Oil 75W80**	**Formulated Engine Oil monograde, SAE 40**	**PAO 11** **(+ZDDP, 0.1%P)**	**Group I** **(+ZDDP, 0.1%P)**
Viscosity at 40/100 C [cSt]	66.6 / 9.7	120.5 / 13.1	66.1 / 11.6	15.1 / 3.4
SRR %	30	30	30	30
Friction coefficient (initial)	0.087	0.086	0.085	0.082
Max Hertz Pressure [GPa]	1.93	1.93	1.93	1.93
Contact semi-width	165	165	165	165
Lambda ratio	0.15	0.19	0.34	0.11
Test Temperature [°C]	100	100	40	100
Entrainment speed [m/s]	1	1.1	0.45	2.4
Roller cycles to failure (10^6)	23.3	16.6	43.5	31
WECs	YES	YES	YES	YES

All tests run until failure (increase in vibration sensor output on the rig) and the final amount of cycles is reported in the table for each case. Indeed, pitting damage was produced in every roller (see Figure 47). A small amount of micro-pitting damage was also evident in the tests with non-formulated oils. The testing method aims to avoid any significant amount of micro-pitting damage, since it is pitting that is of interest here, by monitoring the roller surface development as needed. With this in mind, it should be noted that an attempt of running a test with PAO oil at the same lambda ratio as other tests produced significant micro-pitting after less than 2 million cycles, so to avoid this the lambda ratio in this case was slightly increased as evident in Test 3 conditions in the table above. However, even this slightly higher lambda ratio is still well into mixed/boundary regime and given that this is only an approximate measure of lubrication conditions the difference is not considered significant.

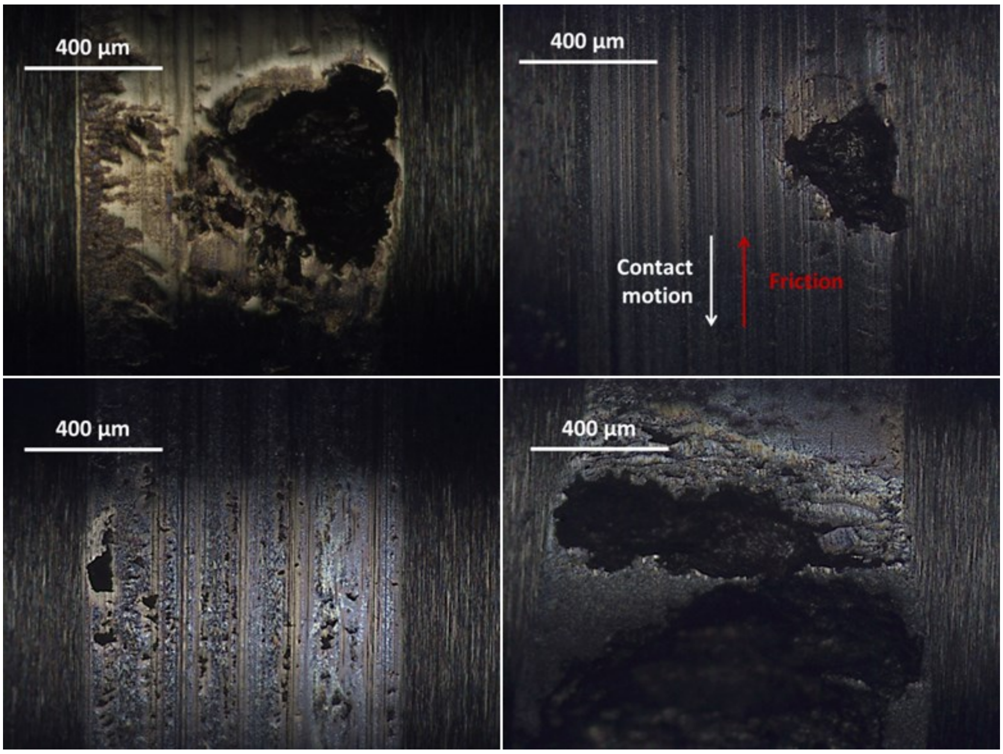

Figure 47 Pitted surfaces of Test 1 (top left), Test 2 (top right), Test 3 (bottom left), and Test 4 (bottom right). Directions of friction and contact are indicated in the photo on the top right and are the same for each case.

Selected polished and etched cross sections in rolling direction from Tests 2, 3 and 4 are shown below, respectively in Figure 48, Figure 49 and Figure 50 (selected WECs from Test1, i.e. the preliminary test, were already shown in 5.1, Figure 46). It is immediately apparent that WECs are found in all tests regardless of the type of oil used. All sections shown here are from the initial 100-200 µm from the same edge of the roller running track.

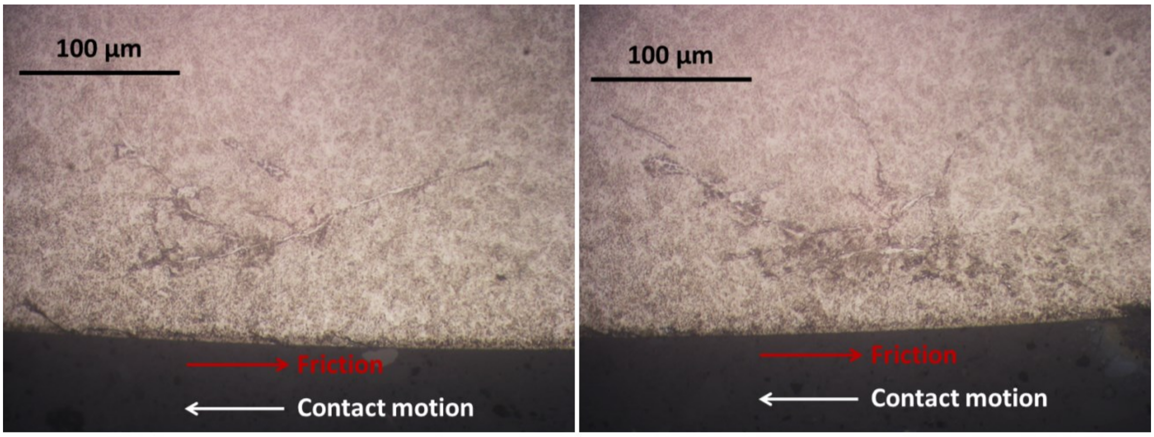

Figure 48 Test 2: WECs produced with engine commercial oil

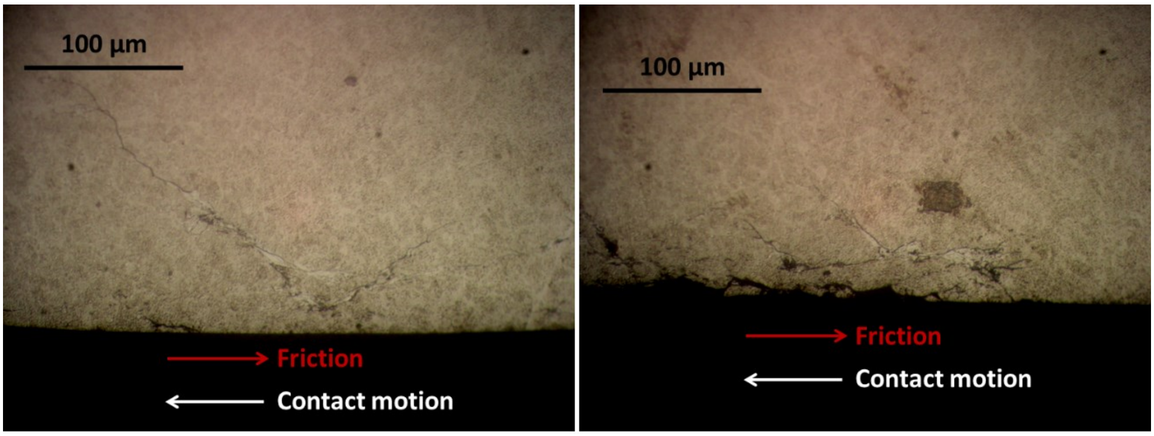

Figure 49 Test 3: WECs produced with PAO + ZDDP

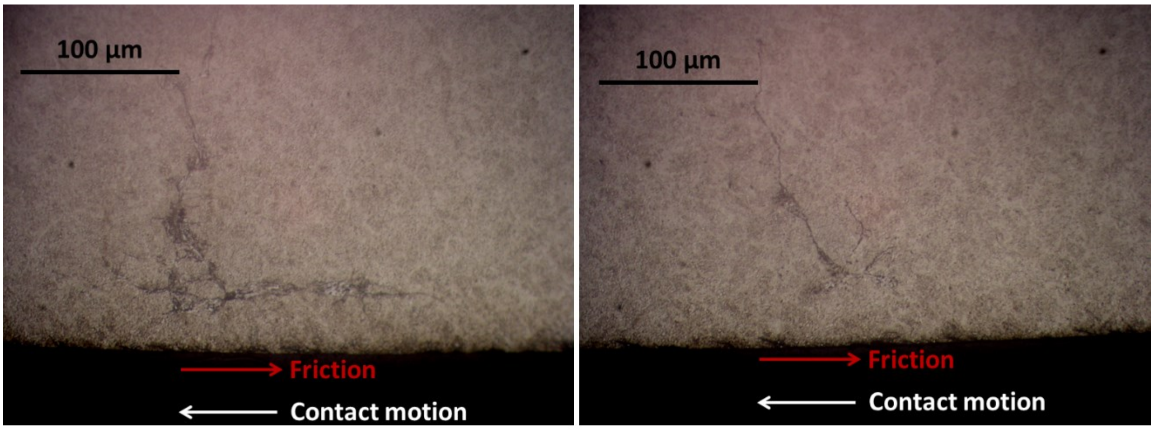

Figure 50 Test 4: WECs produced with Group I mineral oil + ZDDP

5.2.1 Additional tests with pure base PAO oil

The model oils tested here included ZDDP anti-wear additive. This was done in order to prevent excessive wear during the inevitable long fatigue tests, which in turn changes contact conditions (both macro pressure and micro asperity contact pressure change) due to wearing of the roller and ring surfaces. This is discussed at length in the experimental design section and also by other researchers utilising the MPR rig in author's lab [18,28,111].

However, for completeness an attempt was made to run the tests with pure PAO base oil only. To achieve this in a sensible manner, the lambda ratio was increased slightly and slide-roll ratio decreased in an attempt to minimise surface wear. Two tests were run, one at the same pressure as other tests above, 1.93 GPa, and the other at a higher pressure to promote pitting failure over wear. Test conditions are shown in Table 5. In these two tests lambda ratio is increased above the value of 0.6, due to the fact that previous attempts of running with pure PAO oil at lower lambda ratios did not produce pitting failure (see also section 5.2.1 where a comparison between testing with and without ZDDP at lower lambda ratio is presented).

Table 5 Test condition of two tests with pure PAO oil

	Test 5	Test 6
Lubricant	Pure PAO	Pure PAO
Max Hertz Pressure [GPa]	1.9	2.5
SRR	5%	5%
Friction coefficient	0.065	0.065
Test temperature [°C]	65	60
Entrainment speed [m/s]	2.5	3
Lambda ratio	0.9	0.95
Roller cycles (10^6)	180 (micro-pitting)	138 (pitting)

Pictures of final surface and selected etched sections are reported in Figure 51 and Figure 52 for the tests mentioned above.

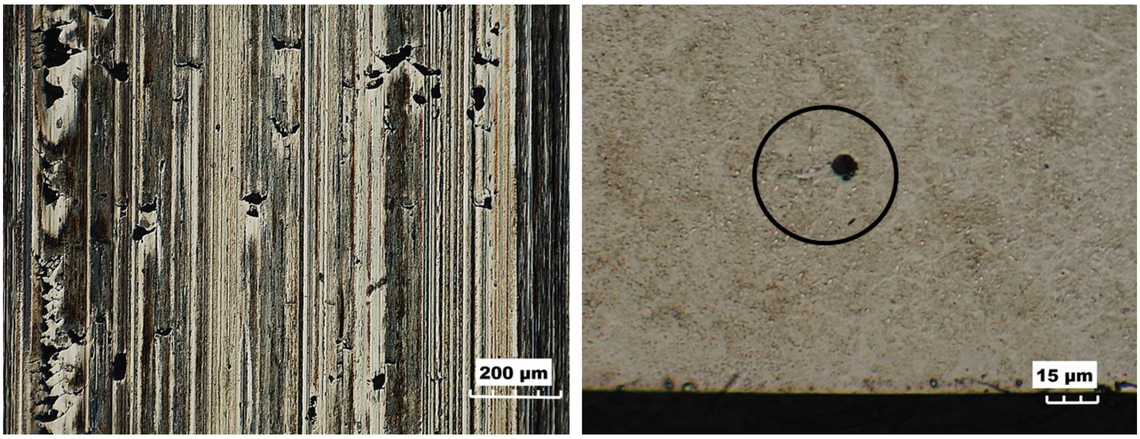

Figure 51 Test 5: final surface (left) after 180 million cycles and sectioned specimen (right) showing presence of a little butterfly

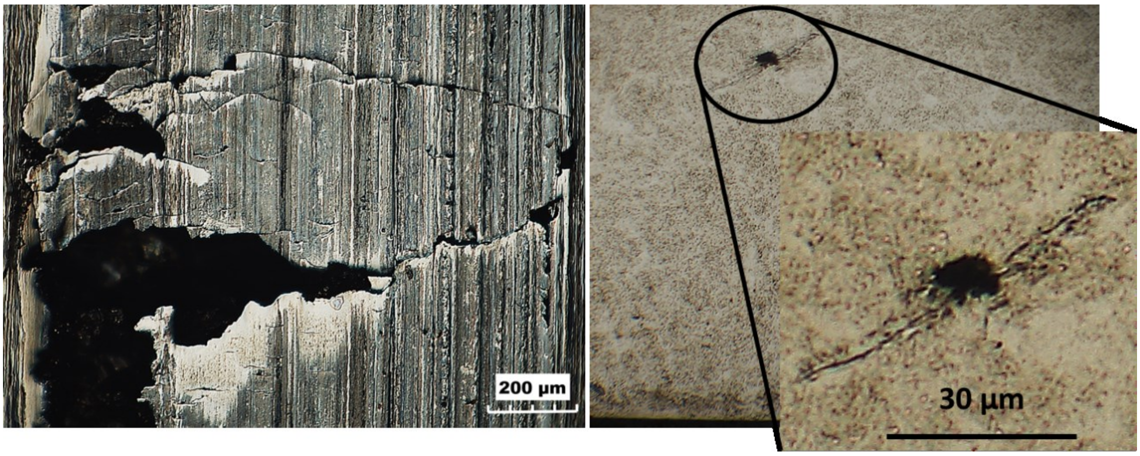

Figure 52 Test 6: final surface (left) after 138 million cycles and sectioned specimen (right); a little butterfly was found also in this case

As can be observes from figures above, Test 5 produced micro-pitting, whereas a pitting failure was obtained in Test 6 which was conducted at higher pressure.

In both cases, WECs starting from inclusions were detected when pure PAO oil was adopted as lubricant. So, it is possible to obtain white etching matter formation also in absence of ZDDP although these are not as extensive and appear to form preferentially around inclusions.

The differences between these tests with pure oil and the previous ones with anti-wear additive are attributed to the evolution of surfaces due to wear in the absence of the anti-wear additive. In particular, the edge stresses that are present in the employed line contact are believed to disappear much quicker in cases with no ZDDP due to rapid wear of the roller and disc surfaces within this edge zone (as also discussed in 7.3.1). To confirm this, further tests were done with PAO + ZDDP and pure PAO where the evolution of the roller surface was followed closely thought the test. Rollers and rings were inspected at the beginning of the test and after 73000, 440000. After this initial inspection, only profiles of the rollers were then analysed until the tests reached a total amount of 20 million contact cycles. The conditions of these tests are reported in Table 6 and results are illustrated below.

Table 6 Comparison between test with pure PAO and test with PAO+ZDDP: test conditions

	Test 7	Test 8
Lubricant	Pure PAO	PAO+ZDDP
Max Hertz Pressure [GPa]	1.93	1.93
SRR	30%	30%
Friction coefficient	0.076	0.070
Test temperature [°C]	78	81
Entrainment speed [m/s]	2.5	2.5
Lambda ratio	0.33	0.33
Roller cycles (10^6)	Up to 20	Up to 20

Tests 7 and Test 8 were carried out at the same lambda which was equal to 0.3. The observations confirm that the evolution of the surfaces is different with and without anti-wear additives as expected, and hence the stress history is very different in the two cases, particularly at the edges of the running track. Test with pure PAO oil did not produce cracks on the running track (see Figure 53). After 20 million cycles damage was present in the form of micro-pits. On the other hand, test with PAO + ZDDP produced cracks starting at the edges already after 440000 cycles and those cracks continued to grow and spread all over the track with increasing running cycles (see Figure 54). It is worth noticing this aspect which will be discussed further later in the thesis as it is of obvious significance to development of cracks in the roller specimens.

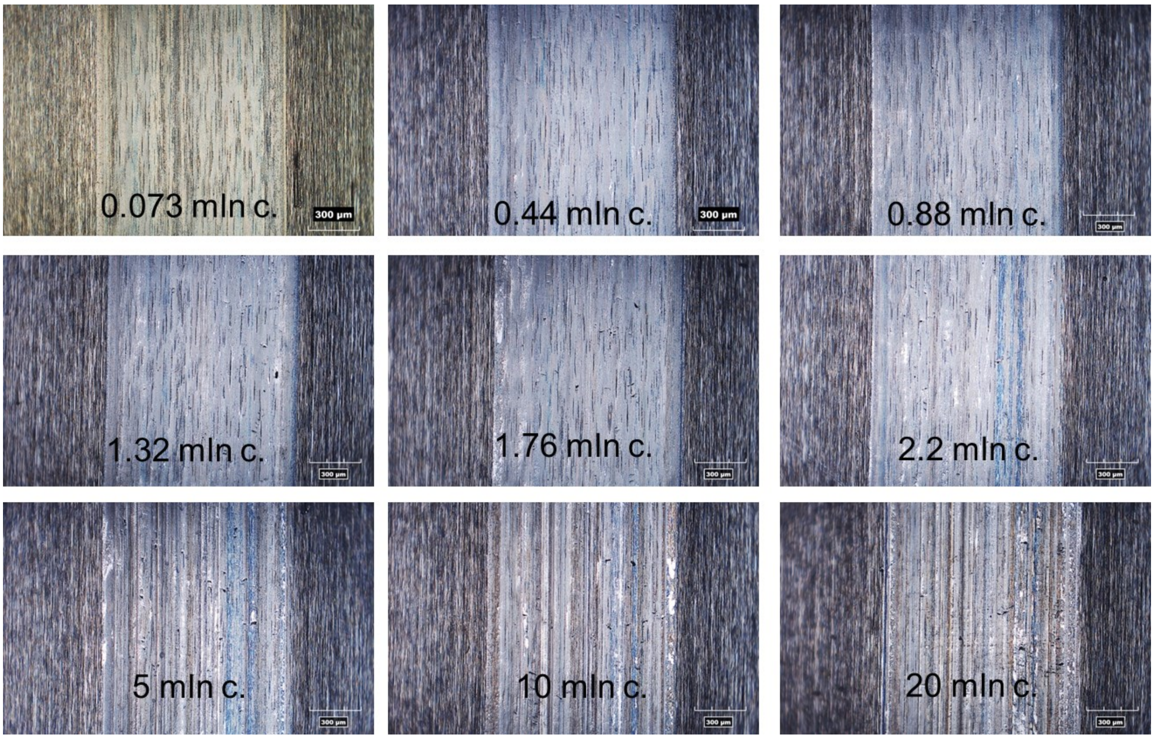

Figure 53 Test 7, pure PAO. A sequence of picture of the test roller is shown after different amount of cycles, indicated in each picture. Little damage in the form of micro-pits is visible after 5 million (mln) cycles

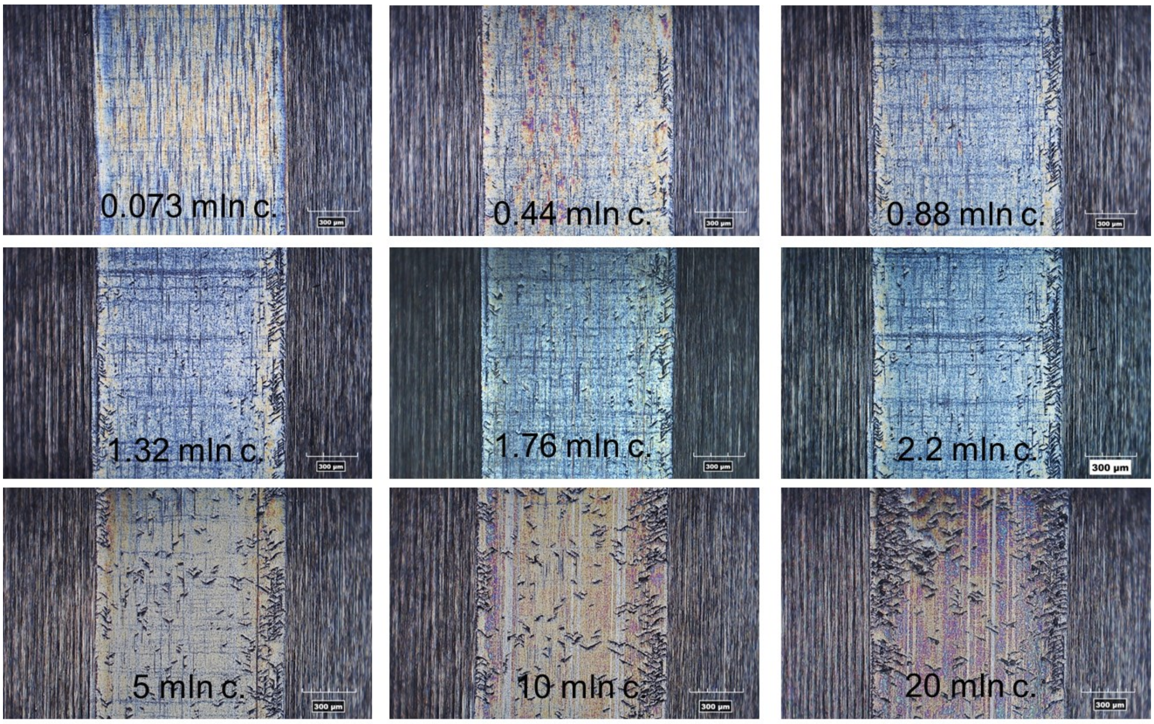

Figure 54 Test 8, PAO + ZDDP. A sequence of pictures at the same intervals as Test 7 is presented. Cracks are visible already after 0.44 million (mln) cycles

5.3 Influence of slide-roll ratio

As suggested from the literature, an important factor to take into account when studying WEC formation is the amplitude and direction of the sliding. Another set of tests is proposed here, varying the amplitude of the SRR from 5 to 30% and considering the direction of sliding as well, by adopting a negative value of sliding, -30%. In the latter case, when sliding is negative, the roller specimen is the driver surface, being faster than the counterface ring. Conditions of tests are reported in Table 7. Since in Test 4 presence of WECs was reported, as already shown previously in the analysis of lubricant composition, this test is here listed again as completeness of analysis for the case of +30 % SRR.

Table 7 Influence of SRR: test conditions

	TEST 4	TEST 10	TEST 11	TEST 12	TEST 13
SRR	30 %	5 %	10 %	20 %	-30 %
Lubricant	Group I (+ ZDDP, 0.1%P)	Group I (+ ZDDP, 0.1%P)	Group I (+ ZDDP, 0.1%P)	Group I (+ ZDDP, 0.1%P)	Group I (+ ZDDP, 0.1%P)
Max Hertz Pressure [GPa]	1.93	2.5	1.93	1.93	1.93
Contact semi-width [um]	165	214	165	165	165
Entrainment speed [m/s]	2.4	2.4	2.4	2.4	2.4
Friction coefficient	0.082	0.078	0.079	0.080	0.080
Lambda ratio	0.11	0.14	0.14	0.12	0.11
Test temperature [°C]	100	100	100	100	100
Roller cycles to failure (10^6)	31	23.9	33	20.4	46.1
WECs	YES	YES	YES	YES	YES

All the tests pitted at the number of cycles indicated in the table. After failure, specimens were analysed as usual. Pictures of sections for the new tests presented here are shown in Figure 55. Direction of friction and contact motion is also indicated for each case. One notes that friction has same orientation as the contact motion in the case of negative slide-roll ratio as already explained previously in 4.1.

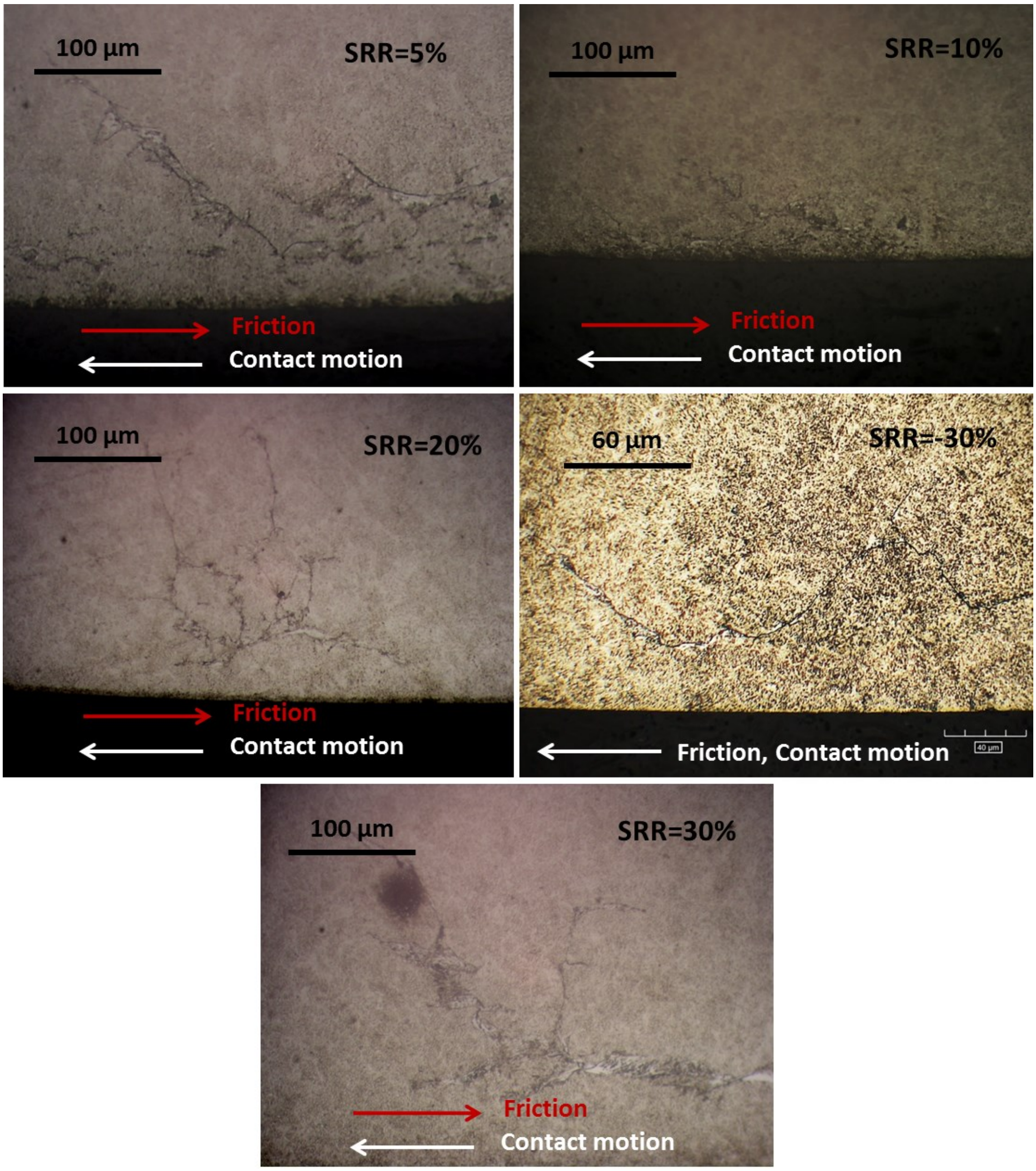

Figure 55 Selected sections from Test 10 (5%), Test 11 (10%), Test 12 (20%) and Test 13 (-30%) and Test 4 (30%). WECs were observed in all the four sectioned specimens subjected to different amount and direction of sliding

As shown in the figure above, WECs are found in each case, regardless of the magnitude or the direction of sliding.

Influence of nominal pressure is treated in the next paragraph.

5.4 Influence of Hertz pressure

This section investigates the effect of nominal Hertz pressure by presenting a new test run at 2.5 GPa, which represents a higher value than the one used for previous tests. For comparison, Test 11 is also reported which was run at the same conditions of SRR and lambda ratio, but at the lower nominal pressure of 1.93 GPa.

Table 8 Influence of nominal pressure: test conditions

	TEST 11	TEST 15
Lubricant	Group I (+ZDDP, 0.1%P)	Group I (+ZDDP, 0.1%P)
Viscosity at 40/100 C [cSt]	15.1 / 3.4	15.1 / 3.4
SRR %	10	10
Friction coefficient	0.079	0.079
Max Hertz Pressure [GPa]	1.93	2.5
Contact semi-width	165	214
Test Temperature [°C]	100	100
Entrainment speed [m/s]	2.4	2.4
Lambda ratio	0.14	0.12
Roller cycles to failure (10^6)	33	12.3
WECs	YES	YES

It was already shown that Test 11 at 1.93 GPa produced WECs. After sectioning, specimen from Test 15 run at 2.5 GPa also revealed presence of WECs just like in Test 11. Figure 56 shows some examples of WECs from Test 15.

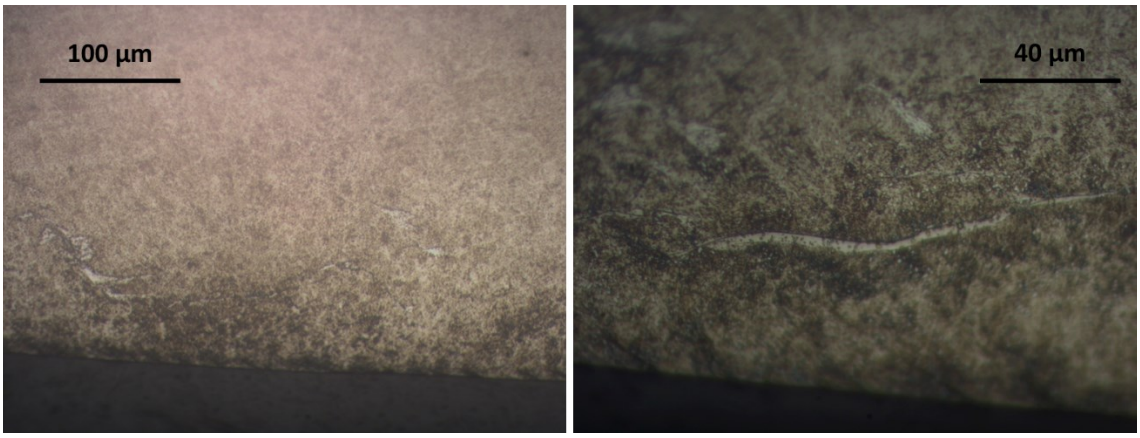

Figure 56 Test 15: WECs observed in the sectioned specimen

Figure 57 and Figure 58 below show respectively WECs from Test 11 and from Test 15. If there is any difference to be noted here, this may be in the extent of WEA and WECs in the two tests. As one can see, the majority of cracks from Test 15 at higher pressure are relatively shorter cracks and tend to be accompanied with less amount of white etching matter. On the other hand, longer cracks were found in Test11 at lower pressure and white etching areas appear to be more wide spread. The duration of the two tests was different; Test 11 pitted after 33 million cycles, whereas Test 15 failed after 12.3 million cycles only, being subjected to a higher nominal pressure. Hence, any cracks would have longer time to grow and rub in Test 15 which may in part explain the differences observed here. A deeper consideration of the effects of pressure, and other conditions, is left for the discussion section of the thesis, whereas this results section focuses on presenting factual results and evidence.

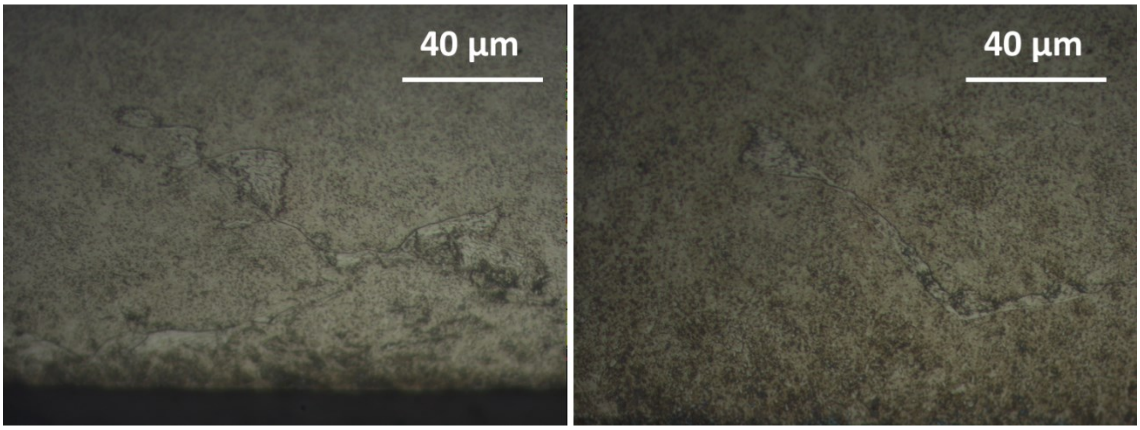

Figure 57 Test 11: WECs show a wider WEA associated with the cracks (if compared with WECs from Test 15 in Figure 58

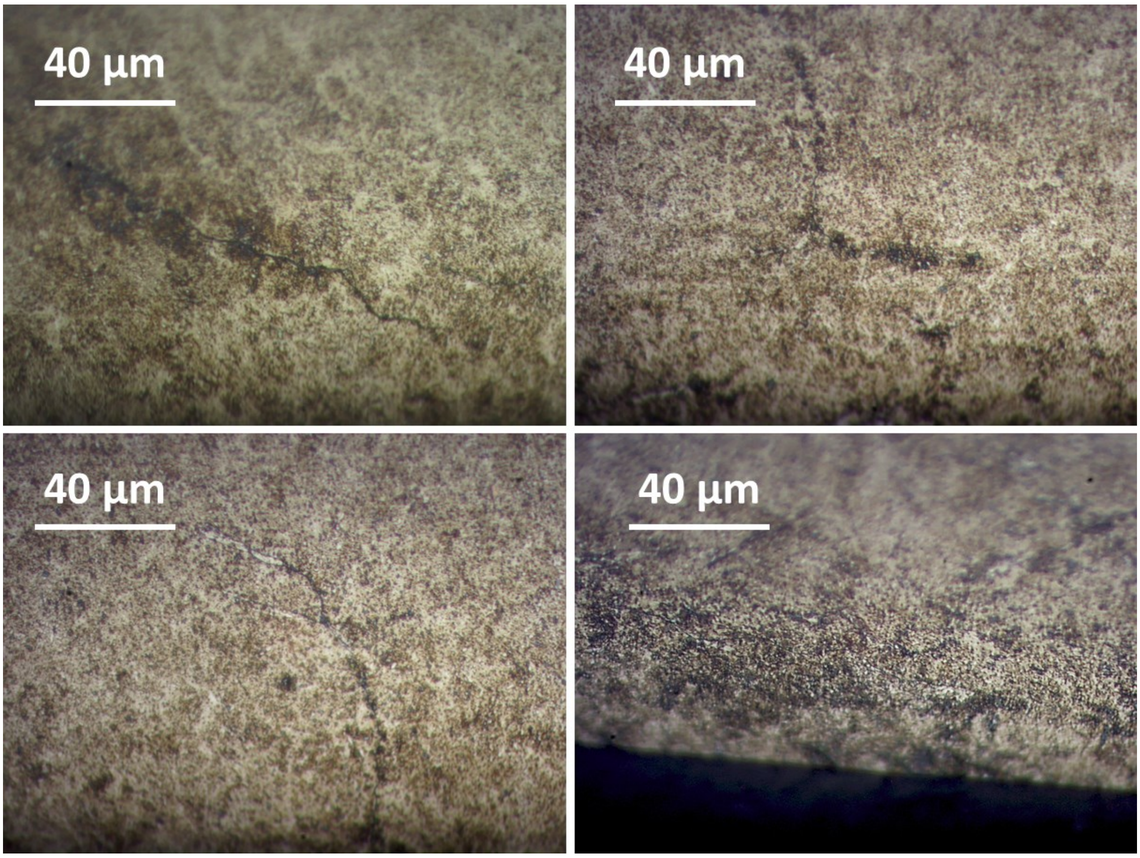

Figure 58 Test 15: the majority of cracks observed in this test is short, presenting less amount of WEA with respect to Test 11

5.5 Influence of lambda ratio

In this sub-section the potential effects of lambda ratio in WEC formation are studied For comparison, Test 3 and test 4 are listed again, plus test 9 at a significantly higher lambda ratio. Conditions are listed in Table 9. Lambda ratio in the three tests was respectively 0.11, 0.32 and 0.7.

Table 9 Influence of lambda ratio: test conditions

	TEST 4	TEST 3	TEST 9
Lubricant	Group I (+ZDDP, 0.1%P)	PAO (+ZDDP, 0.1%P)	PAO (+ZDDP, 0.1%P)
Viscosity at 40/100 C [cSt]	15.1 / 3.4	66.1 / 11.6	66.1 / 11.6
SRR %	30	30	20
Friction coefficient (initial)	0.081	0.078	0.068
Max Hertz Pressure	1.93	1.93	1.93

[GPa]			
Contact semi-width	165	165	165
Test Temperature [°C]	100	40	53
Entrainment speed [m/s]	2.4	0.45	3
Lambda ratio	0.11	0.34	0.65
Roller cycles to failure (10^6)	31	43.5	120
WECs	YES	YES	YES

As one can observe from the table above, the number of contact cycles until failure is higher at higher lambda ratio. This may intuitively be expected; however, given the statistical nature of rolling contact fatigue, no concrete conclusions should be drawn in this respect based on three tests only.

Considering the aspect of WEC formation, it has been already shown that both Test 3 and Test 4 exhibited WECs in their cross-sections. Test 9 ran for 120 million cycles, until a pit was detected; this is shown in Figure 59, which also shows a selected etched section of the failed specimen. WECs were found also in this case of higher lambda ratio. Therefore, at least within this limited lamda ratio range, all within boundary/mixed regime, higher lambdas do not necessarily prevent WEC formation in the present set-up.

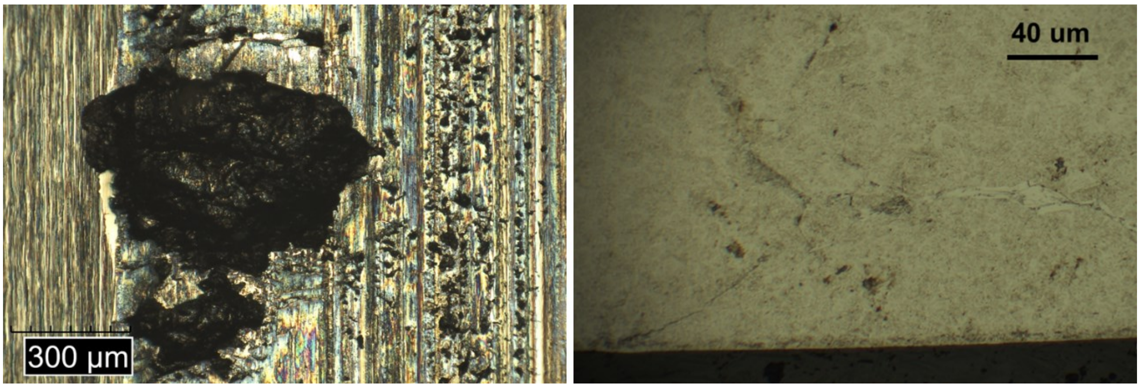

Figure 59 Test 9: final failure (right) of the roller and sectioned specimen (right) showing presence of WECs

5.6 Influence of number of contact cycles

Having established that WECs are consistently generated over a wide range of conditions in the MPR rig, an attempt was made to better understand their initiation and growth over the number of cycles the contact was subjected to. This was particularly important having seen that the development of the surface due to wear and deformation strongly influences crack formation. To achieve this, tests were stopped at 5 and 10 million cycles (i.e. before actual pitting failure occurred) and a series of analysis was performed, including examining the evolution of roller surface profile Conditions employed were the same as in the previous test 4 so that effectively three different values of number of cycles can be compared. Test conditions are listed in Table 10.

Table 10 Influence of contact cycles: test conditions

	TEST 16	TEST 17	TEST 4
Lubricant	Group I (+ZDDP, 0.1%P)	Group I (+ZDDP, 0.1%P)	Group I (+ZDDP, 0.1%P)
SRR %	30	30	30
Friction coefficient	0.084	0.085	0.081
Max Hertz Pressure [GPa]	1.93	1.93	1.93
Contact semi-width	165	165	165
Test Temperature [°C]	100	100	100
Entrainment speed [m/s]	2.4	2.4	2.4
Lambda ratio	0.11	0.11	0.11
Roller cycles	5 (stopped)	10 (stopped)	31 (pit failure)

Specimen were sectioned and etched for analysis. A sequence of pictures is reported in Figure 60 showing the situation found in Test 16, Test 17 and Test 4 with increasing number of cycles. All sections in this figure are from the edge of the roller running track.

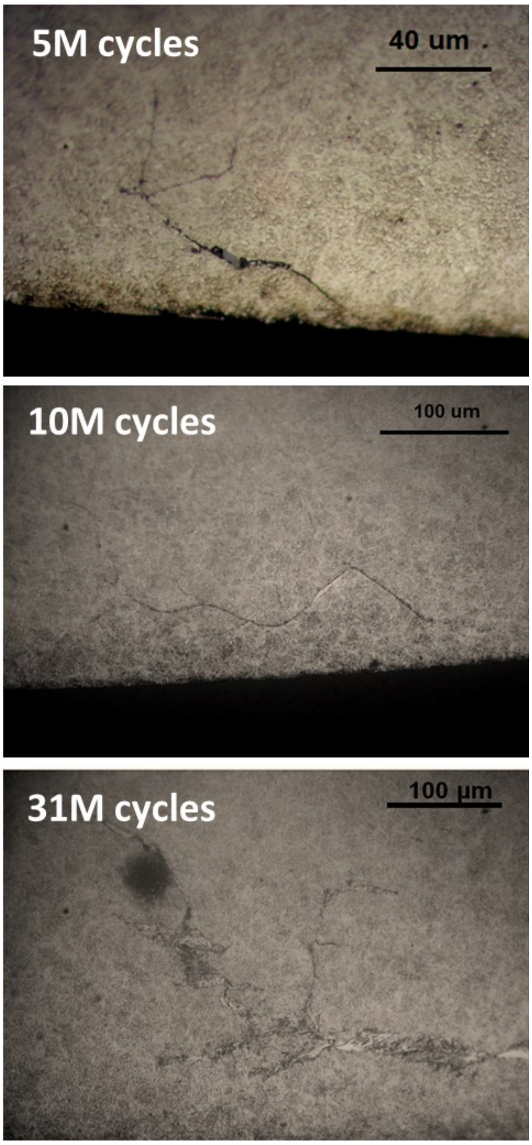

Figure 60 Sequence of pictures showing sectioned specimens (starting from the top, respectively from Test 16, Test 16 and Test 4) after respectively 5, 10 and 31 million cycles. The specimen sectioned at 31 million cycles is after failure, whereas specimens sectioned after 5 and 10 million cycles were sectioned before failure occurred

As visible from the picture, in Test 16, after 5 million cycles only, cracks had already initiated but were relatively short and no presence of white etching area around them is visible. Test 17, stopped after 10 million cycles, had more propagated cracks, and now they were decorated with some white etching areas. Test 4, failed after 31 million cycles, as already shown, produced more branched cracks and extensive WEAs around the cracks are evident.

5.7 Sectioning of the roller at different axial positions within the running track

Consideration of the evolution of roller surface showed clearly that the areas of roller near the edges of the track experience more damage in the early stages of a test. This is to be expected given the stress concentrations that must exist at track edges arising from a flat on flat contact in transverse direction. It was therefore desired to investigate the effect of these stress concentrations in terms of sub-surface damage and crack generation within the different axial position of the roller track. To achieve this, roller sections created at different positions within the 1 mm wide track were created, starting from the first edge and then proceeding towards the centre. Conversely, sections shown up to this point were all from the first 100-300 μm of the track from the edge.

Further sectioning was conducted for Test 1 in order to reach the central part of the running track, i.e. the zone between 400-600 μm from the first edge.

Figure 61 shows a comparison between sections taken at the edge of the track and sections taken at the centre of it, illustrating the different appearance of cracks. other subsurface cracks always at the centre of the running track. As visible from the pictures, cracks at the edge clearly show presence of WEAs along them, whereas cracks at the centre of the track tend to be not associated with white decorations.

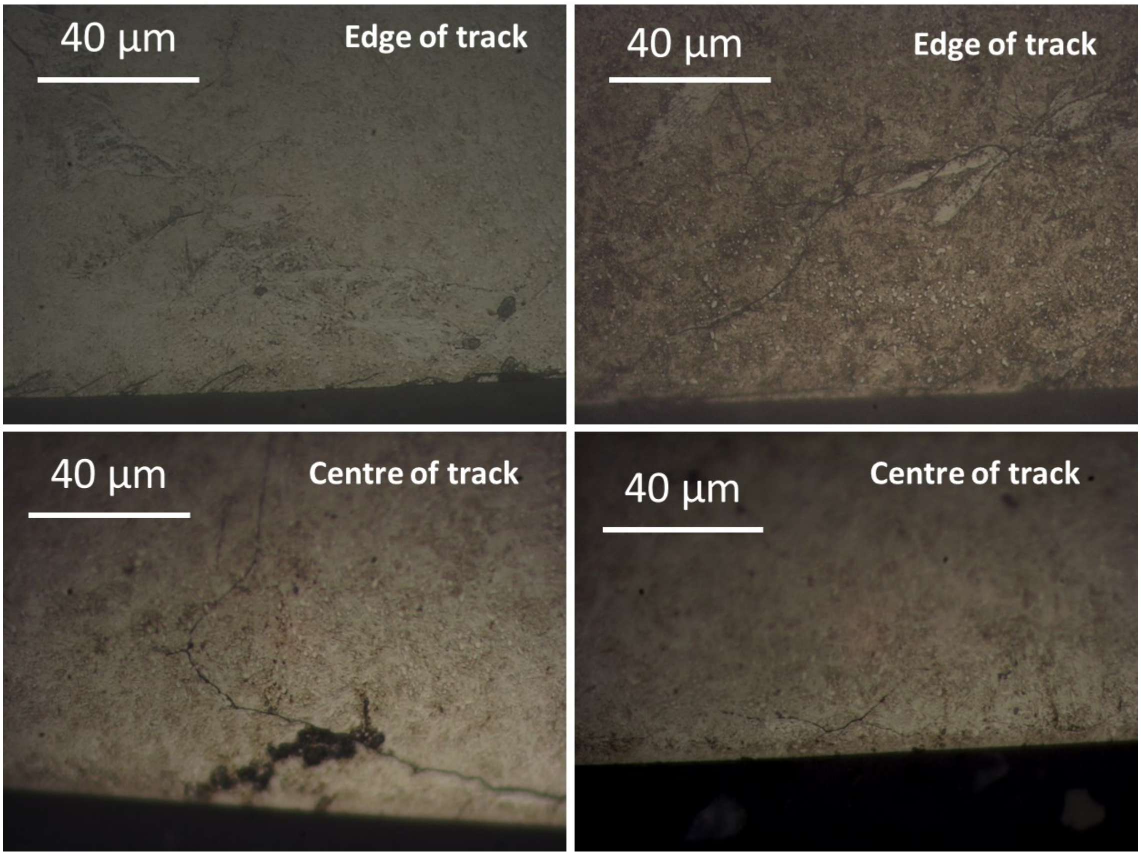

Figure 61 Subsurface cracks at the edge and at the centre of the running track. WEAs are not well-spread in cracks at the centre of the track.

The observation here made, together with others shown in the previous section, regarding the absence of WEAs at a specific location on the track and for a few contact cycles, represent an important aspect in the understanding of WEC/WEA formation and they will be discussed at the beginning of the next chapter.

5.8 Influence of contact geometry (and hence pressure distribution profile)

Tests shown so far utilised a standard configuration of a line contact produced by flat counterface rings on a flat 1 mm chamfered roller. In this section, the pressure distribution effect is taken into account, adopting different specimen geometry, in order to have an elliptical contact. The specimen geometry adopted has been presented in Chapter 4. It is reminded here that the elliptical contact is obtained using crowned rings on a flat roller. Test conditions are shown in Table 11.

Table 11 Pressure distribution: test conditions

	Test 18	Test 19	Test 20
Elliptical contact configuration	80mm crowned rings on flat roller	80mm crowned rings on flat roller	10mm crowned rings on flat roller
Lubricant	Group I (+ZDDP, 0.1%P)	Group I (+ZDDP, 0.1%P)	Group I (+ZDDP, 0.1%P)
SRR %	30	30	20
Friction coefficient (initial)	0.089	0.075	0.077
Max Hertz Pressure [GPa]	1.93	2.8	3.8
Minor contact semi-width	158	235	270
Major contact semi-width	960	1435	492
Test Temperature [°C]	100	100	100
Entrainment speed [m/s]	2.4	2	1
Lambda ratio	0.16	0.1	0.08
Roller cycles (10^6)	55 (test stopped)	55 (test stopped)	10 (Pit failure)
WECs	NO	NO	NO

Test 18 was run at 1.93 GPa. Although the maximum Hertz pressure was the same as in the line contact configuration, the difficulty in this case lied on the fact that it was not possible to produce any crack on the surface of the specimen, even after a considerable amount of contact cycles, as shown in Figure 62.

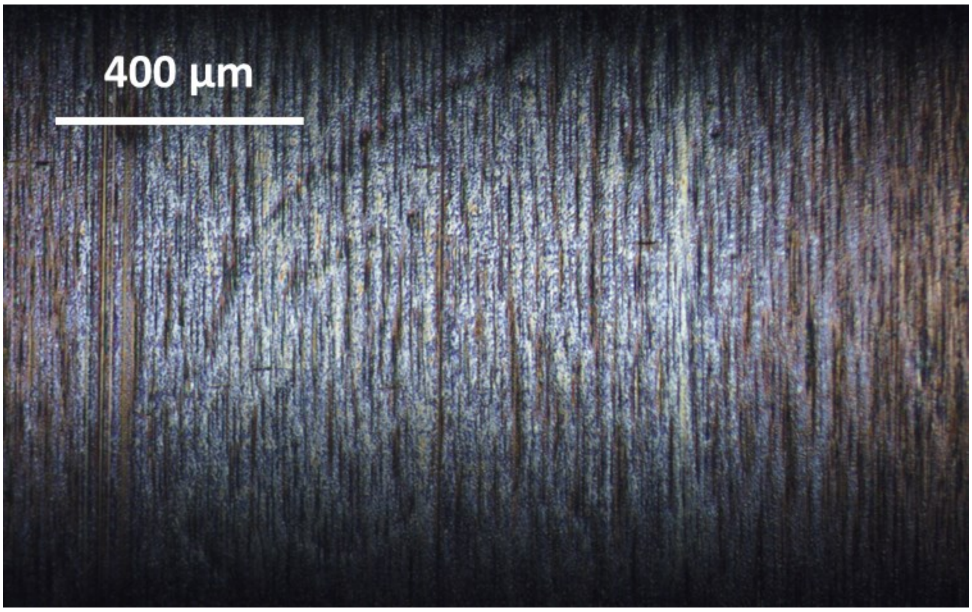

Figure 62 Test 18: Surface of flat roller in elliptical contact configuration. After 55 million contact cycles, the surface is still exhibiting the grinding marks from manufacturing, with no presence of cracks or other sort of damage on the surface

After that, in Test 19 pressure has been raised to the value of 2.8 GPa, so that the medium Hertz pressure of the elliptical distribution is now 1.93 GPa, same as the maximum Hertz pressure used in line contact. This was done in order to account for the different dispersion of pressure along the major axis of the contact area in the elliptical configuration. After the same amount of cycles, no appreciable damage was noticed on the surface. As shown in Figure 63, after sectioning specimens exhibited little dents or micropitting-cracks only, with no presence of WECs.

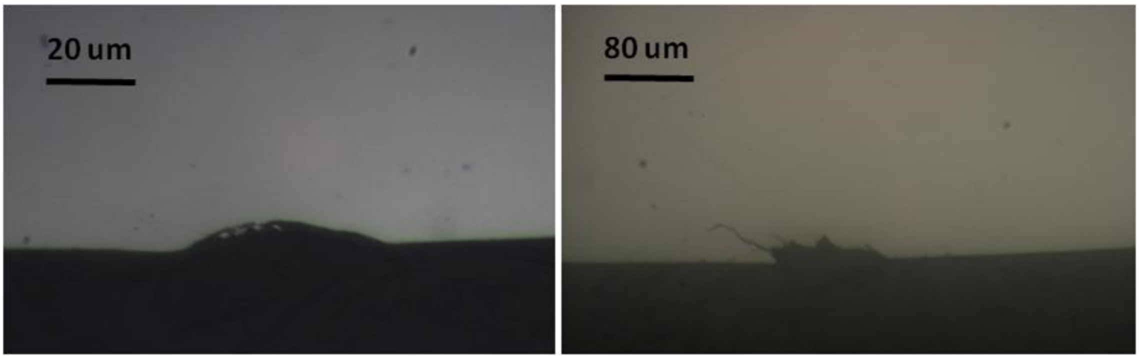

Figure 63 Sections from Test 18 (left) and Test 19 (right). No subsurface cracks were found in both cases. Only surface damage in the form of dents or micro-pitting cracks was detected

With the aim of reproducing a pit failure, pressure was further increased to the value of 3.8 GPa in Test 20. This was done by changing the counterface rings, adopting now 10 mm crowned rings, instead of the previous 80 mm. Failure occurred after only 10 million cycles at this higher pressure. Specimen was sectioned and etched as usual. Figure 64 shows that the specimen did not contain WECs.

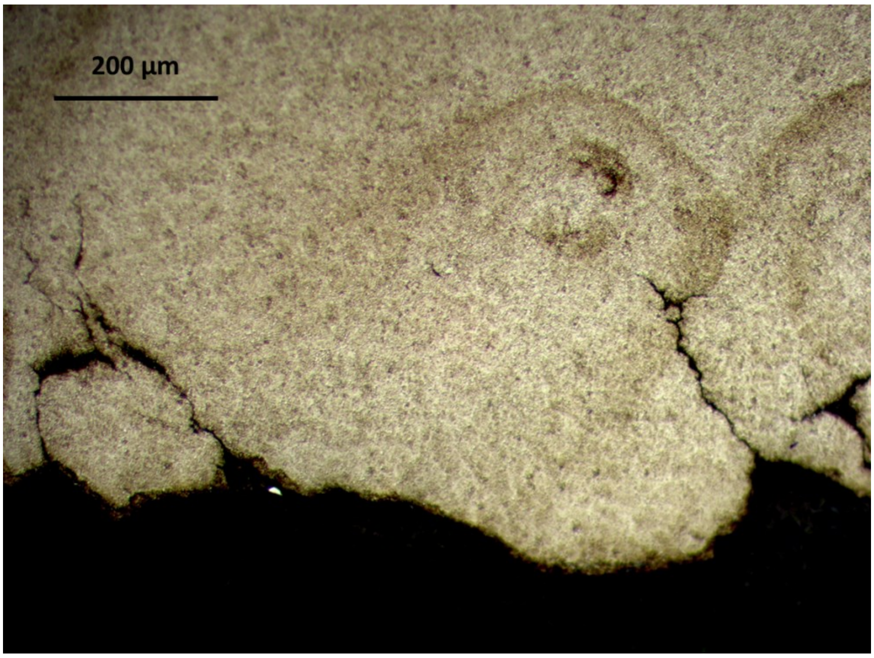

Figure 64 Section form Test 20. Pit-related cracks are shown in the picture, with no presence of WECs after failure

5.8.1 Variable contact pressure history in elliptical contact

Another attempt at reproducing WECs in elliptical contact was made, employing a slightly modified approach. This time, two different steps were used in the test, each run at a different pressure for a set number of cycles, starting with a relatively high pressure (to promote crack formation) followed by a step at a more moderate pressure to allow the crack to grow. This is in contrast to running the whole test at the high pressure level which results in a very quick failure, as was shown in the previous section where no WECs were observed. It should be noted that although this approach of gradually dropping stress is employed in structural fatigue studies, it is not straight forward to achieve because the initial high pressure can create large plastic zones around the crack tip so that the crack does not propagate at the subsequently lower pressure. Hence to increase chances of success, pressure should be dropped very gradually. However, for rolling contact studies this takes a very long time and was out of scope of this project. Nevertheless, an attempt was made employing two pressure levels only to investigate the feasibility of the approach on the MPR rig. The first pressure sequence employed is indicated in Table 12 below.

Table 12 Tests conducted in two different steps: test conditions

	Test 21	
	STEP 1	STEP 2
Elliptical contact configuration	12mm crowned rings on flat roller	80mm crowned rings on flat roller

Lubricant	Group I (+ZDDP, 0.1%P)	Group I (+ZDDP, 0.1%P)
Viscosity at 40/100 C [cSt]	15.1 / 3.4	15.1 / 3.4
SRR %	5	30
Max Hertz Pressure [GPa]	3.6	2.8
Minor contact semi-width	270	235
Major contact semi-width	492	1435
Roller cycles (10^6)	2	Until failure
WECs	NO	
	Test 22	
	STEP 1	STEP 2
Elliptical contact configuration	12mm crowned rings on flat roller	80mm crowned rings on flat roller
Lubricant	Group I (+ZDDP, 0.1%P)	Group I (+ZDDP, 0.1%P)
Viscosity at 40/100 C [cSt]	15.1 / 3.4	15.1 / 3.4
SRR %	5	30
Max Hertz Pressure [GPa]	4.5	2.8
Minor contact semi-width	270	235
Major contact semi-width	492	1435
Roller cycles (10^6)	2	Until failure
WECs	NO	

Initially, 3.6 GPa were applied for Test 21 in the first step for 2 million cycles. Step 2 lasted for other 118 million cycles, after which the test was stopped. No pit was formed on the surface. Sections of the specimen did not reveal formation of subsurface cracks.

A second attempt of the same kind was made in Test 22, adopting 4.5 GPa for the first step. After 2 million cycles, cracks were present on the surface and pressure was then dropped to 2.8 GPa for step 2. Specimen finally pitted after a total amount of 30 million cycles. The initial cracks after step 1 and pit at the end of step 2 are shown in Figure 65.

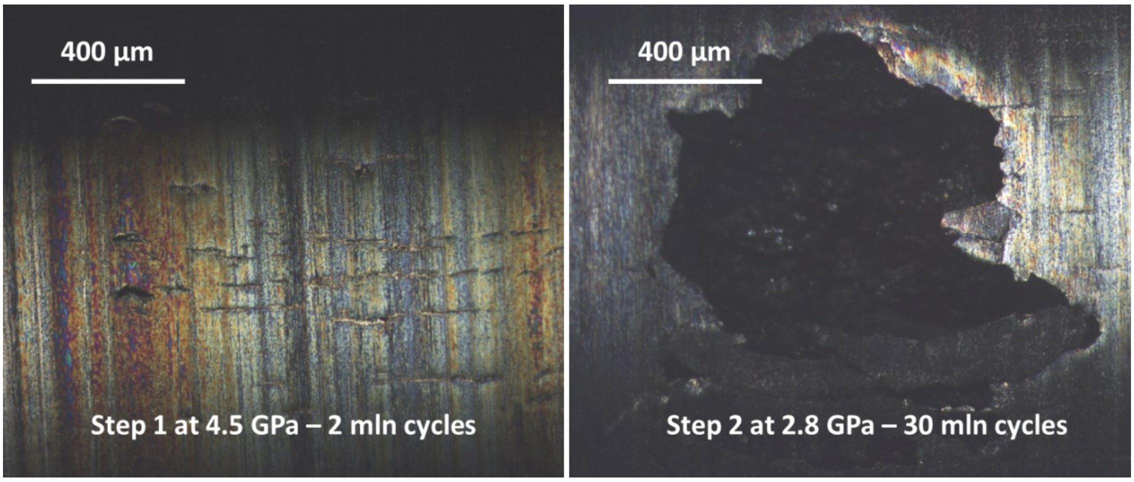

Figure 65 Test 22, roller surface after step 1 (left) and final pit failure after step 2 (right)

Although in the last case it was possible to obtain a pit after a considerable amount of cycles, sections of specimen did not contain white etching cracks, as shown in Figure 66.

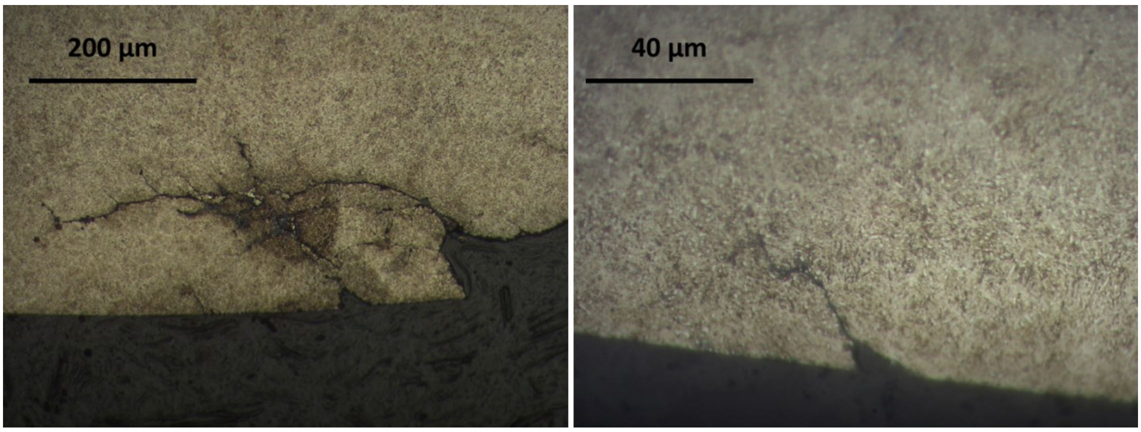

Figure 66 Two sections from Test 22 showing pit-related cracks (left) and a surface crack (right), with no presence of WECs

It appears very complicated to produce WECs when adopting elliptical contact configuration. Although conditions of test were nominally the same as tests in line contact, other than the pressure profile in space and time, not a single white etching crack was detected in any test in elliptical configuration. Every attempt to produce WEC failure with elliptical contact turned out to be a surface pitting failure which occurred too fast if the pressure is above 2.5 GPa; even when adjusting the pressure, either in one single step or in two different steps as described above, only dents, micro-pitting cracks or pit-related cracks were detected, but no presence of WECs whatsoever. The only significant difference between the line contact and elliptical contact tests shown here is the presence of high edge stresses in the line contact (see Figure 67), at least during the early stages of operation before the edges of the roller running track are deformed and worn, after which point the stress throughout falls to the nominal value. Given the differences in results in terms of WEC formation in the two contact configurations as presented here, the presence of these edge stresses appears to be a significant factor in generating WECs and may provide an important clue to the mechanisms of WEC generation. This point will be explored further in the Discussion section.

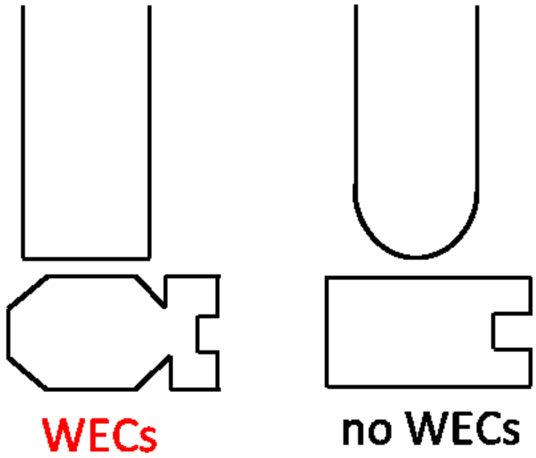

Figure 67 MPR line contact configuration vs elliptical contact configuration. It appears that WECs are easily produced in line contact only

5.8.2 Line contact with chamfered rings on cylindrical roller (potential influence of roller steel batch)

An additional aspect that could be at play here is the potential difference in the steel quality and microstructure between the test roller used in the elliptical and line contact tests. Former is a cylindrical roller and latter a chamfered roller produced from different batches of steel, although the initial steel specifications are exactly the same and come from the same manufacturer. To explore if this aspect is of any significance, further tests were conducted where the cylindrical roller, as used in elliptical contacts and which did not produce WECs, was now tested in a line contact by employing different specimen configuration in the MPR. This is achieved by using a new set of counterface rings, which have a flat profile with a chamfered 3 mm track pressed against the same cylindrical rollers used in the elliptical contact tested above. Essentially this produces the same contact geometry as the flat rings on chamfered roller but the specimen geometry is reversed. The test conditions are the same as in previous line contact tests and are shown in Table 13.

Table 13 Chamfered rings against flat roller line contact: test conditions

	Test 23

Lubricant	Group I + ZDDP
SRR	10 %
Friction coefficient	0.09
Max Hertz Pressure [GPa]	1.93
Contact semi-width	165
Lambda ratio	0.13
Test Temperature [°C]	80
Entrainment speed [m/s]	2.4
Roller cycles to failure (10^6)	14.1
WECs	YES

The geometry of the chamfered rings produced a 3 mm wide track on the roller specimen. Roller was grinded and polished to reach the beginning of the track. Once the specimen was etched, as illustrated in Figure 68, WECs were observed in sections corresponding to the initial 100-300 μm of the track.

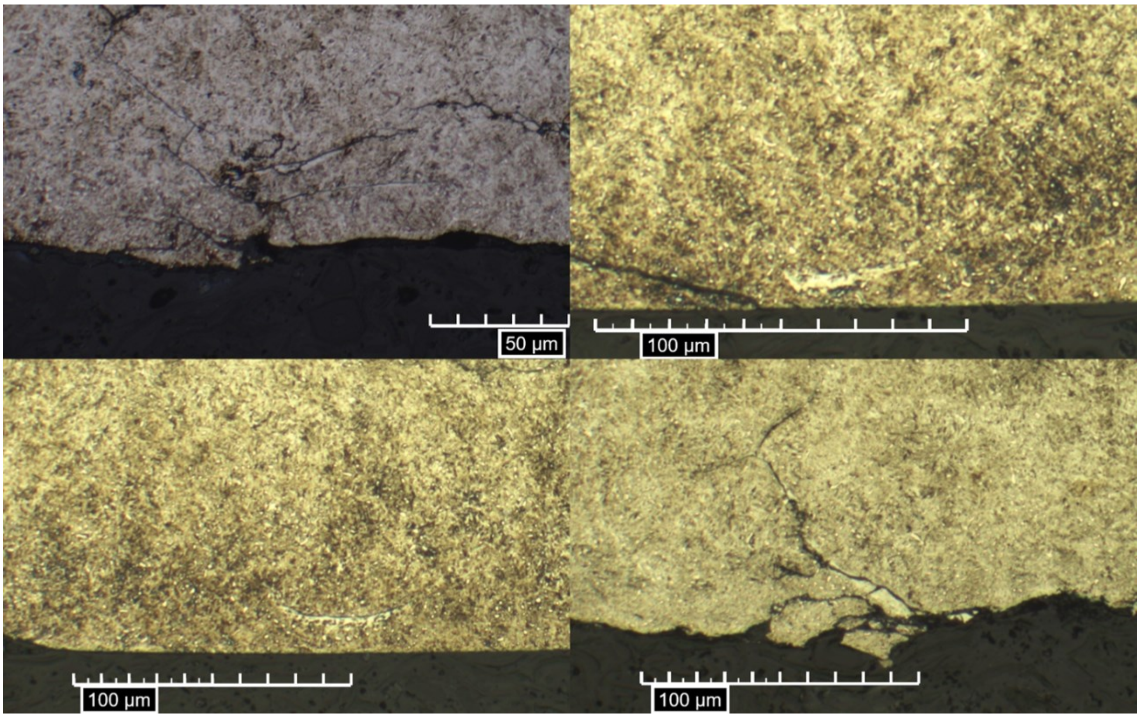

Figure 68 Four different sections of Test 23, showing presence of WECs after pit failure

The specimen was then further polished until reaching the middle of the track. In analogy to what was pointed out in the previous chapter, also in this case, when sections from the middle of the track were etched, only pit-related cracks were found here, which did not present white etching alterations (see Figure 69, right-hand side). In this area two or three short subsurface cracks were found. As visible from the picture, those cracks had the appearance of the one shown on the left-hand side of Figure 69 (circled in red), exhibiting only an initiation of white etching area, less accentuated compared to the WECs found in previous sections right at the edge of the track.

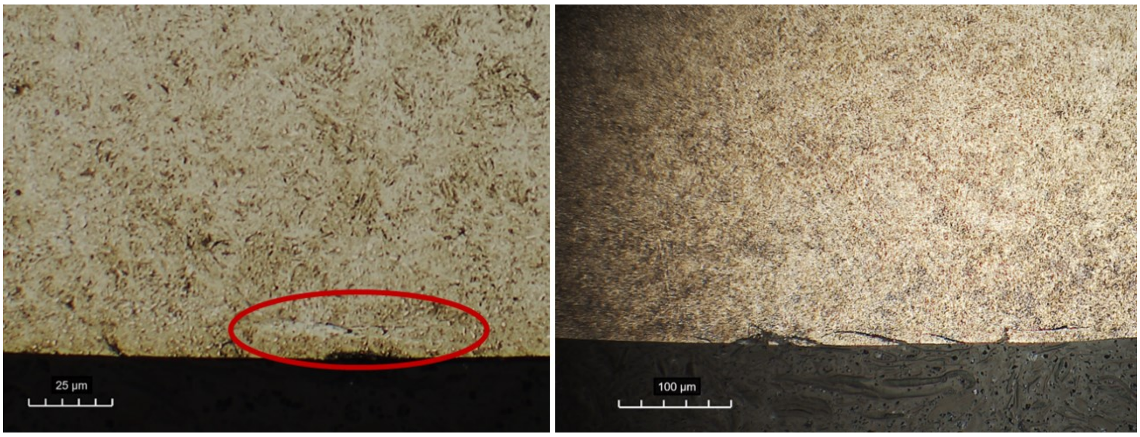

Figure 69 Test 23: two sections from the centre of the track, showing a less accentuated WEC (left) and micro-pitting cracks (right). The situation is analogous to the one observed in section 5.7 where sections from the other line contact configuration: as the sectioning moves towards the centre of the track, less amount of WEAs is noted in subsurface cracks

Therefore, the results obtained with this line contact but with inverted specimen geometry are exactly the same as the ones shown before for the equivalent line contact of chamfered roller against a flat disc. This observation confirms that the material of the roller is not responsible for WEC generation in line contacts, or the lack of WECs in elliptical contact, but that something else is at play, apparently related to the existence of edge stresses in line contacts and their subsequent evolution over test time.

5.9 Characterization of WECs in current tests: TEM analysis

This section presents results of TEM analysis of WECs produced in current tests with MPR. The TEM study was done in order to more closely inspect the microstructural changes associated with observed white etching cracks and white etching areas and confirm that these are representative of those reported in real bearings.

A Focused Ion Beam (FIB) technique has been used for the analysis. FIB stands for Focus Ion Beam. This technique uses an ion beam, usually gallium ion, to prepare an appropriate lamella from the specimens of interest for inspection in TEM.

Coupled with an SEM to form a dual beam station, the FIB becomes a powerful tool for analyzing materials. In the microscopic field, three applications of FIB dual beam can be highlighted: TEM lamella preparation, cross section and tomography. The FIB is able to mill almost any material. Furthermore, precision of the lamella position is high thanks to FIB imaging ability.

In Figure 70, SEM pictures of two WECs from Test 1 are shown. Some distance away from the cracks, the matrix of the steel around the cracks is visible, with its lath martensite patches and carbides. However, nearer to the crack faces, within the so-called white etching area, which appears white under optical microscopy, a much more homogeneous microstructure is apparent which seems to be lacking in carbides and martensite; therefore, WEA appears to be an alteration of the pre-existing microstructure of the steel.

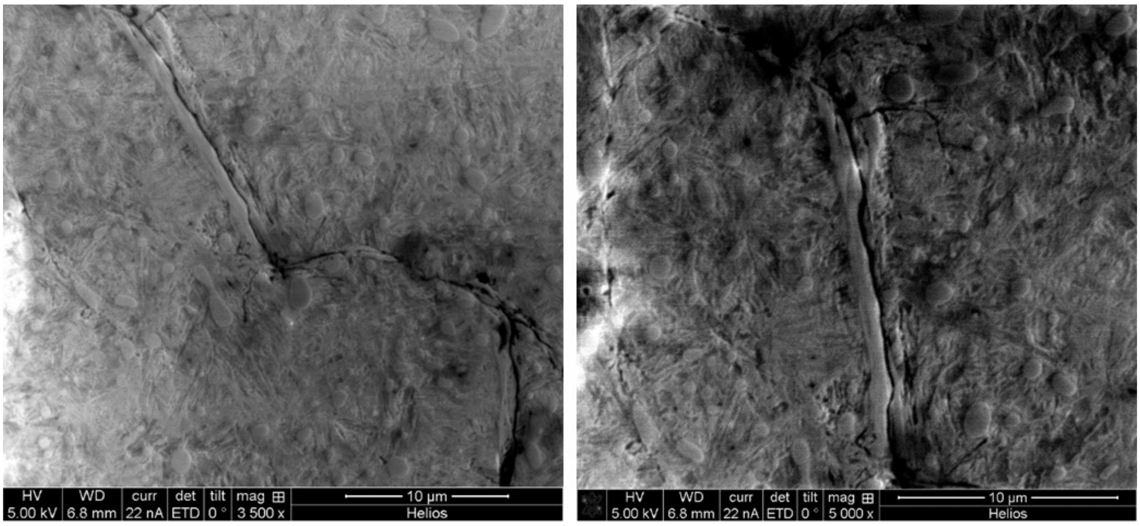

Figure 70 SEM pictures of two WECs from Test 1

A TEM sample preparation is conducted on one of the WEA shown above. The procedure consists of cutting a thin part of the region of interest, which is first covered by a protective material (platinum). Holes are milled on each side of the region and the extrapolation of a lamella takes place by ultra-thin sectioning of a slice of material. After the sectioning, the lamella is lifted-out by a micromanipulator and glued on a support where the final thinning takes place. The final lamella prepared in this way is shown in Figure 71. It is evident that the lamella contains a crack towards its left end.

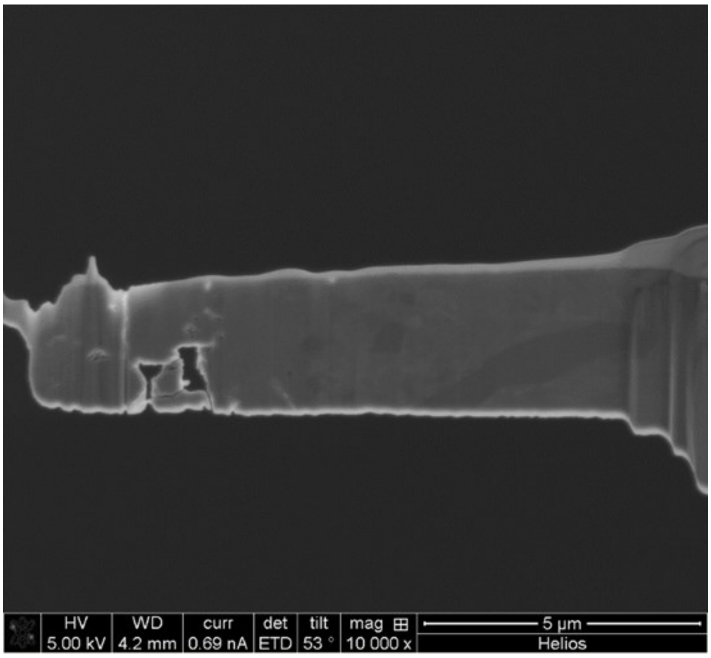

Figure 71 Final lamella after TEM sample preparation

In Figure 72 an SEM picture of the region around this crack is shown; the corresponding TEM results (patterns of X-ray diffraction) from three different zones of this general region are reported in the figure too. The diffraction pattern gives information about the particular (h, k, l) direction of the lattice planes of the crystal. The crystal matrix of the material acts like a grating to the X-rays, whose photons get scattered when they enter into the crystal. Hence, the diffraction pattern is formed. Indeed, one can obtain some information on the grain size which is inversely dependent to the broadening of diffraction spots. In general, discrete spots pattern indicates that grains of the microstructure are quite coarse grains; on the other hand, continuous rings mean that grains are finer.

As shown in Figure 72, the diffraction patterns (framed in red in the figure) of the area surrounding the crack i.e. within the WEA consist of continuous rings, indicating that very small grains are present within this WEA region. Conversely, the diffraction pattern of the region far from the crack is formed by discontinuous spots indicating a coarser grain microstructure. The microstructure within the WEA has been reported to consist of nano-ferrite grains [60,71,76]. The findings here confirm this and indicate that the generated WEA and WECs are representative of those found in real bearings.

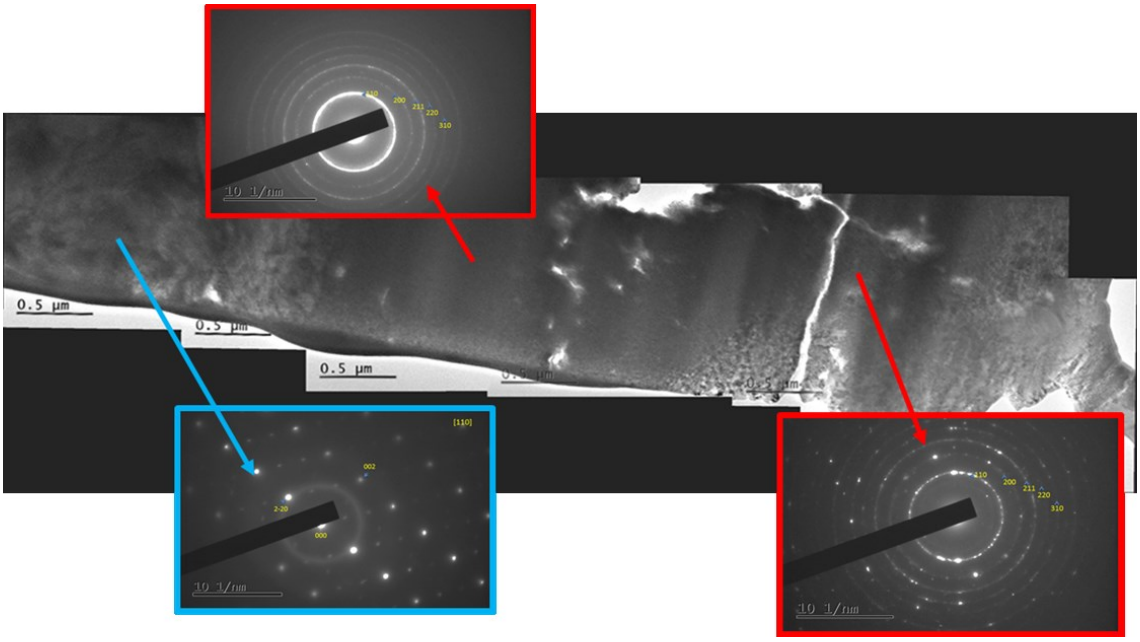

Figure 72 Diffraction patterns of the area surrounding the crack (framed in red in the figure) consist of continuous rings, indicating that ferrite grains are small sized in the proximity of the crack (WEA), whereas diffraction pattern of the region far from the crack is formed by discontinuous spots (framed in light blue)

To further confirm the features of the altered microstructure within the WEA, Figure 73 shows two TEM images of the same WEA taken at different tilt angles. In both pictures, although the orientation of the sample changes, crystals of the steel matrix are always visible, meaning that these are actual features of the microstructure, rather than just an artefact of the imaging.

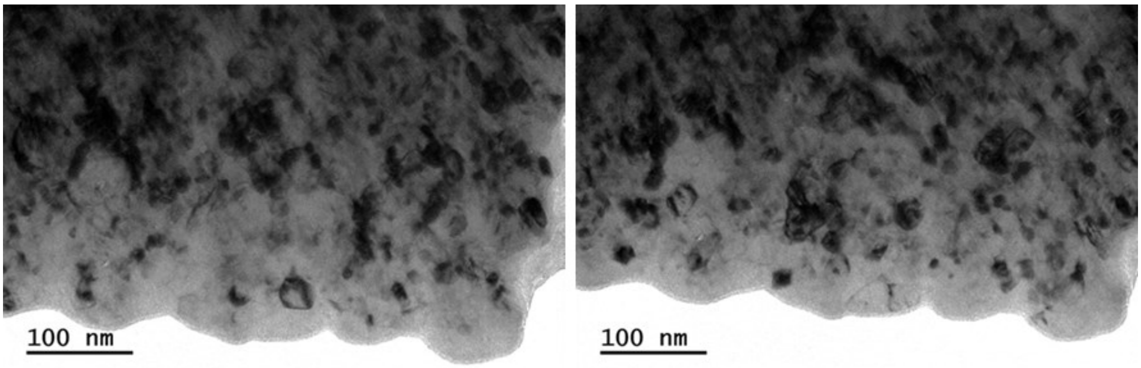

Figure 73 WEA image at different tilt angles. Crystals of the steel matrix are visible as the tilt angle changes

Finally, given the aperture size of the beam and the thickness of the lamella, one estimates the crystal size in the WEA to be 10-30 nm approximately. Figure 74 is a high magnification TEM image. As evident from the scale of the picture, this image supports the fact that ferrite grains in WEA are indeed nano-sized and are in the region of 20 nm.

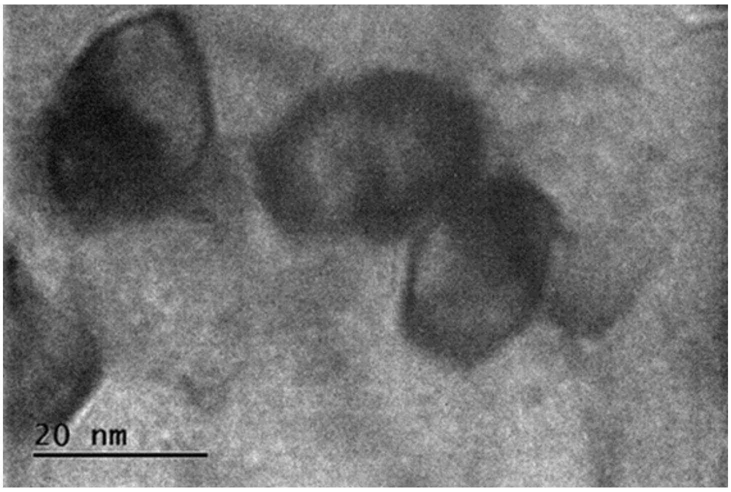

Figure 74 High magnification TEM image of nano-sized ferrite grains

5.10 Characteritic features of WECs produced in current tests

Based on the high number of WECs produced and analysed in this chapter some general observations can be made in terms of most common WEC characteristics. These include:

- they are generally not connected to the surface but appear to be mainly contained in the 'near-surface' regions;
- they start to form at approximately 20 μm from the surface and extend towards the bulk material up to 300 μm from the surface; this range include the depth of maximum shear stress, located at about 130 μm from the surface given the applied load and contact geometry of the line contact tests;
- no WEA is observed without an associated crack, but there are plenty of cracks with no associated WEA;
- whether or not WEA occur around the crack seems to depend on number of contact cycles and particular location in the 1 mm running track of chamfered specimen;
- they are of varying morphology with no particular orientation of the crack network;
- they are always very thin cracks;
- there are plenty of examples where WEC networks interact with inclusions.

Some of these aspects are now explored with relevant supporting evidence provided.

5.10.1 WEC morphology

Regarding the morphology of present WECs observed here, three distinguishing features of WECs seem to commonly be present:

- arc-shaped WECs, in Figure 75;
- irregular branched WECs, in Figure 76;
- vertical branched WECs, in Figure 77

The arc shaped cracks are generally very close to the surface, sometimes just at about 10-20 μm from it and their concavity is always orientated opposite to the surface, in the sense that arc shaped cracks propagate toward the subsurface rather than coming to connection with the surface (see Figure 75).

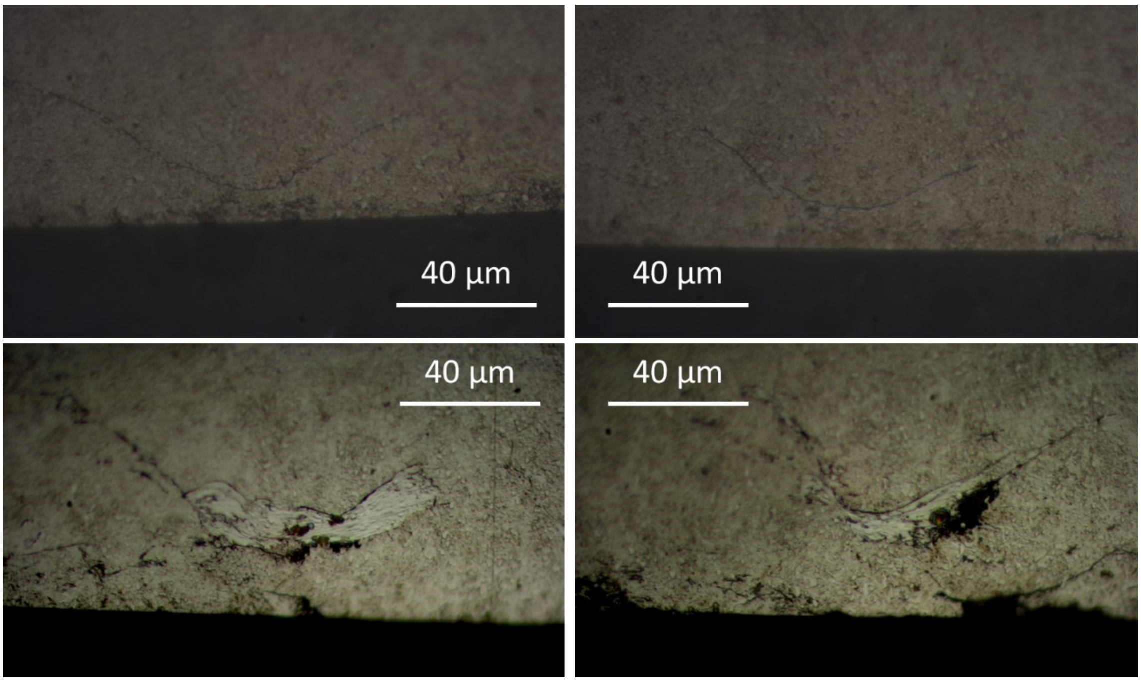

Figure 75 Arc-shaped white etching cracks

Branched cracks, as the ones shown in Figure 76, are very common; they can extend in a direction parallel to the surface, although they are mostly irregular. In fact, pattern of branches in the majority of the cases does not seem to follow a specific orientation related to friction or contact motion. White etching areas tend to be generally more spread where irregular branches are present.

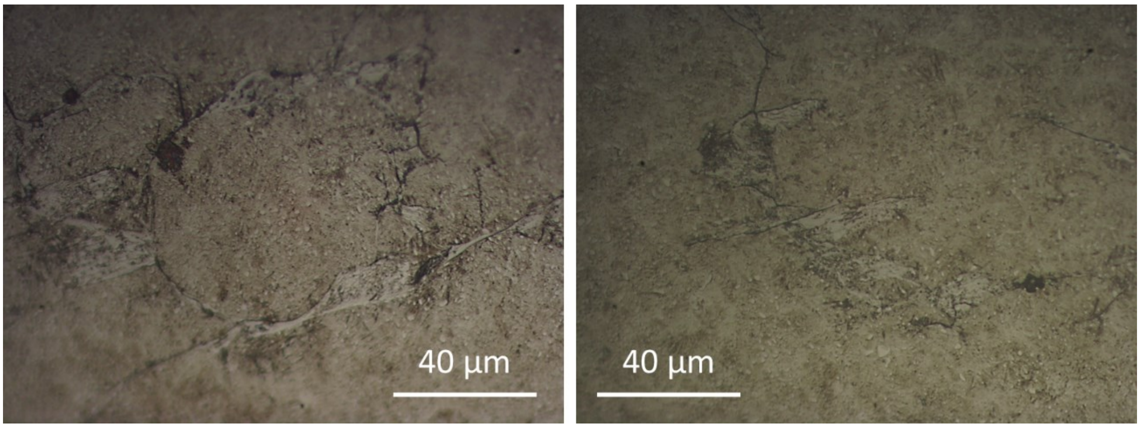

Figure 76 Irregular branched white etching cracks

Vertical branched cracks are generally found at a higher distance from the surface with respect to other cracks, with a range between 50 μm and 300 μm. Generally, vertical cracks tend to be less decorated with white etching cracks if compared with irregular branched cracks. It is observed that these vertical cracks can sometimes produce branches perpendicular to them and parallel to the surface (see Figure 77). In the case of vertical cracks, white etching areas are mostly found at their perpendicular branches or intersections between them.

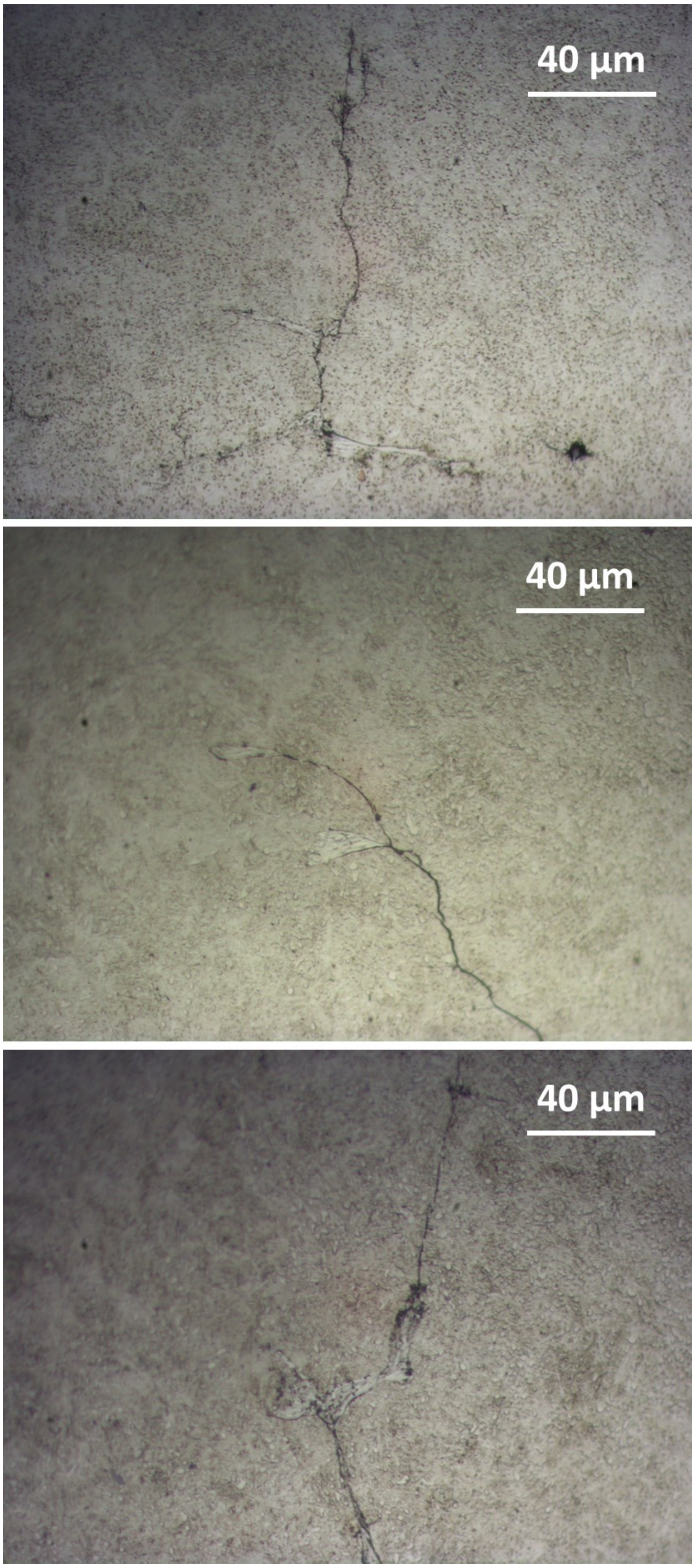

Figure 77 Vertical white etching cracks with some horizontal branches evident

It is also possible to find these three types of recurring cracks forming a single crack network of wider extent. In Figure 78 a common crack network noticeable in current tests is illustrated. Starting from the surface, firstly the arc-shaped crack is found. Little irregular branches seem to form on the left-hand side from the arc shaped crack. A vertical crack is present on the other side of the arc-shaped crack, extending deeper into the sub-subsurface.

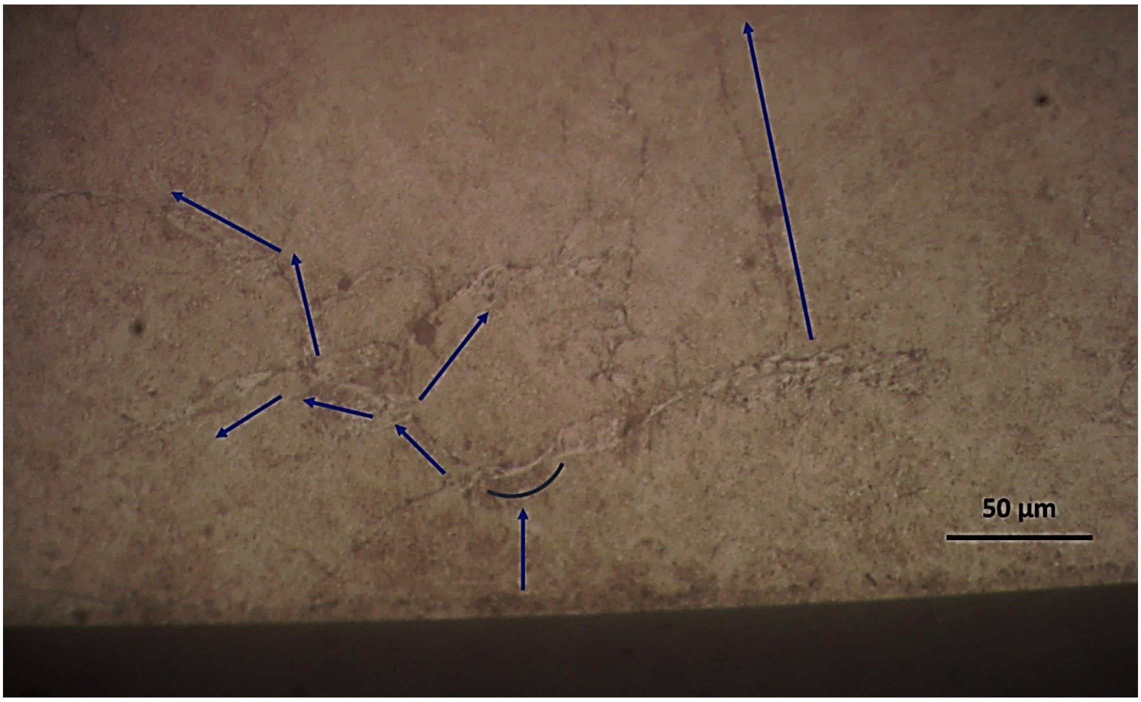

Figure 78 Common crack network presenting the conjunction of arc-shaped cracks, branched pattern and vertical cracks

5.10.2 Interaction of WECs with inclusions

There is plenty of evidence of interaction of WECs produced in current tests with inclusions present in the tested steel specimens. WECs around inclusions sometimes appear as wider crack network that incorporate the inclusion itself (for example in Figure 79) or in a form reminiscent of what is commonly referred to as 'butterflies' (for example in Figure 80)

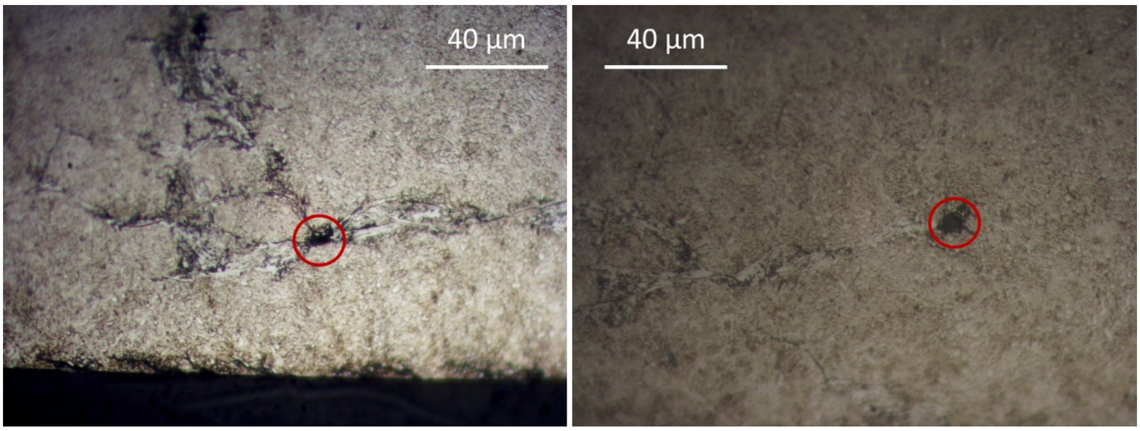

Figure 79 White etching cracks associated with inclusions

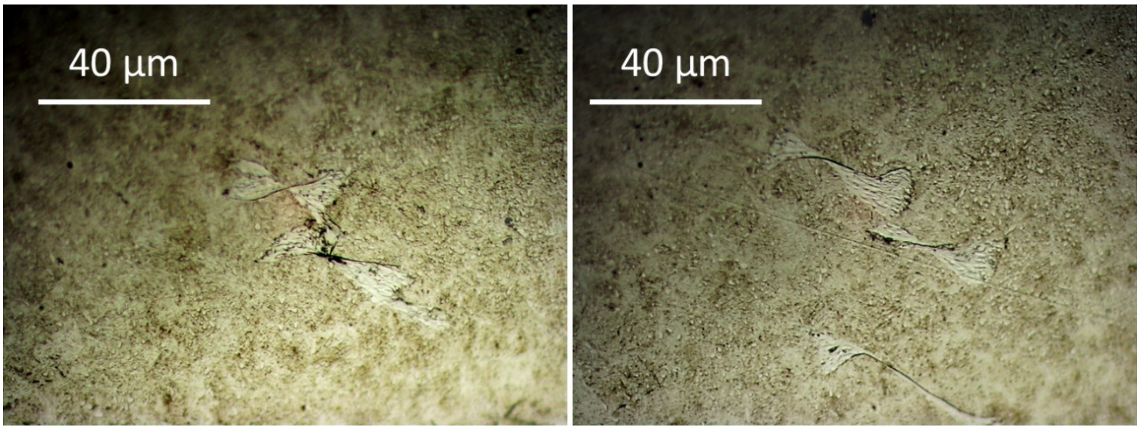

Figure 80 Another type of white etching cracks. Those cracks appear to be isolated, rather than being part of a network and their appearance reminds the shape of a butterfly

5.10.3 Location of WECs: surface or subsurface

In this study, the final pitting failure was generally produced by surface breaking cracks. This is not surprising given that mixed lubrication conditions were used leading to significant metal-to-metal interaction at the surface. However, it is interesting to observe that in general these surface breaking cracks (i.e. cracks directly connected to the rolling surface) that have resulted in failure do not exhibit WEAs. Instead white etching cracks are located elsewhere in the sample and appear not to be directly connected to the surface. This in turn means that WECs themselves are not necessarily the cause of the failure at all. This observation is obviously important in terms of significance of WECs to premature bearing failures, an aspect which does not seem to have been extensively explored in literature at all.

To illustrate the above observations a series of examples are presented here. In general cracks starting from the surface whether or not they are related to the final pit are really unlikely to exhibit white etching areas along them. Indeed, in most failures shown in this study, eventual pitting failures appear to have been caused by surface breaking cracks which are not necessarily white etching at all, while white etching cracks exist in parallel throughout the specimens, mainly subsurface, and are not necessarily connected to the pit itself, i.e. it is not the WECs that have caused the failure directly. This is an important observation in relation to mechanisms of formation of WECs and will be explored further in the discussion section.

Examples of surface breaking cracks from tests in line contact are shown in Figure 81. No white etching areas are evident in those cracks despite the relatively long network.

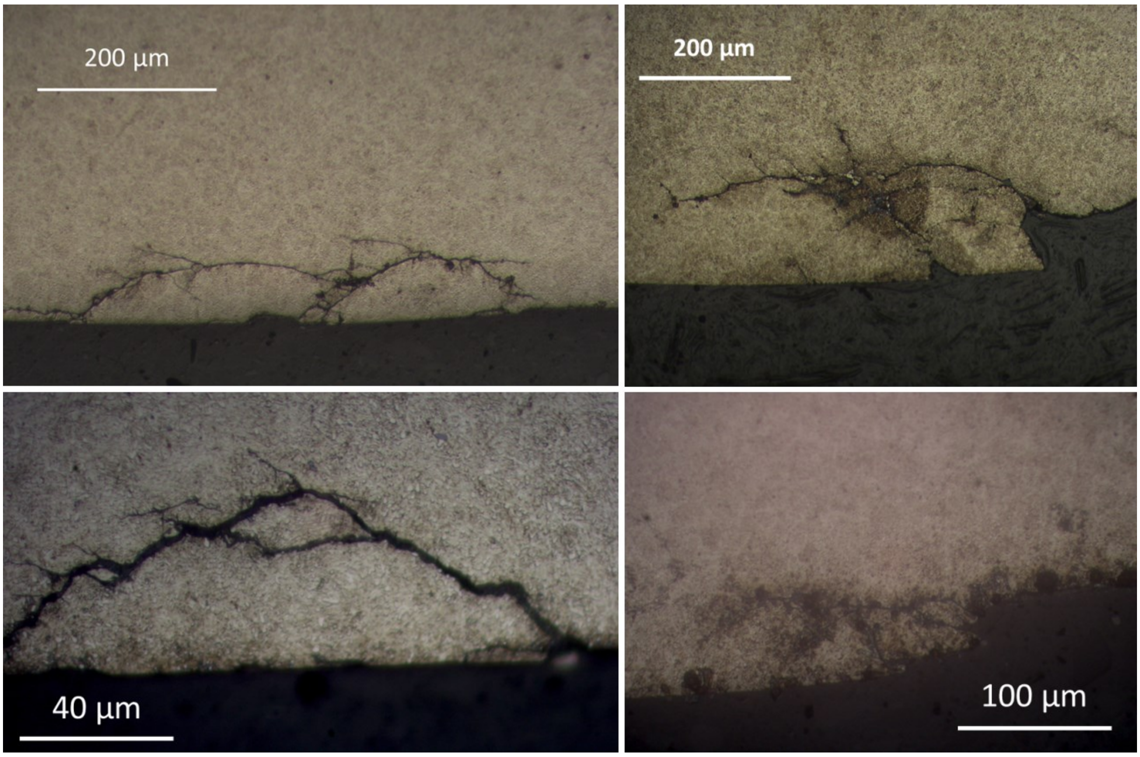

Figure 81 Non-WEA surface cracks from tests in line contact

Essentially, in current tests, surface-breaking cracks, i.e. cracks related to the surface pit or micro-pitting cracks, and WECs do not seem to be related to each other and their main substantial difference is their thickness: WECs are always very thin cracks, tens of nanometers, whereas pit-related cracks are wider.

When considering whether or not WECs are connected to the surface, it is important to bear in in mind the difficulty in making this distinction in the first place. The presence of a pit generally leads to considerable surface damage so that it is difficult to interpret any crack in the vicinity of this damage. This means that if a WEC is present near the pit (which is extremely rare in this study), it is difficult to establish its origin. For example, Figure 82, shows a WEC from an MPR test which appears at a location very close where the final pit detached from the initial contact surface. Because the part of the material above the crack is missing, it is not possible to say if the crack was surface or subsurface initiated, i.e. it started within the detached material or it was always below it.

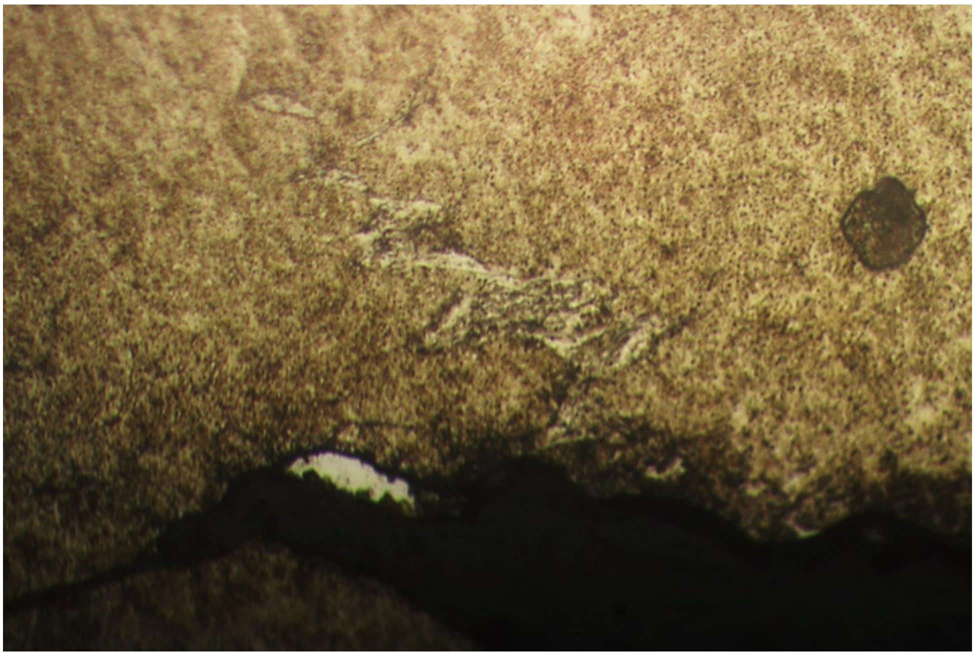

Figure 82 A WEC from an MPR test associated to the presence of the final pit. In this case, it is not possible to assert whether or not there is connection between the crack and the contact surface

In other cases, generally speaking, even far from the pit, it can also be difficult to distinguish the initiation site or make considerations about the nature of the crack (surface or subsurface) if one judges only by looking at one single section. Figure 83 shows a WEC with an apparent direct connection with the surface; however, further sectioning could reveal that one is dealing with two different cracks which came to connect just at one single cross-section, for example, it could be about a junction of a non WEA surface breaking crack with another subsurface crack, that is white etching, and it did not on its own have a connection to the rolling surface.

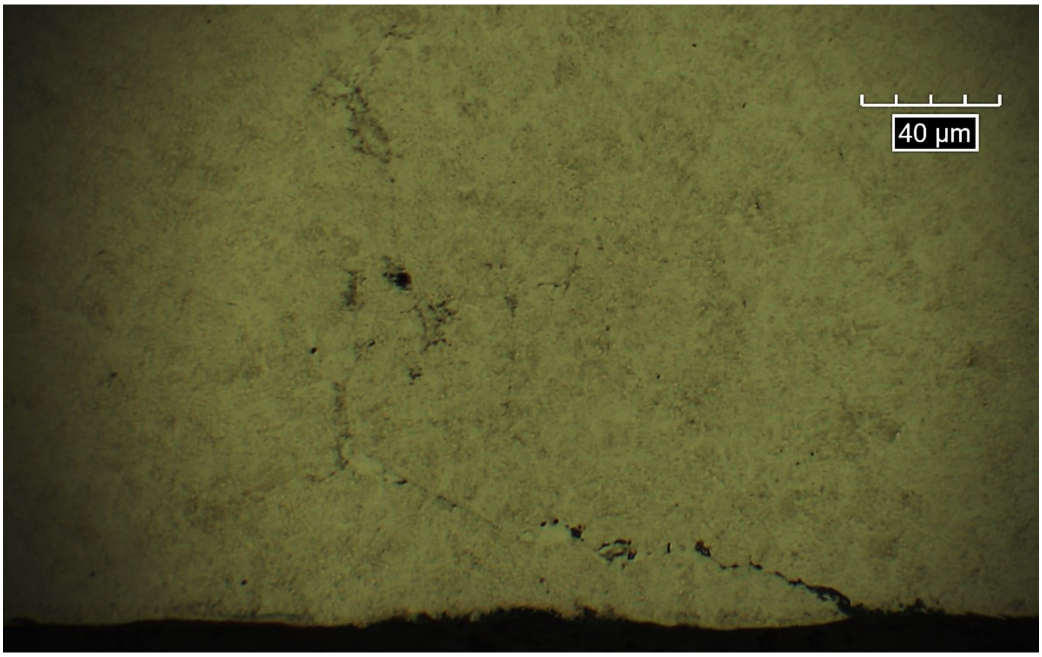

Figure 83 WEC apparently connected to the contact surface

Nevertheless, even such ambiguous cases as the two presented in Figure 82 and in Figure 83, are extremely rare in the present failures, and in a vast majority of cases WECs are clearly not interacting with the surface.

5.10.4 Relationship between WEAs and WECs

It is worth noting here that in the present study not a single white etching area was ever observed without an associated crack. On the other hand here are plenty of cracks which do not show white etching alterations. The large amount of WECs presented here adds weight to this consistent observation. This strongly suggests that the formation of WEAs is consequential to crack formation rather than vice versa. As mentioned in the literature survey of this thesis, this issue is still debated so the consistent results presented here in the regard are very helpful and will be discussed further in the discussion section when the mechanism of formation of WECs are considered. The results presented here suggest that WEA can indeed be formed though rubbing of existing crack faces. It is of course not possible to provide direct observation of this in a rolling contact fatigue test as crack faces are not visible. However, the principle can be confirmed through a different experimental set-up which can provide more direct observations of WEA formation. This is done in the next chapter of this thesis.

It is important to note, that in all etched sections prepared here care was taken to ensure that WEA are real and not artefacts of the preparation process, which can occur if etching and polishing is done incorrectly. To illustrate how a potential artefact of preparation process can be misinterpreted, an example is given here where a sample was re-polished and the etching process was repeated to ascertain that something ambiguous at first sight is not an unwanted product of the etching process. Figure 84 shows a case in which an artefact was found after etching which could appear like a white etching area with no associated crack. Re-etching (same figure, right) clearly shows that this was just an artefact. On the other hand, if a real microstructural alteration in form of WEA is present, it will show up again when the sample is re-etched. This is the case shown in Figure 85, in which re-etching confirmed the presence of white etching areas.

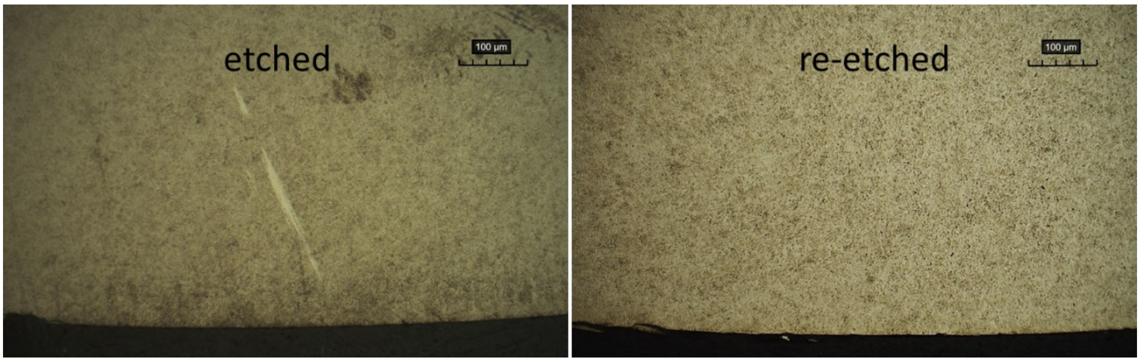

Figure 84 Artefact of etching (left) which vanished after polishing and re-etching (right)

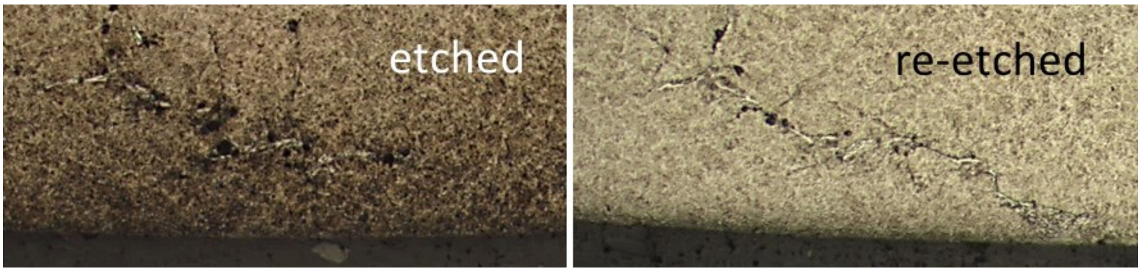

Figure 85 White etching crack in two different consecutive sections

Regarding the effect of etching and possible artefacts, it is here reported the not very common occurrence of local dark etching regions in the steel microstructure which are visible sometimes after etching. The appearance of these dark regions is illustrated in Figure 86.

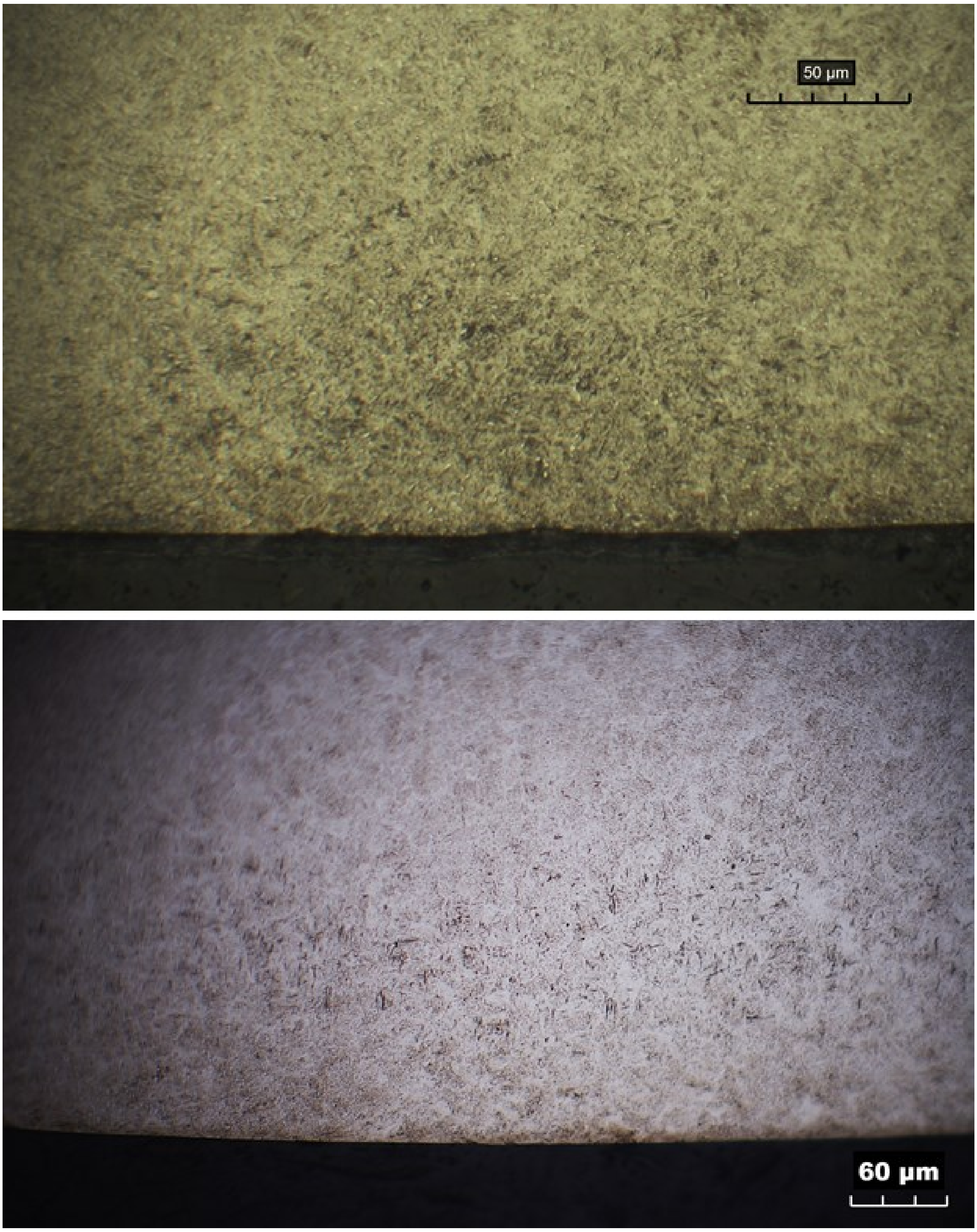

Figure 86 Dark etching regions in specimens from current tests in line contact configuration

There are studies [59,66] which claim that dark etching regions are prior to the formation of WEAs and WECs in bearing steels. However, in this present study no particular correlation was made between these dark regions and WECs, especially considering the fact that in the majority of the cases WECs were not associated with those dark regions shown in the above figure; moreover, it is very difficult to judge, based just on optical microscope observations, if a dark region is an actual microstructural alteration of the steel or a mere artefact from the etching process, unless more accurate investigation is carried out; however, this kind of investigation was beyond the purpose of this study.

5.11 **Conclusions**

A considerable amount of results has been presented in this chapter. They covered various aspects of WEC formation including the influence of lubricant composition, lambda ratio, slide-roll ratio, nominal pressure and contact geometry. The most important observation from tests conducted is that WECs were consistently reproduced in most cases regardless of the applied conditions as long as line contact configuration was employed on the MPR. Conversely, WECS were not produced regardless of conditions when elliptical contact configuration was employed.

Sectioning of specimens in various locations of the running track has been conducted, showing a difference in intensity of white etching area between cracks located at the edge of the track and crack present in the middle of it. The latter were decorated with less accentuated microstructural changes or even with no WEAs at all. In addition, surface breaking cracks generally do not show white alterations; WECs are almost exclusively located in the subsurface region at the depth between about 20 μm and 300 μm (the depth of maximum shear stress being 130 μm). No WEA was ever found without an associated crack but there are plenty of examples of cracks without white etching area decorations.

TEM analysis of WECs in current tests has been presented with the aim to characterize microstructural changes decorating cracks. This indicates that WECs generated in this study are representative of those found in the field.

Finally, some peculiar features of WECs produced in MPR tests have been identified directly from observation of sectioned specimens. The next chapter will explore one of these aspects, namely is WEC or WEA formed first.

6 Results: reproducing WEAs in a rubbing contact

This chapter presents results of experiments designed to provide further insight into the relationship between white etching areas and white etching cracks. The primary objective here is to establish whether WEA can be formed through mere rubbing between two bearing steel specimens. Such a set-up is intended to simulate the rubbing of two crack faces but unlike inside the crack, this experiment allows for a direct observation of WEA formation. The chapter is self-contained in that describes the experimental set-up and the results.

6.1 Introduction to the experimental procedure

One of the questions which still arises from the WEC related literature is whether the crack or the white etching matter comes first. It is, hence, still needed to clarify whether the alteration of the steel microstructure is the cause for crack initiation or just the consequence of an existing crack. A definite answer to this question would allow researchers to focus on what the real cause of damage is so that appropriate solutions can be proposed i.e. is the formation of WEA a problem at all that needs addressing or does the solution lie in preventing crack formation first and WEAs are largely irrelevant.

From direct observation of WECs obtained in the MPR test results presented earlier, two main details have been noticed regarding the relation WECs/WEAs: first of all, white etching areas were never observed without an associated crack, they were always found decorating the crack and differences have been observed when comparing WECs from specific locations of the running track, in the sense that subsurface cracks in some locations or at a lower number of stress cycles were exhibiting less accentuated white etching area or a complete lack of it. This evidence suggests that standard fatigue crack formation occurs first and is therefore the main problem while white etching areas appear to be a consequence of it. In the light of these considerations, the present chapter illustrates an experimental approach to establish the interdependence of white etching areas and white etching cracks, considering the hypothesis of crack-face rubbing.

6.1.1 Rubbing of crack-faces

One of the theories of WEC/WEA relation that appears in some works in the literature implies that WEA is posterior to crack initiation and that the WEA forms through crack-face rubbing [75]. The idea behind this hypothesis is that a crack, i.e. a discontinuity in the material, could be seen as two tri-dimensional surfaces (the crack faces) and that these surfaces come into contact and rub at several different points during bearing operation. This is illustrated in Figure 87. Due to cyclic loading, which allows the bearing to deform elastically at a microscopic level, these point contacts would rub, potentially causing local plastic deformation and leading to alteration of the initial microstructure of the steel to form the nano-ferrite microstructure, i.e. WEAs.

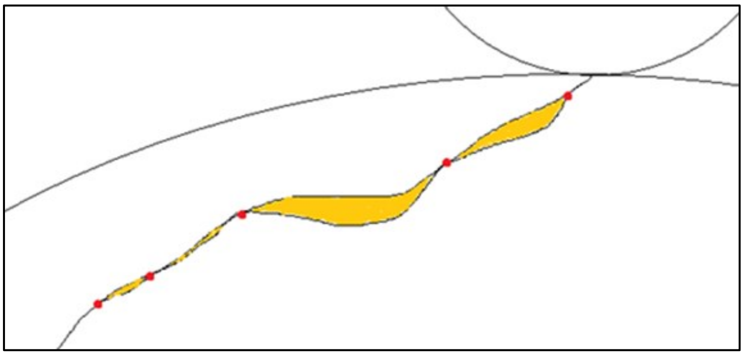

Figure 87 Illustration of two crack-faces rubbing; crack faces contact and rub in certain locations indicated in red in the picture.

It is of course not possible to provide direct evidence for this theory by observing the crack faces rubbing during operation as no access is possible within the specimen. However, it is possible to mimic this crack-face rubbing though a separate experiment where two steel specimens rub against each other at small amplitude, and in this case direct evidence of whether or not WEA can form through rubbing can be obtained. This experiment is now described.

Once this aspect is made clear, the discussion of the present study can focus more appropriately on the interpretation of WEC formation in current tests from MPR.

6.2 Experimental equipment and procedure: reproduction of WEAs under rubbing conditions

In this section, three tests under rubbing conditions are presented. The tests employ a high frequency reciprocating rig, HFRR (PCS Instruments, Ltd).
Subsequent to the rubbing tests, if any alterations from pre-existing microstructure are produced, eventually, one needs to verify that those microstructural changes resulting from reciprocating tests are analogous to those observed in WECs/premature failures from the field. This is made by analysing microstructural alterations with SEM microscopy and via characterisation of their hardness by means of a nano-indenter machine.

The HFRR set-up consists of a ball-on-flat configuration: a ball and a disc are located respectively into an upper specimen holder and a lower specimen holder. Figure 88 illustrates the various parts of the rig; in the bottom part of the figure, the three pictures starting from the left respectively show the upper specimen holder with the ball, the lower specimen holder in which the disc is located and the combination of the two parts in the final ball-on-disc contact configuration. By means of a shaker an oscillatory motion is imparted to the ball so that the ball slides backward and forwards on the disc at different amplitudes and at different frequencies generating a wear scar on the surface of the disc. Both ball and disc are 100Cr6 martensitic steel (AISI 52100), provided by PCS Instrument. Ball and disc specimens had an initial value of R_a less than 20 nm and

50 nm respectively. Lubricant is supplied by filling the lubricant bath where the disc is located (see figure) to a set level every time. The load is applied through a dead weights system.

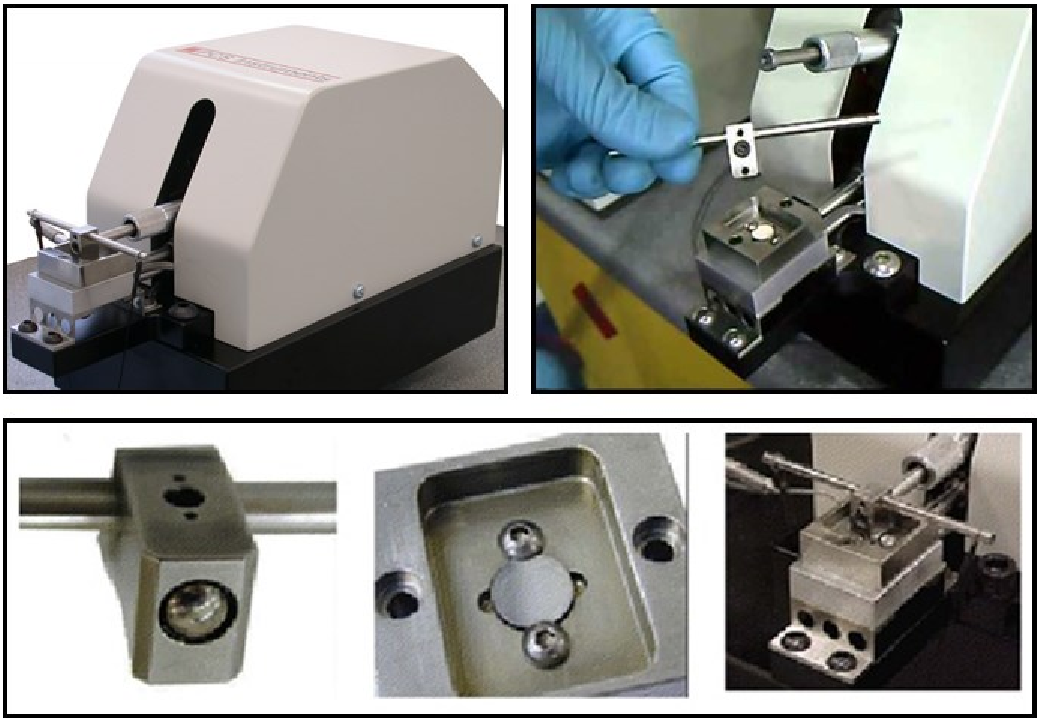

Figure 88 HFRR set-up rig

The idea behind these tests is that the resulting rubbing contact on HFRR reproduces a rubbing contact between two crack faces. Figure 89 illustrates this analogy.

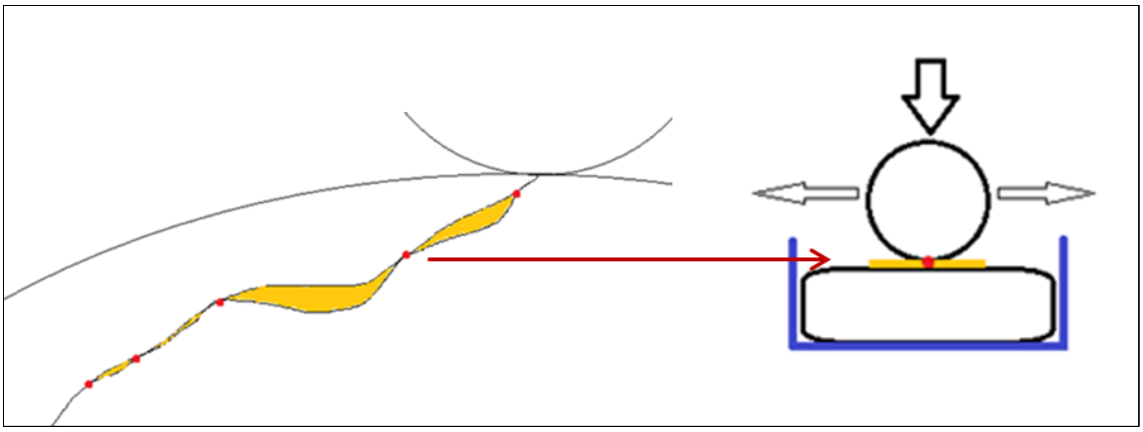

Figure 89 HFRR configuration as a reproduction of a rubbing contact between two crack faces

A number of tests was performed but only a selection is shown here to illustrate the principle. Table 14 lists the conditions of three rubbing tests. Some of the same lubricants used in the MPR tests were used here too. Test *a* was done with the fully formulated engine oil and test *b* with pure PAO oil (with no ZDDP). In order to totally exclude any effect of lubricant, test *c* was run dry. In this case, the test was run at a lower frequency and fewer cycles, in order to decrease the damage on the surface that would otherwise arise, given the dry contact. For the three tests presented here the stroke of oscillation was set to be 25 μm; this is the minimum value achievable on the rig.

Table 14 Test conditions for three selected rubbing tests on the HFRR rig

	Test *a*	Test *b*	Test *c*
Lubricant	Fully formulated Engine oil, mono-grade SAE 40	Pure PAO	Dry contact
Max Hertz Pressure [GPa]	1.26	1.26	1.26
Stroke [um]	25	25	25
Frequency [Hz]	200	200	100
Friction coefficient	0.119	0.152	0.554
Test temperature [°C]	60	60	25
Cycles	13*10^6	4.3*10^6	6*10^4
WEA	YES	YES	YES

Depending on the duration of the test, the maximum depth of the scar on the disc was different, varying from 0.5 μm to 3 μm. After the test has finished, the disc is analysed by following a three step procedure shown in Figure 90: firstly, the initial scar resulting from the test is delimited by three Vickers hardness indents for identification; the disc is then polished until the scar is completely removed, by means of a mechanical polisher and using consecutively three different mono-crystalline water based diamond powders respectively of 9 μm, 3 μm and 0.05 μm; the polished surface is finally etched with Nital.

After this procedure, specimens were analysed using an optical microscope, a scanning electron microscope and indented using a nano-indentation rig.

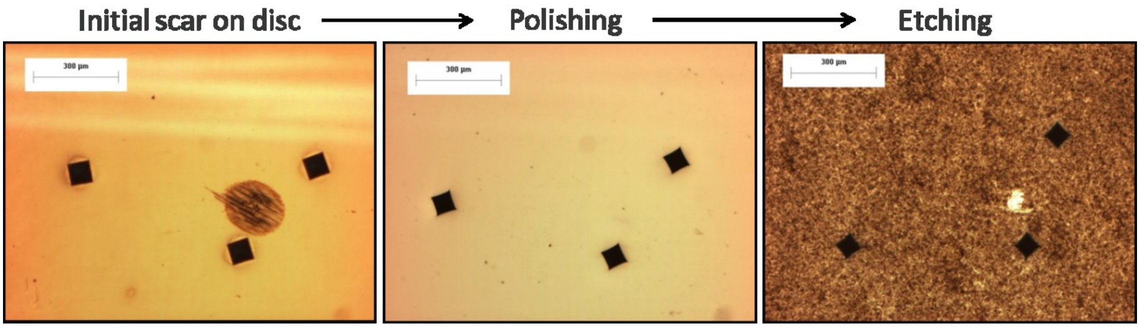

Figure 90 Sequence of sample preparation after a HFRR test. The initial scar is delimited by three indents (left) for identifying the scar area after polishing (centre). Finally, etching is done to reveal possible presence of WEAs (right)

Optical images after etching revealed that in all cases white etching areas were reproduced (Figure 91). It is worth noticing here that even in dry conditions, without using any lubricant, white etching area is formed as well, suggesting that lubricant effects are not the primary factor in forming WEAs in this case.

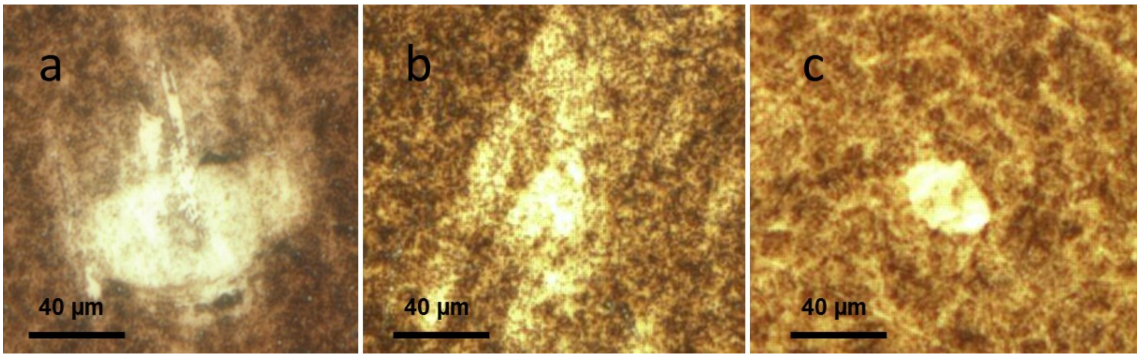

Figure 91 WEAs obtained after tests from HFRR. Test *a* (left), Test *b* (centre) and Test *c* (right)

Those tests presented here confirm that WEA like microstructural changes were taking place under rubbing condition. However, it was still necessary to confirm that the produced WEA are representative of those found in real bearings that exhibited WECs. This analysis is presented in the next sub-section.

6.2.1 Characterisation of WEAs produced in rubbing conditions: nano-indentations

It is known that the WEAs associated with bearing premature failures exhibit 30 to 50% higher hardness than the surrounding matrix, or other types of white etching areas, such as white etching bands or temperature transform layers. The latter can feasibly be formed in a rubbing contact so it is important to confirm that the WEAs observed in the HFRR test do indeed have higher hardness than the surround.

A nano-indentation machine was used to measure the hardness of WEA created under rubbing contact. Test *a* was used for the measurement of hardness. A series of six indentations were made first on the original steel of the specimen (in a zone far from the WEA) and then another set of six indentations was carried out within the white etching area. Figure 92 shows a typical load/deformation curve of a nano-indentation made on the sample.

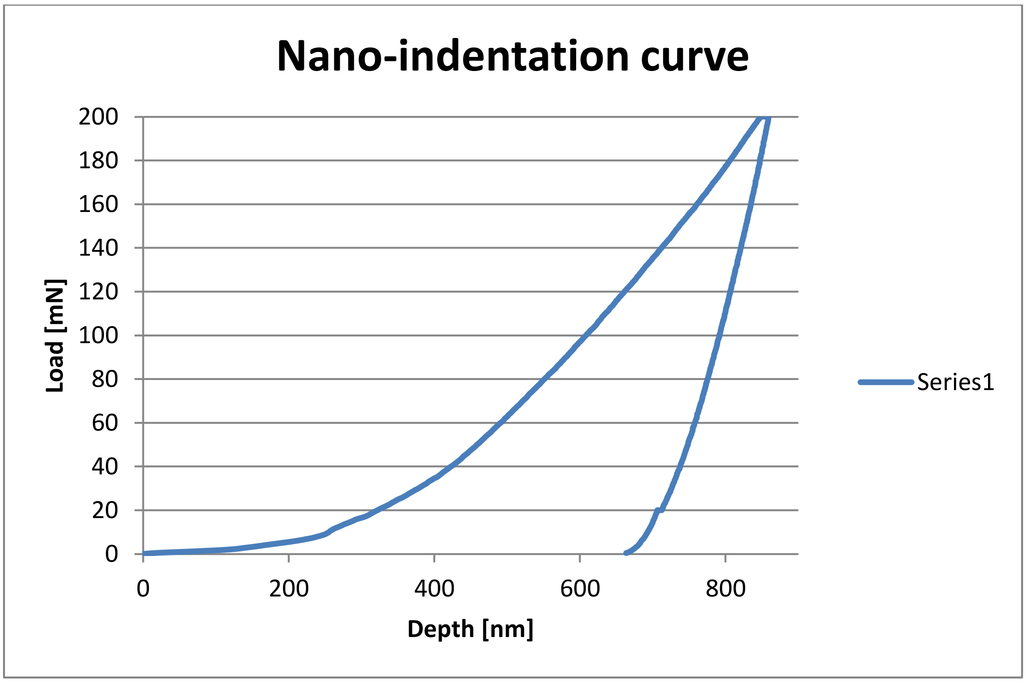

Figure 92 Load-deformation curve of nano-indentation in Test *a* taken inside the WEA

Distance between each indentation was chosen taking into account the deformed region due to the application of the load for indentation; the applied load was 200 mN which gave an induced plastic deformation depth of 880 nm maximum; this considered, the safety distance for each indentation was set to be 7 µm. The measured values of each nano-indentation test and their location are reported in Figure 93 for the original microstructure (left-hand side) and for the WEA (right-hand side) respectively.

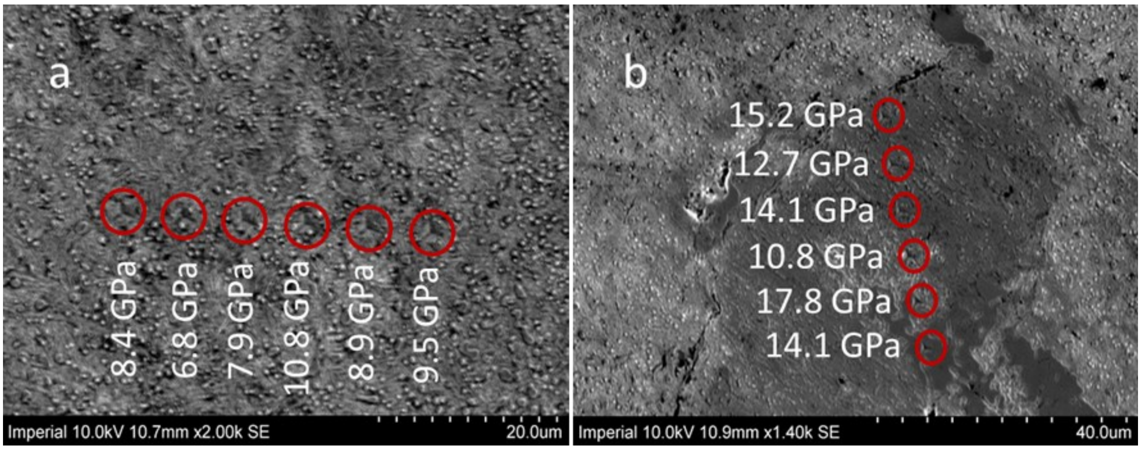

Figure 93 Nano-indentations and relative values of hardness for th eoriginal microstructure (left) and for the microstructural change (right). Results show that WEA is 40% harder than the initial steel

As evident in these results, the WEA created in HFRR test is about 40% harder on average than the original steel matrix. This is in agreement with hardness measurements proposed in the literature, concerning WEAs from the field and hence, confirm that WEA created via rubbing are the same as those found in prematurely failed bearings, rather than some other type of WEA.

6.3 Conclusions

In this chapter an experiment designed to investigate the possibility of reproducing white etching areas under rubbing conditions was presented. The experiment was designed to simulate crack-face rubbing in a cracked half space, and hence confirm whether or not WEA can be formed through rubbing of crack-faces. This in turn confirms that WEA are simply a consequence of an existing fatigue crack rather than being of significance to any bearing failures.

The results show that WEAs can indeed be produced by simply running of two bearing steel specimens. Nano-indentation tests confirm that WEA produced in this manner are representative of those found around WECs in real failures. WEA were produced regardless of lubricant used during the rubbing tests and under dry conditions, confirming that any influence of lubricant composition is not the main driver of WEA formation.

In the next chapter, these results will be discussed together with other results obtained in rolling contact fatigue tests and an overall theory for WEC formation and their relationship to premature failures in rolling bearings will be proposed.

7 Discussion

In this chapter the selected results presented previously will be discussed. The discussion will proceed to answer the initial research questions that were at the base of the motivation of this research. One will begin to recognize that WECs produced in tests are representative of those from the field, through a characterization of their WEAs; then the relationship WEA/WEC will be discussed and explained with the crack-face rubbing hypothesis. Then the attention will be focused on the WEC formation mechanisms, explaining the logical explanation of WEC formation based on the observations provided in earlier chapters. The main root cause for WEC initiation will be proposed. Other mechanisms of WEC formation that have been already proposed in literature will also be discussed in view of the present results including the role of lubricant chemistry by discussing the implications of changing lubricant composition when testing under rolling contact fatigue regime Finally, a relationship with premature failures in bearings from the field will be exposed in the light of the achievements that this study has accomplished.

7.1 Are WECs in current tests representative of those observed in premature failures of bearings from the field?

The aim of this work is to study and understand the main root cause for WEC formation in bearing steel and relate this problem to premature failures in the field.

In the present tests, it was noticed that white etching cracks are not generally associated with the final failure. The final failure is more likely to be due to a non-white etching surface-breaking crack, rather than a WEC which, as observed, are not surface-breaking. It is also not possible to say whether or not observed failures are premature failures due to the statistical nature of RCF failure lifetimes. In order to do that, one would need to test many (20 or so at least) specimens under exactly the same conditions to obtain a Weibull curve and hence get the L_{10} value which can then be compared to that predicted using bearing life theories. This was not the aim of the current research.

As outlined in the literature section of this thesis, it is now widely recognized that the alteration of the steel associated with WEAs is a refined microstructure supersaturated in carbon and composed of nano-sized BCC crystals of ferrite [60,61].

It is important to verify whether WECs produced here in controlled lab conditions are representative of white etching cracks from real bearings.

TEM/FIB analysis has been conducted with this aim and results of this investigation were illustrated. The indexes of the lattice planes identified using X-ray diffraction, were those corresponding to the BCC structure typical of ferrite. Since the diffraction pattern was showing rings, instead of isolated spots, it has been verified that microstructural changes decorating cracks obtained from tests with MPR were indeed composed of a refined microstructure of the steel. With high magnification images and aperture of beam, it was estimated the size of the nano-structure to be 10-30 nm. This is in full agreement with characterization of WECs from the field. Hence, the analogy with lab-produced WECs in term of WEA composition is confirmed.

Once an initial similarity between WEAs in current tests and WEAs in real bearings has been proved, it is now worthy analysing the morphology and some peculiar features of WECs produced in current tests. This will lead to some useful considerations about WEA/WEC duality.

7.2 Does a crack or white etching area occur first?

In the present study, no WEA has been observed without an associated crack, while many cracks were observed without WEAs. This aspect is important because gives a hint about possible relation between white etching areas and cracks. Specifically, in this case, white etching areas are suggested to be a mere consequence of crack initiation.

From direct observations of results, it appears that microstructural changes causing white etching areas are produced via rubbing of pre-existing crack-faces. In fact, several aspects arisen from direct observation of lab-produced WECs are consistent with such crack-face rubbing hypothesis. First of all, WEAs appeared to be more pronounced as the number of contact cycles kept increasing. The fact that WEA extension seems to be related to the number of contact cycles suggests that a longer test causes more rubbing within two faces of a crack and hence produces more extensive WEAs. Secondly, WECs observed were generally much thinner than non-white etching cracks. The small thickness of a crack could cause a more severe rubbing of its faces, hence producing white etching areas. Furthermore, it has been shown that in many cases, cracks are extensively branched; following irregular patterns and their concavity tends to rapidly change very often. More often than not, only the horizontal branches (parallel to the surface) of such a network exhibit WEAs, while the vertical cracks do not. The presence of numerous branches and several intersections of those branches provides preferred locations for rubbing under cyclic loading conditions. The fact that cracks are very thin makes this rubbing even more severe and finally, the dependence of WEA spread with contact cycles corroborate this supposition.

These conclusions follow logically from the observations made here, however, it is not possible to provide direct evidence of the crack face rubbing causing WEA under RCF conditions. To address this, this work employs a different experimental set-up, based on high frequency reciprocating rig (HFRR) to show that it is possible to obtain microstructural changes starting from a rubbing contact condition. Tests under rubbing conditions, presented in Chapter 6 have clearly shown that it is actually possible to obtain microstructural changes causing WEA in bearing steel when two separate bearing steel surfaces rub with each other. An example white etching area produced in reciprocating conditions was inspected using an SEM microscope. Figure 94 shows a white etching area obtained from a HFRR test (on the left-hand side) and an example of WEA associated with a crack from the field (right-hand side) [10]; the similarity between the two is evident. In both situations, in fact, there is a neat differentiation between the microstructural change and the surrounding matrix, so that a homogeneous alteration is clearly originated from the initial microstructure; both in the case of the HFRR test or in the case of the WEC from the field, carbides and lath martensite within this alteration are now replaced with a very fine structure, whose internal features are not distinguishable.

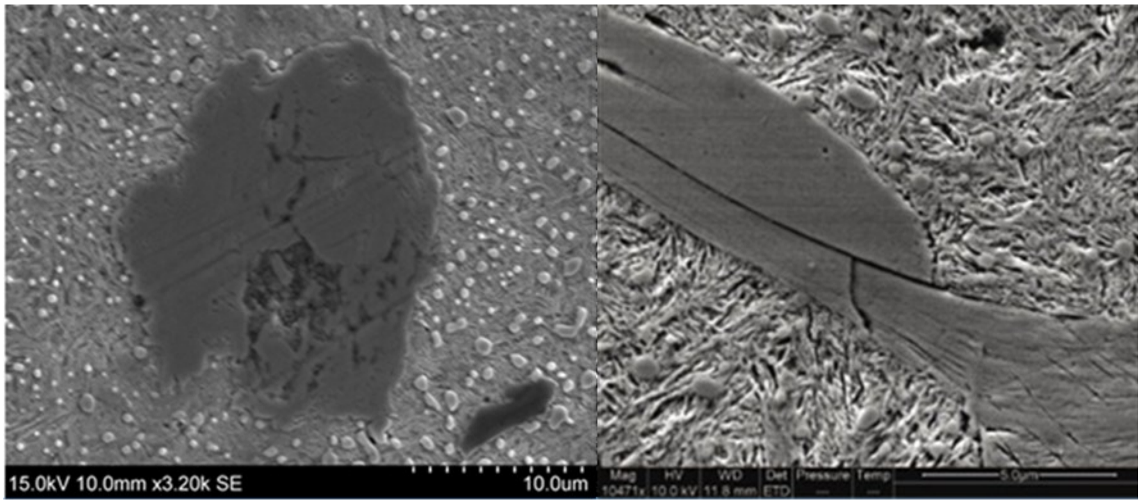

Figure 94 Analogy in the appearance between a WEA from a HFRR test (left) and a WEA associated with a crack from the field [10]

WEAs in HFRR tests have also been characterised with nano-indentations in order to confirm that their hardness is higher than the surrounding matrix as is the case in WEA in premature failures [10] rather than temperature transferred layers for example, which show lower hardness than the matrix. These measurements confirmed that those alterations of microstructure are indeed representative of those found in WECs from the field, being 40% harder than the original steel.

Here, it is important to stress the fact that WEAs were produced in rubbing contact also under completely dry conditions, in Test *c*, presented in Chapter 6. This implies that the presence of lubricant in the contact or inside the crack is not necessary for WEA formation. Notwithstanding this observation, the presence of lubricant inside the crack can affect WEA formation through mechanical means however. Firstly, it could potentially mitigate the effect of rubbing by reducing friction between two crack-faces. In fact, the reduction of friction between crack faces, and hence reduction in WEA formation, due to lubricant action is the most likely reason why surface breaking cracks (which can have lubricant entered in them) do not show WEA where subsurface ones (which rub dry) do show WEA. Conversely, in other instances and other locations, lubricant could prevent crack-face locking, promoting rubbing and hence WEA formation. Both of these factors may be at play under certain conditions and in certain locations, but nevertheless, it is rather obvious that lubricant properties are not the primary cause of WEC formation

Present results provide the strongest evidence yet that crack-face rubbing is the cause of WEA formation. This means that WEAs are just a consequence of an existing crack.

It is believed that the white etching areas observed in WECs, are a result of re-crystallisation process which can occur via dislocation movement and plastic deformation [63,71,78], which require a certain amount of energy in order to take place. Furthermore, a high number of cracks in current tests with the MPR have been noticed with no white etching area related to them, suggesting that in many cases white etching areas starting from an initial crack do not necessarily occur. This observation suggests that certain conditions in terms of stress and/or energy input at crack faces need to exist in order for the transformation to take place. Hence, the magnitude of the friction force between crack faces and pressure exerted between them and frequency of the reciprocating movement between crack-faces are all likely to be important.

7.3 Influence of slide-to-roll ratio, Hertz contact pressure and specific film thickness

Based on the results obtained from the MPR tests some conclusions can be made regarding factors that appear not to be of primary significance in WEC formation.

Section 5.5 presented a set of tests in which lambda ratio was varied, with all lambda ratios employed being less than 1, i.e. within the boundary/mixed regime. WECs were obtained in all cases.

In the literature, lambda ratio is claimed to play a role in WEC formation, with common reason being that lower lambda promotes generation of fresh nascent surface, promoting hydrogen absorption. Some results shown in present study are in fact in contrast to this. For example, in tests shown in section 5.2.1, butterflies were noticed only when lambda was increased. Hence, based on the results presented here, within the lambda ratio range tested (all less than <1), lambda ratio is not seen to be of primary significance for WEC generation. Of course, lambda ratio affects stress history that a surface sees. so it does play a role in the way in which the damage progresses and more importantly, it can alter the type of damage that dominates: micro-pitting and wear for example both occur at low lambda and when they do occur they affect the likelihood of pitting damage, occurring through WECs or otherwise. If pitting damage is to be studied therefore, wear and micro-pitting need to be suppressed. For example, in Test 3, the lambda ratio was deliberately slightly increased to avoid the spread of micro-pitting damage, and so promoting pit failure.

The tests shown in section 5.4 tested the influence of nominal Hertz pressure on WEC formation. No particular difference in term of WEC manifestation was found at different contact pressures. For this reason, nominal contact pressures are not considered here to be of primary importance for WEC phenomenon. In fact, a higher load may cause less WEA considering also what has been shown in this study concerning the crack-face rubbing hypothesis: a higher nominal pressure promotes an accelerated failure where cracks have less time to rub and hence, white etching alterations are likely to be less accentuated if the relative fast failure occurs.

The effect of sliding was taken in consideration in the set of tests presented in paragraph 5.3. In this study different magnitudes of slide-roll ratio have been considered; also, direction of sliding was varied from negative to positive (roller faster and lower respectively). Hence, sliding magnitude and direction do not appear to be of primary significance for WEC generation either. Nevertheless, a consideration is made in the following, concerning the role of sliding in crack formation under rolling contact fatigue. It has long been established that sliding direction affects the surface crack formation and propagation rate and determines the direction of propagation. WECs produced with MPR tests seem to be sub-surface initiated, in the sense that they are not directly linked to the surface. Therefore, it is not surprising that slide-roll ratio seems to be inconsequential to WEC generation.

A good discussion on the role of sliding for surface damage is presented in [27]. As far back as 1935, Way [20] observed that negative sliding accelerates surface damage under rolling contact fatigue. In the 1980s Murakami and co-workers [19] showed that negative sliding, where the friction direction is opposite to the direction of contact movement across the surface, can increase mode I stress intensity factors for surface breaking cracks through the mechanism of fluid entrapment and subsequent pressurisation inside the surface-breaking crack. The theory is also supported by the work of Bower [22], while the increase in stress intensity factors through hydraulic action of lubricants was later modelled in more detail by Balcombe et al [126]. Indeed, it is standard practice in rolling contact fatigue lab level tests to have the test specimen slower than the counterface in order to produce surface cracks in studies of pitting and micro-pitting [27,28,121,122]. As evident in these works, negative sliding does indeed produce and accelerate the propagation of surface-initiated cracks under lubricated rolling contact conditions; however, such cracks do not necessarily have the white etching decorations, as observed in current tests presented in this work.

One theory found in the literature is that negative sliding promotes crack face rubbing and hence, induces microstructural changes through shear stresses acting on the rubbing crack faces [66]. Indeed if WEC are surface breaking, sliding direction may have an important role. If the direction of sliding is such that contact motion and friction are in opposite directions, fluid will be entrained into the crack. This will in turn result in lower friction than in the case of positive sliding where the entry of lubricant into the crack is prevented by the mouth closure caused by the direction of friction force. Lower friction would reduce the shear stress between crack faces, and hence, should reduce the amount of microstructural changes. Furthermore, given that an existing crack would propagate faster under negative sliding than under positive sliding, the crack faces would rub for a shorter time in this case prior to eventual failure, which once again is likely to reduce the amount of microstructural alterations, not increase it. Hence, the observation that negative sliding (damaged surface slower) is associated with white etching cracks, may well be due to the simple fact that, in line with RCF theories, cracks are more likely to exist under negative sliding than positive sliding in the first place.

The next section will discuss the potential role of lubricant chemistry in WEC formation based on the evidence provided in the present tests.

7.3.1 Discussion on the influence of lubricant chemistry on WEC formation: mechanical vs chemical effects

Section 5.2 presented a set of MPR tests performed with different oil formulations. It was shown that WECs were produced with all lubricants tested. No particular difference was noticed between WECs obtained with fully formulated commercial oils (including what is in literature known as 'WEC critical oil') and WECs obtained with mineral oil or PAO synthetic oil. The PAO and base oils used in this study had ZDDP anti-wear additive added for purposes of preventing excessive wear during the long duration of fatigue tests, as described in detail in earlier sections. The supplementary tests that were conducted with pure PAO and mineral oils (with no ZDDP) also showed WECs, although their presence was less and they were focused around inclusions which act as a source of stress raisers, i.e. as long as the critical stress profile is provided WECs are formed. These results emerged from the current study strongly suggest again that lubricant formulation and additive package in particular, are not the primary drivers for WEC formation in this case. The fact that surface-breaking cracks, in which lubricant is very likely to penetrate, do not exhibit WEAs while sub-surface cracks, where lubricant is not present, do, gives further weight to this assertion. Results from HFRR tests that were conducted under dry conditions clearly show that a particular lubricant action is not necessary for WEA formation.

However, it is worth considering this assertion in relation to various works in literature which suggest that additive packages have a primary role in WEC formation. As was discussed in the experimental design chapter of this thesis, it is not straightforward to isolate chemical influences of any particular oil formulation from the mechanical ones. Basically, different lubricant results in different amounts of wear and roughness profiles during the test which directly affects the stress history and given that, fatigue lives are highly affected by stresses, life being inversely proportional to stress raised to power 9 or so, it is very easy to attribute any difference in results to additive formulations. Similar effects are discussed and explained in the micro-pitting studies of Olver and co-workers [28,110,111]. The actual role of chemistry on rolling contact fatigue tests can be isolated and recognised mainly by considering its implications on the stress field during the test.

To illustrate this, surface evolution and wear rates were monitored throughout the tests with and without ZDDP in the present study as shown in section 5.2.1. Generally, due to the low lambda ratios employed here, the surfaces can undergo substantial changes during the fatigue test and these changes differ markedly in tests with and without anti-wear additive as may be expected. In order to have a better insight in this respect, Test 7 and Test 8 were reported in paragraph 5.2.1. The relevant results provide strong clues as to the potential mechanisms of action of the lubricant formulation. As described, counterface rings were inspected to record evolution of roughness during the initial 440000 cycles of testing and then at the end of the test, after 20 million cycles. Also pictures of rollers until 20 million cycles have been taken. The substantial divergence between the two tests is that the surface of roller specimen tested with oil + ZDDP shows presence of cracks at the edges already after 440000 million cycles. As the test progresses, those cracks propagate. On the other hand, the test with pure oil shows a roller surface which is lacking those edge cracks and only limited damage in the form of micro-pitting is observed after 10 million cycles. The reasons for these differences lie in the different wear rates of the roller and ring samples that are obtained with and without anti-wear additive. Figure 95 below shows the roughness of the counterface rings measured over the duration of the test with and without anti-wear additive. It is immediately apparent that there is a remarkable drop in roughness for test with no ZDDP, whereas, roughness of rings tested with ZDDP does not appreciably change if compared to the initial value. These differences in roughness will obviously impart a different stress history to the roller test specimen over the fatigue test given the low lambda ratios, and hence different fatigue failure behaviour is to be expected.

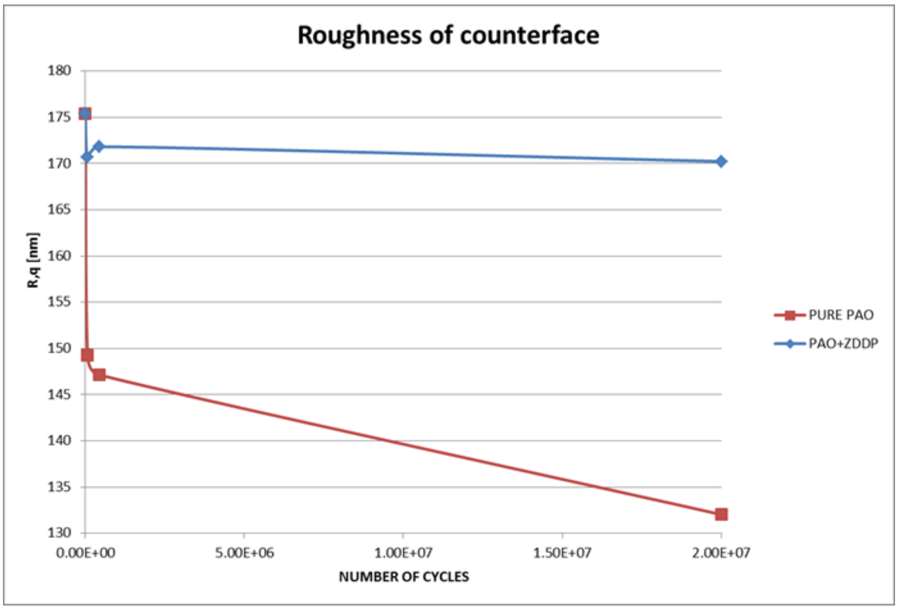

Figure 95 Evolution of roughness of counterface rings when testing with and without ZDDP. It is visible how the roughness is considerably reduced in the test with pure PAO oil

Perhaps more importantly with respect to stress history, the surface of the test roller also undergoes different changes depending on the wear rates. Figure 96 shows roller profiles from the two tests, with and without ZDDP anti-wear additive, at the beginning of the test, after 440000 cycles, after 880000 cycles and after 1.32 million cycles respectively. It is interesting to look at the profiles right at the edges of the running track and notice how they evolve during the test in the two cases. It is visible that edges wear off faster in the case of the test conducted with pure PAO. In this case, apparently, the absence of anti-wear additive is causing more wear which acts to smoothen down the sharp edges very quickly. This is in line with the effect described above where the absence of ZDDP also results in the reduction of roughness of the counterface rings.

In the light of the interpretation of WEC formation in present tests, the observation of these factors helps to explain the limited presence of white etching crack network when testing with pure PAO oil. The absence anti-wear additive is responsible for the wear of the edges which are responsible for the initial pressure spikes. Hence, in the case of pure oil, since these edges are worn off very quickly there is not enough time for the initial cracks to form (a necessary precursor for WEA formation). On the other hand, when ZDDP is present, the roller edges do not wear as quickly (ZDDP is simply doing its job) and associated stress concentration can persist for somewhat longer time so that cracks can be initiated. This fact, coupled with the higher roughness (which also modifies stresses), explains the fewer cracks when pure PAO is used i.e. the effect of lubricant is mechanical via modifying the stress history that the contact is subjected too.

Hence, an important consideration can be made in terms of the effect of oil chemistry: the role of additives (anti-wear additives in particular) is not directly related to WEC formation in MPR tests. Instead, any oil effects are primarily mechanical through helping to ensure a favourable stress state and stress history in time for formation of WECs. In the total absence of an anti-wear additive, or with an anti-wear additive that is less effective than ZDDP, the stress history is changed very quickly due to wear to the conditions that are less likely to promote WEC formation. This does not mean that failure is prevented at all; as seen in this study other non-WEC cracks can still cause the failure regardless or the extensive wear itself can cause the failure, so the use of an ineffective anti-wear additive is not recommended. The correct oil for an application should ensure the right balance between wearing in (which suppresses stress contestations on the surface) and mild wear conditions.

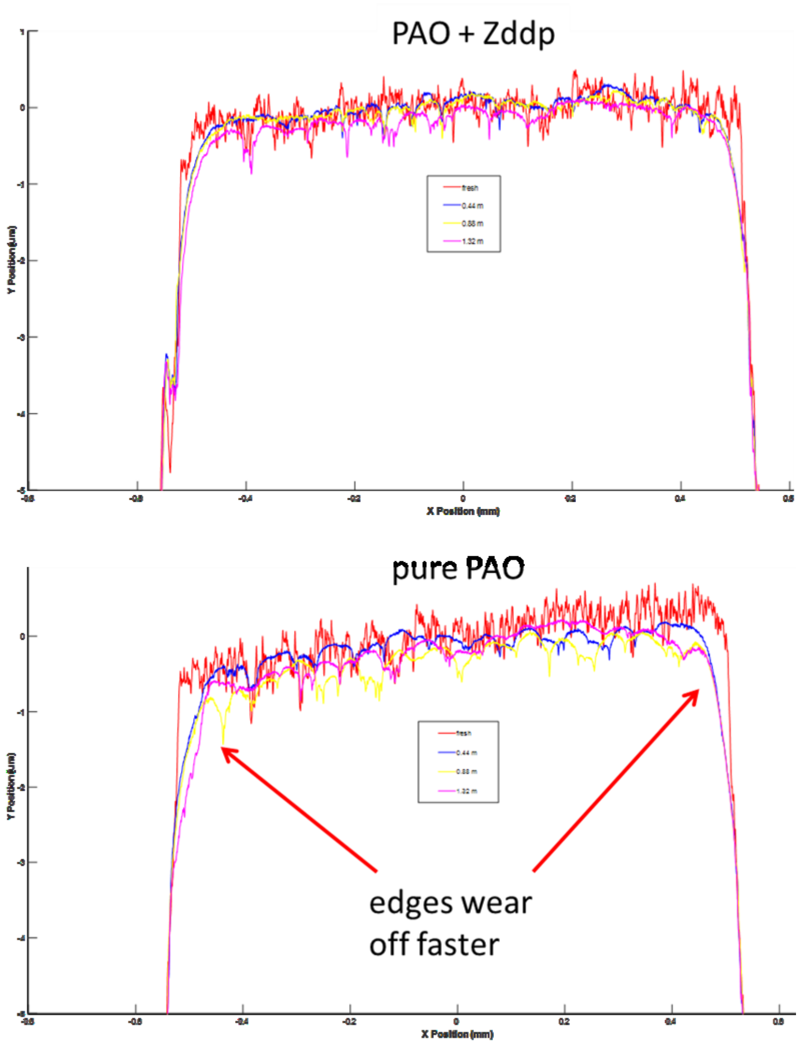

Figure 96 Evolution of roller profiles in test with pure PAO oil and PAO + ZDDP. It is clear how the edges wear off faster in the case with pure PAO which has a direct effect on contact stress history and subsequent formation of WECs

7.4 Mechanism of WEC Formation

(Note: the part of discussion contained in this sub-section 7.4 is based on the equivalent discussion section in the paper submitted for publication by the author [8])

7.4.1 Pressure distribution in a truncated line contact vs elliptical contact

Given that kinematics, lubrication conditions and nominal pressures were all the same in line and elliptical contacts tested here, it is clear that there must be some other major aspect of the line contact employed here that is different to the elliptical contact and is responsible for such consistent generation of white etching cracks in line contact and their consistent absence in elliptical contact.

The most obvious factor in this respect is the difference in the contact pressure distribution between the two contact geometries. The truncated line contact employed on the MPR inevitably produces high edge stresses, at least in the initial period of operation before the disc and roller surfaces wear and deform at the edges to improve conformity in this region. The elliptical contact does not produce such stress concentrations. Indeed, the existence of edge stresses in truncated line contacts on the MPR triple disc machine was mentioned earlier as a factor that received considerable attention in the historical development of this experimental set-up; the purely cylindrical specimens employed by Graham in the early use of the triple-disc set-up for micropittinig studies were replaced by barrel rollers in the later pitting studies of Wilkinson [119] on the same rig with the specific intention of eliminating the edge stresses and unwanted contact damage associated with them.

To further analyse the pressure distribution in the truncated line contact of cylindrical rings and chamfered roller MPR specimens, Figure 97, Figure 98 and Figure 99 show the development of this contact pressure distribution over time in an example MPR test conducted at nominal Hertz pressure of 1.93 GPa. The rough contact pressure distributions shown here are calculated using existing numerical models [122] and actual rough surfaces of the roller and a ring measured using a stylus profilometer at set intervals during the test. In this way any changes in the contact pressure distribution over the duration of the test can be captured. A 3D contact solver is employed but only two dimensional plots in the transverse plane through the middle of the contact are shown, since the edge stresses are visible in this plane. Figure 97 shows the measured roller profile in the transverse direction at the start of the test and at 5 million cycles. It is evident that the area near the edges of the roller is worn/deformed considerably in the first 5 million cycles due to presence of edge stresses in this region.

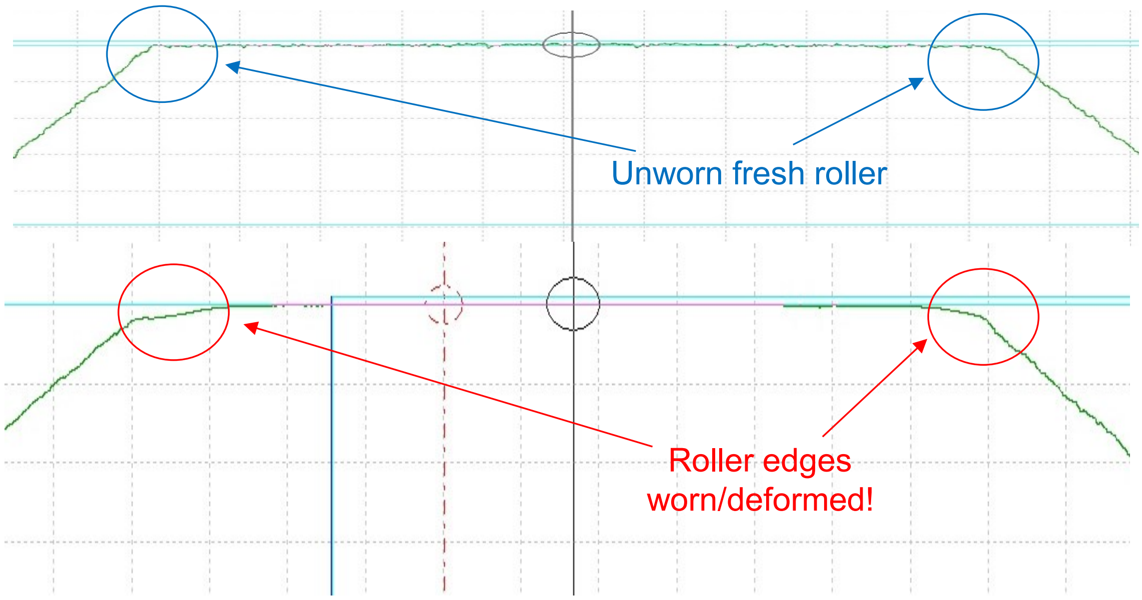

Figure 97 Roller profiles measured using a stylus profilometer at the start of the test and after 5 million cycles

Figure 98 shows the corresponding pressure distributions at the start of the test and at 5 million cycles as well as the nominal Hertz pressure of 1.95 GPa for comparison. The rough surface pressures shown are from an elastic solution to help illustrate the existence of edge effects (note: the use of elastic model obviously means that for a fresh roller some local pressures may be unrealistically high, but the elastic solutions nevertheless better illustrate the presence of stress concentrations at the edge and are therefore used instead of a full elastic-plastic model). For clarity, a hypothetical solution for an equivalent ideally smooth contact is also shown. It is immediately apparent from this figure that at the start of the test, significant stress concentrations exist at the edges of the roller. However, as early as 5 million cycles into the test, these edge stresses have almost totally disappeared producing a flat distribution of pressures in this transverse direction as may be expected, with rough surface pressures in the range 2 to 4 Gpa, i.e. all asperity pressures now lie within the elastic limit of roller material following the wearing-in period.

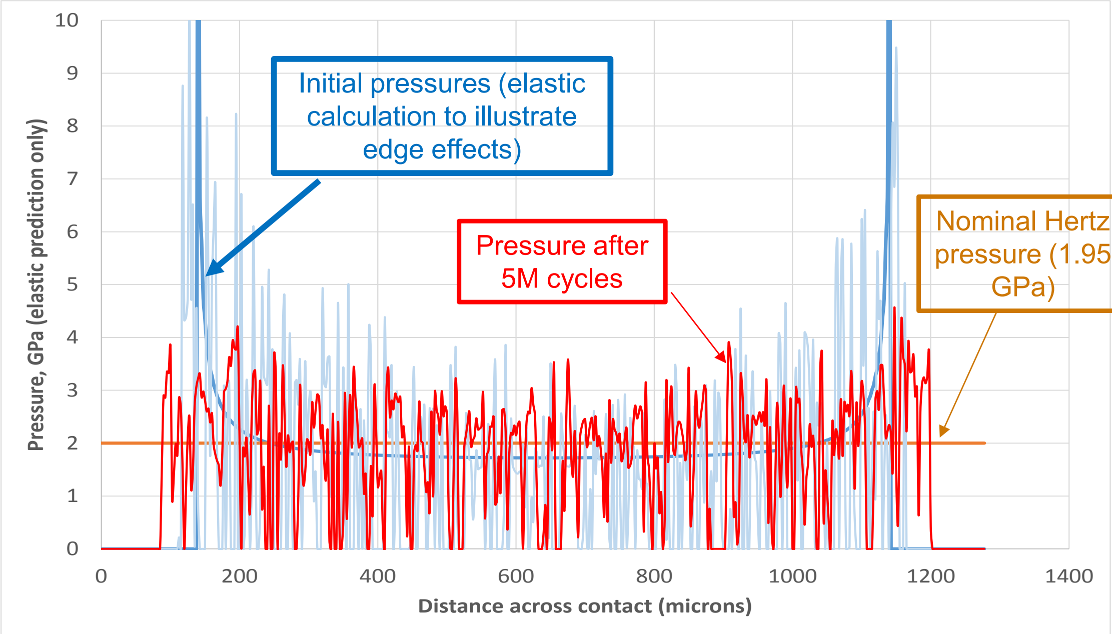

Figure 98 Predicted rough surface contact pressure distributions at the start and 5 million cycles into the test corresponding to the roller profile shown in Figure 97

Figure 99 then superimposes the pressures obtained with the roller profile measured at 10 million cycles onto those existing at 5 million cycles. It is evident that very little further change in the general pressure distribution occurs between 5 million and 10 million cycles i.e. the edge stresses exist for a relatively short period at the start of the test but due to rapid wear and deformation of the roller edges during this early period, they quickly decay to the nominal stress level. This relatively benign pressure distribution then persist for the rest of the test duration.

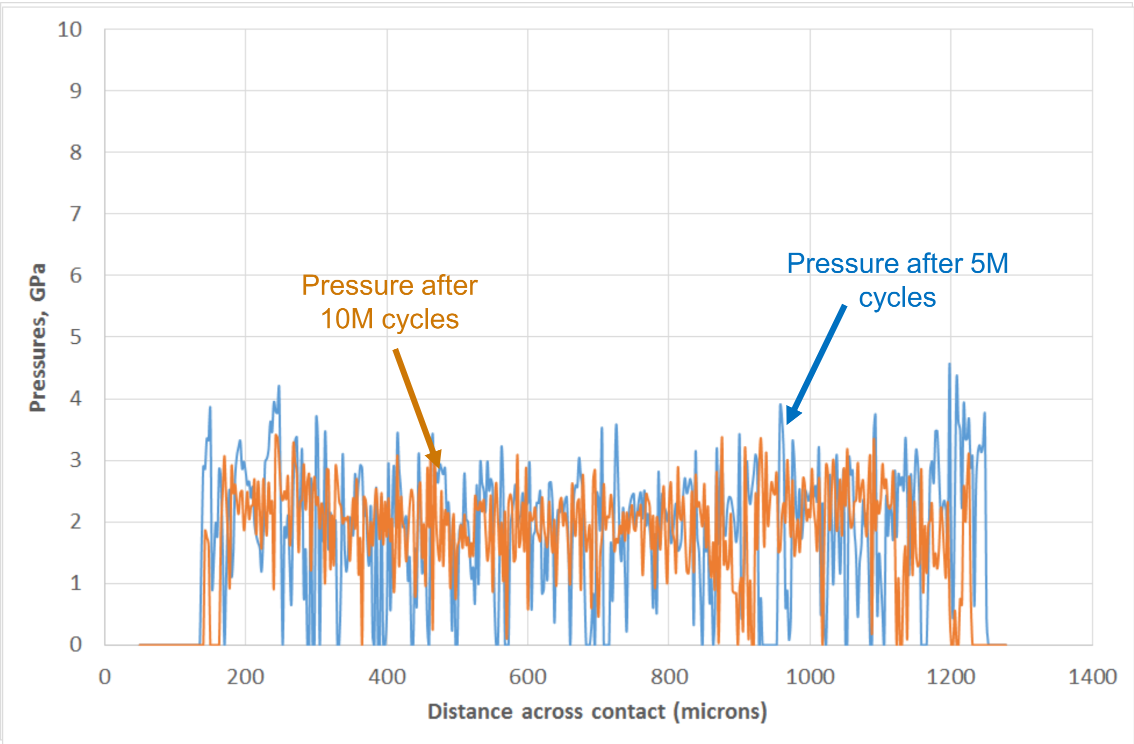

Figure 99 Comparison of pressure distribution after 5 and 10 million cycles showing that no significant changes occur in this interval unlike during the first 5 million cycles shown in Figure 98

7.4.2 Proposed mechanism of WEC Formation

The evolution of contact pressure in the truncated line contact in the MPR tests provides strong clues to the mechanism of white etching crack formation. Based on this and other observations of white etching cracks in this study, the proposed mechanism of white etching crack formation can be summarised as follows:

1. Given the widely accepted high sensitivity of crack initiations and propagation and eventual pitting failure to applied contact stress, with pitting lives being inversely proportional to contact stress to power of 9-12 [127], the high edge stresses in the early stages of the operation result in early crack initiation. The initiation is most likely to occur at any inclusions located subsurface within this high stress region. In the present study the high stresses are produced by the described edge effects. Obviously, such edge effects should not exist in well-made rolling bearings, instead plenty of other sources of stress excursions could exist in operating bearings, such as bearing ring ovality, housing deformations, misalignment, etc.

2. As these stresses drop, due to wear and plasticity at the roller edges, to the general contact stress level which is relatively low in the present tests, these cracks can only propagate relatively slowly.

3. This slow propagation under rolling sliding contact allows ample time for the crack faces to rub and beat together for millions of subsequent cycles. Since they initiated early, this rubbing occurs over a relatively long time. This prolonged rubbing produces the white etching area around the crack. Crack-face rubbing has already been proposed as the likely cause of microstructural transformations that lead to white etching matter. This also means that cracks must form before the white etching areas, a postulate that is supported in this study by the observation that no white etching areas were ever observed without an associated crack being present, but there were plenty of cracks that did not exhibit white etching areas around them. Further evidence of this is provided later.

4. Finally, a pitting failure occurs. Under low lambda ratios, pitting is most likely to be caused by a surface breaking crack, which does not necessarily need to experience white etching at all, since surface cracks generally propagate faster than sub-surface cracks.

This mechanism clearly proposes that it is the stress history in time that is the primary driver of WEC formation. The high stresses excursions must occur early in life in order to initiate cracks early, and must be short lived and followed by a relatively low nominal stress, so that the formed cracks do not propagate to an almost immediate failure but instead grow relatively slowly and therefore have sufficient time to produce white etching areas through prolonged rubbing. This time history, rather than merely the presence of a high stress at some point in the operation, is important – the same high stresses acting towards the end of the component life will clearly not have the same effect since the cracks produced by them will not have sufficient rubbing time to produce the microstructural transformations associated with white etching areas.

7.4.3 Relationship between WECs and premature bearing failures

This link between white etching cracks and time stress history explains the significance of white etching cracks to premature bearing failures. In bearing life predictions, variable stresses are accounted for through application of Palmgren-Miner linear damage accumulation rule [41]. It is well known that perhaps the biggest drawback of this rule is that it totally fails to account for the time history of applied stresses, i.e. a particular stress level is given the same weighting in the overall damage accumulation regardless of when it occurs. This fact is well recognised and discussed in structural fatigue [34] and it is also known for gears. Clearly, an extremely high stress early in components life that initiates cracks at this stage, is more likely to reduce the overall fatigue life of the component than the same stress level acting for the same duration but at a time point that is near the end of the predicted component life. Consequently, bearing life predictions, and fatigue predictions in general, that rely solely on application of Palmgren-Miner rule to deal with a variable stress that contains stress history with high stress excursions early in life, are likely to overestimate the bearing life. Better assessments of loads are needed together with more safety in considering safety factors for peak loads during the design of these bearing applications. The exact stress history, no matter at what stage of life, is also likely to cause white etching cracks in bearing steels, if appropriate conditions of crack-face rubbing apply. Therefore, a variable stress history can independently cause both WECs or early failures (see the scheme in Figure 100).

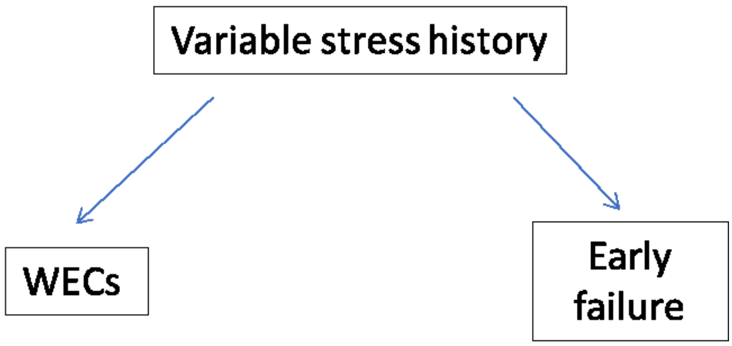

Figure 100 Relation between stress history, WECs and early failure. A variable stress history can cause both WECs and an early premature failure, but there is no direct link between the phenomenon of white etching cracks and premature failure itself

Hence, linking the two, it is the specific stress history, with short lived high stresses early in life and a relatively low nominal stress level that is responsible for both the WECs and shorter than predicted bearing lives (see Figure 101). Considering this cause-effect relationship, WECs themselves are not responsible for early bearing failures, but are simply a consequence of a particular stress history and it is that same stress history that also causes the shorter than predicted fatigue lives.

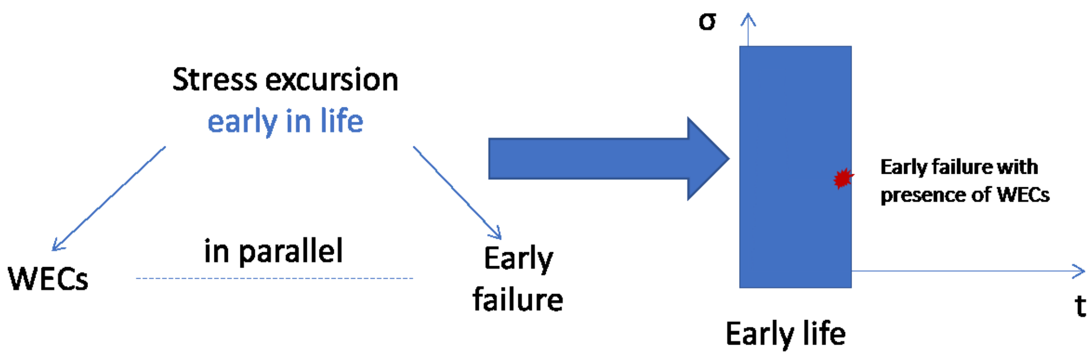

Figure 101 Link between WECs and premature failures. Only when a particular variable stress history (for example a stress excursion) occurs early in the bearing life, following the indicative profile showed in the diagram stress/time on the right of the figure, premature failures and WECs can occur in parallel

7.4.4 Further evidence for proposed mechanism: WECs in elliptical contacts with artificial stress concentrations

The mechanism of white etching crack formation and earlier than predicted fatigue failure relies on short duration high stresses exiting near the start of the contact operation followed by moderate stresses prevailing for most of the remaining stress cycles. A high stress for the whole duration of the operation would be even more damaging of course, and it would likely lead to an earlier failure, however it would be less likely to produce white etching cracks as the faces of the initiated cracks would not have sufficient time to rub against each other and cause the microstructural transformations that manifest themselves as a white etching areas. The stress history of early elevated stresses followed by moderate stress levels is very neatly achieved in the MPR tests through early edge stresses and subsequent roller wear when truncated line contact geometry is employed.

However, for the proposed theory to be universally true, it must also apply to other contact geometries and situations. In the present study, it was shown that tests with elliptical contacts in the MPR, achieved using crowned rings, conducted at the same nominal contact conditions as the line contact tests, do not produce white etching cracks even though they do produce surface initiated pitting failure. In such elliptical contacts there are no elevated early stresses so the fact that white etching cracks are not produced in this situation lends support to the proposed theory. However, if elliptical contacts were subjected to early high stresses, through some external means, then they must also produce white etching cracks if the proposed theory is to hold. To investigate this, further tests were conducted with elliptical contacts where such early stress risers were introduced by artificial means. The most obvious way to create these stress raisers in elliptical contacts is to indent the test roller or the rings with a spherical indenter. Such indent certainly promotes crack initiation and surface failure, as shown for example by Morales-Espejel et al [128]. However, the stress concentrations introduced in this way exist throughout the test and not just in the early stages of contact operation. This is therefore not the situation proposed by the current theory. Hence, in this study a slightly different approach is adopted.

A circumferential groove was created in one of the counterface rings. When the rig is run against the roller high stresses are initially created at the groove shoulders. However, since the roller is significantly softer than the ring, these high stresses very quickly create a mirror image of this groove on the roller surface through wear and plastic deformation. This groove on the roller then conforms to the original groove profile on the ring and due to this conformity the initial high stresses disappear. The process is equivalent to the high edge stresses achieved with the chamfered roller, followed by the wear of the edge roller to increase conformity. Although this approach appears simple in principle, in practice it is quite difficult to create a groove on the ring with controlled geometry so that the groove is not too deep and the shoulders not too steep to produce very fast roller failure, but the groove geometry is just right for the controlled wear of the roller to cause conformity without quick pitting failure. Indeed, the first attempt in this study employed a hard turning tool to create a ring groove but the geometry of the groove created in such a manner was very severe causing a too rapid failure of the roller. Therefore, the final approach employed was to create a groove with controlled geometry via laser etching commonly used for producing controlled surface textures [129]. The geometry of the groove created in this manner is shown in Figure 102. The figure shows that the groove is about 300 μm wide with one very narrow deep valley that reaches a depth of 5 μm.

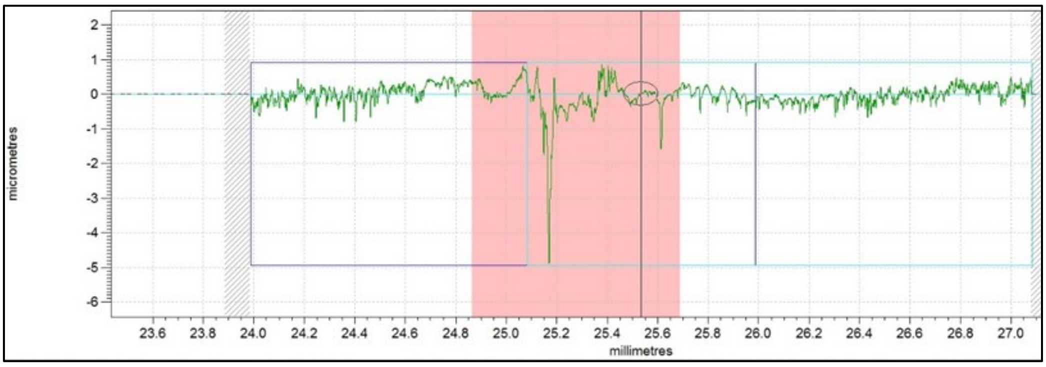

Figure 102 Grooved profile obtained by means of a laser technique [129]. **The controlled process of the laser technique allowed obtaining smaller dimensions of the shoulders with respect to previous attempts**

A normal MPR test with elliptical contact geometry was then carried out but with one of the standard crowned counterface rings replaced with this one containing the laser etched groove. The contact pressure and lambda ratio employed here are slightly less harsh than in the majority of the previous tests, in order to limit the surface damage in the roller due to sharp groove shoulders at the start of the test. After the end of the test, the roller was sectioned circumferentially in a series of planes, including in the centre of the areas where stress concentrations due to groove existed and outside this zone. Conditions of the test are listed in

Table 15.

Table 15

	Test 24
Elliptical contact configuration	n.2 80mm crowned rings + n.1 modified ring with GROOVE -flat roller
Lubricant	Group I (+ ZDDP, 0.1%P)
SRR	5 %
Friction coefficient (initial)	0.085
Max Hertz Pressure [GPa]	1.78
Minor contact semi-width	148
Major contact semi-width	904
Test Temperature [°C]	55
Entrainment speed [m/s]	2.4
Lambda ratio	0.45
Roller cycles (10^6)	30
WECs	YES

The test lasted for 30 million cycles, until a final pit occurred on the surface. The final pit on the roller is shown in Figure 103.

Figure 103 Test 24: surface damage caused by the laser groove on the roller specimen after end of test, 30 million cycles.

After failure, the flat roller was sectioned and inspected. As illustrated in Figure 104, specimen exhibited presence of WECs in its section.

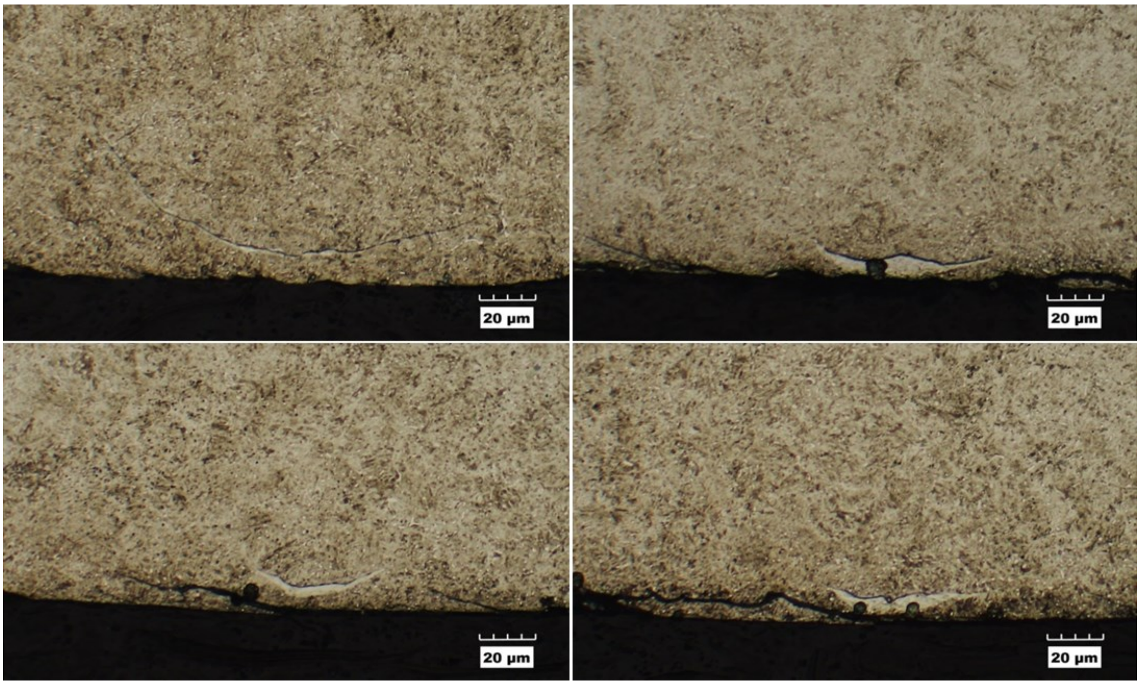

Figure 104 Sections from Test 24 with laser groove revealed presence of WECs

WECs were found in a section correspondent to the central area of contact, where the groove was located. As confirmation for the importance of the stress applied by the action of the grove, further sectioning was carried out until reaching the area of the contact not subjected to the stress of the groove.

Figure 105 shows different sections and their location on the roller surface. The horizontal black line indicated the width of the total area of the elliptical contact. The first section is taken at the middle of the contact area (dark blue line) where WECs were found. The second section is taken at the end of the area subjected by the groove stress (blue line). Here, as seen from the picture, subsurface cracks show initiation of white etching alteration; this is in accordance with what observed under line contact, where sections far from the edge stress zone (in that case in the middle of the contact area, i.e. far from the source of stress excursion represented by the edges) were exhibiting less accentuated white etching matter. The third section is taken far from the location of the groove, but still within the Hertz elliptical contact area. Here only micro-pitting surface cracks are found with no presence of white etching matter whatsoever.

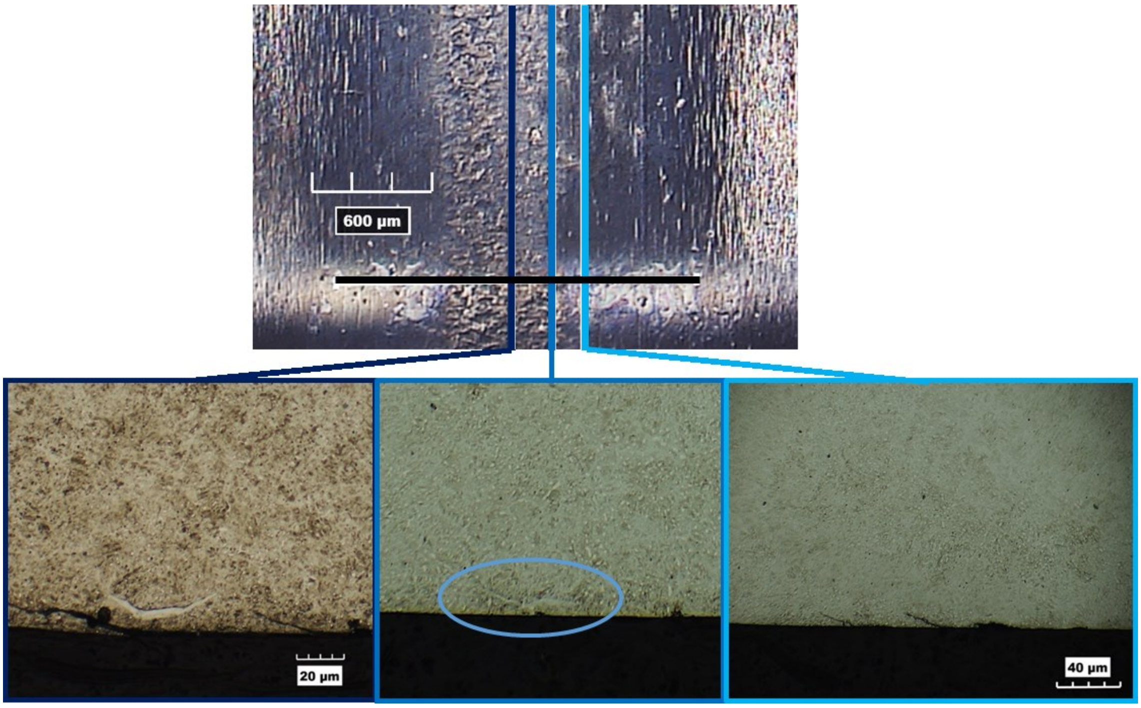

Figure 105 Three different sections from Test 24 taken at different locations of the running track. The black horizontal line in the top picture illustrates the width of full contact area; the cracks visible in the central part of the contact correspond to the region subjected to the action of the grooved counterface. It is visible that sections taken at the centre of the track show presence of WECs (bottom, left). In sections taken further towards the periphery of the contact, subsurface cracks present a less accentuated WEA (picture at the bottom, centre, circled in light blue). No WECs are found if sections are taken outside the centre of the contact area (bottom, right)

As described in the literature review chapter, other studies [7], using same specimen geometry and experimental rig, have attempted to reproduce WECs in elliptical contact configuration, with no success.

In this research, as seen, when running tests under elliptical contact, no WECs were found until a stress concentration was conveniently introduced by modifying the counterface ring by introducing a special grooved profile as a source of stress concentration. This is a remarkable achievement in confirming the validity of the proposed theory and the importance of the stress profile history for WEC formation.

7.5 Comparison with energetical approaches

Some of the recent WEC related research suggests that frictional energy input may be related to WEC formation. In some cases only a potential correlation is suggested while in other actual criteria for WEC risk assessment in terms of threshold frictional energy or frictional heat flux are provided. The proposed criteria inlcude:

- Ruellan et al. [3] were first to propose the product between the local pressure and the sliding velocity to be discriminant for WEC prediction factor based on their tests with angular contact ball bearings;
- Gould et al. [4] proposed a frictional energy [J] criterion based on MPR Test (the same rig as employed in this study). This energy is the product between the applied load, mean friction coefficient, sliding speed and time of the test. The authors state that 'correlation does not imply causation', but suggest a threshold

value of the frictional energy for WEC occurrence. The approach is shown in Figure 106. From the authors indicating the energy threshold value to be about ~5.4 MJ, i.e. below this value of energy no WECs are found in MPR AISI 52100 test rollers.

- Kruhoffer et al. proposed an ‘asperity friction energy accumulation’ parameter which is dependent on the local pressure and local friction coefficient (both at the asperity level), sliding velocity and the ratio between time of contact and time of regeneration. Despite the use of word ‘energy’ in tis name, this parameter has units of Watts [W/m^2] so it is a measure of local heat power flux rather than energy. The threshold values are derived from tests on cylindrical roller thrust bearings but authors claim that it is applicable to ‘arbitrary rolling bearing applications’ where WECs may be formed.

Such energy criteria are usually used for assesment of other types of contact damage, scuffing in particular, and thier use in assessing risk of RCF is unusual. Therefore, it is interesting to relate the present results in terms of frictional heat energy input to the criteria proposed in the literature.

The experimental study from Gould et al. [4] is based on the same MPR rig set-up used in the present research and, for this reason, it is relatively straightforward to make the comparison between the two. Gould et al. identified a threshold value of the frictional energy to be representative of WEC initiation. More precisely, if the frictional energy is below 5.4 MJ in a test, WEC formation is claimed not to occur (see Figure 106 below).

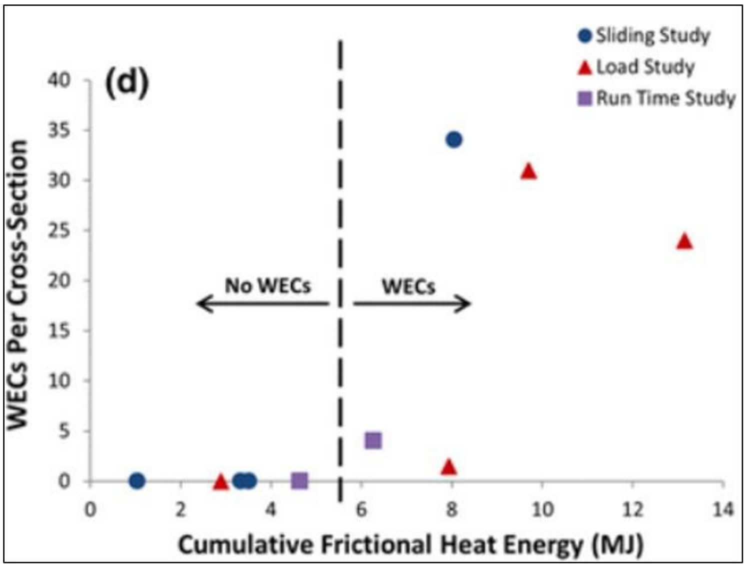

Figure 106 Cumulative frictional heat energy criterion in tests conducted in [66]**. A threshold for WEC occurrence is proposed, below which white etching cracks are claimed not to show up**

Figure 107 shows the cumulative frictional energy values corresponding to some of the tests presented in this thesis. The number of WECs per cross section was not counted in this study so the data is plotted as a bar chart indicating the friction energy values and whether or not WECs were observed (rather than their number); bars in green indicate tests where WECs were not seen, whereas bars in red showed tests where WECs were observed. The horizontal blue line is the threshold observed by Gould et al. As one can notice, there is no correlation between WEC occurrence in present tests and the proposed threshold suggested by Gould et al. In some tests WECs were generated at energies below the threshold value, and in other tests, WECs were not observed even though frictional energy values were higher than the suggested threshold. Therefore, the proposed cumulative friction energy criterion cannot be used to predict WEC generation in the present tests. This is despite the use of the same rig and same specimen geometry in Gould et al.'s tests.

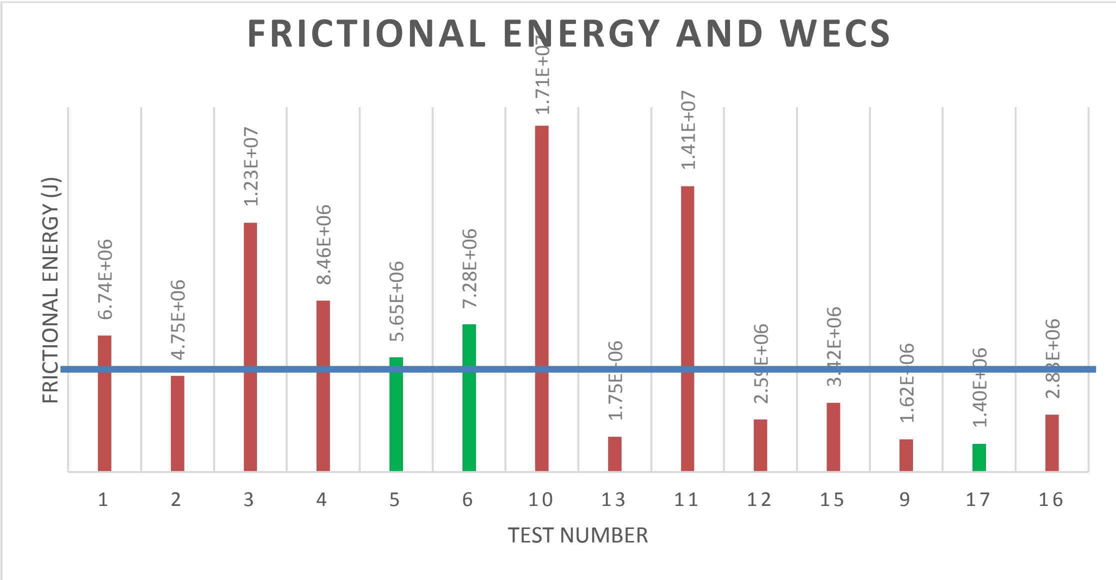

Figure 107 Frictional energy criteria and WECs in current tests. Red columns represent tests which showed presence of WECs; green columns represent WEC-free tests. The blue line in the graph represents the threshold identified by [66]**. As visible, there is no clear correlation between this threshold and WEC appearance in current tests**

The reason for different observations are not clear but are most likely to be in the difference in which the tests are run: it is impossible to say whether or not these were run and designed in the same way, if considering also the fact that they employed very low lambda ratios, as low as 0.06 even without taking into the account thermal heating aspects of the rig, whereas 0.1 was the lowest lambda ratio used here accounting for thermal aspects. The most likely reason for the difference is that Gould et al did not consider the evolution of roller profile and its clear effects on the stress history during the test but instead analysed the data in terms of frictional energy produced in the contact. The stress history is considered to be the main factor in WEC generation as proposed here so its omission from any analysis is significant. Gould et al. only used the 'WEC critical' transmission oil which may affect the stress history in a different manner etc. Whatever the case, the most likely explanation in any difference lies in the interpretation of the generated results.

In general, it is not obvious how a criterion based on frictional energy can explain the initiation and propagation of fatigue cracks. In order to generate and propagate a crack application of *stress* over number of *stress cycles* is required given the fatigue origins. Friction energy input on its own is simply not sufficient; if it were, continuous heating of section of material with external means would produce fatigue cracks and this is not the case. However, one can see how fatigue damage may correlate with any criterion based on energy (provided that stress cycles are applied anyway): any energy criteria include operations time, and for a set rotational speed, this time will correlate directly with the number of applied stress cycles. Since fatigue damage correlates with number of stress cycles, it must correlate with the running time all else being equal.

The criterions proposed by Kruhöffer et al. [5], 'asperity friction energy accumulation', includes additional aspects to describe the quality of lubrication (it considers local asperity pressures for example) as well as the time elapsed between the passage of two rolling elements over a particular area of the raceway. It is not possible to compare the current results with this criterion directly, given the different set-ups. However, some analaysis of the implications of this criterion can be performed using published bearing life data. Using an FE8 bearing test rig, Kruhöffer et al. tested CRTB 81212 bearings in different conditions. The test taken in consideration for the analysis is the one referred in their paper as CRTB1 standard [5], which failed after 20.7M cycles due to WECs. As specified in their paper, the number of cycles to failure is not expressed as number of shaft revolutions or time to failure, but it is considered as the number of contact load cycles until failure.

The proposed 'asperity friction energy accumulation' coefficient is dependent on friction and pressure at the asperity contact, sliding velocity, contact time and regeneration time, according to the following formula [5]):

$$e_{a,c} = \frac{\pi}{4}\,\mu_c p_c v \frac{t_{contact}}{t_{reg}}.$$

As already introduced in the literature review, $t_{contact}$ is the time elapsed during a single contact and $t_{reg,}$ is the so called "regeneration time", i.e. the time span between two consecutive contact cycles; v is the sliding velocity, p_c and μ_c are respectively the local pressure and the local friction at the asperity contact. The higher is the value of the coefficient, the higher the risk to have WEC failure. The authors do not provide explicit values of the coefficient for the tests, but based on the graph retrievable from the paper, here reported in Figure 108; the value of the product p_c*v is obtained and the coefficient proposed as indicator for WECs can be now extrapolated, resulting to be $6*10^4$ W/mm^2.

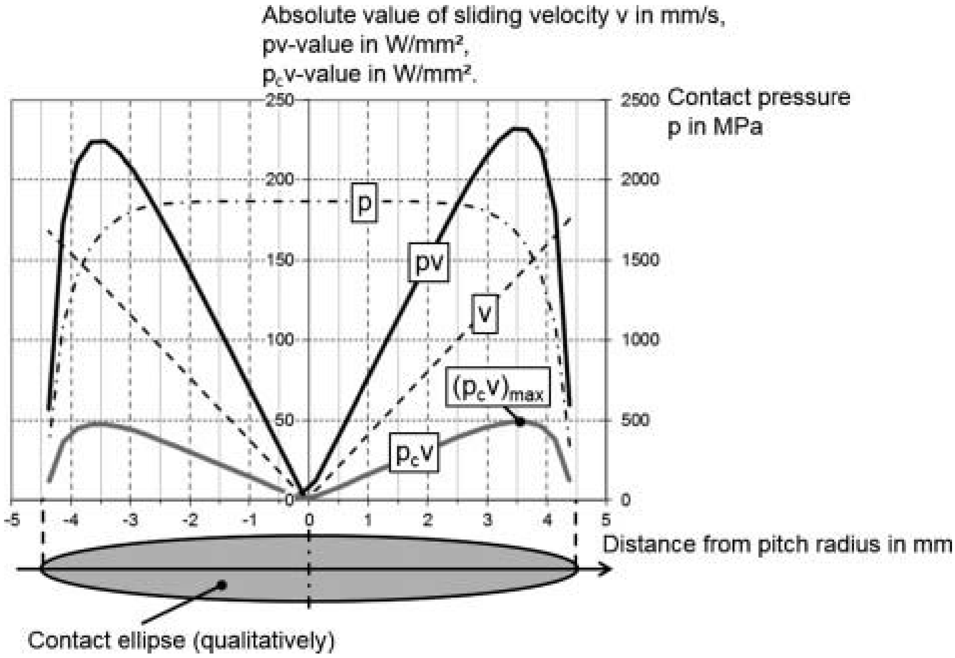

Figure 108 Pressure distribution and sliding velocity in a CRTB tested in [5] **along the major axis of the contact area**

As the authors state, in their calculations the pressure at the asperity contact used was corrected taking into account the value of lambda during the test, considering that the higher the film thickness, the lower is the pressure carried at the asperity contact.

In order to assess whether this proposed criterion is generally applicable to 'arbitrary bearing applications' data from a publication by Morales-Espejel et al. [130] is used for comparison. It is generally difficult to find value of absolute bearing lifetimes in literature, but reference [130] does contain such values for an SRB 22220E tested in a full bearing rig in an endurance test (see extract from the paper shown in Figure 109).

Table 3 Bearing types and operating conditions for the four endurance tests

Test	Designation	F_r (kN)	Speed (r/min)	κ	Mineral oil	L_{10} (Mrev)	Low conf. (Mrev)	High conf. (Mrev)	β slope
1	NU 207E	19.1	6000	0.42	VG 10	20.9	13.5	25.7	5
2	NU 207E	19.1	6000	0.42	VG 10	11.13	6.4	35.8	1.5
3	2222E	140	1500	0.42	VG 10	40	16	58	2.5
4	2222E	140	1500	0.42	VG 10	34	18	50	2.5

Figure 109 Table from with details of endurance test in a full bearing rig for an SRB 22220E

The bearing failed after 40M bearing revolutions without showing presence of white etching cracks. In order to make a comparison with the bearing tested in Kruhöffer et al [5], it is necessary to convert this time to failure into a number of contact load cycles on a given area of the inner ring. Knowing the characteristics of the bearing and the shaft speed as supplied in the paper, one can obtain the number of over-rollings at the inner ring to be 10.9 per bearing revolution; thus the number of contact load cycles for this case is 40M*10.9 = 436M contact load cycles. From the knowledge of the geometry of the SRB 22220E and knowing the test conditions, one can obtain the specific pressure distribution for this SRB bearing case, illustrated in Figure 110 (analogous to graph in Figure 108 from [5].

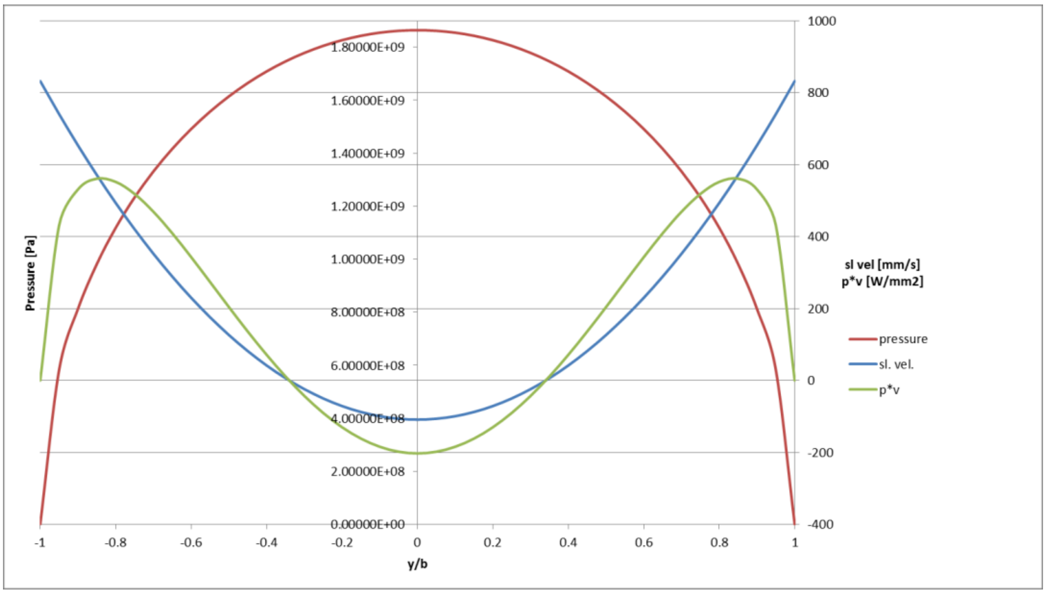

Figure 110 Pressure distribution and sliding velocity for the SRB tested in [130] **along the major axis of the contact area**

In this analysis as well, the pressure was corrected taking into account the asperity load factor from SKF catalogue (Φ_{bl}=0.6, see Figure 111) in order to obtain the 'asperity' pressure as used in the proposed criterion.

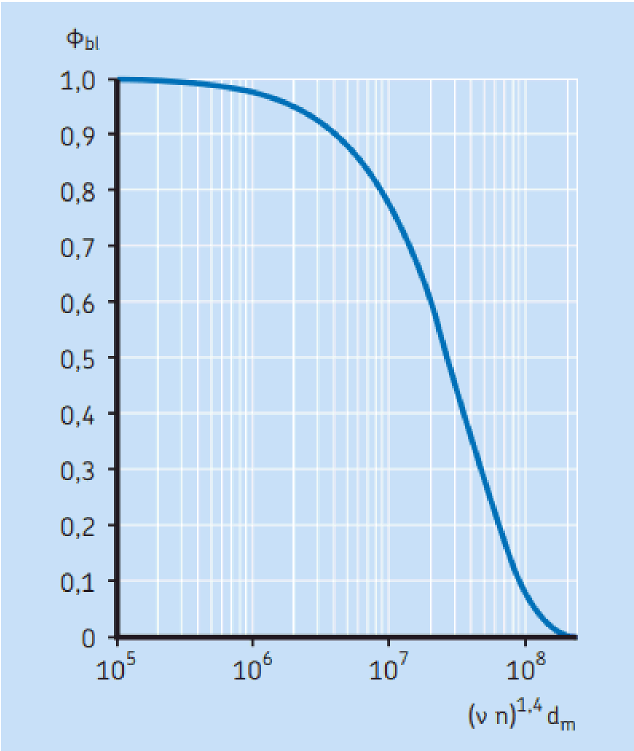

Figure 111 Asperity load factor from SKF catalogue [131]**. Knowing the value of the abscissa for the bearing in** [130]**, Φ_{bl} is equal to 0.6**

Substituting all these values into the equation proposed by Kruhöffer et al, results in the value of the proposed WEC prediction coefficient for this published SRB bearing case equal to $1.26*10^6$ W/mm^2. This is almost two orders of magnitude higher than the value of the previously considered bearing in [5] as outlined above. Although various assumptions had to be made in the analysis presented here, they cannot explain such large mismatch in the value of the coefficient. The fact that the spherical roller bearing considered here did not show WECs, despite much higher value of this proposed WEC indicator suggests that the indicator may not be applicable to 'arbitrary bearing applications' and care should be taken in its use. It was argued above that some correlation between fatigue damage and an energy based criterion may exist owing to the fact that energy criteria contain operational time within them and this scales with the number of stress cycles. This cannot be said about heat flux criteria which have units of W/m^2 and hence do not contain the operational time. Although some correlation may exist in specific cases, it is difficult to see how the magnitude of heat flux power can correlate with the occurrence of fatigue crack generation and propagation since it contains no information on stress cycles at all. If such an approach was to be universally applicable to rolling contacts, it would imply that fatigue crack can be generated and grown by instantaneous supply of high heating power to a spot on bearing steel such as with a laser or similar. This may result in alteration to the steel but is generally not thought to produce and grow fatigue cracks.

The analysis presented here indicates the risks of using a specific single criterion to predict onset of WECs, or any other fatigue damage, Generally, any given criterion based on experimental results may be valid for the set of those specific results obtained and for a given experimental set-up but may not be universally valid for other tests in different configurations or for real applications.

7.6 Conclusions

This chapter has discussed results from this study. A new theory for the mechanisms responsible for the formation WECs is proposed and the relevance of white etching cracks in the problem of premature failures has been addressed and a link between the two phenomena has been presented.

In addition, factors that do not play a relevant role in the phenomenon of WECs have been identified as well.

The relationship between white etching areas and cracks has been clearly pointed out, essentially proposing that WEA alterations of microstructure are a mere consequence of the existence of the crack and crack-face rubbing rather than a cause.

8 Conclusions

This chapter provides a brief summary of the research presented in this thesis. The main achievements arising from the study are listed and a few suggestions on how to continue future research are provided.

8.1 Summary of thesis

This thesis has reported the experimental study of mechanisms of white etching crack formation in bearing steels. The study utilized a lab based triple-disc rolling contact fatigue rig, a reciprocating rubbing rig as well as a series of analytical techniques including SEM and FIB-TEM. The rigs and experimental procedures were designed to provide the means of closely controlling the contact conditions so that the influence of specific parameters of interest can be isolated and valid comparisons made. For example, a thermal network of the rig was used to ensure the same lambda ratio in the contact regardless of the applied slide-to-roll ratios, and the evolution so the fatigue specimen wear on the stress history was accounted for. The research explored the effects of lubricant composition, slide-roll ratio, lambda ratio, nominal pressure and stress history in time. The approach was deigned to address the current gaps in the knowledge of the subject which was found to lack in fundamental understanding of the main factors responsible for WECs formation, as confirmed by the analysis of the literature.

The work presented in this thesis has provided a number of new and significant insights into the mechanism of white etching cracks formation and the latters' relevance to bearing failure as was set out in the initial objectives. The main finding can be summarised as follows:

- It has been shown that white etching cracks can repeatedly and reliably be produced in the triple-disc MPR rolling contact fatigue test machine. The initial MPR tests served to identify the most suitable conditions to adopt in order to testing the influence of various parameters of interest on WEC formation. The initial tests also gave a better understanding of the potential significance of competitive modes of failure, mainly micro-pitting and wear, the occurrence of which can change the behaviour of the contact with respect to WEC generation. In order to study one of these phenomena, it is necessary to design carefully the experiment to suppress the other modes if valid results are to be obtained. The analysis and inspection of the WECs produced under a number of various conditions led to a better understanding of the formation mechanisms.

- FIB-TEM was adopted to analyse a particular WEC and WEA obtained and this showed that the microstructure of the white etching microstructural alterations in the employed test specimens was composed of nano-ferrite BCC grains. This is in agreement with observations in literature regarding WECs in failed bearings from wind turbine applications and showed that WECs obtained in current tests are representative of those observed in real bearings from the field.

- The results presented in this thesis suggest that chemical composition of the lubricant does not constitute a primary role for WEC generation. Two different commercial oils as well as base stock oils were adopted in tests where all other parameters were made equal. WECs have been reproduced in all cases regardless of the package of additives contained in the oil. If chemistry has an effect, this is not directly linked to WEC formation, but it is addressed in a change of mechanical conditions, primarily wearing-on of the surfaces (which affects stress history) and friction (which effects tensile stresses and hence crack initiation and propagation). Comparison of roller surface evolution obtained with different oils supports this fact. In particular, a good anti-wear additive, such as ZDDP, protects the roller and counterface discs from running-in so that any stress concentrations persist for longer than in the case of a bad anti-wear additive or a pure base oil which provide conditions for rapid wearing of roller edges and counterface roughness (and hence elimination of stress concentrations which are a necessary precursor to WEC formation). Additional chemical effects from the lubricant are of course possible, especially if these influence or promote hydrogen absorption, but the results in this study clearly indicate that they are not a primary factor in WEC occurrence, at least in the system studied.

- The effect of other important tribological parameters has been investigated. It has been shown that slide-roll ratio, lambda ratio and nominal pressure are unlikely to represent a root cause for WEC formation in themselves (unless they affect stress fields) since WECs were observed at all values of these parameters within the range adopted here

- The importance of stress history in time has been identified as the main root cause for WEC initiation. Different types of MPR specimen geometry were adopted in this study. In this way, it was possible to study the role of pressure distribution and recognize the importance of its evolution in time. In particular, it appeared that line contact configuration obtained by loading flat rings on chamfered roller specimen, was producing WECs. On the other hand, elliptical contact configuration did not result in WEC formation. This finding provided a cause as to possible mechanisms of WEC formation. The main difference between the truncated line contact and the elliptical contact employed in the MPR is the existence of high edge stresses in the line contact during the early stages of operation. These edge stresses drop to the level of the nominal contact pressure in the first few million cycles of operation due to wear and deformation of the track edges. This evolution of roller profile was confirmed by inspection at different test intervals and the resulting evolution of stresses was evaluated using existing contact mechanics models. This specific stress history is responsible for white etching crack formation and the associated, but unrelated, unpredictable failures (see below for the full summary of the relevant mechanism). In order to confirm the significance of variable stress history in generation of WECs, additional tests were conducted with elliptical contact configuration: a stress concentration was manually introduced in the elliptical contact by engraving the crowned profile of the rings in order to produce a circumferential groove resulting in high early stresses (until the groove wears the softer roller profile); in this case WECs were observed in elliptical contacts too, confirming the significance of stress profile.

- The present study provides direct evidence that it is the stress history in time that is the main driver of WEC formation in the system studied. Namely, occurrence of a short duration stress peak in the load spectrum of the component during its early stage of operation, followed by prolonged operation at moderate stress levels results in formation of WECs. The sequence of events is as follows: the early high stress initiates a fatigue, mostly likely at an inclusion in the subsurface. The stress then drops to a moderate value and hence the crack formed at the start propagates relatively slowly, allowing sufficient time for rubbing and beating of crack faces. This rubbing produced microstructural alterations in the vicinity of the crack-faces that manifest themselves as white etching areas, i.e. the occurrence of white etching is a consequence of a fatigue crack existing in bearing steel subjected to cycles of loading. White etching areas are formed preferentially within the regions where crack rubbing conations favour it, for example horizontal rather than vertical braches. Finally, a pitting failure occurs which will be caused by a single crack which may or may not be a white etching crack. In the present study, the failures are generally caused by non-white etching cracks originated at the surface rather than white etching cracks which are mainly in the subsurface and near surface regions.

- This same mechanism also explains the apparent inability of the current bearing life models to predict failures in which WECs are found: the effects of the specific stress history that causes WECs, is not properly accounted by Palmgren-Miner linear damage accumulation rule on which simple bearing life models are based. Hence, occurrence of WECS is not directly related to the failure at all, rather a third factor, a specific stress history in time, causes both WECs and unpredictable failures in parallel. WECs are simply a side effect and would not be treated as the primary focus of future research in connection to rolling contact fatigue failures.

- The stress history described here can be caused by a number of factors in real bearing operation, rather than only the edge effects which are a specific characteristic of the MPR. Indeed, edge effects do not exist in real bearing that employ line contact configurations (bearings with cylindrical rollers as rolling elements) but plenty of other possible sources of elevated stresses in a real application exist, particularly in wind turbine applications that operate under relatively harsh conditions, such as wind gusts, housing deformations, connections/disconnections from the grid, particular surface roughness structure etc. Although stress history appears to be the predominant cause of early crack development in this study it is, of course, not possible to rule out other possible drivers for early crack development such as hydrogen in other systems.

- Further observations and separate experiments provided a more direct observation that white etching areas are a consequence of crack-face rubbing. In MPR tests, direct observation of specimen sections indicated that WEAs are never present without an associated crack, whereas plenty of cracks are present without WEAs. Appropriate sectioning of specimens at different locations of the truncated line contact and at different amount of contact cycles, revealed more about crack formation and its relation with white etching alterations. By sectioning samples at different number of cycles, one noticed that WEAs were absent at crack initiation and early life, but were then formed gradually with increasing number of cycles, as the crack propagated; this strongly supports the assertion that the alteration of the steel microstructure is posterior to crack formation rather than vice versa, and that crack-face rubbing is the likely cause of WEA formation. A different set-up was adopted to verify whether it was possible to generate WEAs under rubbing conditions, in order to validate the crack-face rubbing hypothesis. This was achieved by adopting a ball-on-flat reciprocating rubbing contact (HFRR rig). In this set-up, WEAs were repeatedly generated under different strokes, frequencies of rubbing as well as different lubricants and also dry conditions. These observations confirmed the initial hypothesis that WEA can be formed through mere running of bearing steel specimen under load. Furthermore, occurrence of WEA in dry conditions indicated that lubricant formation is unlikely to be the primary factor in WEC formation.

8.2 Suggested areas for future work

Although the present study provides some new insights and theories into the root causes of WECs and premature failures in bearing steels, further areas of investigation exist to improve the knowledge of this and related subjects. These include:

- It has emerged from this study that the reason for occurrence of both WECs and premature failure is the existence of a specific stress history in time, with early elevated level of stress followed by more moderate stress levels. This stress history is not accounted for by the current fatigue life models due to their reliance on Palmgren-Miner linear damage accumulation rule which assigns the same significance to stress levels regardless to when they occur in time. Therefore, in order to improve the rolling contact fatigue life predictions, it is necessary to find a better way of taking into account stress profile influence on fatigue life, so that associated failures can be more reliably predicted. This is a difficult task and requires a considerable research effort that is well beyond a scope of a single PhD.

- Given that white etching areas were identified as a consequence rather than the cause of white etching cracks, and it is the early fatigue cracks that are at the heart of the problem, further research is needed to investigate how cracks are initiated and how they propagate to cause the eventual failure. In particular, the effects of stresses, microstructure and inclusions should be studied and better understood. This may lead to potential solutions by improving material response to applied stress fields.

- This research addressed the root cause of WECs and early failures but it did not focused on potential solutions. Hence, any future research should utilise the findings and theories presented here and use these to test and propose potential solutions to early bearing failures (not necessarily WECs themselves as these were shown not to be the main cause of the actual failures). Such solutions would explore how to optimize the stress profile in time through for example optimising the running-in process. It has been suggested that black oxide coatings may help prevent early bearing failures in wind turbine applications. It is possible that the mechanism of their action is indeed optimization of the wearing-in process and hence this is a good first avenue to explore in terms of establishing the significance of wearing-in.
- Hydrogen embrittlement is known to reduce rolling contact fatigue life and indeed has been suggested as one of the drivers of WEC formation. Whether or not hydrogen is related to WECs, there is plenty of evidence to show that hydrogen does affect RCF lives and therefore this deserves further investigation. Hydrogen effects in bearing steel are very difficult to study and any further research requires careful consideration to ensure that observed hydrogen is indeed produced in the contact, rather than pre-existing in bearing steels. Care should also be taken in order to assure that the contact conditions and particular operating environment are representative of those found in real applications.

References

[1] W.E.C., 2011, "GWEC-GLOBAL," W.E.C. Global wind report, annual market update.

[2] Luyckx, J., 2011, "Hammering wear impact fatigue hypothesis WEC/irWEA failure mode on roller bearings," NREL Wind turbine tribology seminar, Broomfield, CO, USA.

[3] Ruellan, a., Kleber, X., Ville, F., Cavoret, J., and Liatard, B., 2014, "Understanding white etching cracks in rolling element bearings: Formation mechanisms and influent tribochemical drivers," Proc. Inst. Mech. Eng. Part J J. Eng. Tribol., **228**(11), pp. 1252–1265.

[4] Gould, B., and Greco, A., 2016, "Investigating the Process of White Etching Crack Initiation in Bearing Steel," Tribol. Lett., **62**(2), p. 26.

[5] Kruhöffer, W., and Loos, J., 2017, "WEC Formation in Rolling Bearings under Mixed Friction : Influences and ' Friction Energy Accumulation ' as Indicator," Tribol. Trans., **60**(3), pp. 516–529.

[6] Holweger, W., Wolf, M., Merk, D., Blass, T., Goss, M., Loos, J., Barteldes, S., and Jakovics, A., 2014, "White Etching Crack Root Cause Investigations," Tribol. Trans., **58**(1), pp. 59–69.

[7] Franke, J., Carey, J. T., Korres, S., Haque, T., Jacobs, P. W., Loos, J., and Kruhoeffer, W., 2017, "White etching cracking - Simulation in bearing rig and bench tests," Tribol. Trans., **60**(3), pp. 1–11.

[8] Manieri, F., Stadler, K., Morales-Espejel, G. E., and Kadiric, A., 2018, "The Origins of White Etching Cracks and Their Significance to Rolling Bearing Failures," Int. J. Fatigue, **under rev.**

[9] Luyckx, J., 2012, "White etching crack failure mode in roller bearings: from observation via analysis to understanding and an industrial solution," Roll. Elem. Bear. ASTM Int., pp. 1–25.

[10] Greco, A., Sheng, S., Keller, J., and Erdemir, A., 2013, "Material wear and fatigue in wind turbine Systems," Wear, **302**(1–2), pp. 1583–1591.

[11] Tamada, K., and Tanaka, H., 1996, "Occurrence of brittle flaking on bearings used for automotive electrical instruments and auxiliary devices," Wear, **199**, pp. 245–252.

[12] Winter, H., Knauer, G., and Gamel, J., 1989, "White etching areas on casehardened gears," Gear Technol., **6**(5), pp. 18–19.

[13] Errichello, R., Budny, R., and Eckert, R., 2013, "Investigations of Bearing Failures Associated with White Etching Areas (WEAs) in Wind Turbine Gearboxes," Tribol. Trans., **56**(6), pp. 1069–1076.

[14] Voskamp, A. P., and Mittemeijer, E. J., 1997, "State of residual stress induced by cyclic rolling contact loading," **13**(5), pp. 430–438.

[15] Hertz, H., 1896, Miscellaneous papers, translated from first German edition (1895) by DE Jones and JA Schott, Cornell University Library.

[16] Johnson, K. L., 1985, Contact mechanics, Cambridge University Press.

[17] Sadeghi, F., Jalalahmadi, B., Slack, T. S., Raje, N., and Arakere, N. K., 2009, "A Review of Rolling Contact Fatigue," J. Tribol., **131**(4), p. 41403.

[18] Rycerz, P., Olver, A., and Kadiric, A., 2017, "Propagation of surface initiated rolling contact fatigue cracks in bearing steel.," Int. J. Fatigue, **97**, pp. 29–38.

[19] Murakami, Y., Kaneta, M., and Yatsuzuka, H., 1985, "Analysis of Surface Crack Propagation in Lubricated Rolling Contact," Tribol. Trans., **28**(1), pp. 60–68.

[20] Way, S., 1935, "Pitting due to rolling contact," Asme J. , Appl. Mech., **2**, pp. A49–A58.

[21] Dawson, P. H., 1981, "Effect of sliding on rolling contact pitting," Mech. Eng. Sci., **23**(6), pp. 289–294.

[22] Bower, A. F., 1988, "The Influence of Crack Face Friction and Trapped Fluid on Surface Initiated Rolling Contact Fatigue Cracks," **110**(4), pp. 704–711.

[23] Hoeprich, M. R., 1992, "Rolling Element Bearing Fatigue Damage Propagation," Tribol. Trans., **114**(April), pp. 328–333.

[24] Littmann, W. E., Widner, R. L., Wolfe, J. O., and Stover, J. D., 1968, "The Role of Lubrication in Propagation of Contact Fatigue Cracks," J. Lubr. Technol., **90**(1), pp. 68–89.

[25] Wren, F. J., and Moyert, C. A., 1964, "Modes of fatigue failures in rolling element bearings," Proc. Inst. Mech. Eng., **179**, pp. 236–247.

[26] Dawson, P. H., 1965, "Further experiments on the effect of metallic contact on the pitting of lubricated rolling surfaces," Proc. Inst. Mech. Eng., **180**, pp. 95–100.

[27] Olver, A. V., 2005, "The Mechanism of Rolling Contact Fatigue: An Update," Proc. Inst. Mech. Eng. Part J J. Eng. Tribol., **219**(5), pp. 313–330.

[28] Laine, E., Olver, a. V., and Beveridge, T. a., 2008, "Effect of lubricants on micropitting and wear," Tribol. Int., **41**(11), pp. 1049–1055.

[29] Nélias, D., Dumont, M. L., Champiot, F., Vincent, a., Girodin, D., Fougéres, R., and Flamand, L., 1999, "Role of Inclusions, Surface Roughness and Operating Conditions on Rolling Contact Fatigue," J. Tribol., **121**(2), p. 240.

[30] Harris, T. A., and Kotzalas, M. N., 2006, Rolling bearing analysis, CRC Press - Francis and Taylor Group, Boca Raton, FL 33487-2742.

[31] Griffith, A. A., 1921, "The Phenomena of Rupture and Flow in Solids," Philos. Trans. R. Soc. London. Ser. A, **221**, pp. 163–198.

[32] Irwin, G. R., 1957, "Analysis of stresses and strains near end of a crack traversing a plate," J. Appl. Mech., **24**(3), pp. 361–364.

[33] Hills, D. A., Nowell, D., and Sackfield, A., 1993, Mechanics of elastic contacts,

Butterworth-Heinemann.

[34] Ellyin, F., 1996, Fatigue damage, crack growing and life prediction, Springer Science & Business Media.

[35] Lundberg, G., and Palmgren, A., 1947, "Dynamic capacity of rolling bearings."

[36] Weibull, W., 1939, "A statistical theory of the strength of materials," Proc. R. Swedish Inst. Eng. Res., **151**, pp. 5–45.

[37] Ioannides, E., and Harris, T. A., 1985, "A New Fatigue Life Model for Rolling Bearings," **107**(84), pp. 367–377.

[38] Gegner, J., 2011, "Tribological Aspects of Rolling Bearing Failures," Tribol. - Lubr. Lubr., **3**(2), pp. 33–94.

[39] Ruellan, a., Ville, F., Kleber, X., Arnaudon, a., and Girodin, D., 2014, "Understanding white etching cracks in rolling element bearings: The effect of hydrogen charging on the formation mechanisms," Proc. Inst. Mech. Eng. Part J J. Eng. Tribol., **228**(11), pp. 1252–1265.

[40] Uyama, H., Yamada, H., Hidaka, H., and Mitamura, N., 2011, "The Effects of Hydrogen on Microstructural Change and Surface Originated Flaking in Rolling Contact Fatigue," Tribol. Online, **6**(2), pp. 123–132.

[41] Miner, M. A., 1945, "Cumulative damage in fatigue," J. Appl. Mech., **12(3)**, pp. A159–A164.

[42] Bruce, T., Long, H., and Dwyer-Joyce, R. S., 2015, "Dynamic modelling of wind turbine gearbox bearing loading during transient events," IET Renew. Power Gener., (ISSN 1752-1416).

[43] Faulstich, S., Hahn, B., and Tavner, P. J., 2011, "Wind turbine downtime and its importance for offshore deployment," Wind energy, **14**(3), pp. 327–337.

[44] Evans, M., 2017, "An updated review : white etching cracks (WECs) and axial cracks in wind turbine gearbox bearings," Mater. Sci. Technol., **32**(11), pp. 1133–1169.

[45] U.S. Department of Energy &, and (NREL), N. R. E. L., 2015, "Statistics show bearing problems cause the majority of wind turbine gearbox failures."

[46] "Jeffreys Bay wind farm; http://jeffreysbaywindfarm.co.za/about-wind-energy/the-wind-turbine/."

[47] "Olympus; http://www.olympus-ims.com/en/applications/rvi-wind-turbine/."

[48] "SKF, evolution.skf.com."

[49] Morsdorf, L., Tasan, C. C., Ponge, D., and Raabe, D., 2015, "3D structural and atomic-scale analysis of lath martensite: Effect of the transformation sequence," Acta Mater., **95**, pp. 366–377.

[50] Verhoeven, J. D., 2005, Metallurgy of Steel for Bladesmiths & Others who Heat Treat and Forge Steel, Ioawa State University.

[51] Voskamp, A. P., Osterlund, R., Becker, P. C., and Vingsbo, O., 1995, "Gradual

changes in residual stress and microstructure during contact fatigue in ball bearings," J. Tribol., **117**, pp. 14–21.

[52] Caballero, F. G., and Garcı, C., 2005, "The Role of Retained Austenite on Tensile Properties of Steels with Bainitic Microstructures," Mater. Trans., **46**(8), pp. 1839–1846.

[53] Scott, B. D., Loy, B., and Mills, G. H., 2015, "Metallurgical aspects of rolling contact fatigue," **I**, pp. 94–103.

[54] Evans, M.-H., Richardson, a. D., Wang, L., Wood, R. J. K., and Anderson, W. B., 2014, "Confirming subsurface initiation at non-metallic inclusions as one mechanism for white etching crack (WEC) formation," Tribol. Int., **75**, pp. 87–97.

[55] Uyama, H., 2011, "The Mechanism of White Structure Flaking In Rolling Bearings," Wind turbine tribology seminar, pp. 1–37.

[56] Gould, B., Greco, A., Stadler, K., and Xiao, X., 2017, "An analysis of premature cracking associated with microstructural alterations in an AISI 52100 failed wind turbine bearing using X-ray tomography," Mater. Des., **117**, pp. 417–429.

[57] Hyde, R. S., 2014, "White etching areas: importance of microstructural characterization and modeling," Gearbox Reliab. Collab. all members Meet. NREL Golden.

[58] Moghaddam, S. M., Sadeghi, F., Weinzapfel, N., and Liebel, A., 2014, "A damage mechanics approach to simulate butterfly wing formation around nonmetallic inclusions," J. Tribol., **137**, pp. 1–13.

[59] Harada, H., Mikami, T., Shibata, M., Sokai, D., Yamamoto, A., and Tsubakino, H., 2005, "Microstructural Changes and Crack Initiation with White Etching Area Formation under Rolling/Sliding Contact in Bearing Steel," ISIJ Int., **45**(12), pp. 1897–1902.

[60] Evans, M.-H., Walker, J. C., Ma, C., Wang, L., and Wood, R. J. K., 2013, "A FIB/TEM study of butterfly crack formation and white etching area (WEA) microstructural changes under rolling contact fatigue in 100Cr6 bearing steel," Mater. Sci. Eng. A, **570**, pp. 127–134.

[61] Grabulov, A., Petrov, R., and Zandbergen, H. W., 2010, "EBSD investigation of the crack initiation and TEM/FIB analyses of the microstructural changes around the cracks formed under Rolling Contact Fatigue (RCF)," Int. J. Fatigue, **32**(3), pp. 576–583.

[62] Evans, M.-H., 2012, "White structure flaking (WSF) in wind turbine gearbox bearings: effects of 'butterflies' and white etching cracks (WECs)," Mater. Sci. Technol., **28**(1), pp. 22–3.

[63] Osterlund, R., and Vingsbo, O., 1980, "Phase Changes in Fatigued Ball Bearings," Metall. Trans., **11**(5), pp. 701–707.

[64] Ruellan Du Crehu, A., 2014, "Tribological analysis of White Etching Crack (WEC) failures in Rolling Element Bearings," INSA, Lyon, PhD Thesis.

[65] Stadler, K., and Stubenrauch, A., 2014, "Premature Bearing Failures in Wind

Gearboxes and White Etching Cracks," Power Transm. Eng., **10**, pp. 34–40.

[66] Gould, B., and Greco, A., 2015, "The Influence of Sliding and Contact Severity on the Generation of White Etching Cracks," Tribol. Lett., **60**(2), pp. 1–13.

[67] Swahn, H., Becker, P. C., and Vingsbo, O., 1976, "Martensite Decay During Rolling Contact Fatigue in Ball Bearings," Metall. Trans. A, **7**(8), pp. 1099–1110.

[68] Carroll, R. I., and Beynon, J. H., 2007, "Rolling contact fatigue of white etching layer: Part 1," Wear, **262**(9–10), pp. 1253–1266.

[69] Lund, T., 1969, "Structural alterations in fatigue-tested ball- bearing steel," Jernkontorets Ann., **153**, pp. 337–353.

[70] Zhang, H. W., Ohsaki, S., Mitao, S., Ohnuma, M., and Hono, K., 2006, "Microstructural investigation of white etching layer on pearlite steel rail," Mater. Sci. Eng. A, **421**(1–2), pp. 191–199.

[71] Grabulov, A; Ziese, U; Zandbergen, H., 2007, "TEM/SEM investigation of microstructural changes within the WEA under RCF and 3D crack reconstruction by focused ion beam," Scr. Mater., **57**(7), pp. 635–638.

[72] Becker, P. C., 1981, "Microstructural changes around non-metallic inclusions caused by rolling contact fatigue of ball-bearing steels," Metall. Technol., **8**, pp. 234–243.

[73] Kang, J.-H., and Rivera-Díaz-del-Castillo, P. E. J., 2013, "Carbide dissolution in bearing steels," Comput. Mater. Sci., **67**, pp. 364–372.

[74] Kang, J.-H., Hosseinkhani, B., Williams, C. A., Moody, M. P., Bagotc, P. A. J., and Rivera-Díaz-del-Castillo, P. E. J., 2013, "Solute redistribution in the nanocrystalline structure formed in bearing steels," Scr. Mater., **69**, pp. 630–633.

[75] Solano-Alvarez, W., and Bhadeshia, H. K. D. H., 2014, "White-Etching Matter in Bearing Steel. Part II: Distinguishing Cause and Effect in Bearing Steel Failure," Metall. Mater. Trans. A, **45**(11), pp. 4916–4931.

[76] Bhadeshia, H. K. D. H., and Solano-Alvarez, W., 2015, "Critical Assessment 13: Elimination of white etching matter in bearing steels," Mater. Sci. Technol., **31**(9), pp. 1011–1015.

[77] Hiraoka, K., Fujimatsu, T., Tsunekage, N., and Yamamoto, A., 2007, "Generation process observation of micro-structural change in rolling contact fatigue by hydrogen-charged specimens," Jpn J. Tribol., **52**, pp. 673–683.

[78] Österlund, R., Vingsbo, O., Vincent, L., and Guiraldenq, P., 1982, "Butterflies in fatigued ball bearings - formation mechanism and structure," Scand. J. Met., **11**, pp. 23–32.

[79] Diederichs, A. M., Barteldes, S., Schwedt, A., Mayer, J., and Holweger, W., 2016, "Study of subsurface initiation mechanism for white etching crack formation.," Mater. Sci. Technol., **32**(11), pp. 1170–1178.

[80] Paladugu, M., Lucas, D. R., and Hyde, R. S., 2018, "Effect of lubricants on bearing damage in rolling-sliding conditions: Evolution of white etching cracks,"

Wear, **398**, pp. 165–177.

[81] Sauger, E., Fouvry, S., Ponsonnet, L., Kapsa, P., Martin, J. M., and Vincent, L., 2000, “Tribologically transformed structure in fretting,” **245**(1–2), pp. 39–52.

[82] Podgornik, B., Kalin, M., Vižintin, J., and Vodopivec, F., 2001, “Microstructural Changes and Contact Temperatures During Fretting in Steel-Steel Contact,” J. Tribol., **123**(4), p. 670.

[83] Franke, J., Holweger, W., Technologies, S., Ag, V., Blass, T., Merk, D., Ag, S. T., and Kg, C., 2014, “Influence of Tribolayer on Rolling Bearing Fatigue Performed on a FE8 Test Rig,” TAE 19th Int. Colloq. Tribol., p. 13.

[84] Bader, N., Wittek, E. C., and Poll, P. G., “Tribological Properties of Fuel Economy Gearbox Oils,” 69th STLE Annual Meeting, pp. 1–29.

[85] Guzmán, F. G., Oezel, M., Jacobs, G., Burghardt, G., Broeckmann, C., and Janitzky, T., 2017, “Reproduction of white etching cracks under rolling contact loading on thrust bearing and two-disc test rigs,” Wear, **390**–**391**(5), pp. 23–32.

[86] Uyama, H., Nakashima, M., Morishige, K., Mine, Y., and Murakami, Y., 2006, “Effects of hydrogen charge on microscopic fatigue behaviour of annealed carbon steels,” Fatigue Fract. Eng. Mater. Struct., **29**(12), pp. 1066–1074.

[87] Evans, M., Richardson, A. D., Wang, L., and Wood, R. J. K., 2013, “Effect of hydrogen on butter fl y and white etching crack (WEC) formation under rolling contact fatigue (RCF),” **306**, pp. 226–241.

[88] Vegter, R. H., and Slycke, J. T., 2009, “The Role of Hydrogen on Rolling Contact Fatigue Response of Rolling Element Bearings,” J. ASTM Int., **7**(2), pp. 1–12.

[89] Mikami, H., and Kawamura, T., 2007, “Influence of electrical current on bearing flaking life,” SAE Int., **113**(1), pp. 25–36.

[90] Thomson, A., and Bernstein, I. M., 1980, “The role of metallurgical variables in hydrogen-assisted environmental fracture,” ’Advances Corros. Sci. Technol. ed. M. G. Font. al.), pp. 53–175.

[91] Ćwiek, J., 2007, “Hydrogen degradation of high strength weldable steels,” J. Achiev. Mater. Manuf. Eng., **20**(1–2), pp. 223–226.

[92] Kohara, M., Kawamura, T., and Egami, M., 2006, “Study on Mechanism of Hydrogen Generation from Lubricants,” Tribol. Trans., **49**(1), pp. 53–60.

[93] Richardson, A. D., Wang, L., Wood, R. J. K., Evans, M.-H., Anderson, W. B., and Ingram, M., 2015, “Investigation of the role of hydrogen in white structure flaking (WSF) of wind turbine gearbox bearings,” STLE Annual Meeting, Dallas, Texas.

[94] Kanezaki, T., Narazaki, C., Mine, Y., Matsuoka, S. ., and Murakami, Y., 2008, “Effect of hydrogen on fatigue crack growth behaviour and ductility loss of austenitic stainless steels,” Int. J. Hydrogen Energy, **33**(10), pp. 2604–2619.

[95] Ruo, P., and Olver, A. V, 2007, “Hydrogen in lubricated contact,” 1st International conference - Artificial intelligence for industrial applications,

Ostravice, CZ, pp. 19–23.

[96] Kohara, M., Kawamura, T., and Egami, M., 2006, “Study on mechanism of hydrogen generation from lubricants,” Tribol. Trans., **49**, pp. 56–60.

[97] Kotzalas, M. N., and Doll, G. L., 2010, “Tribological advancements for reliable wind turbine performance.,” Philos. Trans. A. Math. Phys. Eng. Sci., **368**, pp. 4829–50.

[98] Birnbaum, H. K., and Sofronis, P., 1994, “Hydrogen-enhanced localized plasticity—a mechanism for hydrogen-related fracture,” Mater. Sci. Eng. A, **176**(1–2), pp. 191–202.

[99] Tanaka, S., and Murakami, Y., 2008, “Rolling bearings,” Pat. Trademark Off., **7-435–308**.

[100] Tanimoto, H., Tanaka, H., and Sugimura, J., 2011, “Observation of hydrogen permeation into fresh bearing steel surface by thermal desorption spectroscopy,” Tribol. Online, **6**, pp. 291–296.

[101] Holweger, W., 2014, “Progresses in solving white etching crack phenoma,” Gearbox reliability collaborative all members meeting, NREL Golden, Colorado, pp. 10–45.

[102] Tanaka, S., Mitamura, N., and Murakami, Y., 2004, “Influence of sliding and chromium content in the steel on the white structural change under rolling contact,” Proceedings of the global powertrain conference, Dearborn, MI, pp. 6–13.

[103] Dyson, A. H. P. G. M. C., Evans, H. P., Karami, G., Paliwal, M. C., and Snidle, R. W., 1990, “Scuffing failure of steel discs: conditions for the failure of elastohydrodynamic lubrication.,” Proc. Inst. Mech. Eng. Part C Mech. Eng. Sci., **204**(2), pp. 91–97.

[104] Fujita, S., Mitamura, N., and Murakami, Y., 2005, “Research of new factors affecting rolling contact fatigue life,” World Tribology Congress, Washington, DC, ASME, pp. 1–2.

[105] Beswick, J. M., “Fracture and fatigue crack propagation properties of hardened 52100 917 steel,” Metall. Trans. A, **20**(10), pp. 1961–1973.

[106] Kim, T. H., Olver, A. V., and Pearson, P. K., 2001, “Fatigue and fracture mechanisms in large rolling element bearings,” Tribol. Trans., **44**(4), pp. 583–590.

[107] Janakiraman, S., West, O., Klit, P., and Jensen, N. S., 2015, “Observations of the effect of varying Hoop stress on fatigue failure and the formation of white etching areas in hydrogen infused 100Cr6 steel rings,” Int. J. Fatigue, **77**, pp. 128–140.

[108] Lai, J., and Stadler, K., 2016, “Investigation on the mechanisms of white etching crack (WEC) formation in rolling contact fatigue and identi fi cation of a root cause for bearing premature failure,” Wear, **364–365**, pp. 244–256.

[109] Richardson, A. D., Evans, M. H., Wang, L., Wood, R. J. K., and Ingram, M., 2018, “Thermal desorption analysis of hydrogen in non-hydrogen-charged rolling

contact fatigue-tested 100Cr6 steel," Tribol. Lett., **66**(1), p. 4.

[110] Benyajati, C., Olver, A. V., and Hamer, C. J., 2003, "An experimental study of micropitting, using a new miniature test-rig," Tribol. Ser., **43**, pp. 601–610.

[111] Lainé, E., Olver, A. V, Lekstrom, M. F., Shollock, B. A., Beveridge, T. A., and Hua, D. Y., 2009, "The Effect of a Friction Modifier Additive on Micropitting," Tribol. Trans., **52**(4), pp. 526–533.

[112] Gatzen, M. M., Pape, F., Bruening, C., Gatzen, H. H., Arlinghaus, H. F., and Poll, G. W. G., 2010, "Correlation between performance and boundary layers in high speed bearings lubricated with polymer-enhanced greases," Tribol. Int., **43**(5–6), pp. 981–989.

[113] Vlcek, B. L., and Zaretsky, E. V., 2011, "Rolling-Element Fatigue Testing and Data Analysis—A Tutorial," Tribol. Trans., **54**(4), pp. 523–541.

[114] McParlan, M., and Graville, B. A., 1976, "Hydrogen Cracking in Weld Metals," Weld. J., p. 95s–102s.

[115] Shinozaki, K., and North, L. K. T. H., 1992, "Hydrogen Cracking in Duplex Stainless Steel Weld Metal," Weld. J., p. 387s–396s.

[116] Briant, C. L., 1979, "Hydrogen assisted cracking of type 304 stainless steel," Metall. Trans. A, **10**(2), pp. 181–189.

[117] Craig, B. D., and Krauss, G., 1980, "The Structure of Tempered Martensite and Its Susceptibility to Hydrogen Stress Cracking," Metall. Trans. A, **11**(11), pp. 1799–1808.

[118] Graham, R., 1979, "Pitting of hard steel rolling-sliding elastohydrodynamically lubricated line contacts," Imperial College, PhD Thesis.

[119] Wilkinson, C. M. R., 1998, "The durability of highly loaded, lubricated, case hardened steel gears," Imperial College, PhD Thesis.

[120] Benyajati, C., 2005, "An experimental study of the effect of lubricant composition on micropitting of hard steel," Imperial College, PhD Thesis.

[121] Morales-Espejel, G. E., Rycerz, P., and Kadiric, A., 2018, "Prediction of micropitting damage in gear teeth contacts considering the concurrent effects of surface fatigue and mild wear," Wear, **398**, pp. 99–115.

[122] Kadiric, A., and Rycerz, P., 2016, "Influence of Contact Conditions on the Onset of Micropitting in Rolling-Sliding Contacts Pertinent to Gear Applications," AGMA Tech. Pap. 16FTM21, AGMA, Virginia.

[123] Olver, A. V., and Spikes, H. A., 1998, "Prediction of traction in elastohydrodynamic lubrication," Proc. Inst. Mech. Eng. Part J J. Eng. Tribol., **212**(5), pp. 321–332.

[124] Dowson, D., and Higginson, G. R., 1959, "A numerical solution to the elasto-hydrodynamic problem," J. Mech. Eng. Sci., **1**(1), pp. 6–15.

[125] Chittenden, R. J., Dowson, D., Dunn, J. F., and Taylor, C. M., 1985, "A theoretical analysis of the isothermal elastohydrodynamic lubrication of concentrated contacts. II. General case, with lubricant entrainment along either

principal axis of the Hertzian contact ellipse or at some intermediate angle," Procedings R. Soc. A, Math. Phys. Eng. Sci., **A397**(1813), pp. 271–293.

[126] Balcombe, R., Fowell, M. T., Olver, A. V., Ioannides, S., and Dini, D., 2011, "A coupled approach for rolling contact fatigue cracks in the hydrodynamic lubrication regime: The importance of fluid/solid interactions," Wear, **271**(5–6), pp. 720–733.

[127] Zaretsky, E. V., Poplawski, J. V., and Peters, S. M., 1996, "Comparison of life theories for rolling-element bearings," Tribol. Trans., **39**(2), pp. 237–248.

[128] Morales-Espejel, G. E., and Gabelli, A., 2011, "The behavior of indentation marks in rolling–sliding elastohydrodynamically lubricated contacts.," Tribol. Trans., **54**(4), pp. 589–606.

[129] Gachot, C., Rosenkranz, A., Reinert, L., Ramos-Moore, E., Souza, N., Müser, M. H., and Mücklich, F., 2013, "Dry friction between laser-patterned surfaces: role of alignment, structural wavelength and surface chemistry.," Tribol. Lett., **49**(1), pp. 193–202.

[130] Morales-Espejel, G. E., Gabelli, A., and Ioannides, E., 2009, "Micro-geometry lubrication and life ratings of rolling bearings," Proc. Inst. Mech. Eng. Part C J. Mech Eng Sci., **224**(12), pp. 2610–2626.

[131] SKF, 2003, "SKF General catalogue. Principles of bearing selection and application."